Gαq
regulates mitochondrial motility and interacts with ALEX3, MIRO1 and TRAK proteins

Ismael Izquierdo Villalba

UNIVERSITAT DE BARCELONA

FACULTAT DE FARMÀCIA I CIÈNCIES DE L'ALIMENTACIÓ

$G\alpha_q$
REGULATES MITOCHONDRIAL MOTILITY AND INTERACTS WITH ALEX3, MIRO1 AND TRAK PROTEINS

Ismael Izquierdo Villalba
Barcelona, 2019

UNIVERSITAT DE BARCELONA

FACULTAT DE FARMÀCIA I CIÈNCIES DE L'ALIMENTACIÓ

PROGRAMA DE DOCTORAT DE BIOTECNOLOGIA

$G\alpha_q$
REGULATES MITOCHONDRIAL MOTILITY AND INTERACTS WITH ALEX3, MIRO1 AND TRAK PROTEINS

Memòria presentada per Ismael Izquierdo Villalba
per optar al títol de doctor per la Universitat de Barcelona

Directora:

Dra. Anna M Aragay Combas

Tutora:

Dra. Josefa Badía Palacín

Doctorand:

Ismael Izquierdo Villalba

Ismael Izquierdo Villalba
Barcelona, 2019

Science never solves a problem without creating ten more

George Bernard Shaw

It's been quite long since I first stepped in the lab. Along these years, many people have come by and almost all of them have already left, or better said, begun their new stories. I also came here trying to get my own, a goal that I still pursue and I hope I will have not abandoned by the time you read these lines. Here I would like to thank some of the people who contributed to make one or many of the steps forward to achieve that, not before asking those who I not mention to forgive my lack of memory. First and foremost, I would like to thank Sere, por colaborar con nosotros e implicarte tantísimo con el proyecto, los cultivos de neuronas y los knockouts de Alex a pesar de que nos acaben dando más problemas que alegrías. Difícilmente podría haber encontrado una compi mejor :) I also would like to thank Eduardo for allowing me to carry out a great part of this project in his lab, ¡muchas gracias por hacerme sentir parte de tu grupo y permitirme aprender tantas cosas de neuro! And of course the rest of neuro group, especialment el Marc, l'Alba, la Cris, la Marina, i el Toni, aquest dos amb més motiu encara per haver-los enredat amb els cultius de neurones i les seqüenciacions, i especialment al Toni per haver d'aguantar que un merengue li faci fer els cultius i vingui a robar-li els anticossos i el medi condicionat :p Y bueno, tampoco quiero olvidarme de Ash de la misma forma que me "olvido" cada vez que me paso por el lab de las 4 o 5 paellas del bota-fumeiro que todavía le debo.

In any case, the first pages of this story were not written with those who are currently in the lab, but with old folks who have already started new stages in their lives, and are probably the ones from who I learned the most. Thank you so much to Miriam, per haver-me deixat pendre part del teu projecte,

que al cap i a la fi és com vaig començar a aprendre al grup. També tinc un munt que agraïr-li al la Georgina per tota la paciència que va haver de tenir amb mi quan estava aprenent, per ser tant organitzada i per fer que el grup funcionés tant bé. I per descomptat també agraïr a la Mónica per ajudar-me a resoldre tants dubtes i deixar-me pendre part del projecte de la filamina i els chemokine receptors, suposo que els projectes que donen més problemes també són aquells dels que més s'apren!
Also Cris, que aunque no hayamos coincidido mucho en el lab has aportado una parte importantísima de este proyecto, muchas gracias por tu motivación y por traer buen ambiente y buenas ideas al grupo siempre que vienes!
By that time the only space we had for lunch at the helix building were two small tables in the coffee room, so we all had to struggle to get a seat. It was much worse than now, even if it seems hard to believe. However, once we managed to get a seat, we overcame the lack of space by reading nonsense news at the 20 minutes newspaper and tried to foresee our luck through the horoscopes. Aquí me gustaría agradecer especialmente a Vir y Oscar por ser los impulsores de todo este ritual y por haber aprendido tanto de ellos, pero también a otra gente que por aquella época estaban con Maribel o Tim como Lourdes, Paqui, Erika, Mar, Adrian, Fátima, Isa… Raramente teníamos tanta suerte como para encontrar espacio suficiente para reunirnos todos, pero con coincidir 2 o 3 de nosotros ya era suficiente para leer los horóscopos y pasar un buen rato.
Vielen Dank Adrian für alle Korrekturen meiner Aufsätze! Dank deiner Raten habe ich zwei oder drei Deutschkurse bestanden und viel Deutsch gelernt! Wahrscheinlich bist du (mit Isa natürlich) die zwei Leute die mit mir mehr Zeit im Labor verpasst haben!
I would also like to thank other people from other labs who were especially kind to me and gave me useful advices when I needed. Thanks to Mar and Irene from the crystallography group, also Halal from Marti and Irene from Elisa's group!
After that time, some of them started to defend their thesis and I thought I would eventually stay alone until I defended mine. I already knew it would take me a little longer because my goals have always been… let's say, a bit ambitious. Then new students came to the lab, among them were Oscar Orrios, I really had a lot of fun with you. Also Diego, Mireia, Estel… that was an amazing time with you all. Siempre recordaré las extravagancias de Dass que me contaba Diego, su éxito en los pull-downs con los constructos de Oscar y los momentos surrealistas en aquel amigo invisible irlandés de la cena de Navidad, junto a Fröde y el grupo de Tim, que por aquel entonces estaba lleno de italianos.
I also take this paragraph to thank Fröde for being so nice to us when you came to Barcelona and the Italian group for bringing us that much fun! From them I would like to thank Simona, Emmanuela and Anna, that even though I met them some years later I had sooo much fun with them when we went out! I hope Anna's doing well in Rome and I wish Emmanuela would recommend me another

anime as good as Shingeki no Kyojin :p Moltes gràcies també a Mireia per haver-me fet pasar tant bons moments i haver-me acompanyat a la cafetería a dinar sempre que em volia pendre un cafè amb xocolata per sobre :p Espero que et vagi genial la tesi per Suïssa!!

That was actually a time when I met many people from other groups that I would also like to thank and most specially those who spend over average years to finish their PhD's. Muchas gracias a Raquel, Raúl y Lucia porque al fin y al cabo sois los que más tiempo pasabais en cultivos, quiénes más compañía me hacíais y quiénes me dabais los mejores consejos. La gente suele decir que la experiencia es un grado pero vuestra motivación por la ciencia vale el doble. ¡Seguro que os irá genial mientras sigáis en ciencia! Mención aparte merece Laura, ¡muchísimas gracias por todos los planes que has organizado durante todos estos años, por hacerme descubrir la champaneria y por los findes que pasamos en la playa! Seguro que sin ti mi tesis hubiese sido más aburrida :p But we wouldn't have had that much fun if it wasn't for the people that came with us, and of course I would also like to thank. Muchas gracias Anna, Laura, Aleix, Soraia, Marion y en definitiva toda la gente que se ha unido a nosotros en nuestros viajes a la playa o salidas a la champaneria. Besonders Claus, du bist immer fertig um einen Bier zu trinken, auch wenn wir allein sind und wir zum Kegelbahn gehen müssen. Vielen Dank Claus! But this paragraph would be incomplete without Arkadius. I wish I had finished this work with a protein structure below 2Å, but I will take your advice for a future project.

Then it came the day when Anna suggested me to take part in a, by that time inexistent, IBMB PhD council. I was never good at persuading people to attend meetings and talks, but that was useful to me to know more about other students from other labs. As always, Raul and Laura were among the best organizers, but I want to thank all the members of that PhD council for the nice job you did: Isa, Stella, María, Sandra, Daniel, Raul and Laura thank you all!

And before I jump to a new stage, I want to thank three other people I always admired a lot even though I'm nor really sure if they think the same about me. The first of them is David. Moltes gràcies per fer sempre lo k te surt dels pebrots i callar a qui et critiquen amb millors resultat k ells, ets el model que m'hagues agradat seguir pero k mai m'he atrevit a fer. Segur k t'anirà genial alla on vagis! También agradecer a Iracema, que aún sin haber tenido la suerte de coincidir mucho contigo siempre me anima un montón cuando nos encontramos. And of course Eleni. Seguro que mi experiencia hubiese sido mejor de haber pasado más tiempo contigo, aunque tampoco se puede pedir que todo salga como una espera en una tesis…Se feliz allá donde vayas.

From the people that are still in the lab I should specially thank the group of Maribel, Javi Inés, Laura, Paula and Isa. Muchas gracias Javi por traer experiencia, buen humor y sobretodo jamón de Salamanca al lab, se echa de menos tener mas postdocs como tú! También a Inés, la única murciana que me ha ido cayendo mejor a lo largo del tiempo y espero que la siguiente del lab en defender su tesis!

A Laura por seguir tan agradable y con el valor de meterse a hacer una tesis a pesar de lo que cuesta conseguir que te paguen y ya ni te cuento resultados positivos. A Paula, que espero que todas las penurias de sus compis no la desanimen a seguir más tiempo en el lab! Y por supuesto Isa, porque todo el tiempo que has pasado en el lab debería merecer un reconocimiento especial. Y como no a Maribel, porque junto con Isa y Ana es la única que sigue al pie del cañón desde que empecé. ¡Muchas gracias por tus consejos, por las comilonas en Sant Pol y por dar tan buen ambiente al laboratorio!

I would also like to thank all those students who helped me and Anna during my this time, even though they stayed for a few months. First I should thank Elena, por ayudarnos con los ensayos de mitocondrias a pesar de todos los quebraderos de cabeza que te hecho pasar para reservar horas de confo, ojalá a partir de ahora tengas más suerte y los estudiantes que te encuentres por microscopia sean un poco menos despistados y no te den tantos problemas. También agradecer a Jaume, que aunque me haya tenido que aguantar menos que Elena también ha estado dispuesto a ayudar cuando lo he necesitado. Tampoco quiero que se queden sin agradecer los estudiantes que me han ido haciendo compañía en el grupo todos estos años. Gracias a Lidia, a Ferrán, a Claudia y a Luce. A Alex estudiante, a Jordi, a Effat, a Helena, a Noura y por supuesto a Javi y a Alicia, espero que os vaya genial en el futuro!

And even though I spent most of my time doing experiments in the lab, or better said, trying to find a logical explanation for those experiments that didn't work as expected, I also met many people in congresses and conferences that brought me lot of fun, especially those from Fede's lab in Madrid during the congress in Salamanca. Muchas gracias a Fede y a Cati por su amabilidad y por tener un grupo con tan buen ambiente, la verdad es que me da un poco de envidia. Gracias a Álvaro, Sofía, Guzmán y especialmente Martiña por todos los buenos momentos que pasamos juntos. Espero que te vaya genial en tu nueva etapa en Galicia como farmacéutica, siempre tendrás a alguien encantado de verte por Barcelona o donde quiera que esté en un futuro.

Finally I should also thank the Agaur for providing me the finantial support to carry out a big part of this project and the IBMB institute for hosting us. And last but not least I would also like to thank Anna, moltes gràcies per tots aquests anys aprenent al grup, al capdevall has estat única persona que m'ha acompanyat des del principi fins al final de la tesi. Crec que no s'ha fet mala feina tot i que encara faltin tantes coses per fer. M'hagués agradat acabar una mica més a prop d'aconseguir l'objectiu que em vaig proposar al començar la tesi, però estic satisfet igualment d'haver tingut l'oportunitat d'intentar-ho.

Thank you!

¡Gracias!

Gràcies!

Danke!

CONTENTS

ABSTRACT

G proteins transduce a myriad of signals from receptors at the plasma membrane. Recent reports point to a novel localization of G proteins at the mitochondria and other endomembranes where they regulate the physiology of these organelles. In particular, the $G\alpha_q$ subfamily is required to keep the proper balance between mitochondria fusion and fission acting at both outer and inner membrane, among other functions. In order to unveil the putative effectors of $G\alpha_q$ that mediate those effects at the mitochondria, our group has undertaken a mass-spectrometry analysis based on $G\alpha_q$ immunoprecipitates from cellular endomembranes. The "mito-interactome" study provided evidence of $G\alpha_q$ interaction with the armadillo domain-containing proteins Alex3 and Armc10. Subsequent immunoprecipitation and pull-down studies demonstrated a specific interaction of $G\alpha_q$ with the mitochondrial Rho GTPase 1 (Miro1) and both milton adaptor proteins TRAK1 and 2, that couple mitochondria to kinesin and dynein motor proteins and constitute the main regulators of mitochondrial transport in neurons.

To analyze the physiological role of those interactions, we have performed tracking analysis of mitochondria along the axons of hippocampal neurons overexpressing $G\alpha_q$ or its constitutive-active mutant, $G\alpha_q$R183C, as well as activating a $G\alpha_q$-specific GPCR (DREADD) with its specific agonist. The results of these studies reveal a significant increase in anterograde movement upon $G\alpha_q$ expression, whereas $G\alpha_q$ activation by either expressing the active-mutant or activating the $G\alpha_q$-specific GPCR induces mitochondrial arrest. In contrast, depletion of $G\alpha_q$ using short-hairpin RNAs increases the number of motile mitochondria and their speed and promotes retrograde transport. Both activation of $G\alpha_q$ or its depletion alter mitochondrial dynamics including fusion/fission events, whereas expression of active-$G\alpha_q$ also alters neuronal physiology by reducing their complexity and dendritic branching. In summary, our group postulates a new non-canonical mitochondrial function of $G\alpha_q$ acting as a molecular switch through its association with Alex3, Miro1 and TRAK2. $G\alpha_q$ would associate to Alex3 and Miro1 to allow mitochondrial movement, whereas its GTP-bound conformation would associate to TRAK2 to halt motility. This process would be regulated by Alex3, which could play crucial roles as an adaptor for the protein complex and $G\alpha_q$ transactivation.

ABBREVIATIONS

7TRM 7 Transmembrane receptor

aa Aminoacid

AC Adenyl cyclase

AD Alzheimer's disease

AKT Protein kinase B

ALEX3 Armadillo domain-containing protein lost in epithelial cancers linked to chromosome X 3

ALS Amyotrophic lateral sclerosis

AMP Adenosine monophosphate

AMPA α-amino-3-hydroxy-5-methyl-4-isoxazolepropionic acid

AngII Angiotensin II

APP Amyloid precursor protein

AR Adrenergic receptor

Arm armadillo domain

ARMCX3 armadillo repeat-containing protein located on the X chromosome 3

Armc10 armadillo repeat-containing protein 10

AT1R angiotensin receptor 1

ATP Adenosine Tri-Phosphate

BEX brain expressed X-linked

BSA Bovine serum albumin

BTK Bruton Tyrosyne Kinase

cAMP adenosine 3'5' cyclic monophosphate

CaSR Calcium-sensing receptor

CAT Catalase

CKII Casein kinase II

CNO Clozapina-N-Oxyde

Ct carboxyl terminus

Cyt Cytosol

DAG Diacyl glycerol

DAPI 4',6-Diamidino-2-phenylindole

dH_20 Distilled water

DHC Dynein heavy chain

DIC Dynein intermediate chain

DISC1 Disrupted in schizophrenia 1

DLC Dynein light chain

DLIC Dynein light intermediate chain

DMEM Dulbecco's Modified Eagle Medium

DMSO Dimethyl Sulfoxide

DNA Deoxyribonucleic acid

DREADD Designer Receptor Exclusively Activated by a Designer Drug

DTT DL-Dithiothreitol

EC Extracellular

ECM Extracellular matrix

E.Coli Escherichia coli

EDTA Ethylene diaminetetraacetic acid

EGF Epidermal growth factor

EGTA Ethylene glycol tetraacetic acid

ER Endoplasmic reticulum

ERK Extracellular signa-regulated kinases

ERMES ER-mitochondria encounter structure

ETC Electron transport chain

FBS Fetal Bovine Serum

GABA γ-Aminobutyric acid

GAP GTPase activating protein

GAPDH Glyceraldheide 3-phosphate dehydrogenase

GASP GPCR- associated sorting protein

GDI GDP dissociation inhibitor

GDP Guanosine diphosphate

GEF Guanine nucleotide exchange factor

GFP Green fluorescent protein

GHRH Growth hormone-releasing hormone

GPCR G protein-coupled receptor

GPX Gluthatione peroxidase

GR Glutathione reductase

GRIF-1 GABAA receptor interacting factor-1

GRK G protein-coupled receptor kinase

GST Glutathione S-transferase

GTP Guanosine triphosphate

HA Hemagglutinin (tag)

HAP1 Huntingtin-associated protein 1

HEPES 4-(2-hydroxyethyl)-1-piperazineethanesulfonic acid

Hsp90 heat shock protein 90

IF Immunofluorescence

IP Immunoprecipitation

IP_3 Inositol 1,4,5-trisphosphate

IP_3R Inositol 1,4,5-trisphosphate receptor

IRES Internal ribosome binding site

KDa Kilodalton

KHC Kinesin heavy chain

KI Knock-in

KIF Kinesin

KLC Kinesin light chain

KO knockout

LB Luria-Bertani broth

Leu Leupeptin

MAPK Mitogen-activated Protein Kinase

MEF Mouse Embryonic Fibroblasts

MEK MAPK and extracellular signal-regulated kinase (ERK) kinase

MEKK MAPK kinase and extracellular signal-regulated kinase (ERK) kinase

Miro Mitochondrial Rho

Mfn mitofusin

MPP matrix processing peptidase

mRNA messenger ribonucleic acid

MTOC microtubule-organizing center

NMDA N-methyl-D-aspartate

NP40 Nonidet P-40

NPC Neuronal precursor cells

Nt Amino terminus

OIP106 O-linked N-acetylglucosamine transferase interacting protein 106

OPA1 Optic atrophy 1

p120ctn p120 catenin

PAGE Polyacrilamide gel electrophoresis

PARL PINK1/PGAM5-associated rhomboid-like protease

PBS Phosphate buffered saline

PCR polymerase chain reaction

PDGFR platelet-derived growth factor receptor

PH Pleckstrin homology

PI3K Phosphatidylinositol-4,5-biphosphate 3-kinase

PINK1 PTEN-induced putative kinase 1

PIP2 Phosphatidylinositol 4,5-biphosphate

PIP3 Phosphatidylinositol 3,4,5-biphosphate

PKA Protein kinase A

PKC Protein kinase C

PLC Phospholipase C

PMSF Phenylmethylsulfonyl fluoride

PMSF Phenylmethylsulfonyl fluoride

PVDF polyvinylidene fluoride

RGS Regulator of G protein signaling

RH RGS homology

Ric-8 Resistant to inhibitors of cholinesterase 8

RILP Rab-interacting lysosomal protein

RNA Ribonucleic acid

ROS Reactive Oxygen Species

ROCK Rho-kinase

RT Room temperature

RTK Receptor Tyrosine Kinase

SD Standard deviation

SDS sodium-dodecyl-sulphate

SEM standard error of the mean

shRNA short hairpin ribonucleic acid

Slug Zinc finger protein SNAI2

SR Sarcoplasmic reticulum

SRE serum response element

TAE Tris base, acetic acid and EDTA

TCA Tricarboxilic acid

TE Tris-EDTA

TEMED Tetramethylethylenediamide

TF Transcription factor

TM transmembrane

Tom20 Transporter outer membrane 20

Ub Ubiquitin

UV Ultraviolet

WB Western Blot

Tris Tris(hydroxymethyl)-amino-methane

WEX Wwbp X-linked

WT Wild type

ZNF217 Zinc finger protein 217

INTRODUCTION

1. Mitochondria, the powerhouses of cells

From 2 to 3 billion years ago, a symbiosis between an *alphaproteobacterium* and a primitive eukaryotic cell related to *Asgard Archaea* gave rise to the first primordial mitochondria (Roger, Muñoz-Gómez, & Kamikawa, 2017). As the symbiosis matured, those free-living organisms suffered massive changes including a significant reduction of their genome, transfer of genes to external DNA, generation of membrane transporters to allow the import of proteins and the integration of their metabolism and reproduction to the host cell (Roger et al., 2017). Currently mitochondrial DNA (mtDNA) only encodes for 13 proteins, 22 tRNA and 2 mRNA and the rest of the more than 1500 mitochondrial genes are scattered though the eukaryotic genome (Wallace, 2005).

These organelles are bounded by two lipid membranes, the inner and the outer mitochondrial membrane, that bind together on contact sites. The inner mitochondrial membrane is ion-impermeant and comprises the major barrier between the cytosol and the mitochondrial matrix. It forms multiple infoldings where structural proteins and enzymes are embedded. The outer mitochondrial membrane allows the flux of some ions and small molecules and is tightly regulated. In between, the intermembrane space houses important enzymes for mitochondrial physiology, bioenergetics and apoptosis, like the cytochrome C and the creatine kinase (Castellanos & Lanning, 2019).

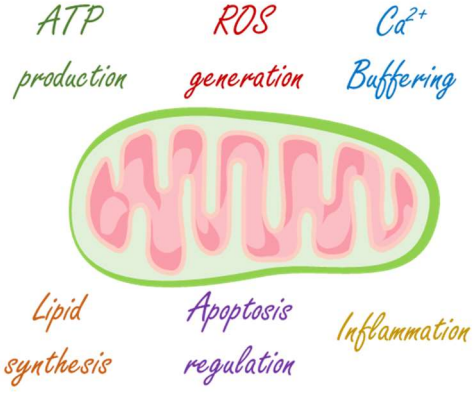

Figure I 1 Overview of the main mitochondrial functions. The main eukaryotic cell functions regulated by mitochondria involve energy production in form of ATP, calcium buffering, regulation of apoptosis and lipid synthesis. They are also the main generators of reactive oxygen species (ROS) and play crucial roles in the process of inflammation.

Mitochondria have evolved to become the "powerhouses" of eukaryotic cells, as their main role is the generation of ATP through the oxidative phosphorylation (OXPHOS). In this process, ATP is generated through the oxidation of nutrients, including sugars, amino acids and fatty acids, which transfer their electrons into oxidized cofactors to generate NADH form NAD^+ and $FADH_2$

from FAD (Meyer, Welchen, & Carrie, 2019). The electron carriers are oxidized back by reducing the first of a series of enzymes embedded at the inner mitochondrial membrane that have O_2 as final acceptor (Duchen, 2004). Those enzymes are all multi-protein complexes and known as complex I (NADH dehydrogenase), complex II (succinate dehydrogenase), complex III (ubiquinol cytochrome c reductase), and complex IV (cytochrome c oxidase) (Duchen, 2004). The electron transferring through the protein complexes is known as electron transport chain (ETC), and is used to pump protons into the inner mitochondrial space and generate a proton motive force, that can flux backwards through the ATP synthase to induce ADP phosphorylation or be used to accumulate cytosolic calcium.

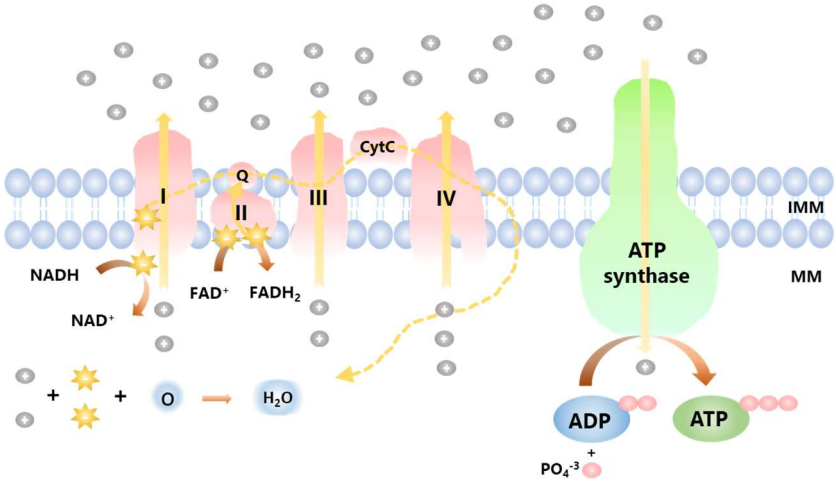

Figure I 2. Schematic representation of oxidative phosphorylation (OXPHOS) and ATP generation through the ATP synthase complex. Electrons derived from cellular metabolism reach complex I or complex II through NADH or $FADH_2$, respectively. These electrons are then transferred to coenzyme Q (ubiquinone), a carrier of electrons from complex I or II, to III. In the latter, particles are shifted form cytochrome b to cytochrome c with a consequent transfer to complex IV (cytochrome oxidase) where they reduce O_2. This electrons transport through mitochondrial complexes is coupled to shipment of protons in the intermembrane space. The electrochemical gradient generated is used by complex V for ATP synthesis. IMM= inner mitochondrial membrane; MM= mitochondrial matrix

Indeed, another important role of mitochondria is to serve as transient calcium warehouses and regulate local calcium fluxes through inositol-triphosphate (IP_3) gated channels (Rizzuto, Brini, Murgia, & Pozzan, 1993). High calcium levels increase tricarboxylic acid (TCA) activity and energy production in response to strong energy demands (Robb-Gaspers et al., 1998). Moreover, mitochondrial calcium allows signaling with other calcium-warehouses like endoplasmic reticulum (ER) or sarcoplasmic reticulum (SR) (Sharma, Ramesh, Franzini-Armstrong, & Sheu, 2000) and even with the voltage-dependent channels of excitable cells (Boitier, Rea, & Duchen, 1999).

The third main function of mitochondria is to regulate apoptosis. Cellular damage and stress activate pro-apoptotic proteins, including Bax and Bak, resulting in changes in mitochondrial inner and outer membrane permeability, loss of membrane potential and release of cytochrome c, which in turn activates caspase signaling and results in apoptosis (Danial & Korsmeyer, 2004; Thornberry & Lazebnik, 1998).

The view of these organelles has equally evolved from kidney-shaped individual entities to a mitochondrial network undergoing fusion and fission events to allow a continuous renewal. Mitochondrial turnover is especially important due to their role of ATP producers through the electron transport chain (ETC). Leakage of electrons during their transport through the four enzymatic complexes leads to their direct binding to oxygen thereby generating reactive oxygen species (ROS). Those ROS are usually neutralized by antioxidant enzymes including superoxide dismutase (SOD), glutathione peroxidases (GPXs), catalase (CAT), glutathione-s-transferase (GST) and glutathione reductase (GR) among others. However, under high activity conditions, the balance between ROS production and neutralization is disturbed, generating an excess of ROS and leading to oxidative stress (Sinha, Das, Pal, & Sil, 2013). Due to their high reactivity, ROS can induce damage by oxidation of proteins (Cabiscol, Piulats, Echave, Herrero, & Ros, 2000), lipids (Biliński, Litwińska, Błaszczyński, & Bajus, 1989) and nucleic acids (Yakes & Van Houten, 1997), which makes degradation of old, damaged mitochondria an essential process to avoid further damage inside the cell. Many human diseases have been associated with ROS-induced oxidative stress, including diabetes (Das & Sil, 2012; Manna & Sil, 2012b, 2012a; Rashid, Das, & Sil, 2013), Alzheimer's disease (Behl C, 1999), Parkinson's disease (Hirsch, 1993), Huntington's disease (Johri, Chandra, & Flint Beal, 2013) and amyotrophic lateral sclerosis (Andrus, Fleck, Gurney, & Hall, 1998; Granatiero, Manfredi, Granatiero, & Manfredi, 2019).

1.1. Mitochondrial transport in neurons

Neurons, probably more than any other cell type, rely on mitochondria for their survival due to their exceptional morphology, their strong dependence on mitochondrial oxidation of glucose to produce ATP and their special need of calcium buffering at the synapses. These post-mitotic cells do not regenerate from progenitors when they die so they must rely on highly regulated autophagy processes to maintain the integrity of their organelles during their lifespan (Chen & Chan, 2009, 2004).

Neurons are highly polarized cells and have a unique morphology usually split into three domains: the cell soma, containing the nucleus and most of its organelles, the dendritic arbor, that can be especially dense in the case of dopaminergic neurons, and the axon, that plays a key role in the synapsis. Both axons and dendrites require long-range transport of vesicles and

organelles, including mitochondria, which in mammals is mainly accomplished though their interaction with the microtubule-based motor proteins kinesin and dynein. In fact, axons can extend for millimeters, centimeters and even up to a meter in the case of human peripheral nerves and cortico-spinal tracts, so neurons represent an extreme case to provide energy into far-reaching points of the cell. Like in other cell types, nearly all neuronal proteins are encoded by nuclear genes, no matter how far that nucleus may be from the protein's site of action. The trafficking machinery is therefore so important in neurons that dysfunctions in the proteins involved in this process that barely have impact in other cells often lead to degeneration in neurons (Baloh, 2008; De Vos, Grierson, Ackerley, & Miller, 2008).

In neurons, the points with highest energy consumption are usually located at the synapses. When a single presynaptic vesicle is released, from hundreds to more than a thousand ion channels at the postsynaptic terminal are opened, allowing millions of ions to enter the cell. This influx requires hydrolyzing a similar amount of ATP molecules in order to pump-back the ions and restore the membrane potential. Because hundreds of synapses can work simultaneously, the number of ATP molecules required can rise to up to several billions (Zhu et al., 2012) and such high requirements can only be matched by placing the "energy generators" at the points where energy is required. Nevertheless, although synapses are crucial for the function of the neuron, they are not the only regions with high energy demands. High levels of ATP are also required at the beginning of the axon, at the growth cones and at the nodes of Ranvier (Sheng & Cai, 2012), the transport machinery of mitochondria itself as well as presynaptic vesicles and other components is energy demanding and neurons, as any other cell type, must fulfill their basal energy requirements. Because energy requirements and calcium buffering needs are constantly varying along time, mitochondrial trafficking and positioning must always be fine-tuned regulated.

In contrast to much of the vesicle trafficking, mitochondrial transport is not one-directional. In order to maintain a functional population of mitochondria, there must be a constant turnover throughout the neuron. That involves retrograde transport of mitochondria to degrade the older, damaged components and synthetize new ones, which usually takes place at the soma and will require anterograde transport to reach distal points within the neuron. However, despite the theoretical assumption it is still controversial whether the anterograde trafficking corresponds to freshly synthesized mitochondria and the retrograde transport to the old, damaged ones (Miller & Sheetz, 2004; Verburg & Hollenbeck, 2008).

The fraction of moving mitochondria depends on the physiological stage of the neuron, but under normal conditions it ranges between 20 and 40%, half of them moving to the tips of the neurites (anterograde) and the other half moving towards the neuronal soma (retrograde)

(Hollenbeck & Saxton, 2005; Misgeld, Kerschensteiner, Bareyre, Burgess, & Lichtman, 2007; Russo et al., 2009). The remaining mitochondria are usually held in place by anchoring proteins and comprise the "stationary pool". Syntaphilin is an example of an outer mitochondrial membrane-embedded protein that tethers mitochondria to the microtubule network (Kang et al., 2008), although mitochondria can also anchor to actin cytoskeleton fibers (Pathak, Sepp, & Hollenbeck, 2010).

1.2. Mitochondrial dynamics

Despite the retrograde transport is responsible of much of the mitochondrial turnover, a single mitochondrion located at far-reaching points within the neurites does not need to be carried back to the soma to renew its components. The mechanisms of fusion and fission between mitochondria allow the exchange of proteins and the renewal of their components even when they take place for short periods of time (Amiri & Hollenbeck, 2008). Mitochondrial dynamics play an important role in the renewal and maintenance of stationary mitochondria. The fraction of motile mitochondria often fuses with those that remain static, so the mechanisms involved in fusion and fission are likely coupled to mitochondrial trafficking (Amiri & Hollenbeck, 2008).

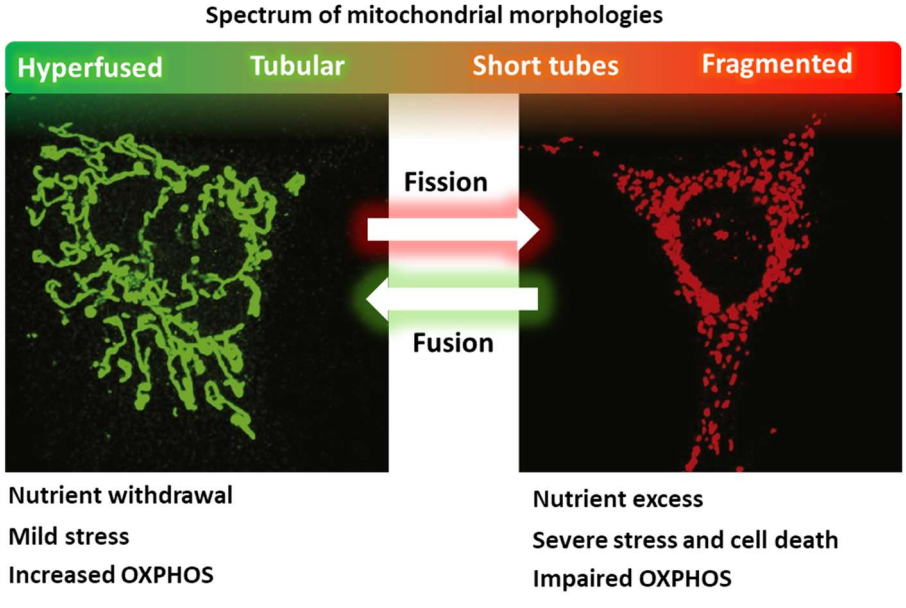

Figure I 3 Metabolic inputs modulate mitochondrial morphology. The morphology of mitochondria can vary significantly over a wide range and is influenced by metabolic stimuli to adopt a hyperfused (left) or fragmented (right) morphology. Pictures represent different mitochondrial morphologies of MEF cells expressing either mito-GFP (green) or mtDsRed (red). Adapted from Wai and Langer, 2016.

Mitochondria usually localize in the soma as interconnected networks that must undergo fission events to be transported to the neurites, where they are usually found as discontinuous entities.

Similarly, fission must occur before cell division to ensure the proper segregation of mitochondria between the daughter cells. The balance of fission and fusion is therefore of foremost importance and is often regulated by oxidative stress and nutrient availability (Wai & Langer, 2016).

1.2.1. Drp1 promotes mitochondrial fission

Mitochondrial fission requires a coordinated function of many factors. It usually occurs at ER-mitochondria contact sites (Friedman et al., 2011) and involves actin polymerization to constrict mitochondria and set the environment for further stages in the division. The main and probably the best-regulated step is the translocation of the dynamin-like GTPase Drp1 from the cytosol to the outer mitochondrial membrane. After translocation, Drp1 self-assembles into ring-like structures that wrap mitochondria at the sites of division. Consecutive cycles of GTP binding and hydrolysis induce conformational changes that result in the ring assembly and promote mitochondrial constriction and scission (van der Bliek, Shen, & Kawajiri, 2013; Xie et al., 2018).

The presence of Drp1 receptors at the OMM facilitates its recruitment to the mitochondria. Among the best characterized receptors stand out MFF, Fis1, MiD49, and MiD51, which exert cooperative but independent functions to promote mitochondrial fission (Labbé, Murley, & Nunnari, 2014). MiD49/51 mediate cristae remodeling during apoptosis and recruit Drp1 in a similar manner as MFF (Osellame et al., 2016), whereas the latest reports point to a complementary role of Fis1 regulating the components of the fission machinery rather than recruiting Drp1 by direct binding (Yu, Jin, Lendahl, Nistér, & Zhao, 2019).

Both Drp1 and its receptors are post-translational modified to regulate their functions in response to cellular needs. For example, Drp1 activity can be enhanced upon Ser616 phosphorylation by many kinases, including Cdk1, Cdk5, CaMII and MAPK. Under normal conditions, Drp1 promotes mitochondrial division to favor segregation during mitosis. However, this phosphorylation has also been associated with neuronal death and tumor growth (Taguchi, Ishihara, Jofuku, Oka, & Mihara, 2007; Xie et al., 2018). Conversely, Ser637 phosphorylation by PKA inhibits Drp1 activity (Chang & Blackstone, 2007), whilst its dephosphorylation by calcineurin enhances its recruitment to the mitochondria (Cribbs & Strack, 2007). In this regard, phosphorylation of MFF by AMPK also promotes Drp1 translocation into mitochondria, thus favoring fission (Toyama et al., 2016).

Besides phosphorylation, Drp1 can be modified by SUMO proteins with different outcomes. SUMOylation by SUMO1 stabilizes Drp1 at the mitochondria and favors fission during apoptosis (Harder, Zunino, & McBride, 2004; Prudent et al., 2015; Wasiak, Zunino, & McBride, 2007), whereas SUMO2/3 reduces its affinity towards MFF, thus promoting mitochondrial fusion. SUMO2/3 can be removed by SENP3 to re-favor fission (Guo, Wilkinson, Evans, Rubin, & Henley, 2017). Further, degradation of Drp1 or its receptor MiD49 after ubiquitination reduces

mitochondrial division and promotes fusion (Cherok et al., 2017; Horn et al., 2011; Wang et al., 2011).

1.2.2. Mitofusins mediate fusion of the outer mitochondrial membrane

The gene encoding the protein that mediates mitochondrial fusion was first described in Drosophila mutants. Male mutants for this gene were sterile and exhibited fuzzy onion like fragmented mitochondria in post-meiotic spermatids (Hales & Fuller, 1997; Hermann et al., 1998). Consequently, the protein involved in this phenotype and subsequently found to mediate mitochondrial fusion was named fuzzy onion (Fzo) (Fritz, Rapaport, Klanner, Neupert, & Westermann, 2001).

The Drosophila and yeast Fzo have two homologues in mammals known as mitofusin 1 (Mfn1) and mitofusin 2 (Mfn2). Both are dynamin-like GTPases and mediate fusion of the outer mitochondrial membrane. Besides their N-terminal GTPase domain, both mitofusins contain in their structure two C-terminal heptad repeat (HR1 and HR2) domains that surround a transmembrane region and are essential for the fusion events. The four stages that lead to mitochondrial fusion require the presence of many regulatory proteins. (Cohen & Tareste, 2018). Those stages comprise:

1. Recognition and docking
2. Membrane approach and deformation
3. Membrane destabilization and merging
4. Formation of the fusion pore, that merges both intermembrane spaces

Mitofusins bind together the outer mitochondrial membranes of adjacent mitochondria by homotypic (Mfn1-Mfn1 and Mfn2-Mfn2) or heterotypic (Mfn1-Mfn2) oligomerization within the same membrane (cis oligomerization) and across two opposing membranes (trans oligomerization) (Fritz *et al.*, 2001; Ishihara, Eura and Mihara, 2004; Koshiba *et al.*, 2004). By analogy with the SNARE mediated fusion of vesicles, mitofusins form trans-oligomers using their C-terminal coiled-coil domains to tether outer mitochondrial membranes of adjacent mitochondria, and after completion of the fusion process the trans-oligomers disassemble to a steady-state process that precedes the formation of cis-oligomers (Koshiba et al., 2004). Most conformational changes in Mfn that promote the tethering process are mediated by GTP binding and hydrolysis within its GTPase domains (Ishihara, Eura and Mihara, 2004).

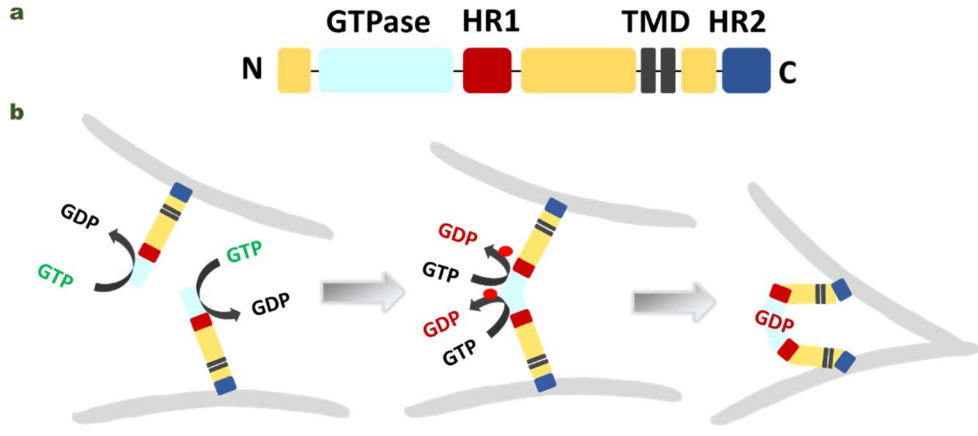

Figure I 4 Structure and hypothetical mode of action of mitofusins in mitochondrial fusion
a, Mitofusins include an N-terminal GTPase domain (light-blue) and two C-terminal heptad repeat domains, HR1 (red) and HR2 (dark-blue), that sandwich a transmembrane domain (black) **b,** Mitofusin molecules may dimerize across outer mitochondrial membranes upon GTP binding, which leads to long-distance (~20 nm) docking of mitochondria. GTP hydrolysis may then induce a conformational rearrangement of mitofusin, through either a "scissor-like" or a "self-folding" mechanism, which brings outer mitochondrial membranes in closer proximity (short-distance docking). These two docking states may be further stabilized by the formation of a ring of trans-mitofusin complexes (not depicted here) at the periphery of the contact zone between mitochondria. Short-distance docking may also be reinforced by the formation of antiparallel trans-HR2 dimers (not shown for clarity). Mitochondrial fusion may proceed as a result of local membrane deformation near the TMD when mitofusin undergoes its GTP hydrolysis-dependent conformational transition and membrane structure perturbation by the HR1 domain. Adapted from Cohen and Tareste, 2018.

Mfn1 and Mfn2 are 741 and 757 amino acids long, respectively. Both share 60% sequence identity and 63% homology and possess the same functional domains (Santel & Fuller, 2001; Yu et al., 2018). Although they are essential for fusion and maintenance of mitochondrial morphology, neither their functions nor their expression patters are overlapped. Mfn1 is predominantly expressed in testes, whereas Mfn2 is abundant in heart, skeletal muscle and brain (Sack, 2011; Santel et al., 2003). Mfn1 is more efficient inducing mitochondrial tethering and plays a more dominant role in fusion than Mfn2, probably due to its 8-fold higher ATPase activity that allows rapid conformational changes (Ishihara, Eura and Mihara, 2004). Together with Mfn2, it mediates the formation of ER-mitochondria contact sites through formation of homotypic or heterotypic complexes that bridge both organelles. Those contacts are especially important for the formation of mitochondrial permeability transition pore (MTPP) that allows calcium flux and regulates apoptosis (de Brito & Scorrano, 2008, 2009). Additional functions of mitofusins include metabolism regulation, ROS generation and mitochondrial transport. In this regard, Mfn2 can interact with Miro proteins to regulate mitochondrial motility in axons, which will be further explained later on (Misko, Jiang, Wegorzewska, Milbrandt, & Baloh, 2010).

1.2.3. Opa1 mediates fusion of the inner mitochondrial membrane

The first mitochondrial dynamin was identified in yeast: mutations of the Mgm1 gene caused deficient mitochondrial DNA distribution during division (Jones & Fangman, 1992). It was later found that such phenotype was a secondary effect of deficient fusion of the inner mitochondrial membrane, where Mgm1 localized (Wong et al., 2000). The human homologue was discovered through genetic mapping of an ocular neurodegenerative disease known as dominant optic atrophy and consequently named Opa1 (optic atrophy 1) (Alexander et al., 2000; Delettre et al., 2000).

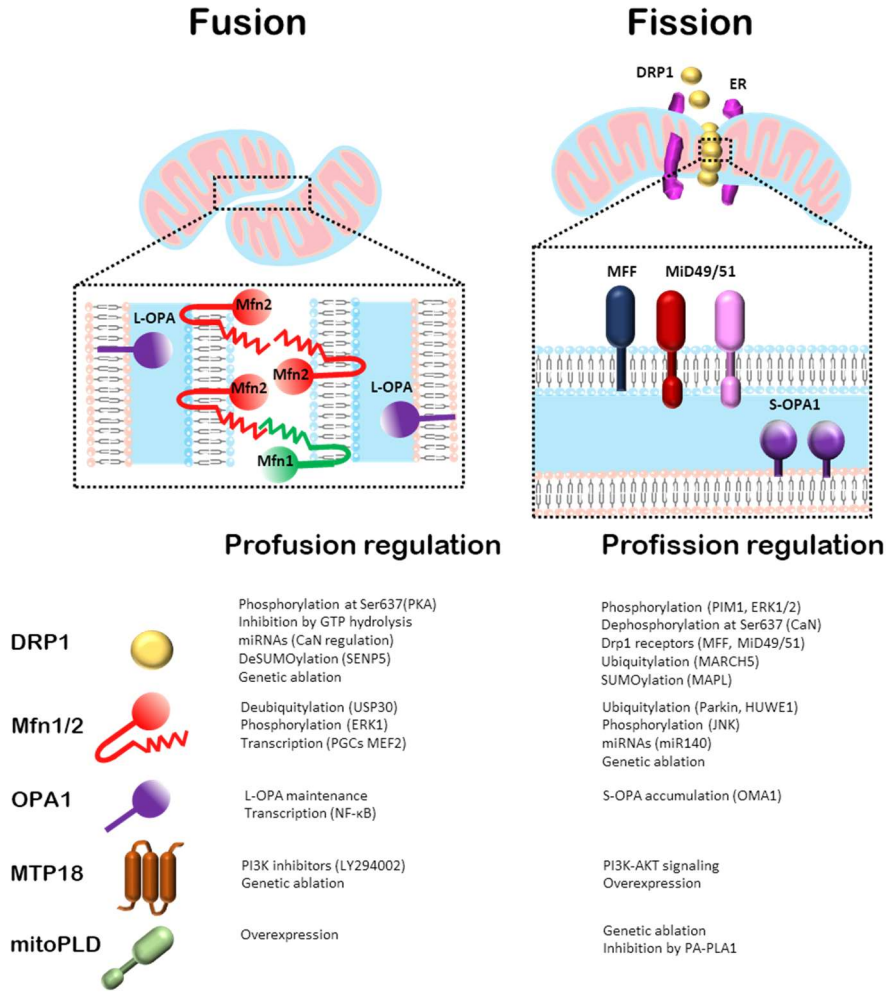

Figure I 5 Regulation of mitochondrial fusion and fission. Mitochondrial fusion is mediated by homo- and heterotypic interactions between Mfn1 and Mfn2 (red) at the outer mitochondrial membrane and L-Opa1 (purple) at the inner mitochondrial membrane. MitoPLD (green) is required for OM fusion. Receptor-mediated recruitment of Dynamin-related protein 1 (DRP1; yellow) from the cytosol to the OM by MFF and MiD49/51 to sites of division marked by endoplasmic reticulum (ER, pink) drives mitochondrial fission. IM fission machinery is unknown. Transcriptional, translational, and post-translational regulation of DRP1, mitofusin 1/2, Optic atrophy 1, MitoPLD, and MTP18 function promote either fusion (lower left) or fission (lower right) Adapted from Wai and Langer, 2016.

Opa1 locates at the inner mitochondrial membrane with the bulk of the protein exposed to the intermembrane space (Olichon et al., 2002; Wong et al., 2000). In lower eukaryotes, Mgm1 is cleaved by the rhomboid protease Pcp1 leaving short (s-Opa1) and long (l-Opa1) forms. The ratio of each form will determine the inner mitochondrial fusion depending on energy availability (Esser, Tursun, Ingenhoven, Michaelis, & Pratje, 2002; Herlan, Bornhövd, Hell, Neupert, & Reichert, 2004; Herlan, Vogel, Bornhovd, Neupert, & Reichert, 2003; Sesaki, Southard, Hobbs, & Jensen, 2003). Mammals have 8 Opa1 isoforms that differ in the presence or absence of short exons at their N-terminal region (Olichon et al., 2007). Those exons determine the presence of up to 3 different cleavage sites. Two of those sites are present in around 50% of Opa1 isoforms and are usually cleaved by the protease Yme1L, leaving similar amounts of l-Opa and s-Opa at the inner membrane (Griparic, Kanazawa, & van der Bliek, 2007; Song, Chen, Fiket, Alexander, & Chan, 2007). A third cleavage site present in all isoforms is recognized by the metalloprotease Oma1 under stress conditions, such as low levels of ATP, mitochondrial damage or loss of mitochondrial membrane potential (Ehses et al., 2009; Head, Griparic, Amiri, Gandre-Babbe, & van der Bliek, 2009). This cleavage produces important changes in cristae structure and results in decreased mitochondrial fusion rates previous to activation of the PINK1-Parkin pathway. The importance of the relative amounts of cleaved and uncleaved forms of Opa1 for fusion of the inner mitochondrial membrane is still unknown.

Given the complexity of matching energy demands to energy requirements while keeping mitochondrial functionality at any time, it is not surprising that mitochondrial transport machinery must be regulated by a myriad of signals and associated proteins. The core of this complex is composed of the kinesin and dynein microtubule-associated motor proteins, the mitochondria-anchored GTPase Miro1 and the motor adaptors TRAK1 and TRAK2 that couple the mitochondria to the motor proteins. Here we will have an insight at mechanisms used for the transport and their main components.

1.3. Transport across microtubules

Neuronal microtubules are key determinants of cell morphology, differentiation, migration and polarity, and constitute the rails of kinesin and dynein motors to promote intracellular trafficking along axons and dendrites (Calogero, Mazzetti, Pezzoli, & Cappelletti, 2019). Microtubule polymers are composed of α and β subunits bound in a head-to-tail manner, a feature that gives rise to microtubule polarity, reflected as a plus and minus ends (Melkov & Abdu, 2018).

In neurons, as in many other cell types, microtubule nucleation occurs at the perinuclear region in a multiproteic structures known as centrosomes. Nucleation is promoted by γ-tubulin, a homologue of α and β subunits that is usually found as part of the γ-tubulin ring complexes

(γTuRC). γ-tubulin is thus not incorporated into the growing filament, but rather serves as a template to begin polymerization. As such, centrosomes function as microtubule organizing centers (MTOC) where the minus end is stabilized by the γTuRC and the plus end extends towards the neurites, resulting in a polarized organization. Microtubule plus ends can undergo rapid polymerization and depolarization events, a phenomenon known as microtubule instability that allows quick adaptations to neurite morphology induced by a wide range of signals.

Axonal microtubules organize in a polar array with the plus end towards the tip of the axon and the minus end towards the soma, whereas in dendrites the polarity is mixed (Hirokawa & Takemura, 2004; Matamoros & Baas, 2016). Nevertheless, lower eukaryotes like *Drosophila* and *C. elegans* display a uniform polarity in dendritic microtubules, so many studies have taken advantage of those models to evaluate dendritic transport (Melkov & Abdu, 2018).

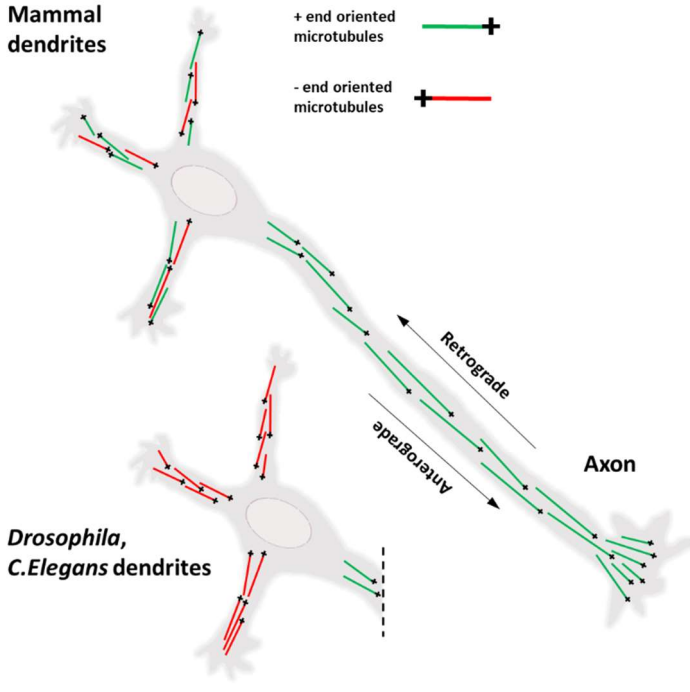

Figure I 6 Microtubule organization in mammalian, *drosophila* and *c. elegans* neurons. Axonal microtubules display a centrosomal array oriented with the plus-ends out (i.e., away from soma). However, whereas mammalian dendrites exhibit mixed MT polarity, in *Drosophila* and *C. elegans*, the dendritic microtubule network is uniformly oriented with the minus ends pointed distally. Adapted from Melkov and Abdu, 2018.

1.3.1. Kinesins, the main mediators of anterograde transport

Microtubule polarity in axons determines the directionality of the associated motor proteins: while kinesins carry most of the anterograde transport (toward the plus end), the dynein-dynactin complex mediate the retrograde transport (toward the soma) (Cai & Sheng, 2009; Pilling,

Horiuchi, Lively, & Saxton, 2006). In dendrites, however, kinesins and dyneins can drive anterograde or retrograde transport depending on the polarity.

The members of the kinesin-1 superfamily were the first identified microtubule-based motors to mediate anterograde transport in vitro (Hirokawa et al., 1991; Vale, Reese, & Sheetz, 1985). Kinesin-1 is composed of 2 light chains (KLCs) and 2 heavy chains (KHCs), known as Kif5, that can use a coiled-coil domain located at their stalking region to form homo- or heterodimers. Dimeric Kif5 heavy chains can interact with the light chains, with adaptor proteins or directly with the cargoes through their C-terminal domain, whereas the N-terminus has ATPase activity and binds to microtubules. To date three isoforms of kinesin-1 have been described, known as Kif5A, Kif5B and Kif5C. Kif5B was the first to be described and is ubiquitously expressed, whereas Kif5A and Kif5C are mostly expressed in neurons.

Kif5A and Kif5B show similar cargo-binding regions and are reported to drive the anterograde transport of synaptic vesicle precursors (Aizawa et al., 1992; Okada, Yamazaki, Aizawa, & Hirokawa, 1995; Yonekawa et al., 1998). Mutations on Kif5B have been related to Charcot-Marie-Tooth disease type 2A, a human peripheral neuropathy (Tanaka & Hirokawa, 2002; Chunjie Zhao et al., 2001). In axons, Kif5 proteins mediate the transport of vesicles containing amyloid precursor protein (APP) and β-secretase, which yields the formation of amyloid-β peptide and whose accumulation is the main source of neurodegeneration in Alzheimer's disease (AD) (Kamal, Stokin, Yang, Xia, & Goldstein, 2000).

In dendrites, kinesins are especially important to transport many receptors involved in the synapsis, as is the case for glutamate, NMDA and AMPA receptors (Guillaud, Setou, & Hirokawa, 2003; Setou et al., 2002). Other cargoes transported by kinesins include mRNAs (Kanai, Dohmae, & Hirokawa, 2004) and multivesicular body-like organelles (Saito et al., 1997).

Aside of receptors, neurotransmitters and nucleic acids, the Kif5 family constitutes the major mediator of the anterograde transport of mitochondria. Early reports point to a perinuclear clustering of mitochondria in cells lacking Kif5B (Tanaka et al., 1998) as well reduced mitochondrial transport and distribution in *Drosophila* larval motor axons depleted of Kif5 (Hurd & Saxton, 1996). Subsequent studies showed that loss of kinesin function also impairs mitochondrial trafficking in hippocampal axons (Cai, Gerwin, & Sheng, 2005) and dendrites (MacAskill, Rinholm, et al., 2009)

In addition to Kif5, Kif1Bα (a member of the Kinesin 3 family) can also interact and transport mitochondria along microtubules, and its mutation leads to neuropathies in mice (Nangaku et al., 1994). Whether anterograde mitochondrial transport is kinesin-specific or there is overlapping of function among different members is still under debate.

1.3.2. Dynein-dynactin as drivers of retrograde transport

Dynein motors are force-generating ATPases that move along eukaryotic microtubules. They were first discovered as the motors that drive flagellar beating in *Tetrahymena pyriformis* (Gibbons & Rowe, 1965). Later, two different isoforms -dynein 1 and dynein 2- were described to be responsible for cytoplasmic transport and cilia movement, respectively (Paschal & Vallee, 1987; Pazour, Dickert, & Witman, 1999; Porter, Bower, Knott, Byrd, & Dentler, 1999). Although most dyneins belong to the axonemal class and regulate flagellar and cilliar movement, a highly conserved cytoplasmic class of dyneins act as minus-end-directed motors in processes like vesicle transport, organelle positioning, chromosome segregation and mitotic spindle organization.

Dyneins are not homologous to kinesins or myosins, but rather a part of the broad ATPase associated with various cellular activities. They have both a very different structure and mode of action to that of kinesins. Whereas the kinesin motor domain is relatively small (around 400 amino acids) and globular, the dynein motor region is larger (around 3000 amino acids) and forms a ring of six AAA+ modules, the first of which is the site of ATPase activity (Kon, Nishiura, Ohkura, Toyoshima, & Sutoh, 2004; Wickstead & Gull, 2007)

Dynein is a 1.4 MDa protein complex formed by 2 dynein heavy chains (DHCs) associated to several dynein intermediate chains (DICs), dynein light intermediate chains (DLICs) and dynein light chains (DLCs) (Holzbaur & Vallee, 1994; Karki & Holzbaur, 1999). The DHC is 4634 amino acids long and contains a dimerization domain at the N-terminus, followed by a series of 9 helical bundles. The last bundle binds the motor domain at the C-terminus, which contains linker, a ring of 6 AAA+ domains and a microtubule binding domain (Kon et al., 2012; Schmidt, Gleave, & Carter, 2012). The motile force is generated by coupling ATP-induced conformational changes in the AAA+ ring with bending and straightening of the linker (Schmidt, Zalyte, Urnavicius, & Carter, 2015).

Dynein complex by itself is barely active in vitro (Trokter, Mücke, & Surrey, 2012) but can be enhanced by binding to a multi-protein cofactor called dynactin. The dynactin complex has 1.1 MDa and forms a filament with 8 copies of actin-related protein α-centractin (ARP1) and 1 copy of β-actin. This filament is capped by CAPZ at the barbed end and ARP11 at the pointed end. Along with ARP11, p25, p27 and p62 constitute the pointed-end complex. Close to the barbed end locates a shoulder domain, composed of the dimmer p150Glued, 4 copies of p50 dynamitin and 2 copies of p24. p150Glued is the main component of dynactin, and has its C-terminus buried in the shoulder, whereas the N-terminus contains 2 coiled-coil domains separated by a globular

region. The most distal N-terminal part contains the CAP-gly and basic domains involved in microtubule binding (Waterman-Storer, Karki, & Holzbaur, 1995).

When recruited to dynactin, DHC binds in grooves between dynactin filaments and induces the alignment of dynein motor domains allowing it to bind microtubules (Urnavicius et al., 2018, 2015). Nevertheless, this recruitment requires the presence of activating factors, which are also involved in cargo binding. So far, 8 activating factors have been described to enhance the formation of dynein-dynactin complex and promote long distance movement on microtubules in vitro. They include BICD2, BICDL1 and SPDL1 (McKenney et al., 2014; Schlager et al., 2014) as well as HOOK1, HOOK3, NIN, NINL and RAB11FIP3 (Olenick et al., 2016; Schroeder and Vale, 2016).

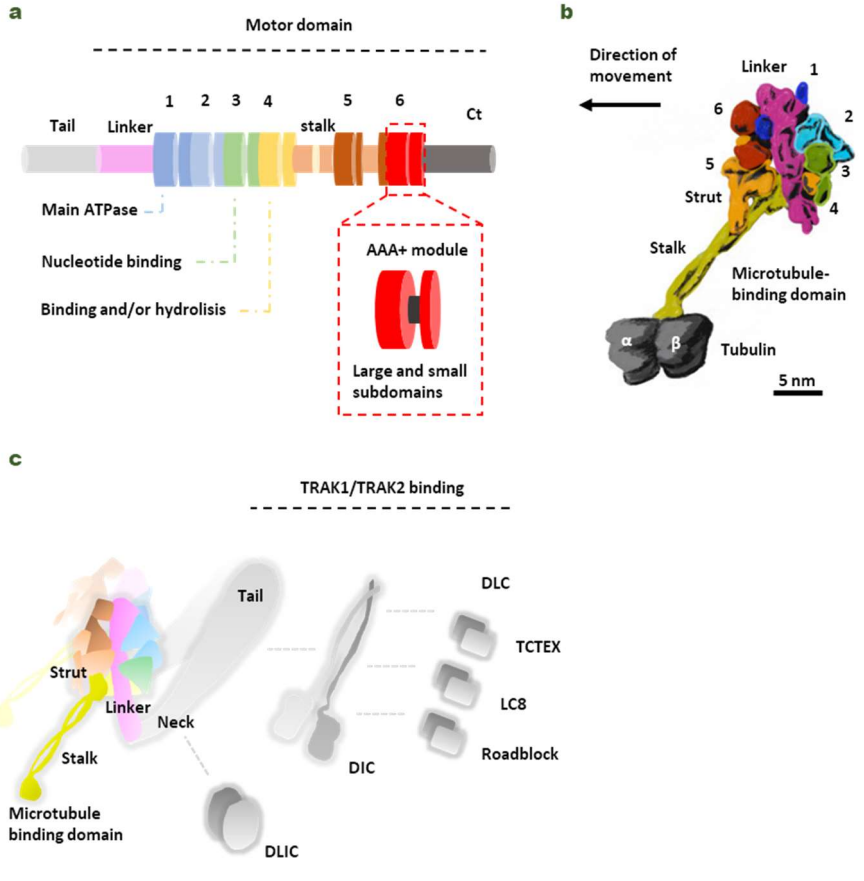

Figure I 7 Overview of dynein structure. a, Linear representation of domains within the dynein heavy chain. The amino-terminal tail domain is involved in dynein oligomerization, cargo-binding and regulation, but is not part of the minimal motor domain capable of producing movement in vitro. The motor domain (~380 kDa) comprises the linker domain, six AAA+ modules (1–6), the coiled-coil stalk and strut, and the C-terminal region (~330 kDa). Each of the AAA+ modules is composed of a large N-terminal subdomain and a smaller C-terminal subdomain. **b,** A 3D model of the cytoplasmic dynein motor domain bound to the microtubule. This model is based on a 2.8 Å crystal structure of the *D. discoideum* dynein motor domain lacking the microtubule-binding domain (Protein Data Bank ID: 3VKG), joined to a cryo-electron microscopy-derived model of the mouse microtubule-binding domain bound to an α-tubulin–β-tubulin dimer (Protein Data Bank ID: 3J1T). Subdomains are shown in surface representation, with the two long α-helices in the stalk rendered separately to emphasize their coiled-coil arrangement. The six AAA+ modules are numerically labelled. **c.** The cytoplasmic

dynein complex contains two identical heavy chains. Within each heavy chain, the six AAA+ modules fold into a ring. The stalk protrudes as an extension from subdomain 4. The tail is connected to domain 1 by the linker domain. The cytoplasmic dynein heavy chains assemble with up to five types of associated subunits. They comprise the intermediate chain, the light-intermediate chain and three classes of light chain: TCTEX, LC8 and Roadblock. Dashed lines indicate reported interactions of the associated subunits with each other and with the tail. Adapted from Roberts et. al. 2013.

		Subunit	Organism	Cell type	Mobility	References
Axon	Kinesin	KHC	*Drosophila*	Motor neuron	↓ anterograde and retrograde	(Pilling, Horiuchi, Lively, & Saxton, 2006)
		KHC	*Drosophila*	Dorsal cluster	↓ distribution	(Satoh, Li, Xia, & Ready, 2008; Satoh et al., 2008)
		KHC	*Drosophila*	Wing nerve	↓ anterograde and retrograde	(Vagnoni, Hoffmann, & Bullock, 2016)
		KHC	Mouse	Embryonic motor neuron	No defects	(Karle, Möckel, Reid, & Schöls, 2012)
		KHC	Rat	Hippocampal neuron	↓ distribution ↓ anterograde and retrograde	(Cai et al., 2005)
		KHC	Rat	Hippocampal neuron	↓ anterograde and retrograde	(van Spronsen et al., 2013)
		KHC	Zebrafish	Peripheral sensory neuron	↓ distribution	(Campbell et al., 2014)
		KHC	Zebrafish	Retinal ganglion	↓ distribution ↑retrograde	(Auer et al., 2015)
		KHC	*C.Elegans*	PHC sensory neuron	↓ distribution Absent movement	(Rawson et al., 2014; Yan et al., 2013)
	Dynein	DHC	*Drosophila*	Motor neuron	↓ retrograde	(Pilling et al., 2006)
		DHC	*Drosophila*	Wing nerve	↓ anterograde and retrograde	(Vagnoni et al., 2016)
	Dynactin	Glued	*Drosophila*	Motor neuron	No defects	(Pilling et al., 2006)
		Arp	*Drosophila*	Larval segmental nerve	↓ anterograde and retrograde	(Haghnia et al., 2007)
		p150	Mammals	Hippocampal neuron	↓ anterograde and retrograde	(van Spronsen et al., 2013)
		Actr10	Zebrafish	Peripheral sensory neuron	↓ retrograde	(Drerup, Herbert, Monk, & Nechiporuk, 2017)
		p150	Zebrafish	Peripheral sensory neuron	↓ anterograde and retrograde	(Drerup et al., 2017)
Dendrites	Kinesin	KHC	*Drosophila*	Dorsal cluster	No effects	(Satoh et al., 2008; Satoh et al., 2008)
		KHC	*C.Elegans*	PHC sensory neuron	Absent movement	(Yan et al., 2013)
		KHC	Rat	Hippocampal neuron	No defects	(van Spronsen et al., 2013)
	Dynein	Dlic	*Drosophila*	Dorsal cluster	↓ distribution	(Satoh et al., 2008; Satoh et al., 2008)
	Dynactin	p150	Rat	Hippocampal neuron	↓ anterograde and retrograde	(van Spronsen et al., 2013)

Table I 1 Roles of motor proteins on neuronal mitochondrial transport. Adapted from Melkov and Abdu 2017.

Although they do not share common sequence motifs, all them have a long coiled-coil domain that binds the C-terminal region of DLIC and a binding site for other proteins, including RAB6 and RAB11, that link adaptors to their cargoes (Schroeder, Ostrem, Hertz, & Vale, 2014).

In addition to the classical activating adaptors, a number of proteins with long coiled-coil domains and binding regions to DLIC are considered putative activating adaptors. Among them can be found the trafficking kinesin-binding proteins (TRAK1 and TRAK2) and the huntingtin-interacting protein 1 (HAP1) (Gama et al., 2017). Other proteins with shorter coiled-coil domains can also mediate the interaction between dynein-dynactin complex and cargo but with much lower activating capacity. Examples of them are the RAB-interacting lysosomal protein (RILP) (Jordens et al., 2001) and the c-Jun-N-terminal kinase interacting protein 3 (JIP3) (Cavalli, Kujala, Klumperman, & Goldstein, 2005).

1.4. TRAK1 and TRAK2 couple mitochondria to kinesin and dynein motor proteins.

The adaptor protein that couples mitochondria to kinesin was first identified in a screening of *Drosophila* mutants. Axonal terminals at photoreceptors of those mutants were devoid of mitochondria, but that did not affect the overall transport of vesicles. (Stowers, Megeath, Górska-Andrzejak, Meinertzhagen, & Schwarz, 2002). Because mutant flies were blind, the protein causing that phenotype was called milton in reference to the blind poet John Milton.

Milton co-fractionates with mitochondria, changes mitochondrial distribution when overexpressed in COS cells and interacts directly with the cargo-binding region of KHC (Glater, Megeath, Stowers, & Schwarz, 2006; Stowers et al., 2002). Surprisingly, Milton interacts with the same mitochondrial region than KLC, which is not detected in the trafficking complex and is dispensable for the transport of mitochondria in *Drosophila* photoreceptors (Glater et al., 2006). A feasible explanation is that Milton can replace KLC as the linker between motor and cargo for the transport of mitochondria. However, it is still unclear whether mammalian Milton isoforms are required to connect mitochondria to kinesin and dynein or they act as regulatory factors instead.

Mammals have two Milton isoforms. γ-Aminobutyric acid type A (GABAA) receptor interacting factor-1 (GRIF-1) was originally found in a yeast-two-hybrid screen aiming to find the elusive GABAA receptor clustering protein (Beck et al., 2002). GRIF-1 binds Kir2.1 K^+ channel (Grishin, Li, Levitan, & Zaks-Makhina, 2006) and regulates endosomal-to-lysosomal vesicle transport by interacting with the endosomal protein Hrs (Kirk, Chin, & Li, 2006). Subsequent studies established that GRIF-1, currently known as trafficking kinesin protein 2 (TRAK2), is a member of the TRAK family of kinesin adaptor proteins. TRAK2 shares around 48% amino acid sequence with O-linked N-acetylglucosamine transferase interacting protein 106 (OIP106), also known as TRAK1. Both bind to Miro GTPases at the outer mitochondrial membrane and contain a long predicted coiled-coil domain that allows their interaction with kinesin and dynein motor proteins (Brickley, Smith, Beck, & Stephenson, 2005). Their coiled-coil domains include a region of

homology with Huntingtin-associated protein 1 (HAP1), a molecular adaptor involved in organelle trafficking (Gauthier et al., 2004). In mature hippocampal neurons, TRAK1 preferentially localizes and regulates mitochondrial transport in axons, whereas TRAK2 mainly localizes and mediates mitochondrial trafficking in dendrites (van Spronsen et al., 2013). The binding affinities of TRAK adaptors for motor proteins are also different, showing TRAK1 equal affinity for kinesin and dynein but TRAK2 with stronger affinity for dynein. Such different localizations and affinities could facilitate differential transport of mitochondria into different compartments of the neuron. In cortical neurons, however, TRAK2 is equally distributed between axons and dendrites (Loss & Stephenson, 2015). TRAK proteins are therefore essential for mitochondrial motility and knocking-down these adaptors or expressing a dominant-negative mutant in hippocampal neurons impairs mitochondrial movement (Brickley et al., 2005).

	Protein	Cell type	Associated motor	Phenotype	Velocity	Reference
Axon	Milton	Photoreceptors/axons	KHC	Terminals lack mitochondria	?	(Górska-Andrzejak et al., 2003)
	Milton	Motor/sensory neurons	KHC	Absence of mitochondria	?	(Glater, Megeath, Stowers, & Schwarz, 2006)
	Milton	Wing axon	KHC	Absence of mitochondria	?	(Fang, Soares, Teng, Geary, & Bonini, 2012)
	Milton	Segmental nerves	KHC	↓retrograde movement	↓ R	(Yu et al., 2016)
	TRAK2	Hippocampal neurons	KIF5C	↓anterograde and retrograde movement	No effects	(Brickley & Stephenson, 2011)
	TRAK2	Hippocampal neurons	KIF5 dynein /dynactin /p150glued	No effect	?	(Brickley & Stephenson, 2011)
	TRAK2	Hippocampal neurons	?	↓ moving mitochondria at early stages	No effects	(van Spronsen et al., 2013)
	TRAK1	Hippocampal neurons	KIF5C	↓anterograde and retrograde movement	No effects	(van Spronsen et al., 2013)
	TRAK1	Hippocampal neurons	KIF5 dynein /dynactin /p150glued	↓ moving mitochondria	?	(Loss & Stephenson, 2017)
	TRAK1	Cortical/Hippocampal neurons	?	↓ moving mitochondria in neuronal development	No effects	(Loss & Stephenson, 2017)
Dendrites	TRAK2	Hippocampal neurons	KIF5 dynein /dynactin /p150glued	↓anterograde and retrograde movement	?	(van Spronsen et al., 2013)
	TRAK2	Pyramidal neurons	?	↓mitochondrial density	?	(van Spronsen et al., 2013)
	TRAK2	Cortical/Hippocampal neurons	?	↓ moving mitochondria in neuronal development	No effects	(Kimura & Murakami, 2014)
	TRAK1	Hippocampal neurons	KIF5 dynein /dynactin /p150glued	↓anterograde and retrograde movement	?	(Loss & Stephenson, 2017)
	TRAK1	Cortical/Hippocampal neurons	?	↓ moving mitochondria at early stages	No effects	(Loss & Stephenson, 2017)

Table I 2 Roles of Milton/TRAK motor adaptors on neuronal mitochondrial transport. ?= not tested/unknown, R= retrograde. Adapted from Melkov and Abdu 2017.

1.5. Additional adaptor proteins

Although TRAK proteins constitute the main mitochondrial adaptors for microtubule-based motor proteins, other adaptors have been proposed to bind mitochondria to kinesin and dynein motors. Among them stands the kinesin-binding protein "fasciculation and elongation protein ζ1"(FEZ1). FEZ1 is the human orthologue of the *caenorhabditis elegans* UNC-76, a brain-specific coiled-coil-containing protein involved in axonal outgrowth. UNC-76 was first identified by yeast-two-hybrid assay as a PKCζ-interacting protein (Kuroda, Nakagawa, Tokunaga, Tatematsu, & Tanizawa, 1999) and drives the anterograde transport of vesicles and organelles. Depletion of *Drosophila* UNC-76 halts mitochondrial movement similar to kinesin mutants (Gindhart et al., 2003).

1.51. FEZ-1

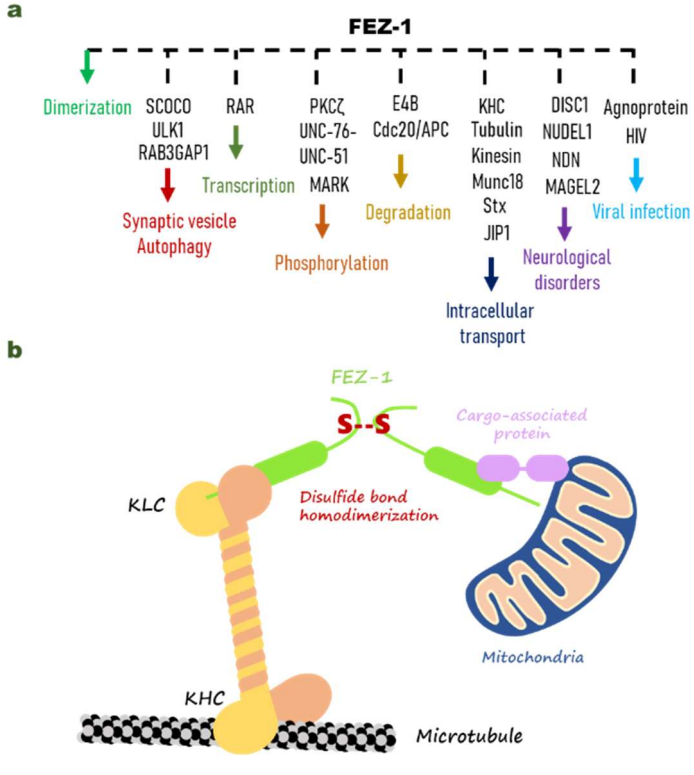

Figure I 8 FEZ1 and proteins reported to associate either by direct binding or by the presence in a protein complex. **a,** The function of the association is depicted in colors. **b,** Schematic representation of FEZ-1 associated with kinesin and mitochondria. DISC1: Disrupted-In-Schizophrenia 1; PKC: Protein kinase C; RAR: Retinoic acid receptor; HIV: Human immunodeficiency virus; NUDEL: Nuclear distribution element-like; NDN: Necdin; ULK1: UNC-51-like kinase; JIP1: c-Jun N-terminal kinase-interacting protein 1; Stx: Syntaxin 1a; MARK: Microtubule-affinity regulating kinase.KHC: Kinesin heavy chain; KLC: Kinesin light chain; FEZ-1: Fasciculation and elongation factor 1. Adapted from Teixeira, Alborghetti and Kobarg, 2019

FEZ-1 forms a dimer at the N-terminal region through a disulfide bond, leaving free the C-terminal region to interact with its many binding partners. FEZ-1 acts as a bridge between the kinesin and the mitochondria, but can also interact with KHC tail and cooperate with the c-Jun N-terminal kinase-interacting protein JIP1 to enhance kinesin motor activity, thus promoting mitochondrial transport (Blasius, Cai, Jih, Toret, & Verhey, 2007). Other FEZ-1 binding-proteins involved in neurodegenerative disorders include the Disrupted-in Schizophrenia 1 (DISC1), necdin (NDN) and MANGEL2, the last two inactivated in the Prader-Willi syndrome and predicted to relate with hypothalamic dysfunction (Teixeira, Alborghetti, & Kobarg, 2019). DISC1 association is essential to promote axonal outgrowth and anterograde mitochondrial transport (Kang et al., 2011), whereas necdin binds FEZ-1 at the centrosomes and prevents its proteosomal degradation (Lee et al., 2005). Overall, FEZ-1 represents an essential motor adaptor to ensure kinesin-mediated transport and axonal viability (Teixeira et al., 2019).

1.5.2. RanBP

The Ran-binding protein 2 (RanBP2), a protein localized at the cytoplasmic periphery of the nuclear pore complex, not only plays an important role regulating nucleocytoplasmic transport, but also drives the transport of the organelles thereof, including mitochondria (Cho, Yoon, Yu, Peachey, & Ferreira, 2019; Delphin, Guan, Melchior, & Gerace, 1997). RanBP2 selectively interacts with the cargo-binding region of Kif5B and Kif5C in the CNS (Cho et al., 2007). Through two of its four RanGTP-binding domains and its kinase binding domain, RanBP2 causes the unfolding, microtubule binding and biphasic activation of kinesin-1 in both neuronal and non-neuronal cells (Patil et al., 2013). It therefore represents another relevant component of the kinesin-mediated transport.

1.6. Miro1, an outer mitochondrial membrane-anchored GTPase that not only regulates mitochondrial movement.

TRAK proteins link mitochondria to kinesin and dynein by interacting with and regulating mitochondrial Rho GTPases. *Drosophila* Miro (dMiro) was first identified and has two mammalian orthologues, Miro1 and Miro2, which are 618 amino acids in length, share 60% sequence homology and are ubiquitously expressed (Fransson, Ruusala, & Aspenström, 2003). They have a unique structure with two GTPase domains flanking two calcium-binding EF hand domains and a C-terminal hydrophobic region embedded at the outer mitochondrial membrane (Nelson, Thulin, Fagan, Forsén, & Chazin, 2009). Their N-terminal GTPase domain shares significant homology to those of Rho GTPases, but due to the lack of G12 and Q61 residues it is probably unable to hydrolyze GTP (Fransson et al., 2003). Miro GTPases are present in many eukaryotes, including fungi and yeast. Gem1p, the only Miro orthologue in *s. cerevisiae*, is essential for cell growth, regulates mitochondrial morphology and distribution and is a component of the ER-

mitochondria encounter structure (ERMES) (Kornmann, Osman, & Walter, 2011; Murley et al., 2013), but unlike in higher eukaryotes does not play a significant role in mitochondrial transport (Frederick, McCaffery, Cunningham, Okamoto, & Shaw, 2004).

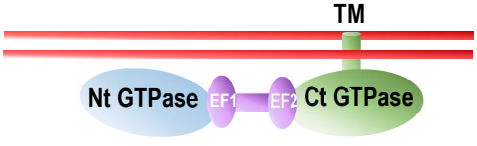

Figure I 9 Domain structure of Miro1. Miro1 contains 2 GTPase domains that are distantly related the Ras superfamily of small GTPases separated by a pair of EF calcium-binding domains. A short trans-membrane (TM) domain is located at the C-terminus anchors the protein to the outer mitochondrial membrane.

The relevance of Miro in mitochondrial transport was first demonstrated in a *Drosophila* screening, where dMiro mutants exhibited locomotion defects and died prematurely due to defective mitochondrial transport in axons and dendrites (Guo et al., 2005; Stowers, Megeath, Andrzejak, Meinertzhagen, & Schwarz, 2002). Miro1 KO mice die shortly after birth and neuron specific knockouts lack mitochondria in their axons and develop upper motor neuron diseases (Nguyen et al., 2014). Miro regulates both anterograde and retrograde transport in a calcium-dependent manner thanks to its EF hand domains (Russo et al., 2009). There are still some uncertainties about the molecular mechanisms by which Miro induces mitochondrial arrest, but the models proposed so far agree about mitochondria dissociating from the microtubules when cytosolic calcium levels are high enough (at micromolar levels) to bind the EF domains. (Chen & Sheng, 2013; Devine, Birsa, & Kittler, 2016; MacAskill, Rinholm, et al., 2009; Wang & Schwarz, 2009) Due to the versatility of its EF domains, Miro1/2 behaves as an intracellular calcium sensor to regulate mitochondrial shape in response to GPCR activation (Nemani et al., 2018). However, the link between calcium and Miro proteins goes beyond mitochondrial motility, as Miro1 interacts with and regulates mitochondrial calcium uniporter (MCU), the main promoter of mitochondrial calcium uptake. MCU not only allows mitochondria to restore cytoplasmic calcium levels after a synaptic outburst, but also fine-tune regulates mitochondrial metabolic activity and transport (Niescier et al., 2018). Expression of a calcium-insensitive Miro1 was sufficient to impair calcium uptake into the mitochondria, and pharmaceutical repression of MCU rescued mitochondrial motility at high Ca^{2+} concentrations, demonstrating that MCU and Miro1 can reciprocally modify their respective functions (Chang, Niescier, & Min, 2011).

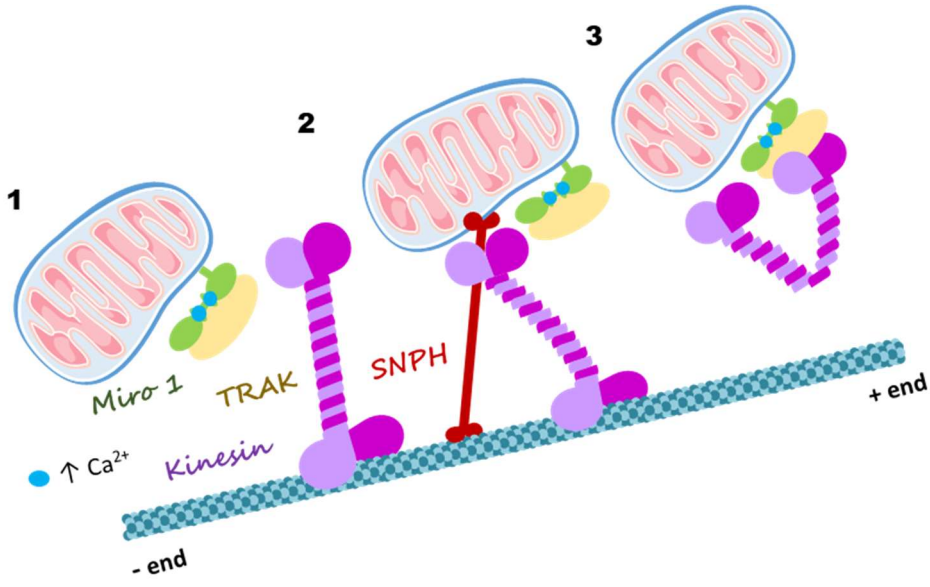

Fig I 10 Proposed models of calcium-dependent mitochondrial arrest. **1,** According to the first model proposed by Kittler's group, the binding of calcium into Miro's EF domains would inhibit Miro interaction with kinesin (MacAskill et al., 2009). **2,** Chen and Seng further improve the previous model, proposing that kinesin would interact with the axonal tethering protein syntaphilin (SNPH) upon calcium-induced uncoupling from Miro (Chen and Sheng, 2013). **3,** According to Wang and Schwartz's model, Miro switches between a calcium-free active state in which kinesin is bound to microtubules and a calcium-bound inactive state in which the motor domain of kinesin interacts with Miro, thereby dissociating from microtubules (Wang and Schwarz, 2009). Adapted from Devine, Birsa and Kittler, 2016

Although the action of Ca^{2+} on mitochondrial motility is well established, the molecular function of Miro's GTPase domains is not fully understood. A constitutive-active mutant for the N-terminal GTPase domain in Miro1 significantly decreases its ability to recruit TRAK2, thus altering mitochondrial distribution. In contrast, a C-terminal GTPase mutant shows no impact on mitochondrial localization (MacAskill, Brickley, Stephenson, & Kittler, 2009). Disruption of the N-terminal GTPase domain on *Drosophila* dMiro also affects kinesin and dynein-mediated mitochondrial movement producing accumulation of mitochondria at the soma, while alteration of the C-terminal GTPase domain selectively disrupts dynein-mediated retrograde transport (Babic et al., 2015). This suggest a putative role of Miro1 on mitochondrial signaling depending on its GTPase domains, whose activity would affect the coupling of downstream signaling partners that mediate mitochondrial motility.

Miro not only regulates intracellular mitochondrial movement, but also intercellular transport as shown with the transfer of mitochondria from mesenchymal stem cells to epithelial (Ahmad, et al., 2014) or neuronal cells (Babenko et al., 2018; Boukelmoune, Chiu, Kavelaars, & Heijnen, 2018). Besides, several studies indicate that Miro1 also mediates peroxisomal transport through its

interaction with Pex19 (Castro & Schrader, 2018), a role that would be supported by the peroxisomal localization of TRAK2 (Okumoto et al., 2018).

Besides its outstanding relevance for mitochondrial on transport, Miro1 is key in the regulation of mitochondrial fission and fusion processes. Miro proteins interact with mitofusins, the dynamin-related GTPases that mediate fusion of the OMM (Misko et al., 2010). Miro1 overexpression increases mitochondrial length in neurons, and this effect is enhanced by mutating the calcium-binding domain (Miro1ΔEF) or the N-terminal GTPase (Miro1 T18N) (Saotome et al., 2008). Such phenotype agrees with the role of EF1 domain mediating mitochondrial shape transition (Nemani et al., 2018). Mfn2-knockout neurons also show a reduction in the number of motile mitochondria and speed similar as the observed in Miro2 knockouts, suggesting a possible regulation of mitochondrial transport by Mfn2-Miro2 interaction (Misko et al., 2010).

Moreover, Miro1 has been proposed as a novel regulator of mitophagy due to its interaction with the serine/threonine kinase PINK1 (PTEN-induced putative kinase 1) and the ubiquitin-ligase Parkin (Liu et al., 2012). Damaged mitochondria are selectively targeted to facilitate their engulfment by autophagosomes, a crucial process to maintain the clearance of damaged mitochondria. Under normal conditions, PINK1 is driven to the inner mitochondrial membrane where is clipped by MPP (matrix processing peptidase) and PARL (PINK1/PGAM5-associated rhomboid-like protease) (Deas et al., 2011; Jin et al., 2010; Meissner, Lorenz, Weihofen, Selkoe, & Lemberg, 2011). However, damage and oxidative stress disrupt mitochondrial membrane potential, which induces stabilization and accumulation of PINK1 at the outer mitochondrial membrane (Lazarou, Jin, Kane, & Youle, 2012; Okatsu et al., 2013). Stabilized PINK1 interacts with and phosphorylates multiple proteins, including Miro1 on Ser156 (Wang et al., 2011). The most relevant substrate of PINK1 is Parkin, which upon phosphorylation is recruited from the cytosol and enhances its E3 ubiquitin ligase activity. When recruited to the mitochondria, Parkin ubiquitinates multiple proteins such as VDAC1, Drp1, Mfn1 and 2, Tom20, Tom40 and Miro GTPases (Birsa et al., 2014; Geisler et al., 2010; Liu et al., 2012; Ziviani, Tao, & Whitworth, 2010). The ubiquitin chains of those substrates will be recognized by autophagy receptors to link mitochondria to autophagosomes and produce mitophagy (Stolz, Ernst, & Dikic, 2014). Although OPTN, NDP52, p62, NBR1 and TAX1BP have been proposed as essential receptors for autophagy (Lazarou et al., 2015), the process requires many other regulators including Rab GTPases to ensure a homogeneous autophagosome formation around the mitochondrion (Yamano et al., 2018).

Phosphorylation of Miro1 on Ser156 by PINK1 and subsequent ubiquitination at K11, K27 and K63 by Parkin targets Miro1 to the proteasome for degradation, thus inducing mitochondrial arrest

(Wang et al., 2011). In the same direction, a phosphorylation-resistant mutant of dMiro increases mitochondrial trafficking and synaptic growth at larval neuromuscular junctions, suggesting a role of Miro1 phosphorylation on mitochondrial motility and neuronal viability (Tsai et al., 2015). Nevertheless, most studies imply a more relevant role of Miro ubiquitination rather that phosphorylation, supporting the fact that Miro stabilizes phospho-serine65 on Parkin and therefore promotes its ubiquitination and degradation (Birsa et al., 2014).

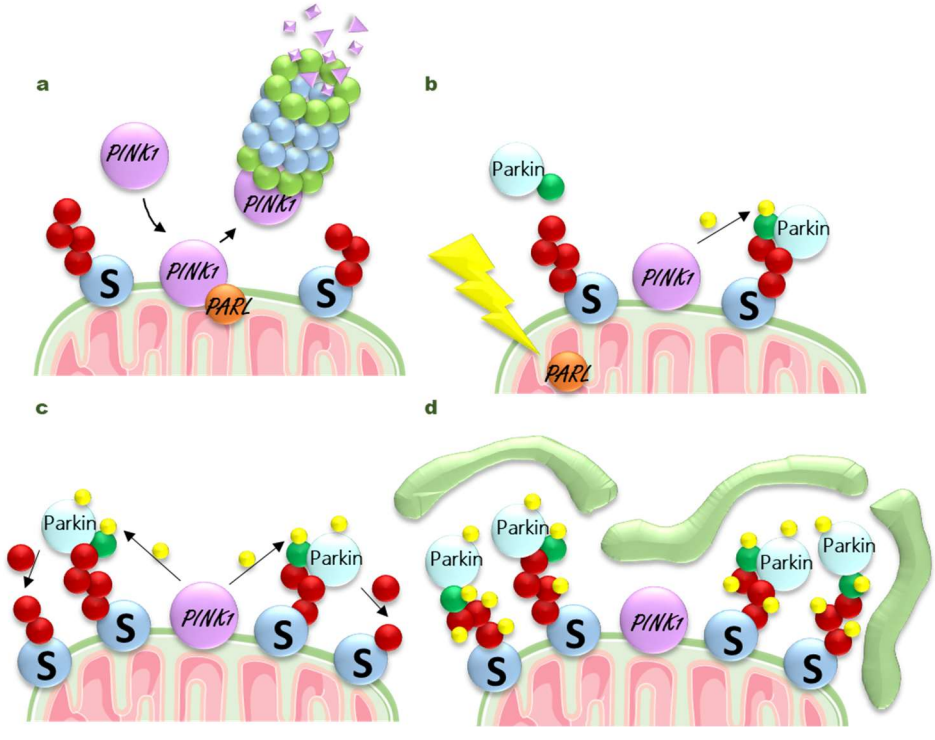

Figure I 11 Stabilization of PINK1 at the outer mitochondrial membrane recruits Parkin to induce mitophagy. a, Under basal conditions, PINK1 is imported into the mitochondria, cleaved by PARL protease and degraded at the proteasome. **b,** After stress or damage, mitochondrial membrane potential is lost, PARL can no longer process PINK1 and the kinase is stabilized at the OMM. From there, PINK1 phosphorylates ubiquitin (red circle) bound to OMM protein substrates (S). Parkin has a high affinity for phospho-Ub (green circle) and translocates from the cytosol to the mitochondrial surface. **c,** PINK1 activates Parkin by phosphorylation of Ser65, enhancing its E3 ubiquitin ligase activity. Activated Parkin ubiquitinates OMM protein substrates and PINK1 phosphorylates ubiquitin leading to further Parkin recruitment and activation. **d,** Phospho-Ub recruit autophagy receptors to engulf mitochondria by autophagosomes for subsequent degradation at lysosomes. Adapted from Pickles *et al.,* 2018

Due to its versatility, Miro1 dysfunction has been linked to many neurological disorders, including Alzheimer's disease (AD), schizophrenia and amyotrophic lateral sclerosis (ALS). Spinal cords of ALS patients, in agreement with mouse models of ALS disease, show low levels of Miro1, indicating an impairment of motor neurons to keep calcium homeostasis in the absence of Miro (Zhang et al., 2015). Reduced levels of Miro and kinesin were also detected cells harboring presenelin-1 E280A mutants, a protein mutated in around 80% of Alzheimer's disease patients

(Falla et al., 2014). *Drosophila* studies also show an inhibitory effect of Miro and Milton on PAR-1 kinase activity and their knockdown correlates with an increase in Tau phosphorylation at S262. This phosphorylation decreases Tau affinity for microtubules and promotes its accumulation at the cytoplasm, thus leading to the major onset of Alzheimer's disease (Ando et al., 2012). Finally, Miro1 interaction with DISC1 has been related with its role promoting anterograde mitochondrial trafficking in axons, and disruption of this complex leads to a pathogenesis that includes schizophrenia, bipolar disorder and severe recurrent depression (Ogawa et al., 2014). Together, these findings imply an outstanding role of Miro in the prevention of neurologic disorders.

1.7. DISC1, a Miro1 regulator disrupted in psychiatric diseases

The disrupted-in-schizophrenia 1 (DISC1) gene was originally identified at the breakpoint of a chromosomal translocation in a scottish family with high prevalence to suffer psychiatric disorders (Millar et al., 2000). Additional studies in broader populations evidenced a link between DISC1 mutations and a wide variety of mental illnesses (Chubb, Bradshaw, Soares, Porteous, & Millar, 2008; Hennah et al., 2003), so it soon became a useful tool to study the molecular mechanisms underlying psychiatric diseases (Sawa, Ishizuka, & Katsanis, 2016). Many of those studies demonstrated the importance of DISC1 in neuronal and developmental processes, including neurogenesis, neuronal migration, synapse formation, and neurotransmission in which it regulates signal transduction through a wide variety of interactions (Brandon & Sawa, 2011; Su et al., 2014; Suh et al., 2019; Zheng et al., 2019).

With over 50 splice variants identified in human brain, DISC1 predominantly localizes at the mitochondria, although in a lesser extend can also be found at the cytoplasm, inside the nucleus or associated to actin fibers (James et al., 2004). Transgenic mice expressing dominant-negative DISC1 revealed abnormalities in dopaminergic neurons, including lower dopamine levels, increased mRNA levels of dopamine receptors in striatum and abnormal behavior after methamphetamine administration (Peled et al., 2013). DISC1 forms a complex with the dopamine D2 receptor after stimulation, thus modulating its downstream signaling and preventing its internalization (Su et al., 2014). It also associates with Krüppel-like factor 16 (KLF16) and translocates to the nucleus to regulate the expression of several genes, among them the dopaminergic receptor D1 (Suh et al., 2019). However, most of DISC1 physiological implications come from its role modulating mitochondrial functions. By associating with Mitofilin, DISC1 regulates NADH dehydrogenase activity, ATP levels and calcium dynamics (Park et al., 2010).

Moreover, DISC1 interacts in a complex with both Miro1 and TRAK1/TRAK2 adaptors and is necessary to couple kinesin1 to the mitochondria, which makes it an essential component of the anterograde-transport machinery (Norkett et al., 2016; Ogawa et al., 2014). Disruption of DISC1-

TRAK-Miro1 complex or expression of the chimeric protein resulting from the translocation in schizophrenic patients inhibits axonal mitochondrial movement and impairs dendritic morphogenesis and arborization (Norkett et al., 2016).

1.8. Syntaphilin docks mitochondria in axonal synapsis

Syntaphylin (SNPH) was originally identified as an axon-targeted protein that competes with SNAP25 to bind syntaxin-1 and inhibits the formation of the SNARE complex, blocking thereby presynaptic vesicle release (Lao et al., 2000). Subsequent studies using knockout mice for *snph* gene allowed to characterize syntaphylin as a static anchor protein that immobilizes mitochondria in axons and acts as a negative regulator of mitochondrial motility (Kang et al., 2008). SNPH knockout neurons show increased mitochondrial motility, but contain fewer mitochondria in axonal tips, which results in defective axonal branching and precedes neurodegeneration (Ohno et al., 2014).

SNPH arrests mitochondrial motility by direct association with microtubules and mitochondria. SNPH also enhances mitochondrial docking capacity by interacting with dynein light chain (LC8) (Chen, Gerwin, & Sheng, 2009) and associates with kinesin1 in response to Ca^{2+} and synaptic activity (Chen & Sheng, 2013), but little is known about proteins that mediate mitochondrial association (Park et al., 2016). The mitochondrial protein DISC1 has been proposed as a negative regulator of SNPH anchoring function. By interacting with SNPH, DISC1 increases mitochondrial movement after synapse stimulation, whereas a SNPH mutant lacking the region of interaction with DISC1 shows stronger docking capacity (Park et al., 2016).

Although SNPH has been characterized in neurons, a recent report showed increased protein levels in metastatic prostate cancer tumors. Hence, SNPH expression also constitutes a novel biomarker for the disease (Hwang et al., 2019).

1.9. Myosins drive mitochondria through the actin cytoskeleton

Although mitochondria are predominantly hauled bidirectionally through microtubule tracks, myosin motors mediate short range movement in presynaptic terminals and dendritic spines, where actin filaments form most of the cytoskeletal architecture (López-Doménech et al., 2018; Oeding et al., 2018). Myosin XIX (Myo19) was the founding member of a novel class of mitochondria-located myosins that mediate movement through actin cytoskeleton (Quintero et al., 2009). Myo19 heavy chain is 970 amino acids long and consists of a motor domain, three IQ motifs, and a short tail (Quintero et al., 2009). In vitro studies revealed that its head domain firmly binds F-actin and mediates a plus end-directed movement (Lu et al., 2014). Conversely, a distal region within the tail domain contains a motif that binds Miro proteins, thereby directing them to the mitochondria and allowing them to act as an actin-driven motor (Oeding et al., 2018).

Interestingly, Miro1 not only acts as a receptor to recruit Myo19 at the mitochondria, but also stabilizes the protein at the outer mitochondrial membrane to couple the actin cytoskeleton (López-Doménech et al., 2018). Depletion of Miro1/2 (López-Doménech et al., 2018) or downregulation of Myo19 (Rohn et al., 2014) leads to defects in the mitochondrial distribution within cells at division, probably due to an impairment on actin-driven mitochondrial movement.

Apart from Myo19, other myosin subfamilies have been linked to different aspects of mitochondrial physiology. For example, Myosin6 (Myo6) is a minus-end directed actin motor that is recruited to mitochondria upon stress and damage. There, it binds to Parkin and drives actin polymerization to encapsulate damaged mitochondria and facilitate the autophagy process (Kruppa et al., 2018). In plants, Myosin XI-K has been linked to the transport of Golgi stacks, peroxisomes and mitochondria in leaf cells of *N. benthamiana* (Avisar, Prokhnevsky, Makarova, Koonin, & Dolja, 2008). Along with myosin XI-K, 5 more myosins (MYA1, MYA2, and myosins XI-C, XI-E and XI-I) were reported to alter Golgi vesicle trafficking and mitochondrial movement in *Arabidopsis thaliana*, evidencing their involvement in the transport of different organelles (Avisar et al., 2009).

2. The armcx/armc10 superfamily

The armcx cluster originated from mRNA retrotransposition and multiple duplication events in common ancestor gene known as armc10/SVH that took place during evolution of eutherian (placental) mammals. Multiple events of gene conversion affected both 5'UTR and coding sequences of the ancestor gene, giving rise to many differences in the structure and length of the derived proteins. However, all components of the armcx family keep a common armadillo-domain-like tandem repeats from that ancestor gene (López-Doménech et al., 2012). Bioinformatic analysis suggest that all members of that family (excluding armc10/SHV) are contained in a single exon and their genes localize in the q22.1-q22.2 region of chromosome X (Kurochkin, Yonemitsu, Funahashi, & Nomura, 2001). The armc10 gene, however, has at least 8 exons and 4 described isoforms (known as A, B, C and D). Unlike armcx genes, it localizes in the human chromosome 7 and mice chromosome 5.

The first three members of the armcx family were described as tumor suppressor genes as their expression was reduced in several epithelial cancers. Consequently, they were named armadillo-domain protein lost in epithelial cancers linked to chromosome X 1, 2 and 3 (also known as Alex 1 to 3). Subsequent studies also placed three previously unrelated gene families into the armcx/armc10 cluster, which include BEX (brain expressed X-linked), WEX (Wwbp X-linked) and GASP (GPCR-associated sorting protein) (Winter & Ponting, 2005). The current GASP family

includes Alex1-6, Armc10, Gprasp1 and 2 and Bhlhb9. Along with the Alex-6 pseudogene, located upstream of Alex6, and Armc10 pseudo gene that locates at the third human chromosome, they form the current 12 members of the armcx/armc10 family (Abu-Helo & Simonin, 2010; Simonin, Karcher, Boeuf, Matifas, & Kieffer, 2004).

Although many of these proteins are ubiquitously expressed, their highest expression is reached at the nervous system and most especially in brain, suggesting a role of the armcx/armc10 members in the mammalian evolution of neocortex. Precisely, the divergence of the armcx/armc10 genes took place with significant evolutionary improvements in mammals, especially for the fully developed placenta and the increase in brain complexity, further supporting the importance of these proteins for neuronal function.

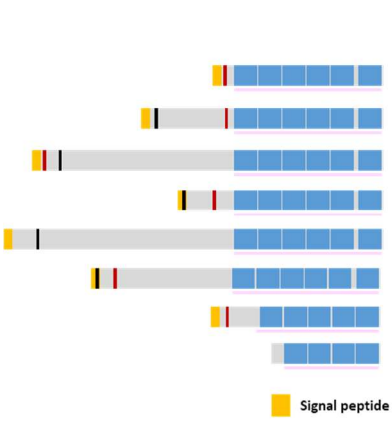

Name	Synonyms	Chromosome region in humans	Gene ID
Armc10	Gasp8, SVH	7(q22.1)	83787
Armcx1	Alex1, Gasp7	X(q22.1-q22.2)	51309
Armcx2	Alex2, Gasp9	X(q22.1-q22.2)	9823
Armcx3	Alex3, Gasp6	X(q22.1-q22.2)	51566
Armcx4	Gasp4	X(q22.1-q22.2)	100131755
Armcx5	Gasp5	X(q22.1-q22.2)	64860
Armcx6	Gasp10	X(q22.1-q22.2)	54470
Armc6-like	Gasp10Ψ	X(q22.1-q22.2)	653354

Fig I 12 Schematic representation of the main Armc10/Armcx proteins. The armcx/armc10 proteins contain several armadillo-domains at the C-terminal region and a putative nuclear localization and mitochondria-targeting signal at their N-terminal. The table at the right indicates the official name and equivalences along with the gene ID number and their localization at the human genome.

2.1. GASP proteins modulate the endocytic fate of GPCRs

GASP proteins regulate the post-endocytic sorting of GPCR-containing endosomes, the recycling and the degradation by lysosomes, thus affecting their signaling. In agreement with their neuronal expression, GASP-1 and GASP-2 interact with and regulate many receptors highly expressed in brain. Specifically, GASP-1 interacts directly with m1/m2-cholinergic, β1-adrenergic and 5-HT7 serotoninergic receptors and is involved in post-endocytic sorting of δ-opioid, cannabinoid CB1 and dopamine D2 receptors (Mathis, Bott, Candusso, Simonin, & Cassel, 2011; Simonin et al., 2004). GASP-2 binds and regulates the endocytic sorting of dopamine D2, β1 and β2 adrenergic and calcitonin receptors (Simonin et al., 2004; Thompson, Pusch, & Whistler, 2007).

Experiments using knockout mice for GASP-1 show no significant abnormalities or health problems in comparison with wild-type animals, but locomotor defects following cocaine

administration were decreased in GASP-1 KO mice (Boeuf et al., 2009). Besides, those animals underwent less self-drug administration, inferring a reduced dependence-effect. Along with GASP-1 interaction with dopamine and cannabinoid receptors, those experiments suggest that GASP-1 increases the time of receptors to recycle back to the plasma membrane, thus reducing the sustained effect of cocaine and cutting down the effect of the drug (Kargl et al., 2012).

Regulating the endocytic pathway of GPCRs is currently just one of the many roles conferred to GASP proteins. Several reports implicate that many of those armadillo-domain proteins translocate into the nucleus and regulate gene transcription due to the presence of a nuclear localization signal at their N-terminus (Mathis et al., 2011). For example, GASP-1 prevents apoptotic cell death when transferred to the nucleus upon NGF treatment in PC12 cells (Kiyama, Isojima, & Nagai, 2006). In another study, the same cell line showed more sensitivity to apoptosis when depleted from GASP-3 (Heese et al., 2004). Precisely, GASP-3 is usually referred to as bHLH-B9 due to its helix-loop-helix basic motif that is typical from the bHLH family of transcription factors. Nevertheless, despite their structure, localization and regulatory function, there is still no direct demonstration of GASP proteins binding to specific DNA sequences and regulating transcriptional activity.

2.2. Implication of armadillo-domain proteins in cancer

The big family of armadillo-domain containing proteins are involved in many signaling pathways leading to embryogenesis, cell adhesion and tumorigenesis, usually by interacting with and regulating a variety of proteins through their armadillo repeats (Hatzfeld, 1999). The best documented is probably β-catenin, a key regulator of cellular homeostasis which acts as a transcriptional co-regulator and as adaptor for intracellular adhesion (Shang, Hua, & Hu, 2017). β-catenin functionality is closely regulated by Wnt canonical pathway (Kobayashi et al., 2000). Accumulation of β-catenin occurs in more than half of the cases of colorectal and liver carcinomas, breast cancer, melanoma and leukemia (Valkenburg et al., 2011).

In a similar manner, members of the armcx family were originally implicated in epithelial cancers and oncogene expression. For example, protein or mRNA levels of Alex1 and 2 are significantly reduced in human lung, prostate, colon, pancreas, and ovarian carcinomas but remain normal in tumors derived from non-epithelial tissues like gliomas, neuroblastomas, and sarcomas (Kurochkin et al., 2001). Consistent with their role as tumor suppressors, Alex1 overexpression impairs the formation of colonies in HCT116 and SW480 cells derived from human colorectal carcinoma. Those cells also show hypermethylation at the promoter and low levels of Alex1 mRNA (Iseki et al., 2012). Expression of Alex3 also decreases in lung cancer cells compared with normal bronchial epithelial cells and correlates with lymph node metastasis and poor prognosis (Du et

al., 2017). Those effects were associated to alterations on AKT/Slug signaling pathway and a down-regulation of E-cadherin expression (Du et al., 2017). Screening studies identified Alex5 as an activated gene by the oncogene ZNF217 (Krig et al., 2007) and Alex6 as an upregulated gene in Hela cells with oncogenic phenotype (Yoshida, Kusama, Tategu, & Yoshida, 2009). Nevertheless, little is known about their precise mechanism of action in epithelial cancers and tumorigenesis taking out what can be inferred from proteins with similar structure. Actually, most reports focus on the mitochondrial targeting signal harbored at their amino (N)-terminal region to propose a role in the regulation of these organelles.

2.3. Alex3 as a novel regulator of mitochondrial physiology

Alex3 sequence contains a transmembrane domain, a nuclear localization signal (NLS) and six arm-like domains (López-Doménech et al., 2012). In agreement with the neuronal expression of armcx cluster, Alex3 was characterized as a gene preferentially expressed in the upper layers of the developing cerebral cortex (García-Frigola et al., 2004). A study carried out by Mou and coworkers identified Alex3 as a Sox10 binding partner in a protein-protein interaction screening (Mou, Tapper, & Gardner, 2009). Sox10 belongs to the E-sox family of transcription factors and plays key roles in neural crest development, neurogenesis, sex determination and cellular differentiation (Wegner, 1999). Alex3 binds to Sox10 in the nucleus and enhances the expression of target genes (Mou et al., 2009). Consistent with the role of Alex3 in neuronal development, electroporation of Alex3 into the spinal cord of chicken embryos reduced neuronal precursor cell proliferation and promoted neuronal differentiation. Both effects depended on its mitochondrial localization and regulation of β-catenin-dependent transcriptional activity (Mirra, Ulloa, Gutierrez-Vallejo, Martí, & Soriano, 2016).

Most of our current understanding of armcx proteins as mediators of mitochondrial dynamics emerged after the work of López Doménech and colleagues. In their report, the authors show that overexpression of Alex3 leads to perinuclear clustering of mitochondria in neurons. Besides, either Alex3 overexpression or knockdown of the protein in hippocampal neurons results in increased mitochondrial arrest in both anterograde and retrograde directions. Such reduction in motility was attributed to its interaction with Miro1 and Trak2 proteins, which occurs in a calcium-dependent manner (López-Doménech et al., 2012).

A subsequent study from the same group demonstrated that Alex3 protein levels are regulated by Wnt/PKC non-canonical pathway, thus affecting mitochondrial aggregation and motility. In particular, Wnt activation reduces protein Alex3 levels, while its phosphorylation by PKC and CKII regulate Alex3 degradation at the proteasome through different mechanisms (Serrat et al., 2013). Nevertheless, there are still many unsolved questions regarding the signaling pathways leading

to Alex3 regulation of mitochondrial motility and the molecular mechanisms by which this protein is necessary for Miro1 and Trak2 functionality.

3. Neurodegenerative diseases related with mitochondrial dynamics

As mentioned before, mitochondria must undergo fusion and fission processes and dynamics are essential to fulfill the energy demands and calcium-buffering requirements of the cell. Dysregulated mitochondrial dynamics or mutations in the proteins that mediate those processes are often associated with neurodegenerative disorders, either directly or indirectly. Here we will give an insight on the most prevalent diseases and the mitochondrial dysfunctions that cause their symptoms.

3.1. Charcot Marie Tooth disease

Charcot-Marie-Tooth (CMT) is the most prevalent category of inherited neuropathy. Individuals with CMT show weakness and atrophy of distal muscles, depressed or absent deep tendon reflexes, and mild sensory loss (Bird, 1993; Zhao et al., 2001). Although the disease is usually manifested as autosomal dominant, some subtypes present an X-linked or autosomal recessive inheritance pattern. Following electrophysiological criteria, the subsets of the disease can be classified into two subtypes: the demyelinating CMT type 1 (CMT1) with decreased nerve conduction velocities and the axonal form, CMT type 2 (CMT2) (Zhao et al., 2001).

Dysfunction of proteins involved in mitochondrial physiology have been related to different subtypes of the disease (Morena et al., 2019). Among them, mutations in the gene coding for Mfn2 are associated with Charcot Marie Tooth 2A (CMT2A). CMT2A is caused by defective mitochondrial fusion and usually affects sensory and motor neurons due to impairment to keep a healthy mitochondrial population (Züchner et al., 2004). The ratio between Mfn1 and Mfn2 in motor neurons may explain the tissue-specificity of the disease and why increasing the levels of Mfn1 can ameliorate the symptoms in a mouse model (Iwata & Scorrano, 2019).

Mutations in genes involved in mitochondrial transport have also been reported to cause CMT2A due to miss-localization of axonal mitochondria, as is the case for Kif5A and Kif5B (Campbell et al., 2014; Kijima et al., 2005). Mice with low levels of Kif5Bβ, a subclass of Kif5B, have defective transport of synaptic vesicle precursors and suffer from progressive muscle weakness similar to the human disease. This indicates that defective axonal transport can underlie peripheral neuropathies (Zhao et al., 2001; Züchner et al., 2004).

3.2. Dominant Optic Atrophy

Dominant Optic Atrophy (DOA) is a neuro-ophthalmic disease primary caused by axonal degeneration of retinal ganglion cells. Those cells are responsible to transfer information from photoreceptors to specific regions of the brain and represent the main components of the optic nerve. DOA patients usually suffer of visual loss with severity ranging from mild to blindness, as well as color vision defects and visual field deficits (Lenaers et al., 2012).

Mutations in the gene OPA1, coding for the inner mitochondrial membrane GTPase responsible for mitochondrial fusion, are the cause of DOA in over 75% of the patients, although mutations in the OPA3 and TMEM126A (OPA7) are also documented (Ferré *et al.*, 2009). As in the case of CMT2A, DOA represents another example of disease caused by alterations in the mitochondrial fusion machinery.

3.3. Alzheimer's disease

Alzheimer's disease (AD) is the most prevalent cause of dementia and the most prevalent neurodegenerative disorder associated with aging, affecting over 25 million people worldwide. This neurodegenerative disease is usually divided into familial AD (fAD), caused by autosomal mutations in β-amyloid precursor protein (APP), presenilin 1 (PS1) or presenilin 2 (PS2) and sporadic AD (sAD), caused by a combination of genetic and environmental risk factors (Waring & Rosenberg, 2008). sAD is the most prominent form of AD and represents around 95% of the diagnosed patients. Clinical manifestations include persistent comprehensive intelligence impairment, cognitive dysfunction, mental and behavioral abnormalities, and inability to live or work independently. Most of those symptoms are caused by progressive atrophy of neurons in the hippocampus and cortex (Zhang et al., 2019).

AD is preceded by the accumulation of extracellular aggregates of β-amyloid protein generated by proteolytic cleavage of APP. The disease also involves the accumulation of intracellular neurofibrillary tangles of the microtubule-associated protein Tau after multiple phosphorylation (Selkoe, 2002). Axonal defects caused by dysfunctions in mitochondrial transport and fusion/fission proteins were also observed in the early stages of AD in humans. In this regard, decreased levels of kinesin1 were associated with accumulation of proteins, vesicles and organelles, including mitochondria, which lead to axonal swelling and regression. Decreasing microtubule-based transport may also stimulate APP processing and enhance the accumulation of senile plaques in AD (Stokin et al., 2005).

Mitochondrial dynamics have also been the focus of several studies to understand the pathology. Deficiencies in several mitochondrial enzymes related to oxidative metabolism are also among the metabolic defects causing AD. Those include the complexes of α-ketoglutarate

dehydrogenase (KGDHC) and pyruvate dehydrogenase (PDHC), cytochrome oxidase (COX) and two enzymes in the rate-limiting step of the tricarboxylic acid cycle (Su et al., 2010). Furthermore, M17 cells expressing high levels of APP exhibit fragmented mitochondria that accumulate around the perinuclear area, reduced protein levels of mitochondrial fusion protein such as Mfn1/2 and Opa1 and increased levels of fusion-related proteins like Fis1 (Wang et al., 2009, 2008).

3.4. Parkinson's disease

Parkinson's Disease (PD) is a chronic and progressive neurodegenerative disorder characterized by selective loss of dopaminergic neurons in the substantia nigra, with presence of intraneuronal inclusions termed as Lewy bodies (LB) and dystrophic Lewy neurites in surviving neurons (Thomas & Beal, 2007). Affecting almost 2% of the current population, PD is the second most common neurodegenerative disease after Alzheimer's. Clinical manifestations include a wide range of motor impairments, bradykinesia, tremor, gait difficulty and rigidity (Forno, 1996). Such pathology is a consequence of both genetic susceptibility and environmental factors.

While the majority of PD cases are sporadic, a series of genes are linked to familiar forms of the disease. Among them, stand those encoding α-synuclein, DJ-1, LRRK2, PINK1 and Parkin. Mitochondrial dysfunction, oxidative damage, abnormal protein accumulation and protein phosphorylation are also considered key processes compromising the survival of dopaminergic neurons and represent an important cause of pathogenesis in both sporadic and familial PD (Thomas & Beal, 2007).

Locus	Gene	Chromosome	Inheritance	Function
PARK1/4	α-Synuclein	4q21	AD	Presynaptic protein, Lewi body
PARK2	Parkin	6q25.2-27	AR	E3 Ubiquitin ligase
PARK3	Unknown	2p13	AD	Unknown
PARK4	Unknown	4p14	AD	Unknown
PARK5	UCH-L1	4p14	AD	Ubiquitin C-terminal hydrolase
PARK6	PINK1	1p35-36	AR	Mitochondrial kinase
PARK7	DJ-1	1p36	AR	Chaperone, antioxidant
PARK8	LRRK2	12p11.2	AD	Mixed lineage kinase
PARK9	ATP13A2	1p36	AR	Unknown
PARK10	Unknown	1p32	AD	Unknown
PARK11	Unknown	2q36-37	AD	Unknown
PARK12	Unknown	Xq21-q25	Unknown	Unknown
PARK13	HTRA2	2p12	Unknown	Mitochondrial serine protease

Table I 3 Gene loci identified for Parkinson's disease. AD= Autosomal dominant; AR= Autosomal recessive. Adapted from Thomas, *et al.,* 2007

Most loci with mutations linked to PD codify for mitochondrial proteins or proteins that exert their function at the mitochondria. The best documented are probably the mitochondrial kinase PINK1 and the E3 ubiquitin ligase Parkin. Both are key proteins for selective degradation of mitochondria in neurons, a process known as mitophagy, although in the last years they have

been implicated in many other functions, including mitochondrial transport. As mentioned before, PINK1 interacts with and phosphorylates Miro1 and Milton adaptors, thus inducing their ubiquitinization by Parkin for subsequent degradation (Wang et al., 2011; Liu et al., 2012). Besides acting as a mitochondrial motility suppressor by decreasing Miro1 protein levels, both TRAK and Miro proteins can act as a bait to enhance PINK1 localization at the mitochondria, even in the absence of its mitochondrial targeting sequence (Weihofen, Thomas, Ostaszewski, Cookson, & Selkoe, 2009). Such findings open a novel window to develop treatments for PD focused on Miro1, TRAK and other proteins of the mitochondrial transport machinery.

3.5. Amyotrophic lateral sclerosis

Amyotrophic lateral sclerosis (ALS) is a debilitating neurodegenerative disorder that causes degeneration of motor neurons in the neuromuscular junction, leading to progressive muscle weakness, respiratory failure, difficulty in speaking and swallowing, and eventually paralysis and death (Bose et al., 2019; Hardiman, van den Berg, & Kiernan, 2011). Around 90% of ALS cases are sporadic with unknown etiology. The remaining 10% are caused by genetic mutations (Emery & Holloway, 1982). The most recurrent mutations occur in the gene of Cu,Zn-superoxide dismutase (SOD1), which codifies for a protein involved in maintaining the homeostasis of ROS, especially after mitochondrial stress. Thus, a great part of neuronal degeneration has been proposed to be a result of increased damage due to oxidative stress, protein aggregation, mitochondrial dysfunction, excitotoxicity and impaired axonal transport, among other factors (Bruijn, Miller, & Cleveland, 2004; Shaw, 2005).

There are two major hypothesis regarding motor neuron dysfunction in ALS. The "dying forward hypothesis" proposes that increased glutamate exitotoxicity exerted by dysfunctional cortical neurons would eventually produce apoptosis in post-synaptic motor neurons (Eisen & Weber, 2001). Astrocytes and other glial cells have also been proposed to mediate toxicity through the release of cytokines and other pro-inflammatory mediators (Nagai et al., 2007; Yamanaka et al., 2008). The "dying-back" hypothesis, however, suggests that motor neuron degeneration begins at the neuromuscular junctions or at distal parts of the axon and spreads towards the soma (Kiernan et al., 2011). According to this second hypothesis, mitochondrial transport alterations that impair the proper mitochondrial supply or the turnover of damaged mitochondria would greatly contribute to axonal degeneration (Fischer et al., 2004; Granatiero & Manfredi, 2019).

In excitable cells with large axoplasm such as motor neurons, loss of viable mitochondria at the synapses of neuromuscular junctions has catastrophic consequences leading to muscle denervation. Numerous lines of evidence indicate that mitochondrial misslocalization contributes to neuronal demise in ALS, producing degeneration of motor neurons and muscle paralysis (De

Vos et al., 2007, 2008). A mouse model of ALS with mutant SOD1 shows reduced vesicular transport in both anterograde and retrograde directions, whereas mitochondrial transport is selectively reduced in the anterograde direction. The selective inhibition of anterograde transport, in turn, enhances the net retrograde movement and depletes mitochondria from distal points within axons (De Vos et al., 2007). Besides, dysfunctional mitochondria accumulate at the soma of motor neurons affected by ALS, suggesting that the inability to maintain a healthy axonal pool of mitochondria plays a pathological role for the development of the disease (Granatiero & Manfredi, 2019).

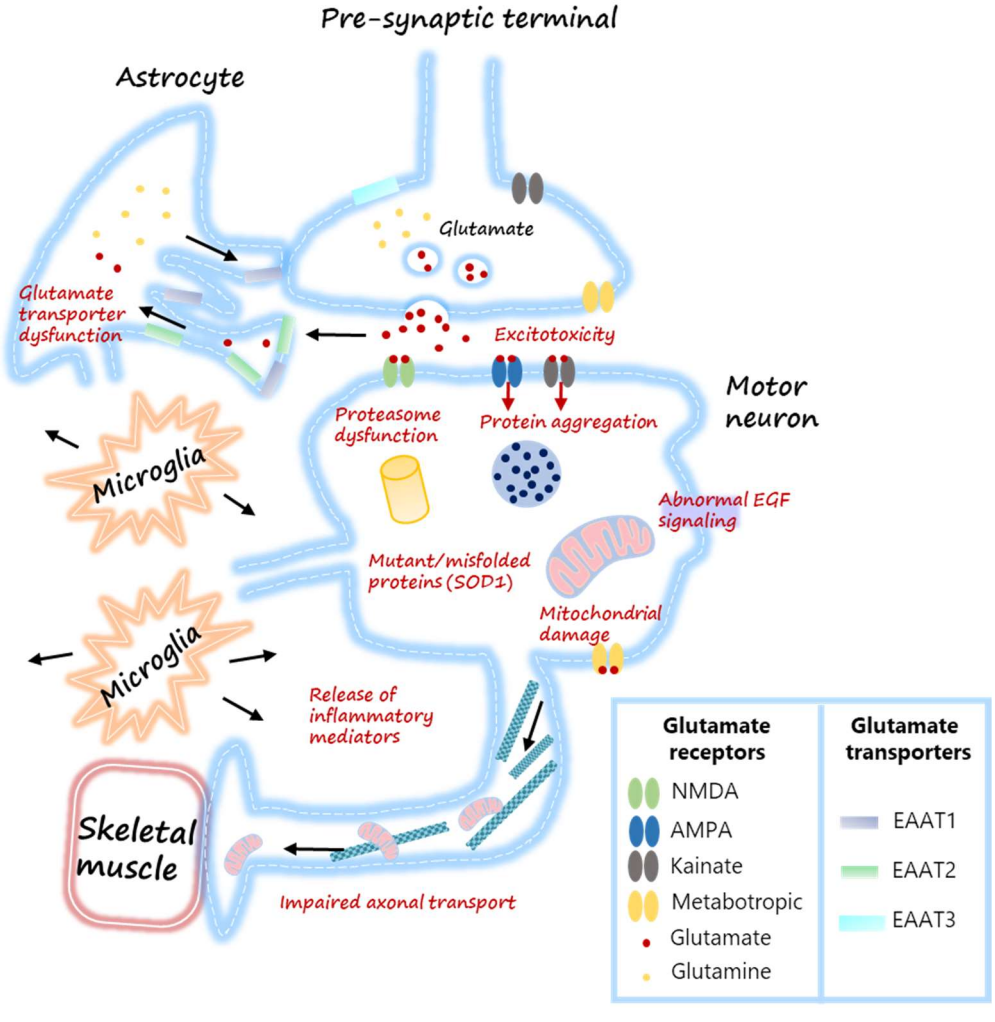

Figure I 13 Molecular mechanisms that contribute to motor neuron injury in a ALS. Adapted from Shaw, 2015

4. Signaling through G protein-coupled receptors

Neurons, as any other cells, can receive, process and respond to a myriad of signals from their environment. Those signals range from hormones, neurotransmitters, lipids and ions to sensory stimuli, such as light and odorants. Many of them elicit their cellular responses through the activation of seven transmembrane (7TM) receptors coupled to heterotrimeric G proteins, usually referred to as G protein-coupled receptors (GPCRs). They include the metabotropic glutamate receptors, muscarinic acetylcholine receptors, $GABA_B$ receptors, and most serotonin receptors, as well as receptors for histamine, dopamine, epinephrine, norepinephrine, neuropeptides, endocannabinoids and many others (Alexander, Mathie, & Peters, 2011).

GPCRs are targets of around 40% therapeutic drugs and represent the most abundant and important family of membrane receptors in the human genome (Bockaert, 2012). Their core is structured in 7 hydrophobic transmembrane α-helices connected by three extracellular and three cytoplasmic loops. Their surface-oriented N-terminal segment is actively involved in ligand-interaction and often modified by glycosylation and other posttranslational modifications, while the intracellular loops and C-terminus mediate the coupling to heterotrimeric G proteins as well as β-arrestins and other downstream regulators and effectors (Katritch, Cherezov, & Stevens, 2012). The over 800 described GPCRs can be classified into five subfamilies based on similarity of their transmembrane sequence: the rhodopsin (family A, with 701 members), the secretin (family B, with 15 members), the glutamate (family C, with 15 members), the frizzled/tasted and the adhesion family (with 24 members each) (Fredriksson, Lagerström, Lundin, & Schiöth, 2003). Although GPCRs where originally conceived as singular entities, there is a growing evidence that they exist as homo- and heterodimers (or oligomers) and that those dimers are essential for G protein activation, ligand binding affinity and cross-talk between different signaling pathways (Angers, Salahpour, & Bouvier, 2002; Gahbauer & Böckmann, 2016). Such a phenomenon is mandatory for the functionality of metabotropic receptors that mediate synapsis, including mGlu and $GABA_B$ receptors, although the dimerization mechanisms for members of other subfamilies such as the rhodopsin is still under debate (Pin, Kniazeff, Prézeau, Liu, & Rondard, 2019).

Further, our current understanding of GPCR signaling seems to indicate that receptor activation does not equally affect all its downstream pathways. GPCRs can acquire multiple conformation states upon ligand binding, giving rise different downstream effects. Receptors undergoing those conformational changes are known as biased GPCRs, and allow some ligands to activate different subsets of signaling events based on the GPCR conformation that they stabilize (Kenakin, 2015; Spangler & Bruchas, 2017). Although biased signaling has been widely studied for angiotensin and adrenergic receptors, those mechanisms can be extended to many of the receptors that mediate the synapses (Smith, Lefkowitz, & Rajagopal, 2018).

Aside from their essential implication in synaptic transmission, GPCRs also play key roles in cell migration and neuronal differentiation. For example, the chemokine stromal cell-derived factor 1 and its receptor, CXCR4, are involved in neuron migration during cerebellar formation (Rahimi-Balaei, Bergen, Kong, & Marzban, 2018). Overexpression of either CXCR4 or its ligand often give rise to neurological disorders, such as multiple sclerosis, stroke, trauma and even the inflammation that occurs in Alzheimer's disease (AD) after accumulation of hyperphosphorylated Tau protein (Bajetto, Bonavia, Barbero, Florio, & Schettini, 2001; Li & Wang, 2017).

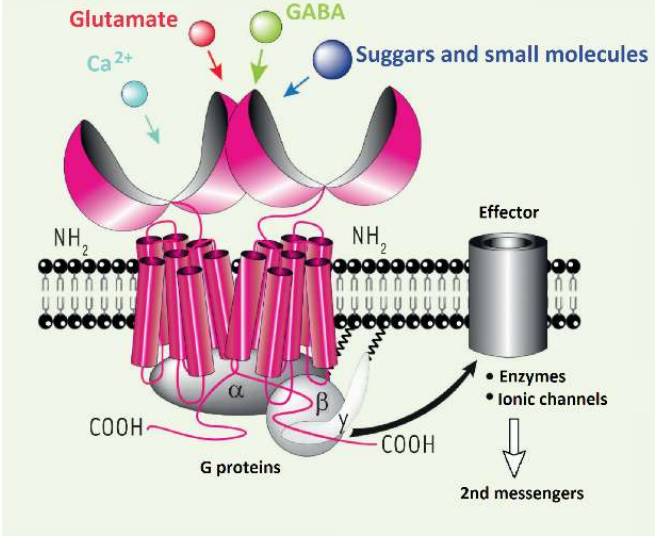

Figure I 14 Schematic representation of a dimeric GPCR. GPCR usually function as dimeric or multimeric complexes and have a wide variety of ligands. In neurons, most of those ligands range from ions and small molecules to neurotransmitters such as glutamate or GABA. Adapted from Bockaert 2012.

5. The G protein activation cycle

Heterotrimeric guanine nucleotide-binding proteins (G proteins) directly relay the signals from GPCRs and are composed of three different subunits: a guanine nucleotide binding Gα subunit a Gβ and a Gγ. Gβ and Gγ are tightly associated and can be referred to as a single Gβγ heterodimer, whereas Gα mediates the cycle between a GDP-bound inactive and a GTP-bound active state. Receptor activation opens the nucleotide-binding pocket of the Gα subunit (Mahoney & Sunahara, 2016), promoting the loss of the GDP and binding of GTP, which is more abundant in the cytoplasm (Traut, 1994). This step leads to its dissociation from the Gβγ dimmer, allowing both Gα and Gβγ to activate their downstream effectors. The GTP within the Gα subunit can be hydrolyzed back to GDP by intrinsic GTPase activity of the Gα, though this process is

usually enhanced by the GAP (GTPase –activating) activity of many RGS proteins (regulators of G protein signaling). This results in the re-association of the Gα with the Gβγ at the plasma membrane and the GTPase cycle termination (Gurevich, 2019). Although the classical model that assumes heterotrimer dissociation is widely established, there is evidence that some heterotrimers may not fully dissociate, but only undergo a rearrangement upon GPCR-mediated activation (Hewavitharana & Wedegaertner, 2012; Lambert, 2008).

Because most of the present work is focused on Gα signaling at the mitochondria, their general and specific features in the case of $G\alpha_q$ will be detailed further on in the introduction. Nevertheless, since the role of $G\alpha_q$ is inherently linked to GPCR signaling, we will outline before the most relevant partners for their function and signal regulation. Among them, stand out the RGS-containing proteins, the GRKs and the arrestins.

5.1. RGS proteins

The GTPase cycle is usually regulated by GEFs (guanine nucleotide exchange factors) and GAPs (GTPase-activating proteins). While the ligand-bound GPCRs actually function as GEFs for the Gα, many binding-partners can stimulate its GTPase activity and act as a GAP. Some of them belong to the regulators of G-protein signaling (RGS) family of proteins, which characterizes by housing a common 120 amino acid "RGS box" used to bind the Gα subunit. To date 37 RGS or RGS-homology (RH) containing proteins have been described, many of which have different functionalities aside from their GAP activity. They range from classical RGS proteins whose GAP activity is limited to the $G\alpha_q$ and $G\alpha_{i/o}$ subfamilies to sorting nexins, axins, AKAPs (A kinase activating proteins) and GRKs (GPCR kinases), which play distinct roles aside from their GAP activity towards the Gα. To this group also belong classical effectors of the $G\alpha_{12}$ subfamily such as p115RhoGEF, PDZ-RhoGEF and LARG whose main function is to activate RhoA but also contain an RH domain to act as a GAP for the Gα (Siderovski & Willard, 2005). In fact, many RGS-containing proteins are actually effectors for the Gα, thus inhibiting further stimulation after their interaction. Regulation of RGS proteins is essential in multiple processes in the central nervous system, including synaptic plasticity, vision and memory. Impairment of their function associates with depression and mental disorders (Senese, Rasenick, & Traynor, 2018).

5.2. Role of GRKs and arrestins

After G protein activation, receptors are desensitized to avoid overstimulation. This process begins when G protein-coupled receptor specific kinases (GRKs) (homologus desensitization) and other kinases such as PKA or PKC (heterologous desensitization) phosphorylate the receptor on multiple residues of its C-terminal tail and intracellular loops (Rajagopal & Shenoy, 2018). GRKs were named and characterized for their kinase activity towards GPCRs. Once the GPCR gets

phosphorylated, arrestins bind the receptor with high affinity, blocking further G protein activation and inducing its internalization in clathrin coated vesicles (Moore, Milano, & Benovic, 2007; Sorkin & von Zastrow, 2009).

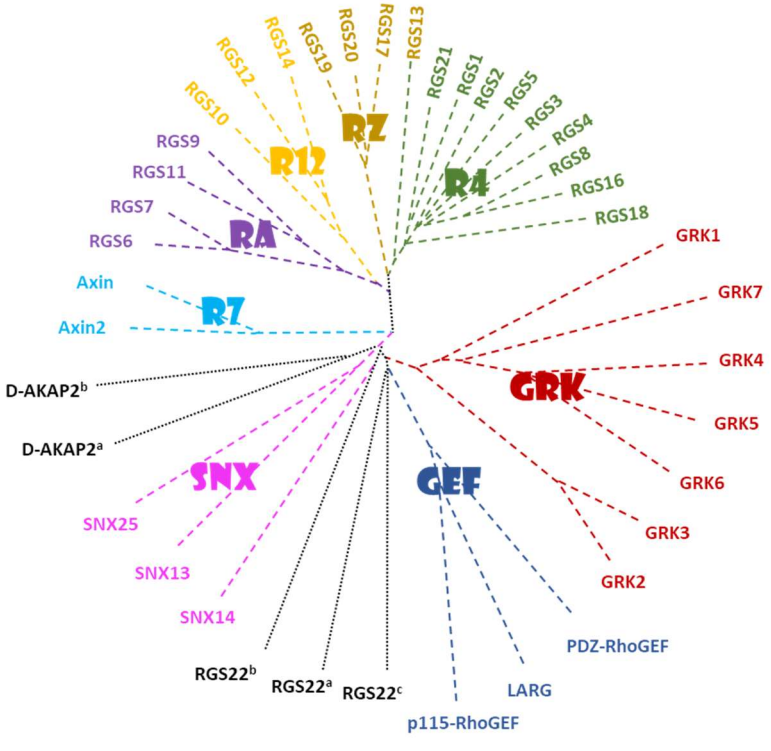

Figure I 15 Relationship between RGS-box sequences of all 37 human RGS proteins identified to date. Unrooted dendrogram generated by Clustal-W and TreeView using sequences identified by the SMART profile for RGS- boxes as well as those identified by protein-fold recognition algorithms. The multiple RGS-box family members D-AKAP2 and RGS22 fall outside the eight established subfamilies. Adapted from Siderovski and Willard 2005.

Beside their role in GPCR phosphorylation, some GRKs bind to Gα subunits, being GRK2 and GRK3 the members with higher affinity for $G\alpha_q$. In the case of GRK2, neither the binding of $G\alpha_q$ through its RH domain nor the interaction with Gβγ with the PH domain are able to induce significant conformational changes in its kinase domain, inferring that both G proteins desensitize the receptors by localizing the GRK near their sites of action. GRKs can nevertheless inhibit G-protein signaling independent of their kinase activity by binding either to Gα or to Gβγ, thus impairing further interactions (Sánchez-Fernández et al., 2014).

As for arrestin proteins, β-arrestins 1 and 2 are the most studied and share 78% sequence homology, but have different expression patterns, GPCR specificity and functional effects

(Srivastava, Gupta, Gupta, & Shukla, 2015). β-arrestins do not only act as terminators of G protein signaling, but also as scaffolders and regulators of many signaling pathways, including the MAPK (Mitogen-Activated Protein Kinase), tyrosine-kinase transactivation, transcriptional regulation and receptor trafficking (Smith & Rajagopal, 2016). Both internalization and intracellular localization of GPCRs and β-arrestins are fine-tune regulated by ubiquitination and other posttranslational modifications, allowing arrestins to mediate endosomal signaling from GPCRs (Lefkowitz & Shenoy, 2005). Strikingly, a recent study using nano-antibodies as biosensors showed that the β_2-adrenergic receptor can be activated and mediates G-protein signaling from endosomes independent of β-arrestins (Irannejad et al., 2013). Such results go against the classical view of GPCRs as mediators of extracellular signaling and opens a new perspective in which GPCRs would transduce signals from diverse ligands in endosomes and other endomembranes.

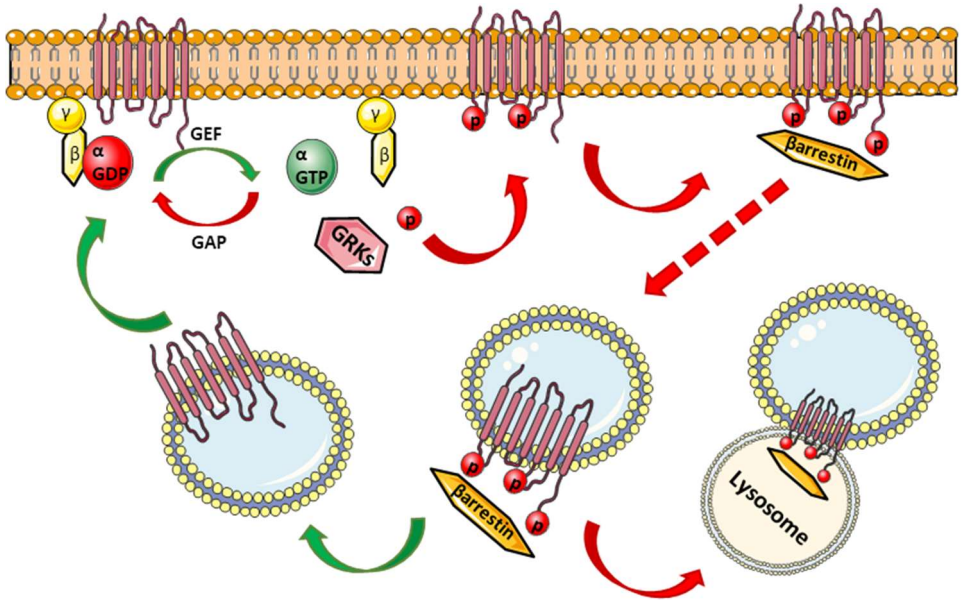

Figure I 16 Schematic representation of the GPCR activation cycle. In the absence of ligand the Gα is GDP-bound and remains associated to Gβγ. Ligand-stimulation of the GPCR enhances its GEF activity toward the Gα, inducing the exchange of GDP for GTP and promoting its dissociation from Gβγ. This step allows both of them to activate their respective effectors. Simultaneously, a short-term desensitization of the receptor begins with its phosphorylation by GRKs and other kinases, enhancing the recruitment of β-arrestins and impairing further signaling from G proteins. Under continuous stimulation, β-arrestins induce the internalization of the GPCR in clathrin-coated vesicles. Internalized receptors can be recycled back to the plasma membrane to transduce further signals or degraded at the lysosomes for long-term desensitization.

5.3. G protein activation by non-canonical GEFs

Although ligand-activated GPCRs were initially considered the only proteins with GEF activity towards the Gα, several activators of G-protein signaling have been found over the last years to bind and activate Gα subunits independent of membrane receptors (Blumer, Cismowski, Sato, & Lanier, 2005). The initially identified as "resistant to inhibitors of cholinesterase 8" (Ric-8) in *Caenorhabditis elegans* was found to interact with $G\alpha_o$ and $G\alpha_s$ in a yeast-two hybrid screen. Subsequent studies showed that its two mammalian isoforms, Ric-8A (also named synembryn) and Ric-8B, could specifically bind and activate $G\alpha_i$, $G\alpha_q$ and $G\alpha_{13}$ or $G\alpha_s$/$G\alpha_{olf}$ subunits, respectively (Chan, Thomas, Sprang, & Tall, 2013; Tall, 2013; Tall, Krumins, & Gilman, 2003). Unlike activated GPCRs, Ric-8 isoforms do not bind heterotrimeric G proteins at their GDP-inactive state, as they have their highest affinity for dissociated nucleotide-free Gα subunits. Ric-8 proteins have thus a complementary role to the one of GPCRs, acting in most cases as signal amplifiers of previously activated Gα proteins. Indeed, after PDGFR (platelet-derived growth factor receptor) activation, Ric-8A can bind to and activate $G\alpha_{13}$ to mediate cytoskeletal reorganization, including dorsal ruffling turnover and cell migration (Wang et al., 2011).

Besides its role in G-protein activation, Ric-8 binds and functions as a chaperone for newly synthesized Gα proteins, thereby facilitating both the folding and the association of Gα subunits with the plasma membrane. Removal of Ric-8A in embryonic stem cells (ESC) complicates the folding and decreases the levels of $G\alpha_i$, $G\alpha_{13}$ and $G\alpha_q$ proteins to <5% of those of wild-type cells at the plasma membrane, leaving them soluble at the cytoplasm and sensitive to degradation (Gabay et al., 2011). On the other hand, overexpression of Ric8-A in COS cells prevents both $G\alpha_q$ and G_{i2} ubiquitination and increases their stability (Chishiki et al., 2013). Conditional Ric-8A knockout mice in neuronal precursor cells present developmental defects in brain, showing thinner cerebral cortex and discontinuous basement membrane, which allows migrating neurons to invade to the marginal zone during neurogenesis (Kask et al., 2015). Animals also display developmental defects in muscles, eyes and heart (Kask et al., 2018).

5.4. Structure of G proteins

The structure of a Gα subunit consists of two domains. The most important is a GTPase domain with catalytic activity to hydrolyze GTP that varies among different Gα members. This domain shares structural homology with the Ras family of small GTPases, and constitutes the binding site for GPCRs, Gβγ subunits and most of its effectors. The GTPase domain is structured in three different switches known as switch I, II and III that vary their conformation according to the guanine nucleotide they hold. Close to it, an α-helical domain is thought to form an inhibitory barrier and provide a regulatory entry point by GPCRs or Gβγ subunits. The N-terminus is usually

modified by attachment of fatty acids to target the protein to the plasma membrane and facilitate its interaction with Gβγ subunits, GPCRs and some effectors.

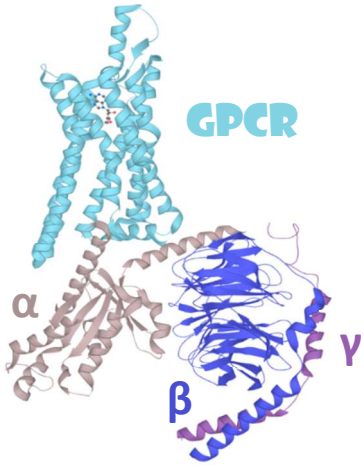

Figure I 17 Crystal structure of human adenosine A1 receptor bound to its endogenous ligand. The **receptor is shown in cian**, the **Gα is shown in light brown**, the **Gβ is shown in blue** and the **Gγ is shown in purple** (Draper-Joyce *et al.,* 2018).

The Gβ subunit is equally structured in two regions: a short α helix at the N-terminus of around 20 residues and seven WD repeats that fold the protein in β strands and form a β propeller ring. The Gγ is a much smaller subunit tightly bound to the Gβ forming a coiled-coil structure through the N-terminal regions of both subunits. Gγ is isoprenylated at the C-terminus to allow Gβγ localization at the plasma membrane

5.5. G protein subfamilies

To date 35 genes are known to encode for G proteins, 18 of which encode for Gα, 5 for Gβ and 12 for Gγ subunits. Different α, β and γ subunits can associate with each other in multiple combinations giving rise to a myriad of cellular responses. Although some subunits express ubiquitously, many others show tissue-specific expression patterns (Milligan & Kostenis, 2006).

G-proteins can be grouped into four different families based on the function and sequence similarity of their Gα subunits. The so-called stimulatory Gα proteins $G\alpha_s$ and $G\alpha_{olf}$ (olf stands for olfactory) stimulate adenylyl cyclase to increase cytoplasmic concentrations of cyclic adenosine monophosphate (cAMP), the main activator of PKA. The inhibitory G proteins $G\alpha_{i/o}$ and $G\alpha_z$ constitute the largest and most diverse subfamily and have the opposite effect. They inhibit adenylyl cyclase and abrogate AMPc production. The $G\alpha_q$ family stimulates phospholipase C, which produces IP_3 to open calcium channels at the ER and DAG to stimulate PKC. Finally, the $G\alpha_{12/13}$ regulates acting cytoskeleton by coupling to RhoGEFs that activate the Rho family of small GTPases. Within the members of each family, each type of Gα shows selectivity to bind specific

effectors and also to associate to a particular subset of GPCRs (Syrovatkina, Alegre, Dey, & Huang, 2016).

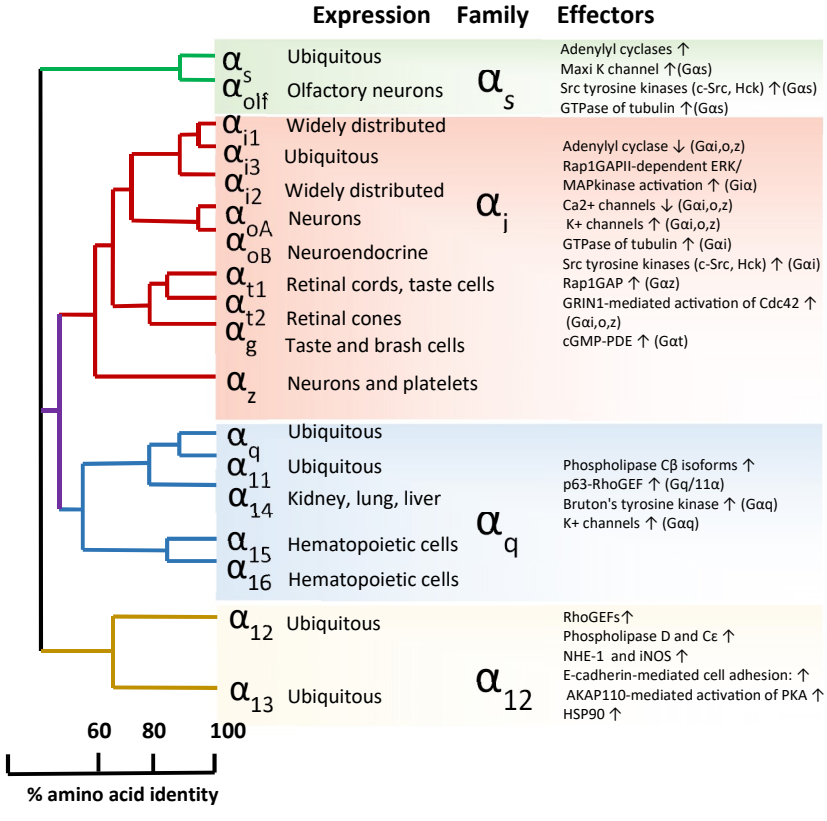

Figure I 18 Phylogenetic relationship of human and mouse Gα subunits, expression and main effectors. Adapted from Syrovatkina *et al.,* 2016

6. The $G\alpha_q$ subfamily

A wide spectrum of cellular processes are known to be mediated by $G\alpha_q$-associated GPCRs, including division, differentiation and function of cells in the immune system, central nervous system and heart, among others (He et al., 2018; Offermanns et al., 1998; Offermanns et al., 1997; Rozengurt, 1998).

The $G\alpha_q$ subfamily is composed of four members. $G\alpha_q$ and $G\alpha_{11}$ are the most abundant ones as they are expressed in a wide variety of tissues. They share a 88% sequence identity, which implies an evident overlapping between their functions (Wilkie, Scherlet, Strathmann, Slepak, & Simon, 1991). $G\alpha_{14}$ is 80% identical to $G\alpha_q$, but only expresses in some cells from liver, lung and kidney.

$G\alpha_{15}$ and $G\alpha_{16}$ are the mouse and human orthologues of the same gene, both share a 57% homology with $G\alpha_q$ and express mainly in hematopoietic cells.

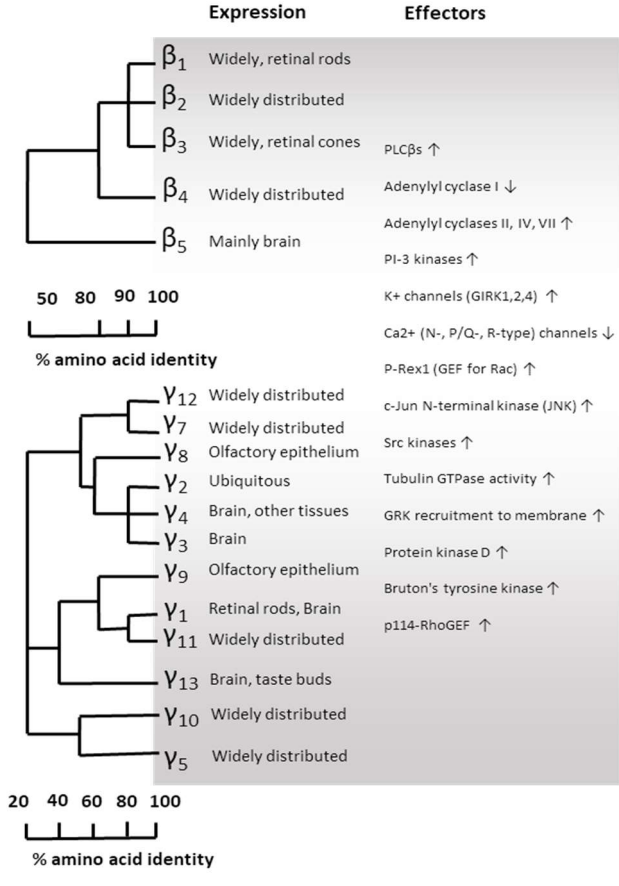

Figure I 19 Phylogenetic relationship of human Gβ subunits, expression and main effectors. Adapted from Syrovatkina *et al.*, 2016

$G\alpha_q$ and $G\alpha_{11}$ mediate the signaling of numerous neuronal receptors, such as the M1 muscarinic-acetylcholine receptor, the 5-HT2 serotonin receptors, the metabotropic glutamate receptors mGluR1 and mGluR5, the α1 adrenergic receptor and many neurotransmitter receptors (Wettschureck et al., 2005).

The physiological significance of the $G\alpha_q$ family has been addressed in several studies using $G\alpha_{q/11}$ depleted mice. An effect of $G\alpha_q$ independent of $G\alpha_{11}$ was studied in platelets, a model with no expression of $G\alpha_{11}$. $G\alpha_q$ knockout mice have impaired platelet activation in response to thromboxane A2 (TX2), ADP and thrombin, thus increasing their bleeding after injury (Offermanns, Toombs, Hu, & Simon, 1997). This phenotype was associated with the high mortality rates after birth of the $G\alpha_{q/11}$ deficient mice along with embryonic defects in cardiomyocyte hypertrophy during development (Offermanns et al., 1998).

The importance of $G\alpha_q$ was further determined in the central nervous system, where $G\alpha_q$ expression is 2 to 5-fold higher than that of $G\alpha_{11}$ (Milligan, 1993). The highest expression pattern of $G\alpha_q$ is reached in dendrites of cerebellar Purkinje cells and hippocampal CA1 pyramidal cells, both enriched in glutamatergic synapses and expressing high levels of the $G\alpha_q$-associated GPCRs mGluR1 and mGluR5. Animals lacking $G\alpha_q$ exhibit slower growth rates and their Purkinje cells remain innervated by multiple climbing fibers (CF), suggesting a role of $G\alpha_q$ in the removal of those synapsis during the firsts 2 weeks of postnatal stage. This translates in mice showing motor coordination deficiencies, loss of balance and ataxic movements (Offermanns et al., 1997). $G\alpha_q$ signaling has also been linked to the hypothalamic effects of ghrelin, the inducer of GHRH (growth hormone-releasing hormone) production and food intake. Selective $G\alpha_{q/11}$ knockout mice in glial and neuronal precursor cells show dwarfism and anorexia due to their low production of GHRH, evoking low levels of GH (growth hormone) and impairment to grow (Wettschureck et al., 2005).

GNAQ, the gene codifying $G\alpha_q$, has a protective effect from oxidative damage on SY5Y cells when stably overexpressed using lentivirus. Reduced levels of ROS are detected on SY5Y cells expressing $G\alpha_q$ (Jia et al., 2017).

In humans, somatic mutations in GNAQ are documented in 83% of blue nevi and 46% of uveal melanomas (Van Raamsdonk et al., 2009). These mutations occur exclusively in the codon affecting glutamine 209, which is essential for GTP-hydrolysis within the Ras-like domain and results in constitutive activation of the Gα, leading to PLCβ overactivation. This makes GNAQ act as an oncogene due abnormal PKC-dependent activation of MAPK, similar as the observed in tumors where the BRAF and NRAS members of this pathway are constitutively active (Van Raamsdonk et al., 2009).

Besides, post-zygotic mosaicism for the activating mutation p.R183Q for GNAQ is the major cause of Sturge-Weber syndrome, a vascular malformation involving the brain, skin, and eye. This rare neurocutaneous disorder produces epilepsy and neurologic impairments such as intellectual disability, visual defects and severe migraines (Comi, 2015; Pinto, Sahin, & Pearl, 2016; Sundaram et al., 2017). The vascular malformation in the eye results in glaucoma and can lead to vision loss. $G\alpha_q$R183Q mutation also decreases the GTPase activity of the Gα and leads to constitutive activation of RAS-RAF-MEK1/2-ERK signaling. This enhances cell proliferation and inhibits apoptosis, resulting in vascularization defects (Comi, 2015; Pinto et al., 2016; Sundaram et al., 2017).

6.1. Main effectors of $G\alpha_q$

6.1.1. Phospholipase C

Phospholipase C-β (PLCβ) was the first effector described for the members of the $G\alpha_q$ subfamily, and probably the enzyme that mediates a big contribution to their signaling effects (Runnels & Scarlata, 1999). The different isoforms of PLC catalyze the breakdown of the phosphatidylinositol 4,5 bisphosphate ($PI(4\text{-}5)P_2$) present at the plasma membrane to yield diacylglycerol (DAG) and inositol 1,4,5 triphosphate (IP_3) (Rhee, 2001). These second messengers serve to propagate and amplify the signal from different pathways. The IP_3 promotes calcium release from the ER stores by binding to and opening IP_3-dependent calcium channels. DAG stimulates the kinase activity from different isoforms of protein kinase C (PKC), promoting the phosphorylation of downstream substrates such as the members of the RAF-MEK-ERK pro-proliferative and anti-apoptotic pathway. In a similar manner as RGS proteins, PLCβ also functions as a GAP for the Gα subunit, thus enhancing its GTPase activity and leading the termination of the Gα signaling.

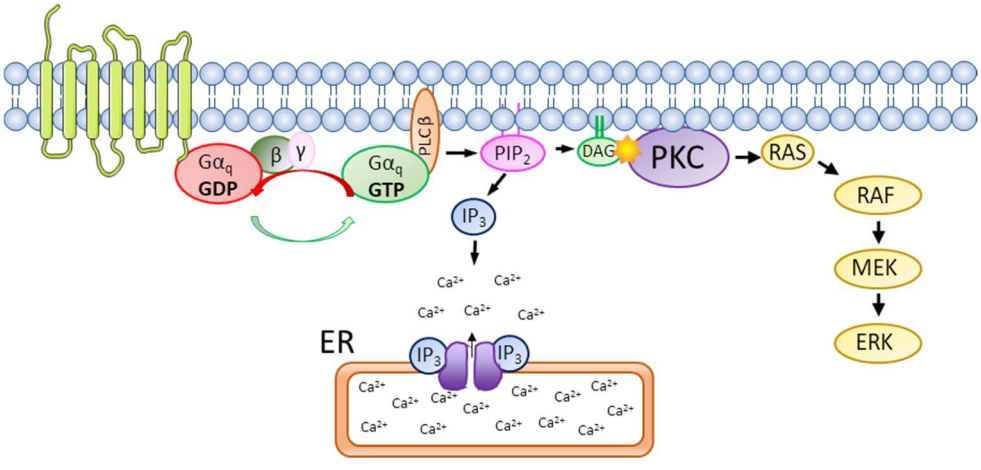

Figure I 20 $G\alpha_{q/11}$-mediated signaling pathways. In the absence of stimuli, the Gα subunit is GDP-bound. Stimulation of the GPCR makes it act as a GEF for the Gα, promoting its dissociation from Gβγ. $G\alpha_{q/11}$ GTP binds and stimulates PLCβ, which breaks PIP_2 into DAG and IP_3. While IP_3 induces calcium release from intracellular stores, DAG activates PKC to phosphorylate many downstream targets.

The mammalian PLCβ isoforms contain an N-terminal pleckstrin homology (PH) domain that, like in the case of GRKs, targets the protein to the plasma membrane and allows its interaction with Gβγ. Close to that region locate four EF hand domain, a poorly conserved catalytic XY domain locates in the center, whereas a C2 domain and a long 400 residue extension locate at the C-terminal region. This C-terminal extension is unique to the PLCβ family and contains the region of interaction with the Gα subunits, as well as the GAP activity towards the Gα. The detailed mechanism by which the PLCβ is activated through this interaction is still unclear, although all

members of the $G\alpha_q$ family can stimulate the four PLCβ isoforms. Studies with purified proteins demonstrate that $G\alpha_q$, $G\alpha_{11}$ and $G\alpha_{14}$ can strongly stimulate PLCβ1, 3 and 4 and in a lesser extent, PLCβ2. Like $G\alpha_{15/16}$, PLCβ2 is only expressed in hematopoietic cells, and both isoforms are good activators of PLCβ1, 2 and 3.

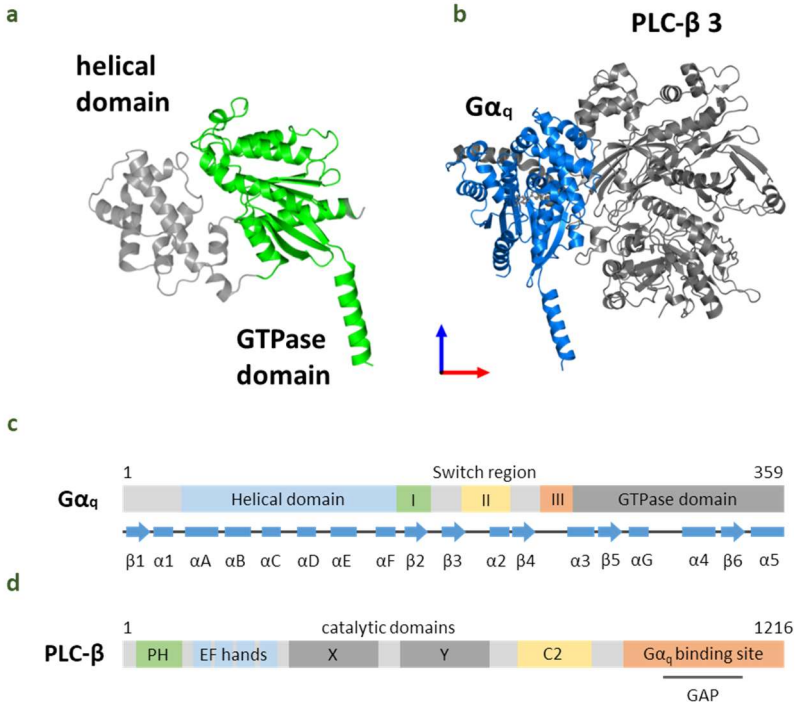

Figure I 21 Structure of activated $G\alpha_q$ and its association phospholipase C β 3. a, Representation of the crystal structure of $G\alpha_q$ with the GTPase domain in green and the helical domain in grey. **b,** Crystal structure of activated $G\alpha_q$ (in blue) bound to its effector PLC-β3 (in grey). **c,** Schematic representation of $G\alpha_q$ showing its helical domain (blue), its three switch regions (green, yellow and orange) and the catalytic GTPase domain (grey) **d,** The schematic representation of PLC-β shows its PH domain (green) four EF hand domains (blue) the X/Y catalytic domains (grey) a C2 domain (yellow) and a C terminal región where it binds $G\alpha_q$ (orange). Adapted from Waldo. *et al.*, 2010 and Mizuno *et al.*, 2009.

6.1.2. Other partners of $G\alpha_q$

Although $G\alpha_q$ signaling is tightly linked to PLCβ, more than 20 proteins are currently known to function as $G\alpha_q$ binding partners and some of them act as effectors independent of PLCβ (Litosch, 2016). One of the first identified non-phospholipase effectors was the Bruton tyrosine kinase (BTK). This kinase gets autophosphorylated upon $G\alpha_q$ interaction, acting as an activator of the p38 MAPK pro-proliferative pathway and NF-κB-dependent gene expression, among others (Sala et al., 2019; Yue et al., 2017). Mutations in this protein lead to X-linked α-gammaglobulinaemia

whereas high levels of expression constitute a marker of human glioblastomas with poor prognosis (Yue et al., 2017).

In a similar manner as $G\alpha_{12}$ and $G\alpha_{13}$, the $G\alpha_q$ family is also known activate RhoA by direct interaction with its main activators, the RhoGEFs. RhoA, along with Rac1 and CdC42, are Rho small GTPases that mediate essential processes like cell cycle progression, migration and adhesion. In particular, RhoA regulates actin cytoskeleton rearrangement and its over-activation is a primary cause of metastasis in many tumors, including colon cancer (Masià et al., 2015) and glioblastomas (Yu et al., 2019). LARG was the first RhoGEF proposed to interact with $G\alpha_q$ through an RGS box, although the relevance of this domain for the binding is still elusive since $G\alpha_q$ is able to bind the catalytic DH-PH region. Subsequent studies characterized other RhoGEFs without the RGS domain as effectors of $G\alpha_q$ that mediate RhoA activation. Trio, Duet and p63RhoGEF are examples of $G\alpha_q$-coupled RhoGEFs (Shankaranarayanan et al., 2010; Williams et al., 2007). The crystal structure of $G\alpha_q$ in a complex with p63RhoGEF revealed that it binds to a similar region than PLCβ, indicating that both effectors could be competing for the same binding site on $G\alpha_q$ (Lutz et al., 2007). Because p63RhoGEF and PLCβ can inhibit each other downstream responses, these novel binding partners allow $G\alpha_q$ to mediate different signaling cascades depending on the levels of expression and subcellular localization of each effector.

In the same direction, the WD repeat containing protein WDR36 can function as a scaffolding protein for the thromboxane receptor A_2, PLCβ and $G\alpha_q$, thus facilitating PLCβ activation (Cartier, Parent, Labrecque, Laroche, & Parent, 2011). WDR36 is necessary for axonal growth in retinal ganglion cells and mutations within its sequence are linked to primary open-angled glaucoma (Chi et al., 2010). The CD9 and CD81 members of the tetraspanin family of cell surface proteins have also been proposed to act as scaffolding proteins for $G\alpha_q$ and $G\alpha_{11}$, bringing them together with the orphan receptor GPR56 and promoting signal transduction (Little, Hemler, & Stipp, 2004). On the contrary, the PDZ domain-containing protein EBP50 can bind to and sequester GTP-bound $G\alpha_q$, which prevents PLCβ activation and inhibits $G\alpha_q$-dependent receptor endocytosis (Rochdi & Parent, 2003; Rochdi et al., 2002).

More recently, PKCζ was reported to stimulate its kinase activity by direct binding to the GTP-bound form of $G\alpha_q$. This interaction appears to be highly specific, since Gα subunits from different subfamilies failed to bind this atypical PKC, nor is $G\alpha_q$ able to interact directly with other atypical PKC isoforms (García-Hoz et al., 2010; Sánchez-Fernández et al., 2014). Interestingly, PKCζ can bind and stimulate MEK5, the upstream kinase responsible for the phosphorylation and activation of the extracellular signal-regulated kinase 5 (ERK5). ERK5 activates MAPK in response stimuli as diverse as cytokines, EGF and stress, most of which elicit their action through GPCRs (Obara et

al., 2008). PKCζ would therefore act as a $G\alpha_q$ effector to activate the MAPK pathway in response to EGF or cytokines independent of PLCβ signaling, GPCR phosphorylation and β-arrestin recruitment (Sánchez-Fernández et al., 2013).

The lipid raft resident proteins flotillin-1/reggie-2 and flotillin-2/reggie-1 also facilitate MAPK activation through $G\alpha_q$ interaction. The p38 MAPK but not ERK1/2 was inhibited upon flotillin depletion, thus evidencing a specific $G\alpha_q$-mediated activation of MAPK signaling through the lipid rafts (Sugawara et al., 2007).

Caveolin-1 and 3 (Cav-1 and Cav-3) are other relevant binding partners and probably some of the main mediators of $G\alpha_q$ localization at the plasma membrane. Caveolin are the structural proteins of caveolae, the 50–100 nm invaginations present at the plasma membrane in most differentiated mammal cells often involved in vesicular trafficking. Those microdomains are highly enriched in GPCRs and other proteins involved in cell signaling, constituting scaffolding domains that facilitate GPCR oligomerization and the recruitment of G proteins as well as many of their effectors (Calizo & Scarlata, 2012). Whilst other Gα subunits such as $G\alpha_i$ and $G\alpha_s$ mainly localize in lipid rafts, $G\alpha_q$ specifically interacts with Cav-1 and Cav-3 and concentrates in caveolae (Oh & Schnitzer, 2001). Caveolin is able to extend $G\alpha_q$ signaling in a dual manner: by binding to GTP-$G\alpha_q$ it stabilizes the active conformation and also promotes the release of Gβγ form caveolae domains, thus delaying their association with the Gα (Guo, Golebiewska, & Scarlata, 2011; Sengupta, Philip, & Scarlata, 2008). In Schwann cells caveolae concentrates $G\alpha_q$ with the metabotropic purinoceptor P2Y2 to generate Ca^{2+} signals (Takahashi-Iwanaga & Iwanaga, 2012), and depletion of Cav-1 impairs the proper interaction of $G\alpha_q$ with GPCRs, as shown with the 5-Hydroxytryptamine 2A ($5\text{-}HT_{2A}$) serotonin receptors (Bhatnagar, Sheffler, Kroeze, Compton-Toth, & Roth, 2004). On the other hand, $G\alpha_q$ interacts with and inhibits the cold-activated TRPM8 ion channel, involved in pain response in inflammatory processes (Zhang et al., 2012). This interaction depends on three arginine residues located N-terminal tail of TRPM8 and has similar outcome as bradykinin receptor B2R stimulation, producing increased pain and inflammation (Zhang, 2019).

Finally, several studies suggest a direct regulation of tubulin cytoskeleton by $G\alpha_{q/11}$. Indeed, tubulin can bind and promote the exchange of GDP to GTP within specific Gα subunits (Roychowdhury & Rasenick, 1994; Wang, Yan, & Rasenick, 1990). In neurons, muscarinic receptor activation induces tubulin relocalization from cytoplasmic subsets to the plasma membrane (Popova & Rasenick, 2000). Tubulin translocation is tightly regulated by Gβ and promotes $G\alpha_q$ transactivation. Hence, a crosstalk between $G\alpha_q$ and tubulin regulates cytoskeletal structures and downstream signaling pathways.

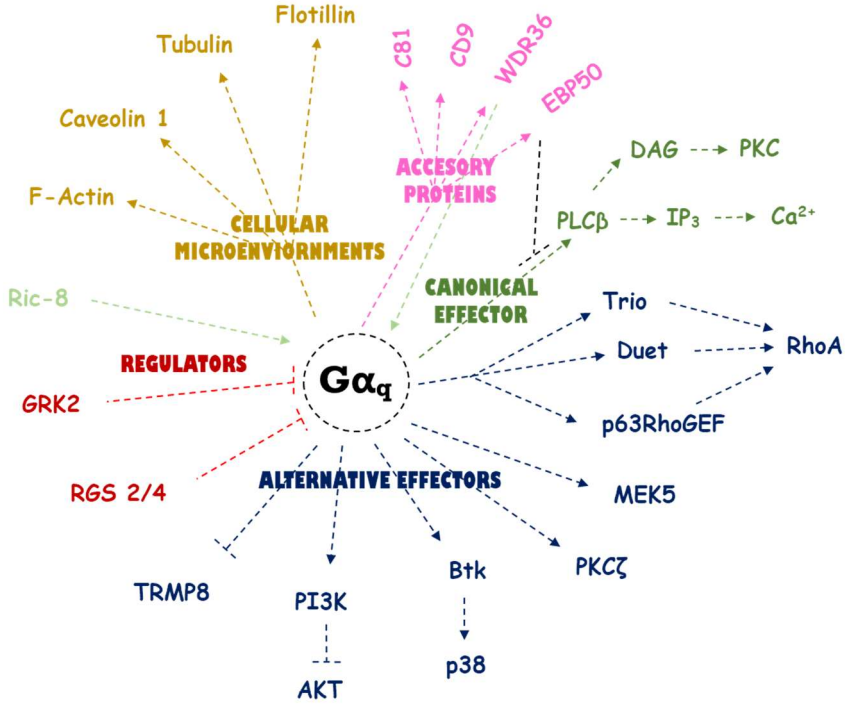

Figure I 22. Summary of the main binding partners and effectors of $G\alpha_q$. $G\alpha_q$ primarily activates PLCβ (canonical effector), although a growing number of alternative effectors mediate $G\alpha_q$ functions independently of PLCβ. They include activating effectors like RhoGEFs (Trio, Duet and p63RhoGEF), PKCζ, MEK5 and Btk and other with inhibitory effects, such as PI3K and TRMP8. The formation of these G protein–effector complexes is negatively regulated by GRK2 and RGS proteins. Ric8 potentiates $G\alpha_q$ signaling in a GPCR activation-dependent manner. Besides, $G\alpha_q$ interacts with components of the cytoskeleton such as tubulin and filamentous actin (F-Actin), and with important organizers of membrane microdomains such as caveolin-1 and flotillin which confine signaling molecules in specific domains. Adaptor proteins WDR36 and EBP50 modulate $G\alpha_q$ coupling to PLCβ, and CD9 and CD81 proteins act as protein organizers for signaling molecules facilitating receptor–$G\alpha_q$ protein coupling. Adapted from Sánchez-Fernández *et al.,* 2014

7. Non-canonical localizations of G proteins

G proteins are typically peripheral proteins tightly associated with the plasma membrane by lipid modifications. For example, all **γ** subunits are stably modified by a farnesyl or gerangeranyl group at a cysteine located at the C-terminus, and most **Gα** undergo palmitoylation on cysteines or become stably modified by myristate at glycines of their N-terminal region (Hewavitharana & Wedegaertner, 2012). But even though G proteins regulate their conventional signaling pathways while bound to the cytoplasmic surface of the plasma membrane, their intracellular localization is highly dynamic. In fact, there is an increasing amount of evidence of their roles controlling the architecture and regulating physiological functions of different organelles, including endosomes,

ER, Golgi, nucleus and mitochondria. Many of those non-canonical functions are exerted by Gβγ subunits, as demonstrated with the Gβγ-induced fragmentation of the trans-Golgi network (Irannejad & Wedegaertner, 2010), the direct binding and activation of IP_3-sensitive Ca^{2+} channels at the ER (Zeng et al., 2003), the interaction with Rab11 to activate AKT at the endosomes (García-Regalado et al., 2008) or the regulation of the transcriptional activity of the glucocorticoid receptor at the nucleus (Kino et al., 2005), to mention some examples. However, it is becoming increasingly evident that Gα subunits also localize on specific organelles including the mitochondria.

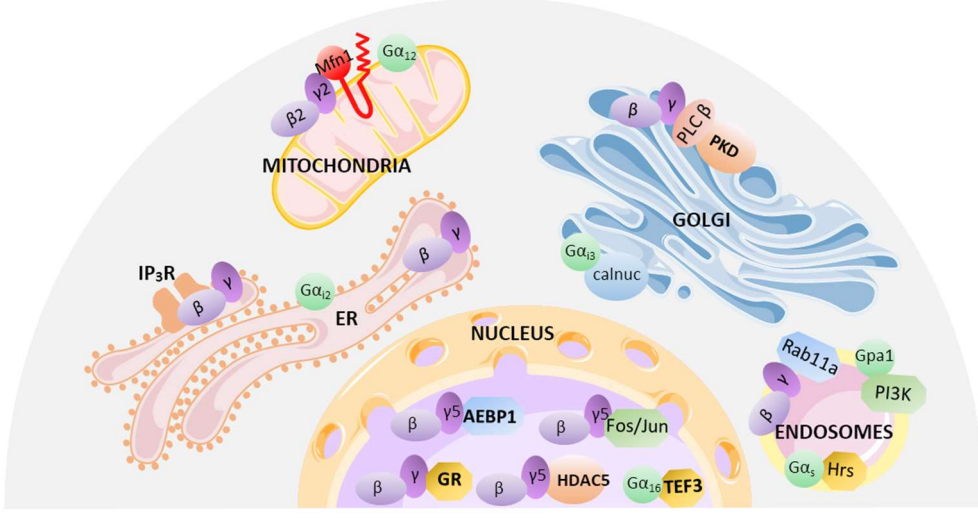

Figure I 23. Novel subcellular localizations of G proteins. Heterotrimeric G proteins have been identified to regulate effectors and their respective signaling pathways at diverse subcellular organelles. Indicated are G protein subunits that have been identified at these subcellular locations, along with their interacting effector proteins. See Table I 4 for details. Adapted from Hewavitharana and Wedegaertner 2012.

An early study detected $G\alpha_i$ and $G\alpha_s$ at the mitochondria of human placenta (Kuyznierewicz & Thomson, 2002), and a subsequent report further confirmed that $G\alpha_i$ co-localizes and co-fractionates with mitochondrial markers (Lyssand & Bajjalieh, 2007). But the first functional evidences of Gα proteins regulating mitochondrial physiology were shown in a study of $G\alpha_{12}$ using HUVEC cells as a model (Andreeva et al., 2008). The study detected a predicted mitochondrial targeting within the N-terminus of $G\alpha_{12}$ and showed that almost 40% of the endogenous G protein co-localized with mitochondrial markers in HUVEC cells. Besides, stimulation of $G\alpha_{12/13}$ signaling using lysophosphatidic acid significantly inhibited mitochondrial motility, while an increase in mitochondrial movement was observed in cells depleted for $G\alpha_{12/13}$ (Andreeva et al., 2008). $G\alpha_{12}$ mutants unable to bind and stimulate RhoA induced mitochondrial

fragmentation and decreased mitochondrial membrane potential, further reported by the upstream activation of the $G\alpha_{12/13}$ homologs in *Drosophila* (Ratnaparkhi, 2013).

Another example of a G protein regulating mitochondrial dynamics came from the interaction of Gβ2 with mitofusin1 (Mfn1). Gβ2 is enriched at the outer surface of mitochondria and localizes with Mfn1. Depletion of Gβ2 using shRNAs results in defective function of Mfn1 thus inducing mitochondrial fragmentation (Zhang et al., 2010).

	Protein	Function	References
Mito-chondri	$G\alpha_{12}$	Regulates mitochondrial morphology, motility and Bcl2-induced apoptosis.	(Andreeva et al., 2008)
	$G\alpha_s$, $G\alpha_i$	Unknown	(Kuyznierewicz & Thomson, 2002)
	$G\beta_2$	Binds to mitofusin1 and regulates mitochondrial fusion	(Zhang et al., 2010)
Golgi	Gβγ	Regulates Golgi to PM transport of proteins including insulin, regulates cellular senescence	(Añel & Malhotra, 2005; Cho, Saini, Karunarathne, Kalyanaraman, & Gautam, 2011; Irannejad & Wedegaertner, 2010; Jamora et al., 1997; Jamora et al., 1999; Saini et al., 2010)
	$G\alpha_{i3}$	Regulates secretion of heparan sulfate, vesicle trafficking, budding of membrane carriers. Interacts with calnuc in neuroendocrine cells	(Berman, Wilkie, & Gilman, 1996; Lin, Fischer, Lavoie, Huang, & Farquhar, 2009; Stow et al., 1991; Weiss et al., 2001; Wylie et al., 1999)
ER	Gβγ	Activates IP_3 receptors and stimulates calcium release, regulates unfolded protein response in *Arabidopsis*	(Wang, Narendra, & Fedoroff, 2007; Weiss, White, Huang, & Ma, 1997; Zeng et al., 2003)
	$G\alpha_{i2}$	Inhibits translocation of Sar1	(Nakagawa et al., 2011)
Endosomes	Gpa1 (yeast)	Regulates pheromone signaling via PI3K in yeast	(Slessareva, Routt, Temple, Bankaitis, & Dohlman, 2006)
	$G\alpha_s$	Interacts with endocytic protein Hrs and regulates the degradation of the EGF receptor	(Zheng et al., 2004)
	Gβγ	Interacts with Rab11 and recruits and activates PI3Kγ and Akt	(García-Regalado et al., 2008)
Nucleus	$G\beta\gamma_5$	Regulates the transcriptional repressor, adipocyte enhancer-binding protein	(Park, Muise, He, Kim, & Ro, 1999)
	Gβγ	Suppresses glucocorticoid receptor (GR) activity; recruits HDAC5 to the nucleus, represses AP-1 transcriptional activity; blocks HDAC5's inhibitory action on MEF2, regulates cardiac function	(Kino, Kozasa, & Chrousos, 2005; Kino et al., 2005; Robitaille et al., 2010; Spiegelberg & Hamm, 2005)
	$G\alpha_{16}$	Regulates activity of Transcription Factor E3 (TFE3) and the cardiomyocyte membrane protein, clauidn 14	(Sato et al., 2011)

Table I 4 Subcellular localization of G proteins at endomembranes. Adapted from Hewavitharana and Wedegaertner 2012.

8. $G\alpha_q$ localization at the mitochondria

In agreement with previous results, a mass-spectrometry analysis aimed to identify G proteins at the mitochondria found that G_{i1-2}, $G\alpha_{12/13}$ but also $G\alpha_q$ and $G\alpha_{11}$ localized on these organelles (Benincá et al., 2014). Specifically, the $G\alpha_q$ was found at the inner and outer membrane, whereas Gβγ was only present at the outer membrane, which indicates that the heterotrimer is probably together at the outer mitochondrial membrane. However, the molecular mechanisms of $G\alpha_q$ translocation into the intermembrane space are still elusive (Benincá et al., 2014). The study identified a putative mitochondrial targeting sequence located within the first its first 124 N-

terminal amino acids that could help to target the subunit to the mitochondrial membrane, although no clear cleavage site was detected. MEF cells depleted of $G\alpha_{q/11}$ showed defects in mitochondrial dynamics and physiology. The knockout cells presented a different pattern of mitochondria distribution, being more clustered at the perinuclear area and also presenting higher fragmentation. They also displayed anomalies at the mitochondrial crest and an altered pattern of Opa1 isoforms. Re-expression of $G\alpha_q$ increases mitochondrial fusion and restores the scattered mitochondrial network (Benincá et al., 2014). In fact, overexpression of $G\alpha_q$ was able to protect mitochondrial fragmentation produced by Drp expression, suggesting a role of the Gα regulating mitochondrial dynamics. The organization of respiratory chain supercomplexes presented alterations in complexes I and III. The differences in morphology correlated with a reduction in mitochondrial membrane potential (ΔΨm), oxygen consumption and ATP production. In fact, depletion of OPA1 and alteration in mitochondria crest was recently linked to efficiency in energy production (Yang et al., 2019).

Taken together, these findings put forward Gα proteins and most specially $G\alpha_q$ as novel regulators of mitochondrial dynamics and potentials transducer of signals at the mitochondria. However, the mitochondrial effectors and the molecular mechanisms that mediate such regulation are still unknown and will require further research.

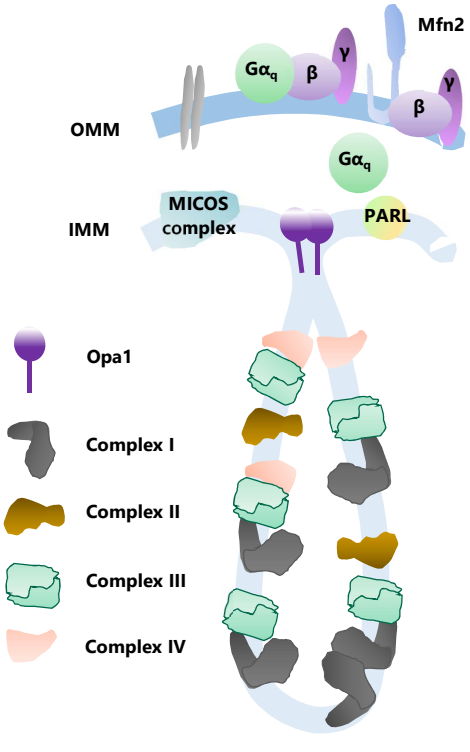

Figure I 24. $G\alpha_q$ regulates mitochondrial dynamics and bioenergetics.

1. $G\alpha_q$ is necessary to keep O_2 consumption and ATP production
2. Opa1 isoforms are altered in the absence of $G\alpha_q$.
3. Mitochondria cristae are altered in the absence of $G\alpha_q$.
4. Alterations in mitochondrial supercomplexes containing complex I and III are present in the absence of $G\alpha_q$.
5. Mitochondria cristae determines the proper assembly of the supercomplexes and the functionality of the respiratory chain.

Adapted from Benincá et. al., 2014.

OBJECTIVES

Studies carried out over the last 20 years have helped us to unveil novel signaling pathways and subcellular localizations for G proteins. In contrast with previous assumptions, signals leading to G protein activation can be diverse and independent from GPCRs, as is the case for Ric-8 and other proteins with GEF activity towards the Gα (Coleman et al., 2016; Siderovski & Willard, 2005; Tall, 2013). Moreover, there is a growing evidence that heterotrimeric G proteins are not restricted to the plasma membrane; they can also localize and signal from cellular endomembranes including endosomes, Golgi, ER, the nucleus and the mitochondria (Andreeva, Kutuzov and Voyno-Yasenetskaya, 2008; Sato et al., 2011; Nakagawa et al., 2011). In this regard, our group provided evidence of a novel localization of $G\alpha_q$ at the mitochondria, where it plays important roles regulating the physiology of these organelles. Depletion of $G\alpha_q$ not only disrupts canonical signaling through PLCβ, but also alters cellular homeostasis by direct disruption of mitochondrial morphology. In particular, $G\alpha_q$ affects mitochondrial dynamics and is required for the proper formation of the infoldings at the inner mitochondrial membrane (Benincá et al., 2014). Its absence impairs the assembly of the complexes involved in electron transport chain and yields significant decreases in oxygen consumption and ATP production (Benincá et al., 2014). Here, we aim to identify the putative binding partners of $G\alpha_q$ at the mitochondria to better understand the molecular mechanisms by which $G\alpha_q$ regulates the function of these organelles. We oriented our work on neurons, highly differentiated cells whose physiology is tightly dependent on mitochondrial function, to link this putative regulation with the onset of neurodegenerative diseases.

Specific objectives

1. Identify possible binding partners of $G\alpha_q$ at the mitochondria.
2. Investigate the molecular mechanism of interaction of novel $G\alpha_q$ partners and their effect at the mitochondria.
3. Unveil the potential implications of the novel $G\alpha_q$ signaling pathways at the mitochondria for neuronal physiology.

MATERIALS AND METHODS

1. MATERIALS

1.1. Buffers and solutions

BUFFER	COMPOSITION	COMMENTS
Alex3 Lysis Buffer	50 mM Tris-HCl pH7.5 150 mM NaCl 5 mM EDTA 1% Triton X-100 10% Glycerol 10 mM NaF 50 mM $Na_2H_2P_2O_7$ 1.5 mM $MgCl_2$	
	200 nM Na_3VO_4 0.5 µg/ml Aprotinin 0.5 µg/ml Leupeptin	Added fresh
Alex3 Wash Buffer	10 mM Tris HCl pH 8.0 300 mM NaCl 1 mM EDTa 1 mM EGTA 1% Triton X-100 0.5% NP-40 1.5 µM $MgCl_2$	
Buffer PD $G\alpha_q$ purified	100 mM NaCl 20 mM HEPES 2 mM $MgCl_2$ 0.5 mM EDTA	
	1 mM DTT 1 µM GDP/GTP/GTPγS	Added Fresh
	10 mM NaF 30 µM $AlCl_3$	When needed, to induce activation of GDP-bound GTPases
Buffer PD	50 mM Tris-HCl pH7.5 150 mM NaCl 1 mM NP-40 0.25% deoxycholate 1 mM EGTA pH 8.0 1 mM NaF	
	20 nM Na_3VO_4 5 µg/ml Aprotinin 5 µg/ml Leupeptin 0.1 µM PMSF	Added fresh
DNA sample buffer 6X	10 mM Tris-HCl pH 7.6 0.15% (w/v) bromophenol blue 0.15% (w/v) xylen cyanol 60% (v/v) glycerol 60 mM EDTA	
HNME buffer	20 mM HEPES-NaOH pH 8.0 100 mM NaCl2 2 mM MgCl2 1 mM EDTA 1 µM GDP 11 µM CHAPS	
LB broth	1% NaCl (w/v) 1% (w/v) bacto-tryptone 0.5% bacto-yeast extract	autoclaved
LB agar	LB broth 1.5% (w/v) agar	

BUFFER	COMPOSITION	COMMENTS
Minimal Medium (MM)	0.4% glucose (w/v) 0.8% Casaminoacids (w/v) 1 mM $MgSO_4$ 0.3 mM $CaCl_2$ M9 salts containing: 33.7 mM Na_2HPO_4 22.0 mM KH_2PO_4 8.55 mM NaCl 9.35 mM NH_4Cl	After adding glucose and casaminoacids, bring it to a volume of 4.5l, autoclave and let it cool. Then add 500 ml of M9 salts x10
NiNTA-Lysis Buffer	50 mM NaH_2PO_4 300 mM NaCl 10 mM Imidazole	Adjust to pH=8
NiNTA -Wash Buffer	50 mM NaH_2PO_4 300 mM NaCl 20 mM Imidazole	Adjust to pH=8
NiNTA -Elution Buffer	50 mM NaH_2PO_4 300 mM NaCl 250 mM Imidazole	Adjust to pH=8
PBS	137mM NaCl 2.7 mM KCl 10 mM Na_2HPO_4 2 mM KH_2PO_4	
Polyacrylamide gel (stacking)	5% Acrylamide 126.7 mM Tris-HCl pH 6.8 0.01% SDS 0.01%APS 0.005% TEMED	TEMED added at the end to induce polymerization
Polyacrylamide gel (resolving)	8-12% Acrylamide 375 mM Tris HCl pH 8.8 0.1% SDS 0.1%APS 0.005% TEMED	TEMED added at the end to induce polymerization
SDS-running buffer(10X)	0.21 M Tris Base 1.92 M glycine 35 mM SDS	
TAE	40 mM Tris-acetate pH 7.6 1 mM EDTA	
TBS (10X)	0.1 M Tris Base 1.5 M NaCl	Adjust to pH 7.4
TBS-Tween (1X)	TBS 1X 0.1% (v/v) Tween 20	
Transfer Buffer (10X)	25 mM Tris base 192 mM glycine 10% methanol	
Triton Buffer	100 mM NaCl 20 mM HEPES 2 mM $MgCl_2$ 0.5 mM EDTA 0.15% (v/v) TritonX-100	

1.2. Oligonucleotides

PRIMER	SEQUENCE	COMMENTS
Alex3 FL BamHI Fw	CGCGGATCCGGCTACGCCAGGAAAGTAG	To generate the GST tagged Alex3
Alex3 (30-x) BamHI Fw	CGCGGATCCGGAAGAAAGCAGAACAAGGAG	To generate the GST tagged Alex3
Alex3 (111-379) BamHI Fw	CGCGGATCCCCTAATTCAGACGATACTGTTTTGT C	To generate the GST tagged Alex3
Alex3 FL His HindIII Rv	GGCAAGCTTTTCCTGACTCTTTGGGAACATC	To generate the His tagged Alex3
Alex3 FL GST EcoRI Rv	GCGGAATTCCTTCCTGACTCTTTGGGAACATC	To generate the GST tagged Alex3
Alex3 (x-111) EcoRI Rv	GCGGAATTCCAGGAGAAGCCCTTTTCTGTAC	To generate the GST tagged Alex3
BPCR1 Fw IRES	CCGGGGTACCGATATCGAATTCCTGCAGCCCG	To sequence the clones from $G\alpha_q$-IRES-DsRed clonning
BPCR2 Fw COX	GGCCACAACCATGTCCGTCCTGACGCCGC	To sequence the clones from $G\alpha_q$-IRES-DsRed clonning
BPCR3 Rv IRES	CAGGACGGACATGGTTGTGGCCATATTATCATC GTG	To sequence the clones from Gq-IRES-DsRed clonning
BPCR4 Rv DsRed	GGAGAATTCTAAGACAGGAACAGGTGGTGGG	To sequence the clones from Gq-IRES-DsRed clonning
Gq fw seq	AGAGGTTGATGTGGAG	To sequence $G\alpha_q$ vectors for the proper mutations
Gq NheI Rv	GGCCCGATCGTTAGACCAGATTGTACTCCTTCAG GTTC	To clone $G\alpha_q$ in IRES-DsRed vector
Gq NheI Fw	CCGGGCTAGCATGACTCTGGAGTCCATCATGGC G	To clone $G\alpha_q$ in IRES-DsRed vector
IRES GqRC fw	GACGTGCTTAGAGTTTGTGTCCCCACTACAGGGA	To mutate R183 to C in IRES- $G\alpha_q$wt
IRES GqRC Rv	TCCCTGTAGTGGGGACACAAACTCTAAGCACGTC	To mutate R183 to C in IRES- $G\alpha_q$wt
IRES Gq QL fw	CGATGTAGGGGGCCTAAGGTCAGAGAGAAG	human sequence
IRES Gq QL Rv	CTTCTCTCTGACCTTAGGCCCCCTACATCG	human sequence
pGW1_M13 reverse primer	CATGGTCATAGCTGTTTCC	Used for sequencing
Primer TRAK HindIII	GGGTCTTTTCTGCAGTCACC	Used for sequencing HA-TRAK proteins

1.3. Primary antibodies

ANTIBODY	SPECIE	SUPPLIER	REFERENCE	DILUTION AND USE
ARMCX3 (Alex3)	rabbit	Proteintech	25705-1-AP	WB 1:1000 IP 1:200 IF 1:500
DsRed	rabbit	Clontech	632496 Lot 1206009	WB 1:2000
FLAG M2	mouse	Sigma	F 1804	WB 1:1000 IP 1:200
GFP	rabbit	Dr. S. Pons (IBMB-CSIC)	Self-made	WB 1:5000
GFP	rabbit	Invitrogen	A11122 Lot #1828014	IP 1:200 WB 1:2000
GFP trap_A beads	alpaca	Chromotek	Gta-20 lot 61102001A	IP 1:200
GST	mouse	Sigma	SAB4200237	WB 1:2000
$G\alpha_q$	mouse	BD biosciences	612704	WB 1:1000 IF 1:200
$G\alpha_q$	rabbit	A. Aragay	MI Simon, Caltech, USA	WB 1:2000
$G\alpha_q$ (E-17)	rabbit	Sta Cruz	sc-393 Lot#3012	WB 1:1000 IP 1:200 IF 1:500
$G\alpha_{q/11}$ (C-19)	rabbit	Sta Cruz	sc-392 Lot#D1212	WB 1:1000 IP 1:200
$G\alpha_q$ specific	mouse	Sta Cruz	Sc-136181 Lot#C1418	WB 1:500
$G\alpha_{11}$ specific	mouse	Sta Cruz	Sc-390382 Lot#A2617	WB 1:500
HA (12CA5)	mouse	Roche	11583816001	IP 1:100
HA high affinity	rat	Roche	11867423001	WB 1:2000 IF 1:500
HA agarose conjugate	mouse	Sigma	A2095	IP 1:25
HSP-90	Mouse	BD	610419 Lot#25560	WB 1:2000
MAP2	rabbit	Abcam	ab32454	IF 1:1000
Miro1	mouse	Abcam	188029 clone 1083	WB 1:1000
myc	mouse	Millipore	05-724 Lot DAM 1632070	WB 1:2000 IP 1:200
Myc 9E10	mouse	Sigma	M4439	IP 1:200 WB 1:2000
MycTrap_A beads	alpaca	Chromotech	61102003A	IP 1:200
MyosinX (c-1)	mouse	Sta cruz	Sc-166720 Lot J0914	WB 1:1000 IP 1:200 IF 1:500
RhoT1 (Miro1)	rabbit	Sigma/Atlas antibodies	HPA010687	WB 1:000
TOM20(F-10)	mouse	Sta Cruz	Sc-17764 Lot#B2018	IF: 1:500
Tom20 (FL-145)	rabbit	Sta Cruz	sc-11415	IF 1:500
Tuj1	mouse	Sigma	MAB1637	IF 1:500
UKHC (F-5)(KIF3)	mouse	Sta Cruz	SC-133184 Lot g1112	WB 1000
β-tubulin	rabbit	Sigma	T2200	WB 1:2000

1.4. Secondary antibodies

ANTIBODY	SPECIE	SUPPLIER	REFERENCE	DILUTION
Alexa Fluor anti-mouse 488	donkey	Thermo scientific	A-21202	IF 1:200
Alexa Fluor anti-mouse 568	donkey	Thermo scientific	A-10037	IF 1:200
Alexa Fluor anti-mouse 647	goat	Thermo scientific	A-21236	IF 1:200
Alexa Fluor anti-rabbit 488	donkey	Thermo scientific	A-21206	IF 1:200
Alexa Fluor anti-rabbit 568	goat	Thermo scientific	A-11011	IF 1:200
Alexa Fluor anti-rabbit 647	goat	Thermo scientific	A-21244	IF 1:200
Alexa Fluor anti-rat 488	donkey	Thermo scientific	A-21208	IF 1:200
Alexa Fluor anti-rat 568	goat	Thermo scientific	A-11077	IF 1:200
Alexa Fluor anti-rat 647	goat	Thermo scientific	A-21247	IF 1:200
IRDye 680 anti-mouse	goat	LI-COR	925-68070	WB 1:20000
IRDye 800 anti-mouse	goat	LI-COR	925-32210	WB 1:20000
IRDye 680 anti-rabbit	donkey	LI-COR	926-68073	WB 1:20000
IRDye 800 anti-rabbit	goat	LI-COR	925-32211	WB 1:20000
IRDye 680 anti-rat	goat	LI-COR	926-68076	WB 1:20000

1.5. Plasmids

PLASMID	VECTOR	SOURCE
Alex3 GFP	pEGFPN1	Prof. E. Soriano, UB
Alex3 myc	pSecTag	Prof. E. Soriano, UB
Alex3ΔNt GFP	pEGFPN1	Prof. E. Soriano, UB
Alex3ΔCt GFP	pEGFPN1	Prof. E. Soriano, UB
Alex3 1-106 GFP	pEGFPN1	Prof. E. Soriano, UB
Alex3 1-45 GFP	pEGFPN1	Prof. E. Soriano, UB
Alex3 GST 30-379(FL)	pGEX2T	Clonned in the lab
Alex3 GST 30-107(Nt)	pGEX2T	Clonned in the lab
Alex3 GST 107-379(Ct)	pGEX2T	Clonned in the lab
Alex3 GST 107-273(Ct1)	pGEX2T	Clonned in the lab
Alex3 GST 273-379 (Ct2)	pGEX2T	Clonned in the lab
Alex3 6xHis	pQE9	Clonned in the lab
Armcx10 myc	pSecTag	Prof. E. Soriano, UB
Armcx10 GFP	pEGFPN1	Prof. E, UB Soriano
Envelope	pVSVG	Addgene
ER-DsRed	pCMV	Prof. A. Zorzano, IRB
Gag/Pol viral proteins	pCMWdR8.91	Addgene
GFP	pEGFPN1	Clontech
GFP	pEGFPC1	Clontech
GST	pGEX2T	Addgene
GST	pGEX4T	Sigma
$G\alpha_q$	pcDNA3.1	clonned from pCis, M. Simon
$G\alpha_q$	pCis	Prof. M. Simon, Caltech, USA
$G\alpha_q$R183C	pcDNA3.1	Clonned from pCis
$G\alpha_q$R183C	pCis	Prof. Melvin Simon
$G\alpha_q$Q209L	pcDNA3.1	Prof. C. Ribas, UAM
$G\alpha_q$Q209L/R256A/T257A	pcDNA3.1	Prof. C. Ribas, UAM
$G\alpha_q$ GFP	pcDNA3.1	C. Berloch
$G\alpha_q$ R183C GFP	pcDNA3.1	Clonned in the lab
$G\alpha_q$Nt GFP	pcDNA3.1	Clonned in the lab
$G\alpha_q$MAS70 GFP	pcDNA3.1	Clonned in the lab
IRES-mtDsRed	pCAG IRES	Prof. J. Kittler, UK
IRES-mtDsRed $G\alpha_q$	pCAG IRES	Prof. J. Kittler, UK
IRES-mtDsRed $G\alpha_q$R183C	pCAG IRES	Prof. J. Kittler, UK
KIF5c myc	pcDNA3.1	Prof. E. Soriano, UB
LifeAct RFP	pCMV	Ibidi
Miro1 Cherry	pCDH	Dr. C. Benincá, MRC, UK

PLASMID	VECTOR	SOURCE
Miro1 GFP	pEGFP	Prof. J. Kittler, UK
Miro1 myc	pRK5	Prof. J.Kittler, UK
Miro1ΔEF myc	pRK5	Prof. J. Kittler, UK
Miro1 6-800 GST	pGEX2T	Prof. J. Kittler, UK
Miro1 6-388 GST	pGEX2T	Prof. J.Kittler, UK
mtDsRed	pcDNA3.1	Prof. A. Zorzano, IRB
pcDNA3.1+	pcDNA3.1	Invitrogen
sh Gαq 1	pLKO1	MISION Sigma (Functional genomics core)
sh Gαq 2 GFP	pLKO3G	Clonned in the lab
sh scr GFP	pLKO3G	MISION Sigma (Functional genomics core)
Synaptophysin GFP	pEGFP	Prof. J. Kittler, UK
TOM20 cherry	pCDH	Dr. C. Benincá, MRC, UK
TRAK1 HA	pGW1	Prof. J. Kittler, UK
TRAK2 HA	pGW1	Prof. J. Kittler, UK
TRAK2 myc	pcDNA3.1	Prof. E. Soriano, UB

1.6. Reagents

NAME	SUPLIER	REFERENCE	COMMENTS
acrilamide	SIGMA	A2792	Add 63 ml $_{dd}H_2O$ to each bottle and mix
Blocking buffer Odyssey	Servicios hospitalarios	9276-50100	
BSA IGg free	SIGMA	A-2058-5G	
CHPG	SIGMA	C7743-5MG	
Clozapine N-oxide dihydrochloride 10	Tocris	6329	
DMEM/F12	Thermo Scientific	31331028	
DMEM high glucose/with glutamax 500 ml	Invitrogen	31966021	
FBS	SIGMA	F7524	
FBS GIBCO 500 ml	Invitrogen	10270106	
FuGENE(R) 6 Transfection Reagent	Promega	E2692	
G418 disulfate	SIGMA	A17201G	Stock 250 mg/ml working concent.: 250 µg/ml
$G\alpha_q$ (purified protein)	Laboratory of Gregory G. Tall, PhD	EUR007 University of Michigan	
GDP	SIGMA	G7127-25MG	Stock: 10 mM Working concent.: 10µM
GDP-β-S	SIGMA	G7637-5MG	Stock: 10 mM Working concent.: 10µM
Gluthatione sepharose 4B slurry	GE Healthcare	GE17-0756-01	
GTP	SIGMA	G8877-10MG	Stock: 10 mM Working concent.: 10µM
GTP-γ-S	SIGMA	G8634-5mg	Stock: 10 mM Working concent.: 10µM
IPTG	Sigma	10724815001	
L-glutamine	Life technologies	25030-024	
Lipofectamine 2000	Thermofiher	Fisher 11668027	
Neurobasal Medium	Thermo Scientific	21103049	
Ni-NTA Magnetic Beads	Thermo Scientific	88831	
Normocin (Invivogen)	Nucliber	ant-nr-1	
Page Ruler Prestained protein Ladder	Thermo scientific	26616	
Pen Strep 100X	Lab Clinics	L0014-100	

NAME	SUPLIER	REFERENCE	COMMENTS
Prolong Diamond Antifade mountant with DAPI	INVITROGEN	P36966	Mounting medium
Protein A-Sepharose	GE healtcare	17-0780-01	
Protein G Sepharose	GE Healthcare	ab193259	
Puromicine dihidrocholide	SIGMA	P8833-10mg	Working concentration: 1 to 10 µg/µl
SYBR Safe DNA gel stain	invitrogen	S33102	
TrackIt 1 Kb Plus DNA Ladder	Invitrogen	10488085	
TRYPAN BLUE STAIN 0.4%	Invitrogen	T10282	
Trypsin EDTA	Thermo scientific	25200056	
YM-254890 ($G\alpha_q$ inhibitor)	Focus Biomolecules	10-1590-0100	

1.7. Cell lines

CELL LINE	DESCRIPTION	SOURCE
COS7	African green monkey kidney, SV40 transformed	Sigma
HEK-293	Human embryonic kidney cells stably expressing the Epstein Barr Virus (EBV). EBNA-1 gene from pCMV/EBNA	Invitrogen
HEK-293T	Human embryonic kidney cells containing Adeno and SV-40 viral DNA sequences	ATCC
HeLa	Human epithelial cells containing papilloma virus	SIGMA
MEF wt	Mouse embryonic fibroblasts	Prof. A. Zorzano
MEF KO $G\alpha_{q/11}$	Mouse embryonic fibroblasts depleted for $G\alpha_q$ and $G\alpha_{11}$	Prof. S. Offermanns
MEF KO $G\alpha_{q/11}$ + $G\alpha_q$	Mouse embryonic fibroblasts depleted for $G\alpha_q$ and $G\alpha_{11}$ stably expressing $G\alpha_q$	Prof. S. Offermanns
SH-SY5Y	Neuroblastoma cells	Prof. C. Gallego

2. METHODS

2.1. DNA manipulations

2.1.2. DNA mutagenesis

Specific residues were mutated using QuickChange® Lightning site directed mutagenesis Kit (Agilent Technologies®) following the manufacturer's guidelines. The mutagenesis kit uses a double-stranded supercoiled plasmid containing the insert of interest and two primers with the desired mutation, each complementary to opposite strands of the vector, to generate a mutated plasmid after extension by PfuUltra HF DNA polymerase. The parental methylated or hemymethylated DNA is subsequently digested for 5 min at 37ºC using Dpn I endonuclease and the resulting nicked DNA vector with the desired mutation is transformed using Heat-shock to XL10-Gold ultracompetent cells (provided by the kit) and plated onto LB-Agar plates. Resulting colonies are grown onto LB-ampicilin (10 µg/ml) for mini-prep preparation and plasmids are sent for sequencing. After proving the integrity and desired mutation, cDNAs are amplified in larger scale using either Quiagen® MaxiPrep Kit to transfect cell lines or Quiagen® MaxiPrep Kit Endo-Free to transfect primary neurons.

2.1.3. Storage, transformation and purification of plasmid DNA

Plasmids were transformed into bacteria by electroporation (*E. coli* strains DH10B) or heat shock (*E. coli* strains DH5α) and kept in the presence of 10% glycerol at -80ºC.

- Electroporation

For electroporation, 30 µl of DH10B electrocompetent bacteria stored at -80ºC were thaw on ice for 10 min before addition of 1 µl of plasmid DNA (containing around 10 ng of plasmid DNA) and incubated 15 min on ice, transferred to the electroporation cuvette and electroporated using a GENE PULSER II from BioRad® at 200 Ohms, 25 mF and 2.5 V. Following electroporation, 1 ml of LB medium (see buffer and solutions list) was added, the bacteria mix was incubated at 37ºC for 30 min. Finally, 100 µl of the bacteria were plated onto LB plates containing the appropriate antibiotic and incubated overnight at 37ºC.

- Heat shock

To transform bacteria by heat shock, 100 µl of DH5α competent cells stored at -80ºC were thaw on ice before addition of 2 µl of the desired plasmid (containing around 20 ng of DNA). The mixture was incubated on ice for 20 min, placed on the water bath at 42ºC for 60 s and back to ice 2 more min. Next, 1 ml of LB medium pre-warmed at 37ºC was added to the mixture and incubated 30 to 60 min at 37ºC with continuous shaking. Around 200 µl of the resulting culture

was planted onto pre-warmed LB plates containing the appropriate antibiotic and incubated overnight at 37ºC

2.1.4. DNA purification from bacteria cells

To purify plasmid DNA from bacterial cultures, a single colony was picked up from LB plates, added into 3 ml LB medium with the proper antibiotic and incubated overnight at 37ºC with continuous shacking. Small-scale purification of plasmid DNA (Mini-Preps) was performed from 1.5 ml of bacterial culture harvested by RT centrifugation at 6800xg, using the GeneJET Plasmid miniprep Kit (Thermo scientific®) following the manufacturer's guidelines.

For large-scale DNA purification (Maxi Preps), bacterial culture was expanded by incubating overnight 500 µl of the previous culture with 200 ml of LB medium containing the proper antibiotic, at 37ºC with continuous shacking. Cells from the saturated culture were harvested by centrifugation at 6000xg for 15 min at 4ºC, and DNA was purified using either Quiagen® MaxiPrep Kit (to transfect cell lines) or Quiagen® MaxiPrep Kit Endo-Free (to transfect hippocampal neurons) following in each case the manufacturer's instructions. Plasmid DNA was resuspended into 200 µl of TE buffer and stored at -20ºC.

2.1.5. DNA integrity and quantification

The fidelity of the cDNAs from MaxiPreps was determined by digestion with the proper restriction enzymes and samples were resolved in a 0.8% (w/v) agarose gel. DNA concentration was measured using a ND-1000 Nanodrop spectrophotometer (Thermo Scientific®) at 260 nm. The ratio 260/280 nm was used as measure of quality control.

2.1.6. PCR and agarose gel electrophoresis

For PCR, specific oligonucleotides complementary to the flanking regions of the target sequence were designed. When using the PCR products for cloning, restriction endonuclease cleavage sites were included at the desired ends of the oligonucleotide. To mutate specific residues, forward and reverse oligonucleotides were designed from the region containing the desired mutation and PCR reaction was performed using QuickChange® Lightning Site-directed mutagenesis kit (Agilent®) according to the manufacturer's guidelines. Up to 50 µl of PCR mixture were prepared and the reaction was carried out in the Thermal Cycler MJMini (BioRad®) under the conditions described on table M1.

PCR mixture
1 ng/µl DNA template
1x HF or GC Phusion Buffer
10 mM dNTPs
2.5 µM oligonucleotide forward
2.5 µM oligonucleotide reverse
20 U/ml Phusion

STEP	CYCLES	TIME (sec)	TEMP (ºC)
1	1	120	95
2	30	20	95
3	30	30	55
4	30	240	65
5	Repeat steps 2 to 4, 18 times		
6	1	300	65

Table M 1. Composition of the PCR mixture (left) and thermocycling conditions (right)

Plasmid DNAs, PCR fragments and products of digestion with restriction enzymes were analyzed by electrophoresis in 0.8 %-1% (w/v) agarose gel in TAE buffer (see buffer list). To make the agarose gel, electrophoresis grade agarose (Invitrogen®) was added into TAE solution, heated in the microwave and swirled until no suspension particles were visible. To visualize DNA, 1:10000 (v/v) SYBR Safe DNA gel stain (Invitrogen®) was added into the agarose before letting it solidify in a mold adapted with the suitable wells. DNA samples were loaded into the wells in DNA sample buffer (see composition in materials) and run along-side 5 µl of 2-Log DNA ladder (BioLabs®). Gels were run 15 to 30 min at 70 V and visualized using a GeneGenius image system (SynGene®). To cut the bands for cloning the Safe Imager 2.0 Blue Light transilluminator (Invitrogen®) was utilized.

2.1.7. DNA digestion

PCR products were purified using ilustra GFX DNA and Gel Band Purification Kit (GE Healthcare®) following manufacturer's protocol and digested with the appropriate restriction endonucleases (NEBiolabs® or Fermentas®). Approximately 1 µg of vector was also digested with 2 U endonuclease in a final volume of 50 µl. The digestion reaction was performed at 37ºC for at least 2 h using a suitable buffer to allow activity of both enzymes. In case a single buffer could not match good activity of both endonucleases, sequential digestion using a specific buffer and optimal reaction conditions for each enzyme were required. In such case, DNA purification was carried out after each digestion using the GFX™ PCR DNA and Gel Band Purification kit (GE Healthcare®). The digested insert and vector were separated by agarose gel electrophoresis and purified using the same purification kit following manufacturer's instructions.

2.1.8. DNA ligation

The ligation reaction was performed at 16ºC using 50 U/ml of T4 DNA Ligase (NEBiolabs®). The optimal ration of insert and vector was estimated using the following formula:

$$\text{Insert concentration} \times \text{Vector (bp)} = \text{Insert (bp)} \times \text{Vector concentration}$$

The ligation products were transformed by heat shock and the resulting cells were incubated overnight at 37ºC. Grown colonies were picked and checked by PCR under the previous

conditions or amplified for mini-prep (GeneJET Plasmid miniprep Kit, Thermo scientific®). In such case, plasmid DNA was digested with the proper enzymes and an agarose gel electrophoresis was run to verify the presence of the band corresponding to the insert. Positive colonies were then sequenced to avoid undesired mutations and amplified by MaxiPrep (Quiagen®) after verification.

2.1.9. DNA sequencing

Plasmids coming from cloning or mutagenesis experiments were sequenced using BygDye v1.1 kit and the 3730 Sequencer at the Sequencing Capillary Service of the CRAG (Center for Research in Agrigenomics, Autonomous University of Barcelona). Specific primers were used to verify the mutations and fidelity of the cDNAs. Sequenced plasmids were analyzed using BLAST program (NIH) and compared side by side with the suitable sequences from UNIPROT library.

2.2. Cell culture

2.2.1. Maintaining and subculturing the cells

Manipulation of mammal cells was carried out in a laminar flow cabinet (ESCO Labculture). Cells were cultured using the suitable medium (table M2) and maintained at 37ºC in a humidified atmosphere with 5% CO_2. (Core scientific services-PCB). To subculture the cells, 10 cm plates or T75 flasks (Thermo Scientific®) containing adherent cells were washed with 10 ml PBS, incubated with 1 ml trypsin-EDTA (Invitrogen®) for 2 min at 37ºC until cells detached and resuspended in fresh pre-warmed medium. The usual passage ratio ranged between 1:5 and 1:20 and passages were carried out twice a week, depending on the cell line and their confluence.

Cells	Medium	FBS (v/v)	L-Glu	Pen/Strep	Normocin	G418
EBNA293	DMEM (Gibco) +G418	10%	2 mM	0.01%/0.063%	0,1 mg/ml	200 µg/ml
HEK293T MEF HeLa COS7	DMEM (Gibco)	10%	2 mM	0.01%/0.063%	0,1 mg/ml	-
SHSY5Y	DMEM F12 (Gibco)	15%	2 mM	0.01%/0.063%	0,1 mg/ml	-
Primary neurons	Neurobasal (Gibco) +Glia conditioning medium	10%	2 mM	0.01%/0.063%	-	-

Table M 2. Composition of the cell medium for the different cell lines cultured throughout this work.

2.2.2. Cell counting

Cell counting after trypsinization was performed with the Countess II Automated Cell Counter (ThermoFisher Scientific®). For that, around 100 µl of suspension cells were separated into

Eppendorf tubes to avoid possible contaminations, while the remaining cells to be used were kept into a sterile 50 ml Falcon tube. A small volume of cells from the Eppendorf aliquot were mixed with 0.4% trypan blue (Sigma®) in a 1:1 dilution to allow detection of death cells, and 10 µl of the resulting mixture were loaded into the provided slides. Cells were then analyzed in the cell counter. The counter was set to automatically detect the number of cells in the initial suspension assuming the 1:1 trypan blue dilution (Sigma®), and provides the total number of cells as well as the living cells that were not stained with the dye. Only the number of living cells was considered for all our experiments.

2.2.3. Storage and Freezing

Cells from a 10 cm dish at 90% confluence (approximately 3-4x10^6 cells) were collected by trypsin digestion, centrifuged at 900xg, resuspended in 1.5 ml of fresh medium and kept on ice for 5 min. The same volume of cold freezing medium containing 20% DMSO, 50% FBS and 30% DMEM was added dropwise to the cell suspension and aliquots of 1 ml were made on 1.5 ml cryo-tubes (Nunc®). Cells were stored at -80ºC on isopropanol-filled containers (Mr. Frosty) for 3-4 days and transferred to liquid nitrogen tank for long-term storage.

2.2.4. Thawing

Cells were thaw quickly in a 37ºC water bath, diluted 1:10 in fresh pre-warmed medium and centrifuged at 900xg for 5 min. The pelleted cells were resuspended in fresh medium and plated.

2.2.5. Transient transfections

Transfections were performed on a 50-60% confluent monolayer using FuGENE (Promega®) for HEK293T and EBNA293 or Lipotransfectine (Biontex®) for MEF and HeLa cell lines following the manufacturer's instructions. Hippocampal neurons were transfected using Lipofectamine 2000 (Invitrogen®). The transfection mixtures are shown in **table M3**.

	FuGene		Metafectene		Lipofectamine 2000	
Culture plate	P60 28.2 cm²	12-well 4 cm²	P60 28.2 cm²	12-well 4 cm²	Fluoro Dish 9.6 cm²	IBIDI 2.5 cm²
DNA (µg)	4	1	4	1	2	1
Volume to dilute DNA (µl)	100	25	300	50	100	50
Reagent (µl)	12	1,5	12	2	4	2
Volume to dilute reagent (µl)	100	25	300	50	100	50
Volume of mixture (µl)	212	51,5	612	52	204	52

Table M 3. Summary of the conditions of transfection with the three reagents used throughout this work.

2.2.6. Transfection of neurons

Neurons were transfected at 4-5 DIV using Lipofectamine 2000. Before transfection, 2/5 of media was removed from each plate. For each plate to transfect, 2 µg of DNA were mixed with 50 µl of OptiMEM (Invitrogen) in a 1.5 ml tube and 2 µl of Lipofectamine 2000 were mixed in 50 µl of OptiMEM in a second 1.5 ml tube. After 5 min, both mixtures were put together and incubated for 20 min. The resulting mixture was added dropwise to the plates and neurons were incubated 30 min at 37ºC. Afterwards, the transfection medium was replaced for a fresh one composed of 40% of the previously removed medium, 40% of stuffed Neurobasal and 20% of glia conditioning medium.

2.3. Cell lysis and protein concentration

To prepare cell lysates, cells on p60 plates were washed with 5 ml of cold PBS before adding 300 µl of cold Lysis buffer (Alex3 Lysis buffer or buffer PD). Cells were harvested using a scrapper and transferred to pre-chilled 1.5 ml tubes. Lysates were left on ice before centrifugation at 16000xg for 15 min to pellet big debris and DNA. Supernatants containing cellular proteins were used for immunoprecipitation, pull-down or western blot analysis.

When needed, protein concentration was determined using the BioRad Protein Assay reagent (Biorad®). Growing volumes of lysates (from 1 to 10 µl) were mixed with 800 µl of ddH_2O in plastic buckets and a BSA standard with known concentrations of protein was prepared in parallel. A volume (200 µl) of BioRad reagent was added to the lysates and the BSA standard buckets. After 5 min of incubation, the absorbance at 595 nm was measured and protein concentration was calculated by extrapolating the sample values using the BSA standard as reference.

2.4. SDS-PAGE electrophoresis and western blot

Polyacrilamide-SDS electrophoresis (PAGE) was carried out to separate proteins from a sample, as described by Laemmli (Laemmli, 1970). Samples were mixed with 5x Laemmli buffer and heated for 5 min at 95°C. Samples were loaded in an acrylamide gel (from 8 to 12% of acrylamide/bis) and run in 1xSDS-PAGE running buffer at 100 V until the proteins reached the desired separation, visualized by the marker PageRuler prestained protein ladder (Fermentas®). Separated proteins were transferred onto PVDF membranes (Immobilion-FL, Millipore®) using Mini-trans Blot system (Biorad®) for 3 h at 70 V.

To immunodetect the proteins, PVDF membranes (activated for 1 min in 100% methanol) were blocked with TBS-Tween containing 3% BSA for 1 h and incubated overnight with a primary antibody solution in TBS-tween (by default, 1:1000) while shaking at 4°C. Membranes were

washed 3 times with TBS-tween and incubated with the suitable secondary antibody solution for 1 h at 4°C, at the rocking platform. The secondary antibodies were IRDye 600 or 800 (Odyssey) conjugated to allow detection by Odyssey infrared scanner. After incubation, membranes were washed 3 times with TBS-tween and another 3 times with TBS or PBS. Membranes were analyzed using the Odyssey infrared scanner and quantification of the bands was carried out using ImageStudio Lite software (LI-COR®).

2.5. Immunoprecipitation

To immunoprecipitate proteins form cells, whole cell lysates on lysis buffer (Alex3 buffer) were incubated with a specific antibody (1-5 µg) and 1.5 µg of IgG free BSA for 3 h or overnight at 4°C on a rotating wheel. Antibodies were bound to beads by addition of 10-20 µg protein G or protein A sepharose beads (Sigma®) to each sample and subsequent incubation in a rotating wheel for 1 h. Beads were equilibrated with three washes of lysis buffer prior to use. When using a bead-TRAP-conjugated antibody (anti-myc and anti-GFP TRAP, Chromotek®) or antibodies conjugated to protein G agarose beads (anti-HA sepharose beads, Sigma®), 1-5 µl of antibody-beads were added per sample and incubated in a rotated well for 1-2 h at 4°C. After incubation, samples were washed 4 to 6 times with 1 ml of Alex3 wash buffer, leaving them 5 min on rotation at 4°C between each wash. After the final wash, beads containing the immunoprecipitated protein were resuspended in 5-7 µl of 6xLaemmli buffer and resolved by SDS-PAGE.

2.6. Immunoprecipitation of endogenous $G\alpha_q$ for proteomics

Eight 35 cm diameter plates of confluent MEF WT, MEF KO $G\alpha_{q/11}$, MEF KO $G\alpha_{q/11}$ stable expressing $G\alpha_q$ and NIH3T3 cells were lysed and mitochondria were isolated from cultured cell lines using the protocol described by Schägger (1995), with slight modifications. Samples were immunoprecipitated using 2 different polyclonal antibodies (C-19 and E-17, Santa Cruz ®). NHS-Activated Magnetic Beads were incubated with both antibodies following manufacturer´s instructions before used for immunoprecipitation. Immunoprecipitation was done following Pierce IP kit (Thermo Scientific®) instructions; proteins were eluted in ultrapure water and sent for MS analysis (Proteomic facility CNIC, in collaboration with Dr. Benincà and Prof. Enríquez). Samples were digested with trypsin (1:50 w/w) and the resulting peptides were separated by inverted phase HPLC and injected into an Orbitrap Velos spectrophotometer (Thermo Scientific®) measuring with a 60000 resolution, 400 m/z ratio and 300-1800 m/z acquisition range.

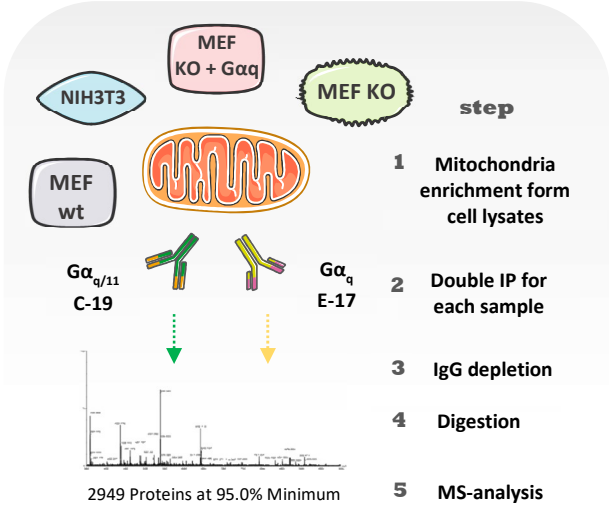

Figure M 1. Schematic representation of the steps followed in the proteomic analysis. Cell lysates from MEF wt, MEF knockout for $G\alpha_{q/11}$ (MEF KO), MEF knockout for $G\alpha_{q/11}$ stably expressing $G\alpha_q$ (MEF KO + $G\alpha_q$) and NIH3T3 were enriched for endomembranes. For each cell line, endogenous $G\alpha_q$ or $G\alpha_{q/11}$ was immunoprecipitated using the polyclonal antibodies E-17 or C-19 (Santa Cruz®). Immunoglobulins were removed from immunoprecipitates previous to trypsin digestion and mass-spectrometry analysis was carried out for each of the 8 samples. The resulting data was analyzed using the Scaffold software.

2.7. Expression and purification of GST-tagged proteins

The protease deficient *E.Coli* strain BL21 was used to produce GST-proteins. BL21 competent cells were transformed with the GST-containing plasmids (pGEX-2T or pGEX-4T) by heat shock and plated onto LB plates containing ampicillin. Plates were incubated overnight at 37ºC, then a single colony was picked and incubated overnight in 100 ml of LB containing ampicillin at 37ºC with continuous shaking. Next day, the overnight culture was diluted 1:100 and incubated first 2 h at 37ºC until the OD_{595} reached 0.4, and then around 1 h at 24ºC until the OD_{595} reached 0.8. At that point, protein production was induced by addition of IPTG (Sigma®) to a final concentration of 100 µM. For proteins that express at high levels (including GST-Alex3 and GST-Alex3 Ct), cultures were incubated for 3 h at 24ºC with shaking before bacteria collection. For proteins with lower stability or those that express at lower levels (Including GST-Alex3 Nt, GST-Alex3 Ct1, GST-Alex3 Ct2 and GST-Miro1 constructs) cultures were incubated in minimal medium at 16ºC overnight with continuous shaking. After protein production, bacteria were collected by centrifugation at 4000xg for 10 min at 4ºC, then resuspended in ice-cold PBS and aliquoted into 4 o 5 15 ml Falcon tubes. Tubes were centrifuged once more at 4000xg for 15 min, the supernatant was discarded and samples were stored at -20ºC before proceeding with the purification protocol.

For each GST-construct, an aliquot was used to estimate the protein production yield before proceeding with the experiment. First, bacterial pellets were resuspended in 5 ml PBS-Tween 0.1% containing protease inhibitors and sonicated on ice for 6 pulses of 15 s, leaving them 15 s off between each pulse. Samples were clarified by centrifugation at 20000xg, 30 min at 4ºC, the supernatant was collected into new falcon tubes and a 20 µl sample were loaded into an SDS-PAGE gel along increasing concentrations of a BSA standard. The gel was run at 70 V for around 3 h, stained with Coomassie dye for 30 min and distained overnight in a 1% acetic acid solution at the rocking platform. GST-proteins and BSA standard bands were visualized using the Odyssey infrared imaging system and quantified using ImageStudio Lite software, and the protein concentration of the supernatant of each of each aliquot after clarification was estimated by extrapolating the values of the GST-protein to those of the BSA standard.

2.7.2. Purification of GST-tagged proteins

After determining the protein yield of each bacterial aliquot, samples were sonicated and clarified as previously indicated before incubation with Glutathione Sepharose Magnetic Beads (Sigma®). Because the purification yield was previously calculated, the volume of clarified supernatant containing from 5 to 10 µg of GST-tagged protein was incubated with 20 µg of beads (gluthatione sepharose 4B slurry, GE Healthcare®) in falcon tubes at the rotating wheel for 1 h at 4ºC. The total volume of all samples was set to 5 ml and the required volume of PSB-tween 0.1% with protease inhibitors was added to each sample. After incubation, beads bound to GST-proteins were washed three times with 5 ml PBS-tween and three more times with PBS with protease inhibitors, keeping the beads at 4ºC and precipitating them at 1000xg for 5 min between each wash. After the final wash, beads were resuspended in 20 µl of PBS and incubated with the cell lysates or buffer solution containing the purified protein of interest.

2.7.3. Pull-down from transfected HEK293 cells

In assays from transfected cells, $8x10^5$ HEK293 were seeded on p60 plates 24 h before transfection. Cells were transfected with plasmids containing $G\alpha_q$ or $G\alpha_q$R183C using FuGene reagent (Promega®) according to the manufacturer's guidelines. Plates were washed twice with 5 ml of ice-cold PBS before addition of 300 µl of Alex3 lysis buffer, then harvested using the cell scrapper and transferred into pre-chilled 1.5 ml Eppendorf tubes. Samples were centrifuged at 16000xg, 15 min at 4ºC and supernatants containing around 700 µg of protein were pre-cleaned by incubating them 30 min with 10 µg of unconjugated sepharose beads, at 4ºC in the rotating wheel. Then, beads were pelleted by 5 min centrifugation at 1000xg and pre-cleaned supernatants were incubated with the glutathione bead-conjugated GST-containing proteins of interest. Incubation was performed in the rotating wheel, at 4ºC and for at least 1 h. Next, beads

were washed 4 times with 1 ml of Alex3 wash buffer, pulling the beads down by centrifugation at 1000xg for 5 min between each wash. After the final wash, beads were resuspended in 5-7 µl of Laemmli Buffer and stored at -20ºC until SDS-PAGE analysis.

2.7.4. Pull-down from SHSY5Y cells

In pull-down assays from SHSY5Y lysates, confluent p100 plates of cells were used for each experimental condition. Plates were washed with 10 ml of ice-cold PBS before lysis with 1 ml of Alex3 lysis buffer, then scrapped and transferred into 1.5 ml per-chilled Eppendorf tubes. After centrifugation at 16000xg for 15 min, supernatants containing 1.5 mg of protein were transferred into new tubes and incubated with the gluthatione bead-bound GST-protein of interest in the rotating wheel at 4ºC for 1 h. Beads were washed 4 times with Alex3 wash buffer, pulling the beads down by centrifugation at 1000xg for 5 min between each wash. After the final wash, beads were resuspended in 5-7 µl of Laemmli Buffer and stored at -20ºC until SDS-PAGE analysis.

2.8. Expression and purification of His-Alex3

A 3 ml LB-culture was grown overnight with a single colony of transformed BL21 cells and incubated overnight at 37ºC with shacking. Next day, the culture was amplified into 100 ml minimal medium culture and from that a 1:100 dilution of the over-night culture was incubated first 2 h at 37ºC until the OD_{595} reached 0.4, and then around 1 h at 24ºC until the OD_{595} reached 0.8. At that point, protein production was induced by addition of IPTG (Sigma®) to a final concentration of 100 µM. Cultures were incubated o/n at 16ºC with continuous shaking, and bacteria were pelleted, aliquoted and quantified as with GST-proteins.

Pelleted bacteria was resuspended in ice-cold NiNTA lysis buffer, sonicated and clarified as explained for GST-tagged proteins. Supernatants containing approximately 10 µg of protein were incubated with 20 µg of HisPur Ni-NTA Magnetic Beads (Thermo Scientific®) in a total volume of 5 ml, in the rotating wheel at 4ºC. Beads bound to His-Alex3 were washed three times with 5 ml NiNTA lysis buffer and three more times with NiNTA wash buffer. After the last wash, beads were resuspended in 20 µl of NiNTA wash buffer and incubated with the cell lysates.

2.8.1. Pull-down of His-Alex3

Lysates from transfected HEK293 cells were obtained as with the GST-pull downs. Incubation was carried out by adding 20 µg of conjugated Ni-NTA beads into the cell lysates, for 1 h at 4ºC in the rotating wheel. As with GST-pull-downs, beads were washed 4 times with 1 ml of Alex3 wash buffer, resuspended in Laemmli Buffer and stored at -20ºC until SDS-PAGE analysis.

2.8.2. Elution of purified His-Alex3 from Ni-NTA Magnetic Beads

To address the impact of His-Alex3 on GST-pull-downs with purified components, His-Alex3 was eluted from Ni-NTA Magnetic Beads by incubation for 30 min with 100 µl of elution buffer (NiNTA wash buffer containing 350 mM imidazole) at 4ºC at the rotating wheel. Then beads were pelleted, the supernatant was transferred into new pre-chilled Eppendorf tubes and stored at -80ºC after addition of glycerol to a final concentration of 10% (v/v). The remaining beads were incubated once again with 100 µl of elution buffer and the process was repeated 4 more times until 5 different eluates were obtained. The concentration of His-Alex3 in each eluate was determined by loading a 20 ul sample of each eluate into an SDS-PAGE gel along with a BSA standard and subsequent Coomassie staining. Gels were imaged using an Odyssey Infrared scanner system and band intensity was quantified using ImageStudio Lite software. Protein concentration of each eluate was finally determined by extrapolating the values of each sample with the BSA standard.

2.9. In-vitro pull down of purified components

In pull-down assays with purified components, 10 µg of the bead-conjugated GST-tagged protein of interest were incubated with 10 ng of purified $G\alpha_q$ in 1 ml of PD Purified $G\alpha_q$ Buffer, for 1 h in the rotating wheel at 4ºC. In pull-down of GST-Miro1, up to 40 ng of eluted His-Alex3 were added to the buffer in some experimental conditions. The incubation buffer was changed to "triton" or "HMNG" when indicated. After incubation, samples were washed 4 times with 1 ml of the incubation buffer, pulling-down the beads by centrifugation at 1000xg for 5 min between each wash. After the final wash, beads were resuspended in Laemmli Buffer and stored at -20ºC until SDS-PAGE analysis.

Pull-down of GST-Miro1 in the presence of His-Alex3 was carried out under the same conditions in the presence of growing concentrations of eluted His-Alex3 (50, 100 and 200 ng of purified protein).

2.10. Immunofluorescence

For immunofluorescence experiments on HeLa cells, cells were plated and transfected on p60 dishes before transferring them onto cover-glasses. Around $4x10^5$ cells were plated on p60 dishes, transfected 6 h later with Lipotransfectine or FuGene following the manufacturer's guidelines and reseeded 12 h later on 18 mm cover glasses placed in 12-well plates under sterile conditions. Cells were fixed 6 h after being reseeded. This protocol reduced non-specific DAPI

staining caused by the transfection reagent and allowed cells to be homogeneously distributed onto the cover glasses.

To fix the cells, either Hela cells seeded on 18 mm cover glasses (calibrated 1.5 mm knottel glass) and neurons plated on dishes with a glass cover (Fluoro Dish 9.6 cm^2 and IBIDI 2.5 cm^2 dishes) were rinsed twice in PBS, fixed in 3.7% formaldehyde solution for 15 min at room temperature and washed 3 times with PBS. Permeabilization was done by rinsing the cells twice for 10 min with PBS-Tween 0.1%. To avoid non-specific interactions, cells were pre-incubated with a blocking solution (PBS containing 0.5% NP-40 and 1% IgG free BSA) for 1 h at RT. Samples were then incubated for 1-2 h at RT with a precleared primary antibody dilution (1:100 to 1:500 in blocking solution). Cover-glasses with the antibodies were placed in hand made humidified chambers to avoid evaporation of the antibody. Next, cells were washed 3 times with PBS-Tween-20 0.1% and incubated for 1 h at RT with the suitable precleared secondary antibody dilution (1:200 in blocking solution with the proper AlexaFluor antibody). Cells were washed 3 times more with TBS-tween 0.1% and 3 additional times with PBS to eliminate traces of Tween 20. Cover-slides were mounted using 7-10 µl of Prolong Diamond (containing DAPI) and let them dry overnight before imaged, while neuron dishes were stored on PBS at 4ºC and imaged no longer than 7 days after immunostaining. All solutions used on this protocol were filtered through 0.22 µm filters (Fisher Scientific®) and preclearing of antibody dilutions was done by centrifugation at 16000xg for 5 min.

2.11. Super resolution Imaging

COS7 were transfected with $G\alpha_q$ and DsRed-tagged Miro1. Cells were fixed with 3.7% formaldehyde after 24 h, then permeabilized with 1% Triton X-100 and 0.1% sodium deoxycholate in PBS and immunostained in blocking buffer (5% goat serum and 0.1% IgG-free BSA in PBS) with anti-$G\alpha_q$ (Santa Cruz®) and the respective secondary antibody (Alexa Fluor 488, Invitrogen®) and mounted with Prolong Diamond. Acquisition was performed using an N-SIM microscope system (Nikon®) equipped with a super-resolution Apo TIRF 100× 1.49 NA objective and a DU897 Ixon camera (Andor Technologies). Three-dimensional SIM image stacks were acquired with a Z-distance of 0.15 µm. All of the raw images were computationally reconstructed using the reconstruction slice system from NIS-Elements software (Nikon®) while keeping the same parameters.

2.12. Image acquisition

For the Alex3 or Miro1 expression experiments on MEF cells, images were acquired using a Leica SP5-TSC confocal microscope and the software LAS AF (Leica®), whereas the TRAK overexpression experiments on HeLa cells as well as live and fixed primary neurons were imaged

using a Zeiss LSM780 confocal and multiphoton microscope with a 63x oil objective along with the ZEN software (Zeiss®).

2.13. Culture of primary hippocampal neurons

OF1 mice embryos (Iffra Credo, Lyon, France) were used to obtain primary cultures of hippocampal neurons. Pregnant females were euthanized by cervical dislocation, embryos at 17-18 days (E17-E18) were taken, their brains were extracted in dissecting medium (0.1 M PBS + 0.6% w/v glucose) and the hippocampus were carefully and quickly isolated. Hippocampus were trypsinized in 3 ml of dissecting medium containing 1xTripsin-EDTA during 12 min at 37ºC before inactivating the enzyme adding 1.5 ml of normal horse serum (NHS). Next, neurons were incubated with 10 U/ml DNAse during 12 min at 37ºC and then mechanically disaggregated by pipetting up and down around 40 times. Neurons were centrifuged 5 min at 1000xg and 4ºC and resuspended in stuffed Neurobasal medium (Neurobasal containing 2% B27, 1xGlutamax and 20 U/ml pen-strep) supplemented with glial conditioning medium (stuffed neurobasal medium kept for 15 days in confluent cultures of glia cells). Neurons were then counted using Neubauer chambers and plated on FluoroDish (150.000 cells per plate) or IBIDI plates (for KO Alex3 neurons 75.000 cells per well) pre-treated with 0.5 mg/ml poly-D-lysine for 12 h. Plated neurons were stored humidified incubator at 37ºC with 5% CO_2.

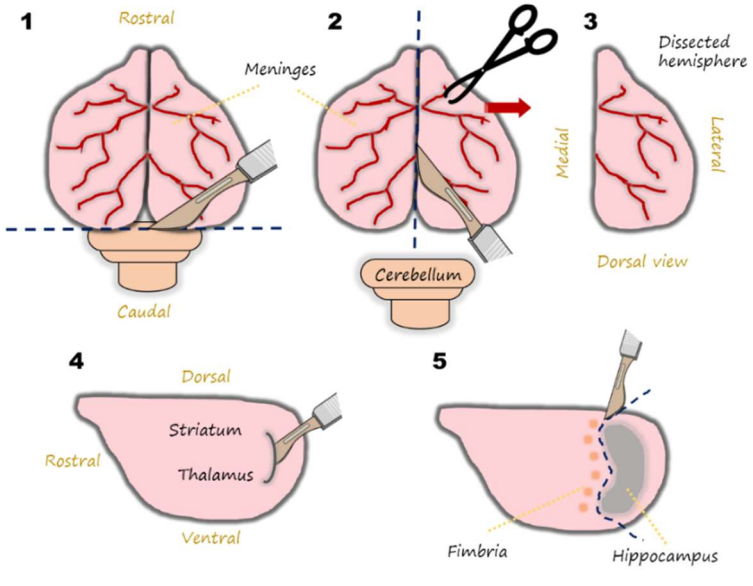

Figure M 2. Schematic representation of hippocampus isolation from mouse brain. Once the brain has been released from the skull of the embryo, the caudal region is removed using a scalpel (1). Next, the two cerebral hemispheres are divided with using scalpel and forceps (2,3). After releasing the section containing the striatum and the thalamus (4), the hypppocampus is carefully released from each of the two hemispheres (5).

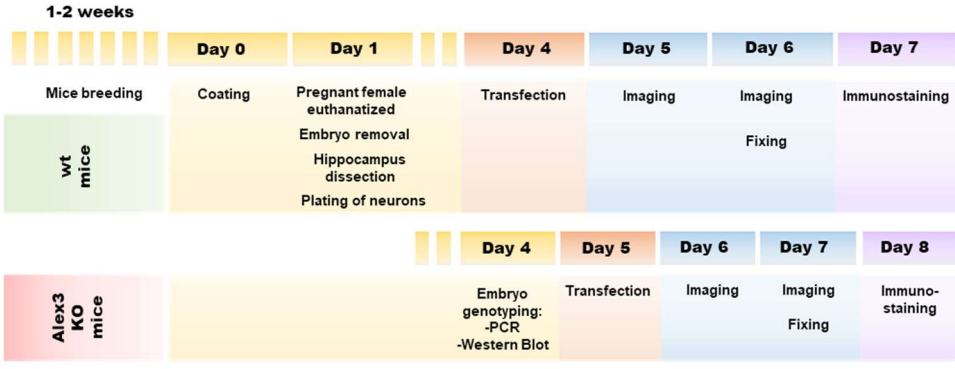

Figure M 3. Time-course diagram of live-imaging experiments with hyppocampal neurons. To perform live-imaging experiments, hyppocampus from embryos were removed and neurons were plated on poly-D-lysine pre-treated plates. Neurons were transfected at 4DIV and live-imaged 24 and 47h post-transfection using an incubation system at 37ºC and 5% CO_2. Cells were fixed after imaging and immunostained with specific antibodies to verify the proper expression or depletion of our proteins of interest. In the case of Alex3(-/-) neurons, transfection was carried out at 5 DIV to allow genotypic of the knockout embryos before transfection. Imaging was performed at 6 and 7 DIV instead of 5 and 6 DIV.

2.14. Live imaging and quantification of mitochondrial transport

Hippocampal neurons seeded on FluoroDish plates (World precision instruments®) pre-coated with poly-D-lysine and transfected with cDNAs using Lipofectamine2000 were filmed 24 to 48 h after transfection using a Zeiss LSM 780 confocal microscope with a 63x oil objective. On the microscope, neuronal cultures were kept at 37ºC using a temperature-sensitive adaptor with a cover that allowed the flow of warm air and CO_2 to avoid pH variations. Films were taken using the ZEN software (Zeiss). For each neuron, an axonal segment located approximately de diameter of 6-10 nuclei away from the soma (from 90 to 160 µm) was filmed with 800x100 pixel resolution and an extra 2x digital zoom. Stacks of 7 images were acquired every 6 s during 15 or 10 min from the selected region. Kymographs were generated and processed using Fiji software (ImageJ 1.51j) along with a macro program (Fig. M4) to automatize the process.

```
name=getTitle();
run("Z Project...", "projection=[Max Intensity] all");
selectWindow(name);
close();
selectWindow("MAX_"+name);
run("Z Project...", "projection=[Max Intensity]");
rename("time projection");
run("Enhance Contrast", "saturated=0.35");
setTool("polyline");
waitForUser("paint line");
selectWindow("MAX_"+name);
run("Restore Selection");
selectWindow("time projection");
run("Close");
```

Figure M 4. Summary of the macro used to generate kymographs from time-lapse images of axonal mitochondria.

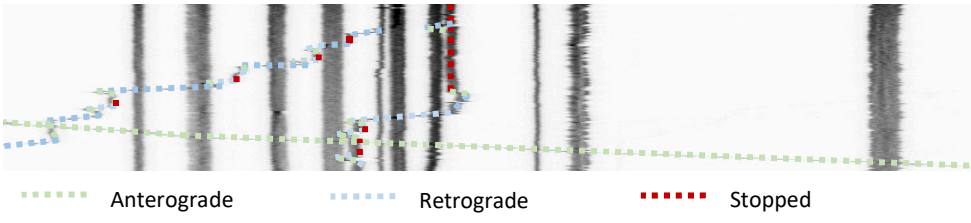

Figure M 5. Example of kymograph analysis to calculate mitochondrial velocities. Kymographs were processed automatically from time-lapse videos using a specific macro for Fiji software. From kymographs, each mitochondrial displacement was traced manually and sorted according to the anterograde or retrograde directions. Mean velocities per mitochondria (shown as bar graphics in results section) are the result of calculating the weighted average of all segments traced for a mitochondrial run, including those in which they remain stopped (in red). Instant velocities (shown as dot charts in results section) are arithmetic average of those segments in which mitochondria move (skipping those in red).

2.15. Neuronal treatments

For live-imaging experiments using the $G\alpha_q$ specific inhibitor, neurons transfected with the plasmids of interest were incubated with 10 µm of YM-254890 (Focus biomolecules®) during 30 min prior to imaging, as previously reported (Takasaki et al., 2004; Uemura et al., 2006).

In GPCR-activation assays, neurons were cotransfected with mitoGFP along with a cherry-tagged hM3D (Gq) DREADD receptor (Armbruster, Li, Pausch, Herlitze, & Roth, 2007). After transfection (24 h), axons of DREADD-expressing neurons were imaged before and 15 min after the addition of 1 µm clozapine-N-oxide (Tocris).

2.16. Sholl analysis, dendritic length and mitochondrial morphology

Sholl analysis was calculated using the plugin NeuronJ (1.4.3) available for the Fiji (ImageJ 1.51J) software. Sholl intersections were analyzed every 10 µm. The same software was used to determine dendritic length. Primary dendrites were considered those emerging directly from the soma, whereas those originated from primary dendrites were classified as secondary and tertiary.

Mitochondrial length was calculated from those mitochondria located within the time-lapse imaged axonal region using the Fiji software. Morphological parameters (aspect ratio and form factor) were calculated using a specific macro for Fiji software (Anna Bosh and Maria Calvo, CCiTUB UMOA-Campus Clínic), following the guidelines described in previous reports (Harwig et al., 2018; Koopman, Visch, Smeitink, & Willems, 2006; Mortiboys et al., 2008).

2.17. Stable and transient knock-down of $G\alpha_q$ using short-hairpin RNAs

pLKO.1-shRNAs used to stable knock-down endogenous $G\alpha_q$ in HeLa cells were obtained from MISSION shRNA human system (Sigma®) and the oligonucleotides used to generate proteins were also obtained from Sigma® at 0.05 µM scale. pLKO.1-shRNAs transfected to neurons to transiently knock-down the expression of $G\alpha_q$ were from MISION shRNA mouse system (Sigma®). In this case, the insert containing the targeting sequence against the coding region of GNAQ gene was removed from its original vector using restriction endonucleases, purified through agarose-gel and re-cloned into a pLKO.3G vector digested with the same enzymes to allow expression of GFP in knocked-down neurons.

-Lentivirus particles production to stable knock-down $G\alpha_q$ expression

$2.5x10^6$ HEK293T cells were seeded on p100 plates for each lentivirus to be produced containing either the mRNA sequences to target $G\alpha_q$ or the control vector (CV) that does not target any sequence in the genome. Cells were co-transfected using FuGene with pLKO.1 vectors (containing the shRNA sequences), pCMWdR8.91 (to express gag and pol viral proteins) and pVSVG (to generate viral envelope) at 4:3:1 ratio. Medium containing viral particles was collected 24 and 48 h after transfection, filtered through 0.45 µM MCE filters (Millipore®) and stored at -80ºC.

- Viral transduction to stable knock-down $G\alpha_q$

Cells ($2x10^4$) seeded on 6 well plates were incubated for 24 h with 1 ml of medium containing viral particles. Transduced cells were incubated with 3 µg/ml puromycin for 3 to 6 days. The optimal concentration of puromycin was calculated using a standard and impaired the survival of non-transduced cells without significant effects on infected cells. After selection, cells were incubated with 1 µg/ml of puromycin to keep selective pressure on stable knock-down cell line. The effectiveness of the shRNAs against $G\alpha_q$ was confirmed by SDS-PAGE of cell extracts and western blot analysis using antibodies against $G\alpha_q$.

2.18. Statistics

2.18.1. Gene ontology analysis

For the proteomic analysis, p-values were calculated using the gene ontology resource (GO) (http://geneontology.org). The GO terms of our proteomic database were compared to the background database of the GO software. The closer the p-value is to zero, the more significant the particular GO term associated with our mass-spectrometry results is. Said in another way, the less likelihood our data are assigned to a particular GO term by chance.

2.18.2. Statistical analysis

Data in all figures are expressed as mean ± SEM of the number of experiments indicated. The experiments were repeated at least 2-3 times to confirm the results. Data were analyzed using a Student's t-test to compare between two conditions or a one way ANOVA for multiple comparisons. The statistical significance was set at p-value<0.05 (*p<0.05, **p<0.01,***p<0.001). Statistical analysis was carried out using Graph Pad Prism 6 software.

RESULTS

G proteins are no longer considered signal transducers restricted to the plasma membrane, but rather dynamic GTPases that localize in a wide variety of organelles and endomembranes, including endosomes, endoplasmic reticulum, Golgi, mitochondria and even the nucleus (Hewavitharana & Wedegaertner, 2012; Sánchez-Fernández et al., 2014). Previous results from our group demonstrated that $G\alpha_q$ not only associates with $G\beta\gamma$ at the outer mitochondrial membrane, but also localizes at the intermediate space, where it has a clear impact in mitochondrial dynamics and bioenergetics (Benincá et al., 2014). MEF cells depleted from $G\alpha_q$ and $G\alpha_{11}$ show a fragmented and less distributed mitochondrial network and defective cristae organization. As a result, mitochondria are unable to keep the proper membrane potential and show lower oxygen consumption and ATP production compared to the wild-type cells. Such defects seemed caused rather by direct impact of $G\alpha_q$ at the mitochondrion than an indirect effect of impairing $G\alpha_q$ downstream signaling from the plasma membrane (Benincá et al., 2014). If that was the case, $G\alpha_q$ would probably have a downstream effector at the mitochondrion involved in those alterations in dynamics and bioenergetics.

1. Identification of putative mitochondrial effectors for $G\alpha_q$

1.1. Mass spectrometry analysis

In order to identify putative binding partners of $G\alpha_q$ and $G\alpha_{11}$ at the mitochondria, our group followed an approach based on $G\alpha_{q/11}$ immunoprecipitation from endomembrane-enriched cell lysates and subsequent mass spectrometry analysis of co-immunoprecipitated peptides. Essentially, cell lysates from MEF and NIH3T3 cells as well as MEF $G\alpha_{q/11}$ (-/-) recovered for the expression of $G\alpha_q$ and MEF $G\alpha_{q/11}$ (-/-) (used as a control) were enriched for the particulate fraction. This fraction contains a high amount of endomembranes including ER, Golgi, endosomes and mitochondria, though it also includes nuclear membranes and ribosomes. Endogenous $G\alpha_q$ and $G\alpha_{11}$ were immunoprecipitated from the endomembrane-enriched cell lysates using the two most reliable commercial antibodies at that time: the E-17 against $G\alpha_q$ and the C-19 against $G\alpha_q$ and $G\alpha_{11}$ polyclonal antibodies from Santa Cruz. Both antibodies were selected from a previously tested pool and embedded in agarose beads. Immunoprecipitates were digested with trypsin and analyzed by mass spectrometry. The peptides identified were assigned to their respective proteins for each of the eight samples ("NIH3T3", "MEF wt", "MEF $G\alpha_{q/11}$ (-/-)" and "MEF $G\alpha_{q/11}$ (-/-) + $G\alpha_q$ " immunoprecipitates with either E-17 or C19 antibody) using the Scaffold 4.8.9 software.

The Scaffold software classifies the proteins according to the number of peptides identified and allows a customized sorting from the user. To our study, we only considered those proteins with at least two peptides in two different samples (appearing either in at least two cell lines or with both antibodies) as long as no peptides were found in the $G\alpha_{q/11}$ (-/-) immunoprecipitates. The proteins obtained were subsequently sorted according to their function, main expression and subcellular localization. The protein list was shortened-up by discarding ribosomal components and those proteins whose expression was restricted to the nucleus, as we considered their presence a result of their abundance and the overall "protein dragging" during the immunoprecipitation process rather than a specific protein-protein interaction. The remaining proteins were classified according to criteria of UNIPROT database and processed by gene ontology software (**Fig. R1**).

As shown in **Figure R1a**, over 9% of the immunoprecipitated proteins localize at the mitochondria, a fraction that was around 2-fold enriched from what would be expected. Most $G\alpha_q$-interacting proteins were involved in signal transduction or have catalytic activity (**Fig. R1b**). Besides, most of those putative binding-partners were either enriched in the nervous system or expressed in neuronal cells at some stages during development (**Fig. R1c**). The gene ontology analysis revealed

an enrichment of mitochondrial components (**Fig. R1d**) besides an up to 9-fold enrichment of proteins involved in vesicle and organelle transport, standing out those involved in the retrograde transport towards the Golgi. As expected for a G protein, data also shows a noticeable enrichment of proteins implicated in signal transduction and heterooligomerization (**Fig. R1e**). Furthermore, the gene ontology results for molecular function unveiled an enrichment of several proteins involved in signal transduction including Rho and Ras small GTPases or ATPase activators (Coleman, Topalidou, & Ailion, 2018), but also dynein intermediate and light-intermediate chains, two of the main components of the motor complex involved in microtubule-based retrograde transport (**Fig. R1f**)

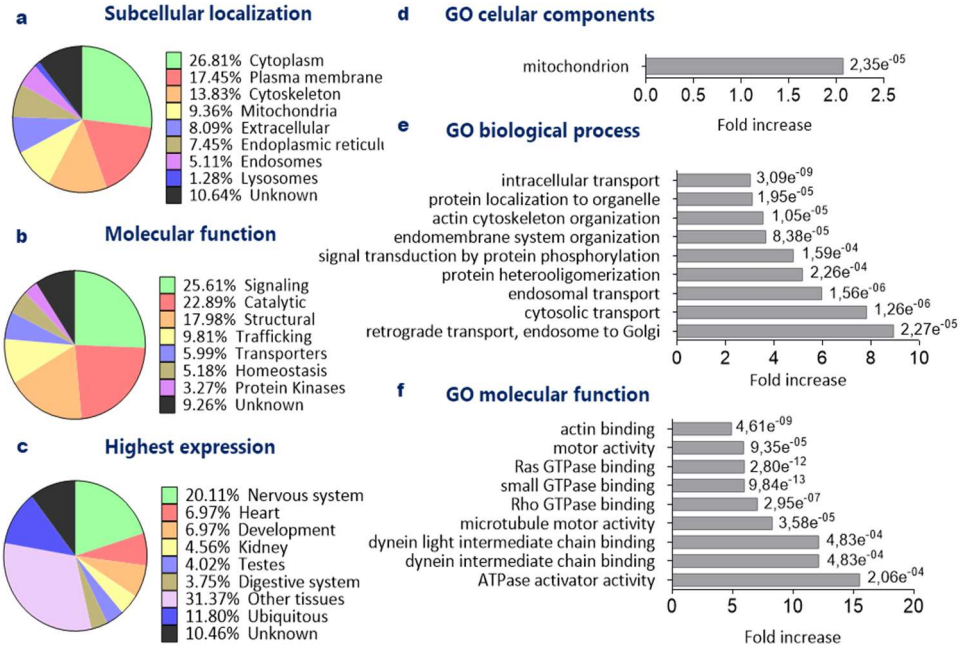

Figure R1. Ontology analysis of the data obtained from the mass-spectrometry analysis. From the 2949 proteins identified in all the samples of this study, those obtained with at least 2 peptides in two different samples with $G\alpha_q$ and without peptides in the MEF $G\alpha_{q/11}$ (-/-) immunoprecipitates were short-listed. The 375 non-ribosomal proteins whose subcellular localization was not restricted to the nucleus were selected for further analysis. The pie charts on the left represent: **a,** the relative subcellular distribution **b,** the main function of the protein and **c,** the tissue where the protein is mainly expressed. The graph bars on the right represent: **d,** the fold enrichment of mitochondrial proteins **e,** the fold enrichment of proteins involved in specific cellular functions and **f,** the fold enrichment of proteins with the described molecular functions. The analysis was carried out using the gene ontology software. For each condition, p-values of the enrichment were calculated using the same software and are shown on the right side of each bar.

				Peptides antibody C19			Peptides antibody E17		
ID	**Gene**	**Name**	**MW kDa**	**KO +Gq**	**3T3**	**WT**	**KO +Gq**	**3T3**	**WT**
NIPS1	Nipsnap1	Protein NipSnap homolog 1	33	3	1	9		4	8
Q3TA68	Wdr36	Protein Wdr36	98	3	11		2	24	
HXK1	Hk1	Hexokinase-1	108		12			19	
OXR1	Oxr1	Isoform 4 of Oxidation resistance protein 1	93		9			16	
ARMX3	Armcx3	Armadillo repeat-containing X-linked protein 3	43			13		2	7
RIPK3	Ripk3	Receptor-interacting serine/threonine-protein kinase 3	53		6	6		3	6
D3ZL86	Heatr1	HEAT repeat containing 1 (Predicted)	?	1	3			17	
Q3UNW7	Heatr1	Putative uncharacterized protein (Fragment)	?		2			10	
FAKD2	Fastkd2	FAST kinase domain-containing protein 2	79	1		3	2	1	2
GLSK	Gls	Glutaminase kidney isoform, mitochondrial	?		8	3		4	1
ARM10	Armc10	Armadillo repeat-containing protein 10	33	1		7	2		6
CEP89	Cep89	Centrosomal protein of 89 kDa	90			2	1	4	
COASY	Coasy	Bifunctional coenzyme A synthase	62		4			5	
OAT	Oat	Ornithine aminotransferase, mitochondrial	48		2			6	
CPSM	Cps1	Carbamoyl-phosphate synthase	165	1	1		1		2
RT02	Mrps2	28S ribosomal protein S2	32	1	1	3	3		1
AOFA	Maoa	Amine oxidase [flavin-containing] A	60			2		2	3
RUSD4	Rpusd4	RNA pseudouridylate synthase domain-containing protein	?	1		2	2	1	1
Q32Q54	Uqcc	RCG37273, isoform CRA_a	?			3	1		3
SHC1	Shc1	SHC-transforming protein 1	63	1	3		1	2	1
KITH	Tk1	Thymidine kinase	26	2	2		3	1	
TIM44	Timm44	Mitochondrial import inner membrane translocase subunit TIM44	51			2	1		1
Q9D8W6	Ak3	Putative uncharacterized protein	?		3			4	1
CAV1	Cav1	Caveolin-1	21		4			3	
DIC	Slc25a10	Mitochondrial dicarboxylate carrier	32	1		2	1		
RM38	Mrpl38	39S ribosomal protein L38	45	1		5			1
KTHY	Dtymk	Thymidylate kinase	24		4	1			
FBX7	Fbxo7	F-box only protein 7	58		2			4	
BAX	Bax	Apoptosis regulator BAX	21		3			2	
TARA	Triobp	Isoform 4 of TRIO and F-actin-binding protein	218		4			3	
DCAKD	Dcakd	Dephospho-CoA kinase domain-containing protein	26	2		2		1	1
RM19	Mrpl19	39S ribosomal protein L19	34	3			1		2

AOFB	Maob	Amine oxidase [flavin-containing]	?	2			2					1
MAOM	Me2	NAD-dependent malic enzyme	66				3					4
RNZ2	Elac2	Isoform 2 of Zinc phosphodiesterase ELAC protein 2	92			3				2		
PKHH2	Plekhh2	Pleckstrin homology domain-containing family H member 2	168					2		2		1
A2AQ17	Ndufaf1	Complex I intermediate-associated protein 30	38	1			3					1
CHCH3	Chchd3	Coiled-coil-helix-coiled-coil-helix domain-containing protein 3	26			3				3		
PPOX	Ppox	Protoporphyrinogen oxidase	51				3					1
PRDX5	Prdx5	Isoform Cytoplasmic+peroxisomal of Peroxiredoxin-5	17				3			2		
ARLY	Asl	Argininosuccinate lyase	?			1				2		
RT18B	Mrps18b	28S ribosomal protein S18b	29	1								2
Q9CZN7	Shmt2	Serine hydroxymethyltransferase	?			1				2		
USMG5	Usmg5	Up-regulated during skeletal muscle growth protein 5	6				2					1
Q3V1X6	Heatr1	Putative uncharacterized protein (Fragment)	?			1				2		
ATPA	Atp5f1a	ATP synthase subunit alpha	?				2					1
ACSF2	Acsf2	Acyl-CoA synthetase family member 2	68				2					2
ABD12	Abhd12	Monoacylglycerol lipase ABHD12	45				1			2		
RM28	Mrpl28	39S ribosomal protein L28	30				1	3				
ACAD9	Acad9	Acyl-CoA dehydrogenase family member 9	?							2		1
FIS1	Fis1	Mitochondrial fission 1 protein OS=Mus musculus	17				2			1		
HIBCH	Hibch	3-hydroxyisobutyryl-CoA hydrolase	43			1				2		
PGAM5	Pgam5	Isoform 2 of Serine/threonine-protein phosphatase PGAM5	?				2					1
NDUAD	Ndufa13	NADH dehydrogenase [ubiquinone] 1 alpha subcomplex subunit 13	17	2				1				
SAM50	Samm50	Sorting and assembly machinery component 50 homolog	?			2				1		

Table R1. List of the main proteins identified by the mass spectrometer that co-immunoprecipitate with $G\alpha_q$ and are present at the mitochondria. $G\alpha_q$ immunoprecipitates from endomembrane-enriched cell lysates of MEF wt, MEF $G\alpha_{q/11}$ (-/-), MEF $G\alpha_{q/11}$ (-/-) stably expressing $G\alpha_q$ and NIH3T3 fibroblasts were analyzed by mass spectrometry. Data obtained were processed using Scaffold software and proteins were sorted according to their number of peptides. Those proteins present either in the $G\alpha_{q/11}$ (-/-) immunoprecipitates or with less than 2 peptides between two other experimental conditions were omitted for the analysis. The resulting proteins were classified individually according to their function and subcellular localization, and those present at the mitochondria were listed. The list represents the number of peptides obtained for each protein in the cell lines utilized using either the anti- $G\alpha_q$ E-17 or the C-19 antibodies for the immunoprecipitation. Proteins previously found to interact with $G\alpha_q$ are highlighted in **green** (Calizo and Scarlata 2012; Cartier et al. 2011; Lecat et al. 2015; Sánchez-Fernández et al. 2014; Takahashi-Iwanaga and Iwanaga 2012). The arm-containing proteins Alex3 (Armcx3) and Armc10 are shown in **blue** (López-Doménech et al. 2012; Mirra et al. 2016; Serrat et al. 2013). Protein probability legend: 100%-95% **green**, 95%-40% **yellow**, 40%-5% **red**.

Because the main goal of this approach was to identify $G\alpha_q$ effectors located at the mitochondria, only those proteins known to play a role on these organelles were considered and appear listed according to the relative amount of peptides found in the different samples (**table R1**). The resulting list contains between 50 and 60 proteins and includes some previously described binding-partners for $G\alpha_q$ that elicit their function at the mitochondria, such as wdr36, caveolin-1, TRIO and Pleckstrin homology domain-containing family H member 2 (Pkhh2) (highlighted in green) (Cartier et al., 2011; Feng et al., 2019, 2014; Preuß, Kurig, Nürnberg, Orth, & Aktories, 2009; Sengupta et al., 2008). Fis1, a mitochondrial binding-partner for $G\alpha_q$ previously identified by our group (unpublished data) also appears in the list, which further validates our experimental approach. Among the proteins with more peptides identified stand out Alex3 (Armcx3) and Armc10, two arm-containing proteins enriched in brain recently proposed to mediate mitochondrial trafficking in neurons (López-Doménech et al. 2012; Serrat et al. 2014).

Both armadillo-domain proteins were proposed to regulate mitochondrial dynamics by interacting with and regulating Miro1 and TRAK2 (López-Doménech et al. 2012; Serrat et al. 2014), a phenotype that could be related with the changes in mitochondrial morphology and distribution previously observed in $G\alpha_{q/11}$ (-/-) cells (Benincá et al. 2014) . It is well documented that $G\alpha_{q/11}$ mediate Rho activation in a similar manner as $G\alpha_{12/13}$, which makes those arm-containing proteins a possible link for $G\alpha_q$ to regulate Miro1 activity. Interestingly, previous results from our group demonstrated that catenins and other arm-containing proteins could regulate G-protein signaling leading to RhoA activation. For example, $G\alpha_{12}$ interacts with the N-terminal region of p120 catenin (p120ctn) and regulates its function, thus compensating for its inhibitory activity towards RhoA and promoting cell adhesion in a cadherin-dependent manner (Ardawatia et al., 2011; Krakstad, Ardawatia, & Aragay, 2004). Besides, $G\alpha_{12}$ co-immunoprecipitates with the armadillo repeat protein deleted in velo-cardio-facial syndrome (ARVCF), a protein with 10 identified arm-repeats (unpublished data from our group).

	Cell line	Antibody	Number of peptides	coverage	Peptides spectra
Armadillo repeat-containing X-linked protein 3 (ARMCX3)	MEF WT	C-19	13	41%	MGYARKVGWVTAGLVIGAGACYCIYRLTRGRKQNKEK MAEGGSGDVDDAGDCSGARYNDWSDDDDDSNESKSI VWYPPWARIGTEAGTRARARARARATRARRAVQKRAS PNSDDTVLSPQELQKVLCLVEMSEKPYILEAALIALGNNA AYAFNRDIIRDLGGLPIVAKILNTRDPIVKEKALIVLNNLSV NAENQRRLKVYMNQVCDDTVTSRLNSSVQLAGLRLLTN MTVTNEYQHILANSISDFFRLFSAGNEETKLQVLKLLLNLA ENPAMTRELLRAQVPSSLGSLFNKKEYKEVILKLLIIFENIN DNFKWEENEPAQNHFSEGSLFFFLKEFQVCADKVLGIES RHDFQVRVKVGKFVAKLTERMFPKSQE
	MEF WT	**E-17**	7	24%	
	NIH 3T3	E-17	2	7,9%	
Armadillo repeat-containing protein 10 (ARMC10)	MEF WT	C-19	7	33%	MGGARDVGWVAAGLVLGAGACYCIYRLTRGPRRGGRR LRPSRSAEDLTDGSYDDILNAEQLKKLLYLLESTDDPVITE KALVTLGNNAAFSTNQAIIRELGGIPIVGNKINSLNQSIKE KALNALNNLSVNVENQTKIKIYVPQVCEDVFADPLNSAV QLAGLRLLTNMTVTNDYQHLLSGSVAGLFHLLLLGNGST KVQVLKLLLNLSENPAMTEGLLSVQVDSSFLSLYDGQVA NEILLRALTLFQNINNCLKVEGRLANQIPFAKGSLFFLLYG EECAQKMRALACHHDVDVKEKALAIKPKF
	MEF KO+ Gq	C-19	1	3,6%	
	MEF WT	**E-17**	6	28%	
	MEF KO+ Gq	*E-17*	2	5,9%	

Table R2. Representation of the peptides found for Armcx3 and Armc10 in the mass spectrometry analysis. Table shows the peptides contained in Armcx3 and Armc10 sequences detected by the mass spectrometer. For Armcx3, green residues were detected in MEF wt cells using the C-19 antibody, those in bold were also detected using the E-17 antibody and underlined sequences were found in NIH3T3 with E-17 antibody. For Armc10, green residues were detected in MEF wt cells with the C-19 antibody, the underlined peptide was also found in MEF $G\alpha_{q/11}$ (-/-) + $G\alpha_q$ cells, peptides in bold were found in MEF wt cells with the E-17 antibody and peptides in italics were found in MEF $G\alpha_{q/11}$ (-/-) + $G\alpha_q$ cells with the same antibody.

2. Alex3 is a novel binding partner of $G\alpha_q$

2.1. Alex3 binds $G\alpha_q$ in neuronal cells

Alex3 (Armcx3) appeared in MEF wt cells with 20 peptides detected in both C-19 and E-17 immunoprecipitations, but also 2 of its peptides were detected in NIH3T3 using the E-17 antibody. Similarly, all peptides of Armc10 were found in MEF cells using either E-17 or C-19 antibodies, most of them in MEF wt cell line but with a few peptides appearing in MEF $G\alpha_{q/11}$ KO cells recovered for the expression of $G\alpha_q$ (table R2). The relatively high amount of peptides found for both proteins in diverse experimental conditions provides a strong support for the specificity of protein interactions.

To validate the findings, we performed a series of immunoprecipitation experiments of endogenous proteins. First, a corroboration using MEF whole cell lysates control and $G\alpha_{q/11}$(-/-) cells was performed (Fig. R2a). As shown in figure R2a, Alex3, which appears as two main bands, is present in both cell lines, but only immunoprecipitates with the $G\alpha_q$ antibody when the G protein is present (in MEF control cells), thus validating our previous analysis.

To address if $G\alpha_q$ immunoprecipitates specifically with Alex3 in neuronal cells, endogenous $G\alpha_q$ was first immunoprecipitated from lysates of SHSY5Y neuroblastoma cells. A band corresponding to the molecular weight of Alex3 was detected with the Alex3 specific antibody in $G\alpha_q$ immunoprecipitates (**Fig. R2b**). Next, Alex3 and $G\alpha_q$ were immunoprecipitated from mouse brain homogenates using specific antibodies for each protein. Alex3 immunoprecipitation revealed a band corresponding to the molecular weight of $G\alpha_q$ and, in the same direction, a band was detected by the Alex3 specific antibody in $G\alpha_q$ immunoprecipitates, which was absent in the GFP immunoprecipitates used as a control (**Fig.R2c**). In those experiments, we noticed that the higher molecular weight band of Alex3 is predominantly detected in $G\alpha_q$ immunoprecipitates. Although the significance of the different bands detected by the anti-Alex3 antibody is yet to be experimentally determined, such band pattern is consistent with data shown in previous studies (López-Doménech et al. 2012; Serrat et al. 2014). Moreover, the band corresponding to Alex3 in $G\alpha_q$ immunoprecipitates shows a slight shift compared to the upper-molecular weight band of Alex3 (**Fig.R2c, third track**). This band though, was specific for the armadillo protein since the antibody was previously tested using Alex3 KO mice as a control (Prof. Soriano's laboratory). Such variation could be due to putative post-translational modifications, suggesting $G\alpha_q$ would only bind Alex3 under a specific modification stage. Overall, those results confirm that Alex3 can from a complex with $G\alpha_q$ and that both proteins associate in neuronal cells.

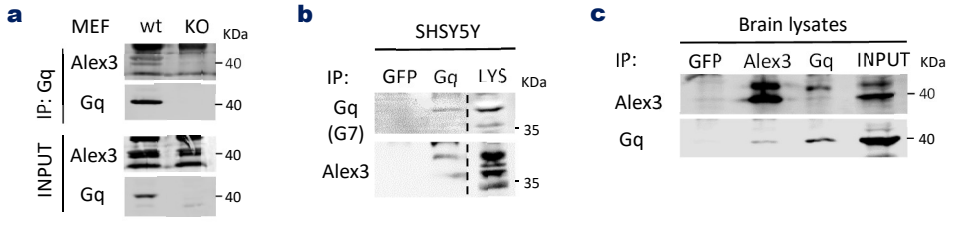

Figure R2. Endogenous $G\alpha_q$ associates with Alex3 in mouse embryonic fibroblasts, SHSY5Y neuroblastoma cells and mouse brain lysates. a, Immunoprecipitation of endogenous $G\alpha_q$ was performed in MEF wt and MEF $G\alpha_{q/11}$ (-/-) by incubating 1 mg of total lysates with 1 µg of $G\alpha_q$ specific antibody (E-17, Sta. Cruz). **b,** As in (a), 1.5 mg of SHSY5Y lysates were incubated with 1 µg of $G\alpha_q$ specific antibody and endogenous $G\alpha_q$ was immunoprecipitated. **c,** $G\alpha_q$ and Alex3 were immunoprecipitated from mouse brain homogenates by incubating 1.5 mg of homogenates with 2 µg of $G\alpha_q$ (E-17, Sta. Cruz®) or 1 µg of Alex3 (Proteintech®) specific antibodies, respectively . 1 µg of GFP antibody was incubated with 1.5 mg of homogenates as a control. 20 µg of homogenates were loaded as input. In all cases, antibodies were precipitated using sepharose G beads previous to SDS-PAGE analysis. Western blot was performed using anti-$G\alpha_q$ (Sta Cruz®, G-7 for (b) and Sta. Cruz® E-17 for (a) and (c)) and Alex3 (Proteintech®) antibodies. Data are representative of 3 independent experiments.

2.2. $G\alpha_q$ shows higher capacity to complex with Alex3 in its GTP-bound stage

G proteins are not static entities, but rather molecular switches that cycle between a GDP-bound inactive state and a GTP-bound active conformation. Their intracellular function and binding partners depend in great measure on the guanine nucleotide they have incorporated. With the goal to determine if $G\alpha_q$ interaction with Alex3 was depending on its nucleotide-bound stage, we performed a series of immunoprecipitation and pull-down experiments using the GTPase-deficient mutant $G\alpha_q$R183C. This mutant is unable to hydrolyze the GTP into GDP, so as long as it is able to incorporate GTP, it will remain constitutively in its GTP-active conformation.

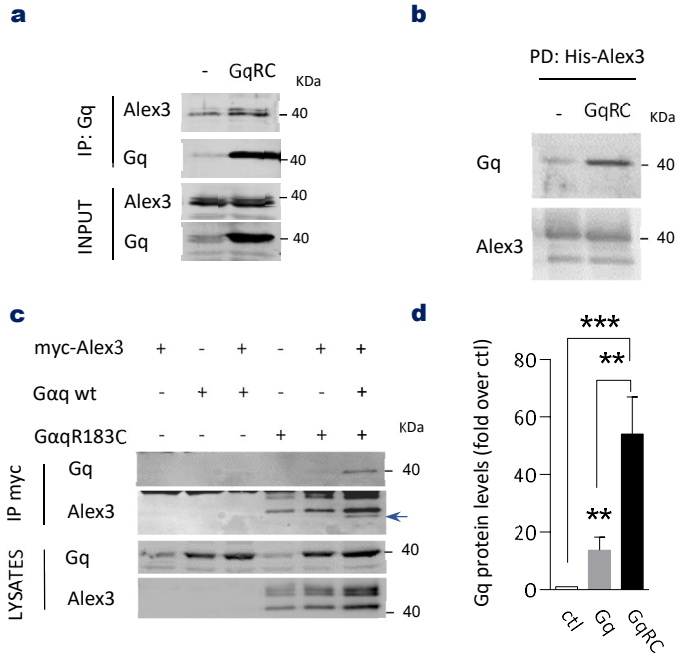

Figure R3. Alex3 binds preferentially to the constitutive active mutant $G\alpha_q$R183C. a, Lysates (700 µg) from HEK293 cells expressing $G\alpha_q$R183C were immunoprecipitated with $G\alpha_q$-specific antibody (E-17, Sta. Cruz®). **b,** Pull-down of 6xHis-tagged Alex3 (200 ng) from 700 µg of HEK293 cell lysates expressing $G\alpha_q$R183C **c,** Immunoprecipitation with anti-myc (9E10, Millipore®) from 700 µg of HEK293 extracts expressing myc-Alex3 and $G\alpha_q$ or $G\alpha_q$R183C, as indicated. In all cases, precipitates and total cell lysates were analyzed by western blot with specific antibodies for $G\alpha_q$ (BD Biosciences®) and Alex3 (Proteintech®). The blot developed with anti-Alex3 was previously developed with anti-$G\alpha_q$ (blue arrow indicates the $G\alpha_q$ band). **d,** Quantification of $G\alpha_q$ immunoprecipitated with Alex3 was done after western blot analysis using Odyssey and ImageStudio® software. Data are represented as the fold increase in $G\alpha_q$ co-immunoprecipitation over the control condition. Data are mean±SEM of 3 independent experiments. **p<0,005, ***p<0,001 two tailed Student's T-test.

$G\alpha_q$R183C was then expressed in HEK293 cells and its capacity to interact with Alex3 was compared to that of the endogenous protein (**Fig.R3a**). The GTPase-deficient mutant co-immunoprecipitates with the endogenous Alex3. Pull-down of 6xHis-tagged Alex3 also precipitated $G\alpha_q$R183C from lysates, further supporting the previous result (**Fig.R3b**). Comparing the immunoprecipitation from HEK293 cells expressing either mouse $G\alpha_q$ or $G\alpha_q$R183C, we observed the constitutive-active $G\alpha_q$ co-immunoprecipitates more efficiently with Alex3 than the wild-type form, although certain immunoprecipitation was observed with the GDP form. In principle, these results suggest that Alex3 interaction is favored by the active state of $G\alpha_q$ (**Fig.R3c** and quantified in **Fig.R3d**).

2.3. $G\alpha_q$ interacts with the arm-containing region of Alex3

To determine the region of interaction of $G\alpha_q$ in Alex3, a series of pull-down experiments were carried out using GST-tagged truncated forms of the protein. For those experiments, we designed an N-terminal fragment comprising the first 107 residues that contain both the mitochondrial and nuclear localization sequences and a C-terminal segment comprising the last 272 residues with the armadillo repeats (**Fig.R4a**). In a first approach, GST-Alex3 truncated proteins were pulled-down from cell extracts of HEK293 cells expressing $G\alpha_q$R183C (**Fig.R4b**). In the same direction as the previous IP experiments, $G\alpha_q$ pulls-down the full-length Alex3 protein and it does so with a similar efficacy as the C-terminal region. The N-terminal region pulls-down in a lesser extent but more than with the GST used as a control. The higher binding capacity of the C-terminal construct was confirmed by band quantification (**Fig.R4c**). Further, pull down of the same constructs from SHSY5Y undifferentiated cells revealed a clear interaction of the endogenous $G\alpha_q$ with the full-length Alex3, which was similar as the shown by the C-terminus and barely detectable using the N-terminal fragment (**FigR4d,e**). Both results are consistent with the idea that the arm-containing region of Alex3 is needed for the interaction with $G\alpha_q$.

The interacting region within Alex3 was further delineated by pulling-down two additional GST-tagged constructs, comprising the residues 107 to 273 (Ct1) and 274 to 379 (Ct2) (**Fig.R4a**). The results revealed a stronger interaction with the proximal armadillo domains (Ct1) compared with the distal segment (Ct2), but even though those constructs pulled-down lesser ammounts of $G\alpha_q$ than the full C-terminal region (Ct) (**Fig.R4f**). This might be due to conformational changes suffered after truncating the arm domains, which would indicate that a complete arm-containing region is necessary for the proper interaction between both proteins.

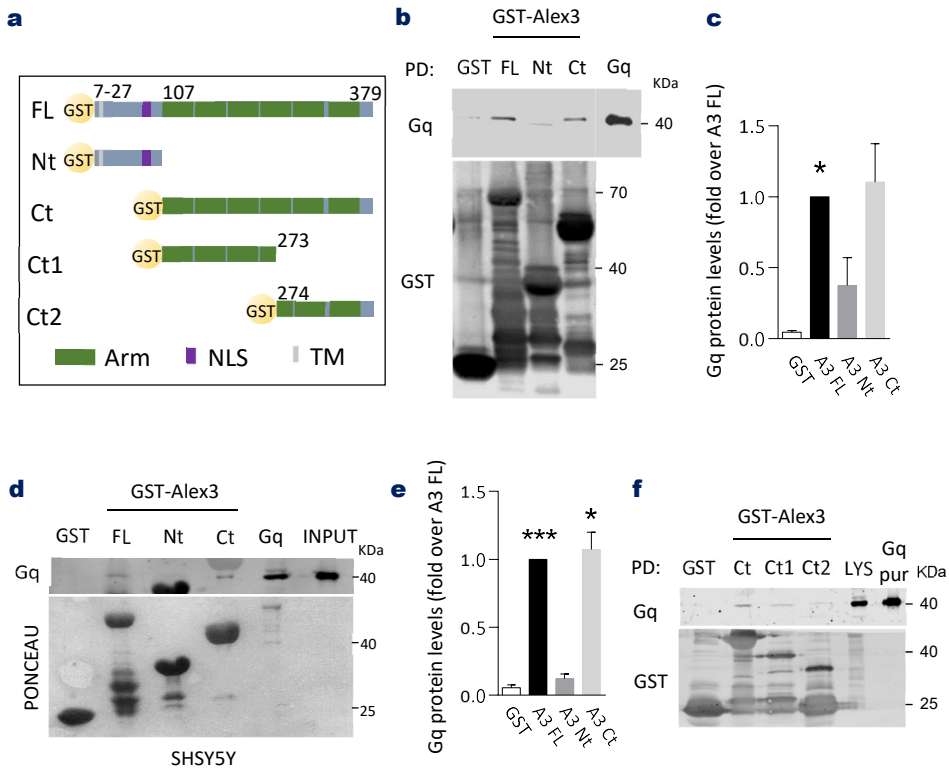

Figure R4. Gα$_q$ binds the armadillo-containing region of Alex3. a, Schematic diagrams of the GST-tagged Alex3 proteins utilized in de pull-down experiments; full-length (FL), N-terminus (Nt), C-terminus (Ct), C-terminus proximal (Ct1), C-terminus distal (Ct2), arm domains (Arm), nuclear localization signal (NLS), transmembrane domain (TM). **b,** Pull-down of the GST-proteins shown in (a). GST-beads (20 µg) were incubated and pulled-down from 700 µg of HEK293-Gα$_q$R183C cell lysates. **c,** Bands from pull-downs as (b) were quantified and represented as the fold increase of Gα$_q$ pull-down over the GST-Alex3 full-length (FL). **d,** Pull-down of the GST-proteins (5 µg) shown in (a) with 1.5 mg of SHSY5Y cell lysates. **e,** Bands from (d) were quantified and represented as the fold increase in precipitated Gα$_q$ over the GST-Alex3 full-length (FL). **f,** Pull-down of the GST-tagged C-terminal proteins shown in (a) with 700 µg of HEK293-Gα$_q$ cell lysates. In all cases, Gα$_q$ was analyzed by western blot using anti-Gα$_q$ (BD biosciences®) and anti-GST (Sigma®) when indicated. Data are mean±SEM of 3 independent experiments. *p<0,05, ***p<0,001 two tailed Student's T-test.

The previous results were corroborated by immunoprecipitation experiments using the previously characterized GFP-tagged Alex3 truncated proteins (**Fig.R5a**) (Serrat et al., 2013). Unexpectedly, immunoprecipitates revealed a stronger binding of Gα$_q$ with the Alex3 mutant lacking the last 16 amino acids compared with the full-length construct. In this case, the arm-lacking 1-106 protein showed an affinity comparable with Alex3 full length, but neither the first 45 residues nor the mitochondria localization signal-lacking mutant (ΔNt), which localizes exclusively to the nucleus (Serrat et al., 2013), reached a substantial degree of Gα$_q$ co-immunoprecipitation. A feasible hypothesis to explain the increased affinity of Gα$_q$ for the Alex3ΔCt mutant could come for posttranslational modifications within the last 16 residues in Gα$_q$ interaction. For example, phosphorylation of threonine 370 or serine 377 could difficult Gα$_q$ binding. Another explanation would be the easier access for Gα$_q$ to the arm-domains in the

absence of those amino acids. Whatever the case, the armadillo domains of Alex3 seem to have the foremost importance for $G\alpha_q$ interaction (see table R3 for a resume of results), as they have for other binding partners such as Miro1.

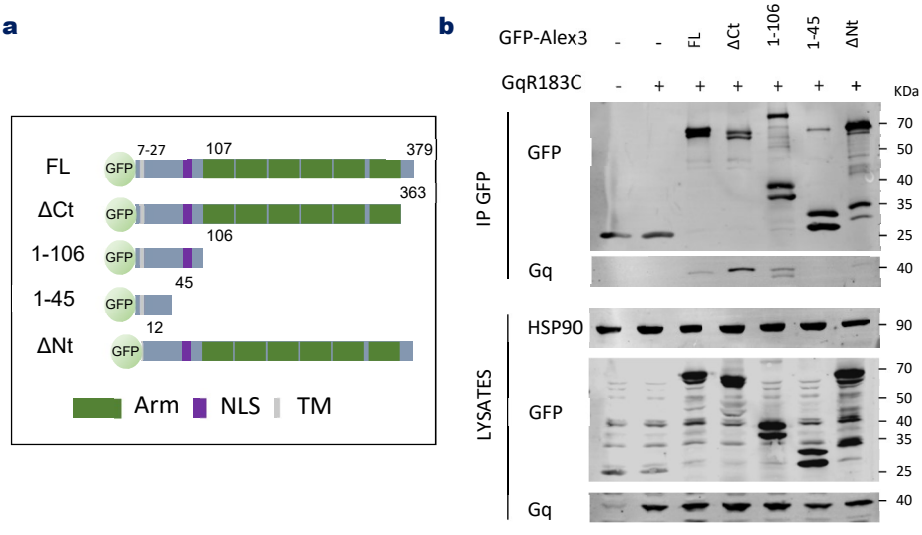

Figure R5. The most distal C-terminal region negatively regulates $G\alpha_q$ interaction with Alex3. a, Schematic diagrams of the GFP-tagged Alex3 proteins utilized in the immunoprecipitation experiment; full-length (FL),1-363 (ΔCt), 1-106, 1-45, 12-379 (ΔNt) arm domains (Arm), nuclear localization signal (NLS), transmembrane domain (TM). **b,** Immunoprecipitation of the GFP-tagged Alex3 proteins shown in (a) from HEK293 cells expressing GFP alone (indicated as -) or with $G\alpha_q$R183C. For each condition, 700 µg of lysates were incubated with 2 µg of GFP-trap (Chromotek®). Immunoprecipitates and total cell lysates were analyzed by western blot with specific antibodies for $G\alpha_q$ (BD biosciences®) and GFP (Invitrogen®) as indicated. HSP90 was used as a loading control. Data are representative of 3 independent experiments.

Name	Structure	Relative binding to $G\alpha_q$	Assay
FL	1 7-27 379	+++	IP/PD
ΔCt	363	++++	IP
ΔNt (nuclear)	12 379	-	IP
Ct	107 379	+++	PD
Ct1	107 273	++	PD
Ct2	274 379	-	PD
1-106	1 106	+	IP/PD
1-45	1 45	-	IP
Miro1	Miro1 binding region		

Arm NLS TM GTPase EF

Table R3. Relative binding to $G\alpha_q$ of the different Alex3 truncated proteins. The table indicates the symbol, a schematic representation of the protein, the relative capacity to interact with $G\alpha_q$ and the assay performed to determine the interaction. arm domains (Arm), nuclear localization signal (NLS), transmembrane domain (TM), GTPase domain (GTPase), EF calcium-binding domains (EF), immunoprecipitation (IP), pull-down (PD).

3. Miro1 is a novel binding partner of $G\alpha_q$

3.1. Miro1 interacts with Alex3

To date only a few partners have been proposed to explain the physiological role of Alex3 at the mitochondria. One of the best characterized is the atypical GTPase Miro1, which along with TRAK2 associates to the C-terminal region of Alex3 to promote mitochondrial motility (López-Doménech et al. 2012). The significance of Miro1 in mitochondrial transport has been widely addressed (Schwarz, 2013; Tang, Tang, & Luen, 2015). Miro1 is considered the main anchoring protein of the outer mitochondrial membrane to kinesin and dynein motors. The pair of EF-hand domains located between its two GTPase-homology regions allow Miro1 to function as a calcium-sensor that uncouples mitochondria from motor proteins under high calcium concentrations, thus halting mitochondria. The molecular function of both GTPase domains is still unclear, as their conformational changes due to the presence of GTP or GDP do not clearly correlate with an effect in mitochondrial movement. However, they represent most of the Miro1 structure and are involved in the interaction with many binding partners, including TRAK1/2 adaptors (Brickley et al., 2005; Brickley & Stephenson, 2011), PINK1 (Kane & Youle, 2011; Liu et al., 2012; Tsai et al., 2015; Wang et al., 2011; Weihofen et al., 2009) and mitofusins (Misko et al., 2010). In this regard, Miro1 is known to specifically bind the arm region of Alex3 in a calcium-dependent manner (López-Doménech et al. 2012). High cytoplasmic calcium concentrations promote Ca^{2+} binding within the EF domains and induce conformational changes in Miro1 that disrupt its interaction with Alex3. Nevertheless, the immunoprecipitation assays from whole cell lysates carried out so far do not allow to discern whether Miro1 and Alex3 interact directly or through an intermediate adaptor like TRAK2 (López-Doménech et al. 2012).

3.2. Alex3 interacts directly with Miro1

We first addressed the question whether Alex3 associates directly to Miro1. For that, we performed *in vitro* pull-down experiments using purified tagged proteins. First, GST-Miro1 was pulled-down in a buffer containing 50, 100 or 200 ng of purified His-Alex3. Western-blot analysis using an Alex3 specific antibody revealed a clearly distinguishable band at 40 KDa whose intensity reaches its maximum at the highest Alex3 concentrations (**Fig.R6a**). Non-specific interaction with the GST was barely detectable and did not correlate with the amount of purified Alex3 (**Fig.R6a**). The interaction between Alex3 and Miro1 was reported to be dependent on calcium concentrations (López-Doménech et al. 2012). To check whether high levels of calcium could disrupt the binding between both purified proteins, we pulled-down GST-Miro1 in the presence of purified His-Alex3 with or without 2 mM Ca^{2+} in the buffer (**Fig.R6b**). Consistent with the previous report (López-Doménech et al. 2012), increasing calcium levels up to 2 mM diminished

the interaction of purified His-Alex3 with Miro1, further validating our approach. With these results, we demonstrate for the first time the existence of a direct protein-protein interaction between Alex3 and Miro1.

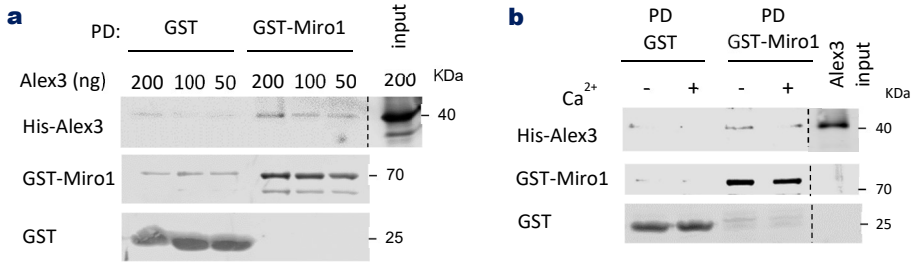

Figure R6. Alex3 interacts directly with Miro1. **a,** Pull-down of GST and GST-Miro1 was performed by incubating 5 µg of the bead-conjugated GST-proteins with 50, 100 and 200 ng of purified 6xHis-Alex3. **b,** Pull-down of GST and GST-Miro1 was performed by incubating 5 µg of the bead-conjugated GST-proteins with 100 ng of purified 6xHis-Alex3 in the presence or absence of 2 mM Ca^{2+} in the buffer. In both experiments, GST-Miro1 was analyzed by western blot with antibodies from Abcam®, Alex3 was analyzed with antibodies from Proteintech® and GST was analyzed with antibodies from Sigma®. 200 ng of purified Alex3 were loaded as input. Data are representative of 3 independent experiments.

3.3. $G\alpha_q$ interacts in a complex with Alex3 and Miro1

Since Miro1 immunoprecipitates with the same region of Alex3, we hypothesized that Miro1 and $G\alpha_q$ could be competing for the same binding domain in Alex3. To address that question, GFP-Alex3 was immunoprecipitated from HEK293 lysates expressing myc-Miro1, $G\alpha_q$R183C or both. Consistent with previous experiments, $G\alpha_q$ co-immunoprecipitated with Alex3 (**Fig.R7a,** tracks 5 and 6). As expected, Miro1 was also present in Alex3 immunoprecipitates. (**Fig.R7a,** tracks 3 and 6). Quantification of relative amount of proteins in the bands revealed an increased co-immunoprecipitation in the presence of $G\alpha_q$ (**Fig.R7b,c**). This raises the possibility that $G\alpha_q$ and Miro1 are both present in a protein complex with Alex3 to regulate mitochondrial dynamics. Here we observed that when the three proteins are expressed together, the lowest band of Alex3 is more prominent.

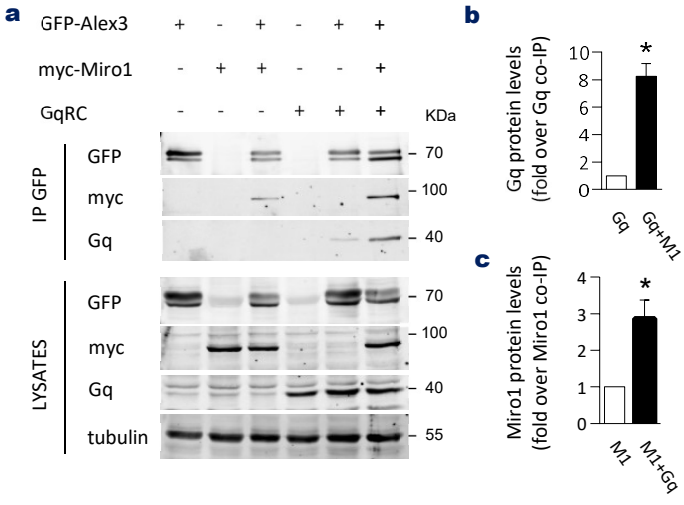

Figure R7.Alex3 co-immunoprecipitation with Miro1 and Gα$_q$. a, Immunoprecipitation of GFP-tagged Alex3 from HEK293 cells expressing GFP-Alex3 with myc-Miro1, and/or Gα$_q$R183C, as indicated. Cell lysates (700 µg of) were incubated with 5 µg of anti-GFP (made at IBMB) and GFP-Alex3 was immunoprecipitated using G-sepharose beads. **b,** Gα$_q$R183C precipitation in the presence or absence of Miro1 was quantified and represented as the fold increase. **c,** Miro1 precipitation in the presence or absence of Gα$_q$R183C was quantified and represented as the fold increase. Data are mean±SEM of 3 independent experiments. *p<0,05, two tailed Student's T-test.

3.4. Gα$_q$ interacts with Miro1

After finding that Gα$_q$ promotes the co-immunoprecipitation of Miro1 with Alex3, we hypothesized if Miro1 could also function as a binding partner for Gα$_q$. To find out, a series of pull-down and immunoprecipitation assays were done using different tagged constructs of Miro1 (FigR8a). First, GST-Miro1 was pulled-down from SHSY5Y lysates (FigR8b). Consistent with our previous experiments, endogenous Alex3 precipitated with the GST-Miro1, but not with the GST alone. Besides, a band at 40 kDa was present after developing with the Gα$_q$-specific antibody, indicating that endogenous Gα$_q$ also precipitates with Miro1 (FigR8b).

The precipitation of endogenous Gα$_q$ with Miro1 prompted us to think whether this interaction occurs during the active or the inactive conformation of the Gα. To address that, we first tested the precipitation capacity of the GTPase-deficient Gα$_q$R183C with GFP-tagged Miro1. Consistent with the previous pull-down, immunoprecipitation of GFP-Miro1 also precipitated active-Gα$_q$ (FigR8c). Next, a comparative IP between the wild-type and the active Gα$_q$ mutant was performed by immunoprecipitating myc-Miro1 in the presence of each Gα$_q$ form (FigR8d). This time, we did not notice substantial differences in co-IP between the mutant and the wild-type form.

Interestingly, we did notice an increase in co-IP of endogenous Alex3 when $G\alpha_q$ was expressed, thus reinforcing the idea of a putative complex between the three proteins (FigR8d). With that data, we propose that Miro1 could also function as a binding partner for both Alex3 and $G\alpha_q$. Overall, $G\alpha_q$ interaction with Miro1 suggests a possible role of $G\alpha_q$ regulating mitochondrial motility, as it has Alex3.

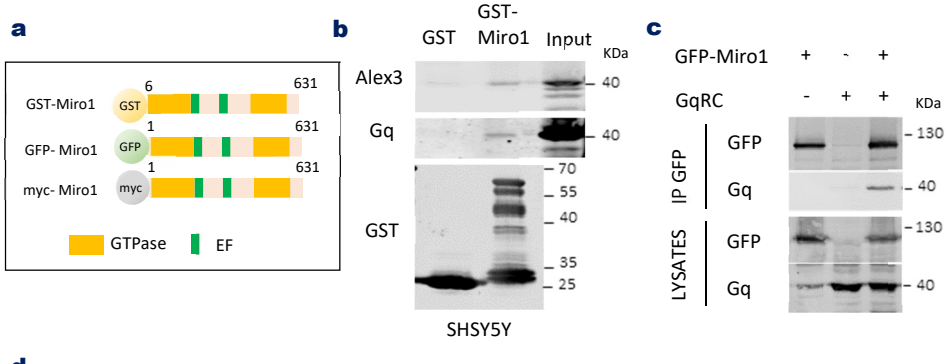

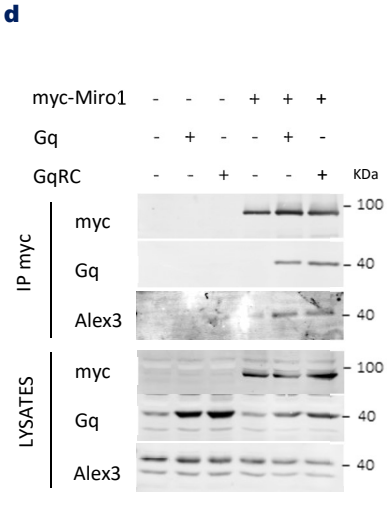

Figure R8. $G\alpha_q$ immunoprecipitates with Miro1 in SHSY5Y and HEK293 cells. a, Schematic diagrams of the GST-tagged Miro1 proteins. **b,** Pull-down of GST-Miro1 (10 µg) from 1.5 mg of SHSY5Y cell lysates. After SDS-PAGE analysis, endogenous $G\alpha_q$ and Alex3 were detected by western blot using specific antibodies. **c,** Immunoprecipitation of GFP-Miro1 from HEK293 cells expressing GFP-Miro1 and/or $G\alpha_q$R183C, as indicated above. 700 µg of lysates were incubated with 5 µg of GFP antibody (Invitrogen®) and GFP-Miro1 was immunoprecipitated using G-sepharose beads. **d,** Immunoprecipitation of myc-Miro1 from HEK293 cells expressing myc-Miro1 and $G\alpha_q$ or $G\alpha_q$R183C. For each condition, 700 µg of lysates were incubated with 5 µg of myc antibody (Millipore®) and myc-Miro1 was immunoprecipitated using G-sepharose beads. For all cases, western blot analysis was performed with anti-$G\alpha_q$ (BD biosciences®), anti-myc (Millipore®), anti-GFP (Sta. Cruz®), anti-GST (Sigma®) or anti-Alex3 (Proteintech®) when indicated, and data are representative of 3 independent experiments.

3.5. $G\alpha_q$ interaction with Alex3 and Miro1 is independent of its PLCβ binding region

After determining that both Alex3 and Miro1 interact with $G\alpha_q$, we asked whether they would use the same binding region on the Gα than its canonical effector, the PLCβ, and thus interfere in the canonical $G\alpha_q$ signaling. To address that question, Alex3 and Miro1 were immunoprecipitated in the presence of a $G\alpha_q$ mutant unable to bind PLCβ ($G\alpha_q$Q209L/R256A/T257A). In the same experiments, we also tested whether Alex3 and Miro1 would bind to the fully active $G\alpha_q$ mutant,

the $G\alpha_q$Q209L. Unlike $G\alpha_q$R183C, the $G\alpha_q$Q209L is constitutive active regardless of the presence of RGS proteins.

The results showed that the PLCβ binding region was not necessary to precipitate neither Alex3 nor Miro1, since both mitochondrial proteins co-precipitated with the $G\alpha_q$Q209L/R256A/T257A mutant (**Fig.R9a,b**). This result indicates that both proteins bind $G\alpha_q$ through a different motif, as described for other binding partners (Sánchez-Fernández et al., 2014). Surprisingly, we observed an important decrease of Alex3 and Miro1 interaction with the fully active mutant $G\alpha_q$Q209L (**Fig.R9a,b** third track). As mentioned, the only known difference between $G\alpha_q$Q209L and $G\alpha_q$Q209L is the ability of the last to bind RGS-containing proteins (Kasom, Gharra, Sadiya, Avital-Shacham, & Kosloff, 2018; Takasaki et al., 2004), so this result may indicate the presence of a RGS-like domain within Alex3 and Miro1 or the involvement of additional proteins in their interaction.

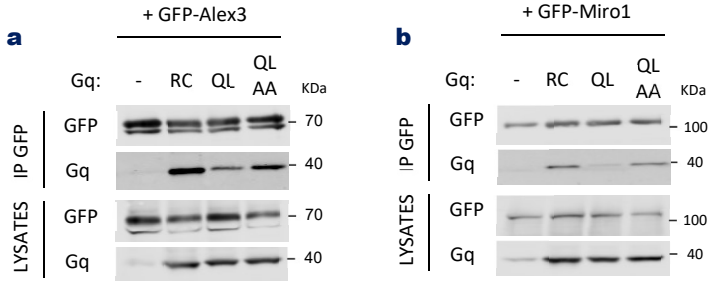

Figure R9. The PLCβ binding mutant $G\alpha_q$Q209LR256A/T257A, but not the fully active $G\alpha_q$Q209L, associate with Alex3 and Miro1. a,b, Immunoprecipitation of GFP-Alex3 (a) or GFP-Miro1 (b) from HEK293 lysates expressing $G\alpha_q$R183C (RC), $G\alpha_q$Q209L (QL) or $G\alpha_q$Q209L/R256A/T257A (QLAA), as indicated. 700 µg of cell lysates were incubated with 2 µg of GFP-trap antibody (Chromotek®). Immunoprecipitates and total cell lysates were analyzed by western blot with specific antibodies for $G\alpha_q$ (BD biosciences®) and GFP (Invitrogen®). Data are mean±SEM of 2 independent experiments.

3.6. Molecular basis of $G\alpha_q$ precipitation with Miro1

To address the molecular mechanisms that regulate $G\alpha_q$ precipitation with Alex3 and Miro1, we focused on the main mechanism of regulation of Alex3-Miro1 interaction: the cytoplasmic calcium concentrations. Because the regulatory activity of Alex3 towards Miro1 depends on the EF hand in the mitochondrial GTPase (López-Doménech et al. 2012), we aimed to determine whether $G\alpha_q$ association could be regulated in a similar manner. To address that, a myc-Miro1 protein with dysfunctional EF-hand domains (Miro1ΔEF) was precipitated in the presence of $G\alpha_q$ or $G\alpha_q$R183C (**Fig.R10b**). Interestingly, both $G\alpha_q$ and $G\alpha_q$R183C showed increased co-IP with the Miro1ΔEF mutant. Such unexpected result seems to indicate that point mutations in the Miro1ΔEF

promote a conformational change that favors $G\alpha_q$ interaction, probably though a more accessible conformation. To rule out a possible artificial precipitation, the experiment was further validated though the inverse IP, in which $G\alpha_q$ and $G\alpha_q$R183C were precipitated from cells expressing either the wild-type Miro1 or the EF mutant (**Fig.R10c**). Consistently, this other experiment showed almost identical results in the western blot analysis, thus reinforcing the importance of Miro1 central domain for $G\alpha_q$ interaction.

Considering that mutations in the EF-calcium binding domains affect $G\alpha_q$ precipitation with Miro1, we decided to investigate if $G\alpha_q$ binding to Miro1 was dependent on cytoplasmic calcium levels. For that, IP and pull down experiments were performed in a buffer containing 2 mM Ca^{2+}, as previously documented for Alex3 (López-Doménech et al. 2012). The results only showed a slight decrease in $G\alpha_q$ co-IP under high calcium concentrations (**Fig.R10d**), which contrasts with the almost undetectable precipitation of endogenous Alex3 in the presence of 2 mM Ca^{2+}. Importantly, this reduction in Alex3 precipitation agrees with the previous report (López-Doménech et al. 2012) and validates our assay. However, we cannot rule out that exogenous expression of $G\alpha_q$ might diminish the differences in the co-IP, since the reduction in Alex3 co-IP is detected with the endogenous protein (**Fig.R10d**).

The previous experiments seem to indicate that calcium concentrations are not as important to regulate $G\alpha_q$ interaction with Miro1, as they are in the case of Alex3. Therefore, we tested whether conformational changes on Miro1 would regulate this putative interaction by pulling-down mutant Miro1 proteins lacking the C-terminal GTPase (M1-388) or the entire form only lacking six amino acids (M1-6-800) in lysates from HEK293 cells expressing $G\alpha_q$R183C (**FigR10e**). $G\alpha_q$ pulls-down with both Miro1 constructs, although the C-terminal GTPase-lacking mutant form (M1-388) showed a greater association with $G\alpha_q$R183C (**FigR10f**), suggesting that the N-terminal region containing the first GTPase and EF domains is important for interaction and that the C-terminal domain behaves as a inhibitory region. These results are in agreement with the previous experiments, and strongly suggest that $G\alpha_q$ interaction with Miro1 depends on conformational changes on the atypical GTPase that may differ from those regulated by calcium concentrations.

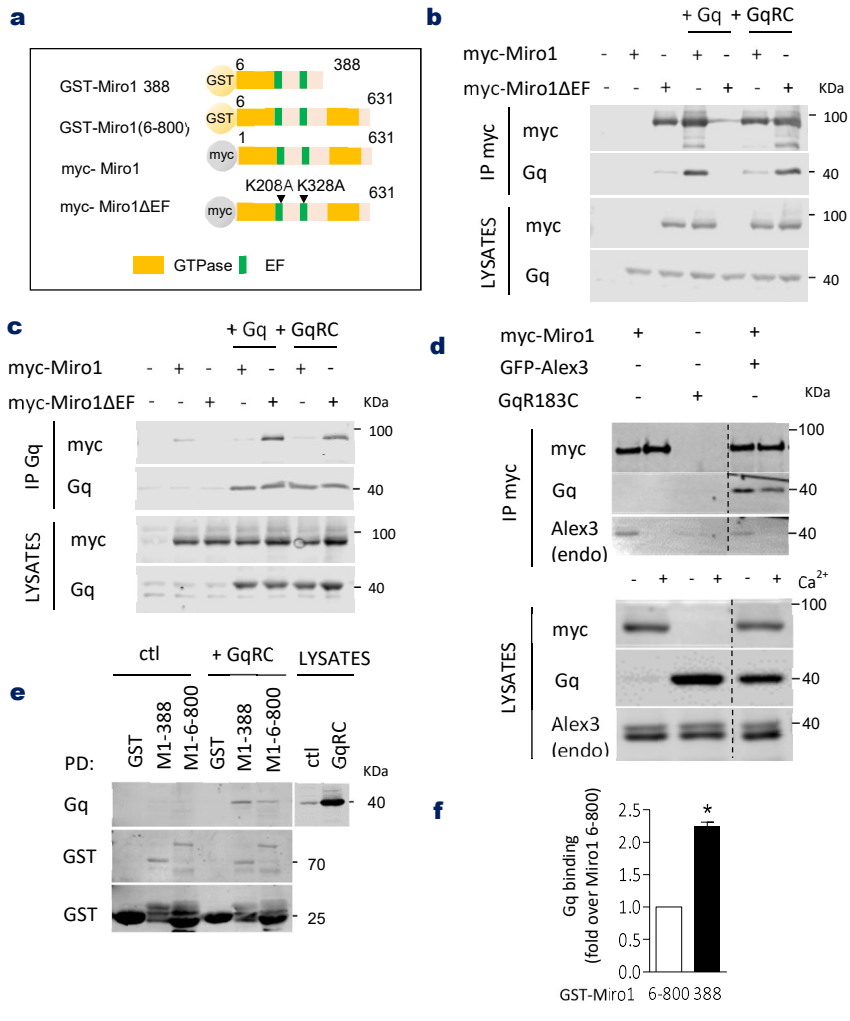

Figure R10. Molecular basis of Gα$_q$ precipitation with Miro1. a, Schematic diagram of the Miro1-tagged proteins utilized in the immunoprecipitation and pull-down experiments **b,** Immunoprecipitation of myc-tagged Miro1 or mutant (Miro1ΔEF) from HEK293 transfected cells in the presence or absence of Gα$_q$ or Gα$_q$R183C. Cell lysates (700 µg) were incubated with myc-trap antibodies (Chromotek®) previous to SDS-PAGE analysis. **c,** From cells transfected as in (b), Gα$_q$ was immunoprecipitated with anti-Gα$_q$ (BD Biosciences®) using G-sepharose beads previous to SDS-PAGE analysis. In both experiments, immunoprecipitates and total cell lysates were analyzed by western blot with specific antibodies for Gα$_q$ and myc. Data are representative of at least 2 independent experiments. **d,** Immunoprecipitation of myc-Miro1 from HEK293 cells expressing myc-Miro1 and Gα$_q$R183C. For each condition, 700 µg of lysates were incubated with 1 µg of myc antibody (Sigma®) in the presence or absence of 2 mM Ca^{2+} **e,** Pull-down of GST-Miro1 was performed from HEK293 either transfected with empty vector or containing Gα$_q$R183C. Cell lysates (700 µg) were incubated with 10 µg of bead-conjugated GST-Miro1. Gα$_q$ and GST were analyzed by western blot using a specific antibodies from BD biosciences® and Sigma®, respectively. **f,** Blot bands from experiments as in (e) were quantified and represented as the fold increase in Gα$_q$ interaction with the truncated protein GST-Miro1 388 compared with the GST-Miro1 6-800. Data are mean±SEM of 3 independent experiments. *p<0,05, two tailed Student's T-test.

3.7. $G\alpha_q$ interacts directly with Alex3 and Miro1

Because $G\alpha_q$ barely decreases its co-IP with Miro1 in the presence of high calcium levels, it is unlikely that it associates to Miro1 indirectly through Alex3, as could be initially inferred. Despite no peptides of Miro1 were detected in the preliminary proteomic analysis, the atypical GTPase could be acting as a direct binding-partner for $G\alpha_q$ as proposed for Alex3. To confirm a possible direct interaction of Alex3 and Miro1 with $G\alpha_q$, pull-down experiments with purified components were performed with the previously utilized GST-tagged constructs of Miro1 and Alex3.

We first tested the interaction of purified $G\alpha_q$ with both Alex3 and Miro1 full-length proteins using two different buffers (**Fig.R11a**). Interestingly, $G\alpha_q$ interacted with both mitochondrial proteins with similar affinity in the two buffers tested. Besides, $G\alpha_q$ affinity towards Miro1 was slightly decreased upon addition of His-Alex3 to the buffer, suggesting a possible competition between Alex3 and $G\alpha_q$ for the binding region on Miro1. This results contrasts with the previous immunoprecipitation assay, and suggests the presence of additional proteins in the putative Miro1-Alex3-$G\alpha_q$ complex. Next, we tested the affinity of purified $G\alpha_q$ towards the previously characterized Alex3 and Miro1 constructs. Consistent with our previous experiments, $G\alpha_q$ showed increased affinity towards the C-terminal armadillo-containing region of Alex3, although some interaction with the N-terminus was also present (**Fig.R11b,c**). Besides, the binding capacity of $G\alpha_q$ was also increased when pulling-down a construct lacking the C-terminal GTPase domain (M1-388), as previously demonstrated in cell lysates (**Fig.R11b**). This assay further validates our previous experiments and proves that $G\alpha_q$ interacts preferentially with the C-terminal Alex3 and the N-terminal Miro1.

Finally, we tested the capacity of Alex3 to compete for the binding region of Miro1 by pulling down GST-Miro1 in the presence of constant concentrations of purified $G\alpha_q$, but increasing amounts of His-Alex3. The results only showed Alex3 interaction with Miro1 when the protein concentration was high enough and this interaction did not produce a detectable decrease in Miro1 affinity towards $G\alpha_q$ (**Fig.R11d**). Overall, these results suggest a putative regulation of Alex3 and Miro1 functions through direct binding to $G\alpha_q$.

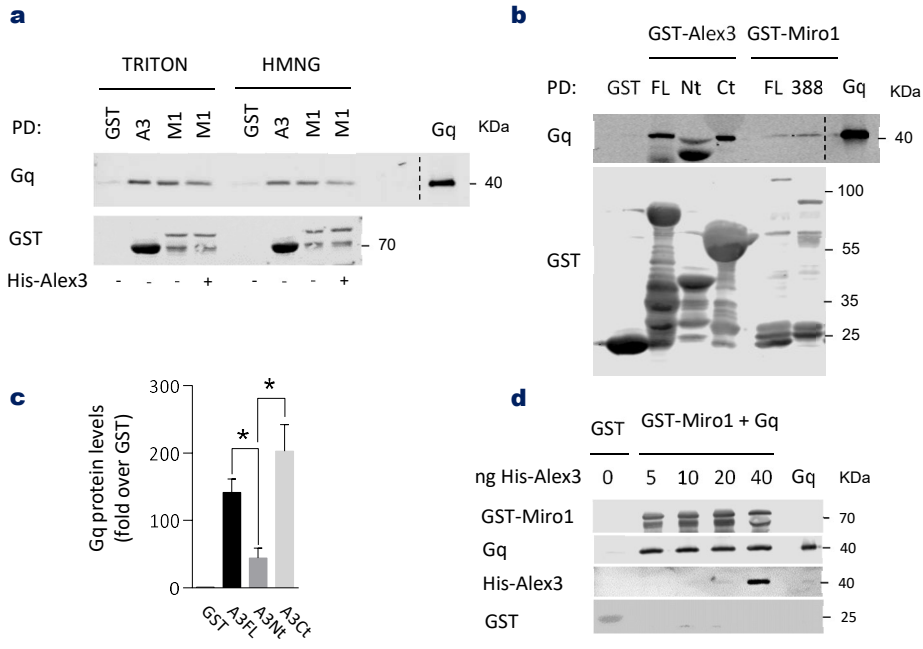

Figure R11. Purified $G\alpha_q$ interacts directly with Alex3 and Miro1. a, Pull-down of GST-Alex3 (A3) and GST-Miro1 (M1) was performed by incubating 10 ng of purified $G\alpha_q$ with 10 µg of the bead-conjugated GST-proteins in Triton or HMNG buffer (as detailed in materials) with or without 20 ng of His-Alex3. **b,** Pull-down of the GST-Alex3 constructs (shown in R4a) and the Miro1 constructs (shown in R8a) was performed by incubating 10 ng of purified $G\alpha_q$ with 10 µg of the bead-conjugated GST-proteins in PD buffer. **c,** Quantification of the fold increase in pulled-down $G\alpha_q$ by the different GST-Alex3 constructs over the control condition (GST). **d,** Pull-down of GST-Miro1 was performed by incubating 10 ng of purified $G\alpha_q$ with 10 µg of the bead-conjugated GST-proteins in $G\alpha_q$ buffer in the presence of 5, 10, 20 or 40 µg of 6xHis-Alex3. Experiments were analyzed by western blot using specific antibodies (BD biosciences® for $G\alpha_q$, Proteintech® for Alex3, Sigma® for Miro1 and GST) and 20 ng of purified $G\alpha_q$ were loaded as a control. Data are mean±SEM of 3 independent experiments. *p<0,05, **p<0,005 two tailed Student's T-test followed by Mann-Whitney test.

3.8. $G\alpha_q$ localizes at the mitochondria within the same structures as Miro1

In light of our previous results from immunoprecipitation and pull-down experiments, we aimed to find whether $G\alpha_q$ localizes with Miro1 at the mitochondria. For that, we utilized COS-7 cells taking advantage that mitochondria are easy to visualize. We addressed whether $G\alpha_q$ was localizing within the same mitochondrial structures by co-expressing the $G\alpha_q$ with a Cherry-tagged Miro1 (**Fig.R12**). Consistent with previous reports (Guo et al., 2005), Miro1 expression was detected along the outer mitochondrial membrane in a patch pattern. As expected, $G\alpha_q$ expression (**Fig.R12a,** green) shows a scattered staining throughout the cytoplasm, but also displays a clear localization along the outer and inner mitochondrial membranes (**Fig.R12b**). These results agree with previous reports that suggest the presence of $G\alpha_q$ in the outer and intermembrane space using trypsin digestion experiments (Benincá et al., 2014). Here we observe $G\alpha_q$ localization at the most external region of the outer membrane, where it localizes close to Miro1 at specific patches, resembling membranous intra-mitochondrial domains. $G\alpha_q$ expression

was also present in the intermembrane in a pattern that resemble the mitochondria crest structures. With that data, we first visualize the specific localization of $G\alpha_q$ at the outer and inner mitochondrial membranes. These results also suggest that Miro1 and $G\alpha_q$ are positioned together in certain subregions as molecular aggregates.

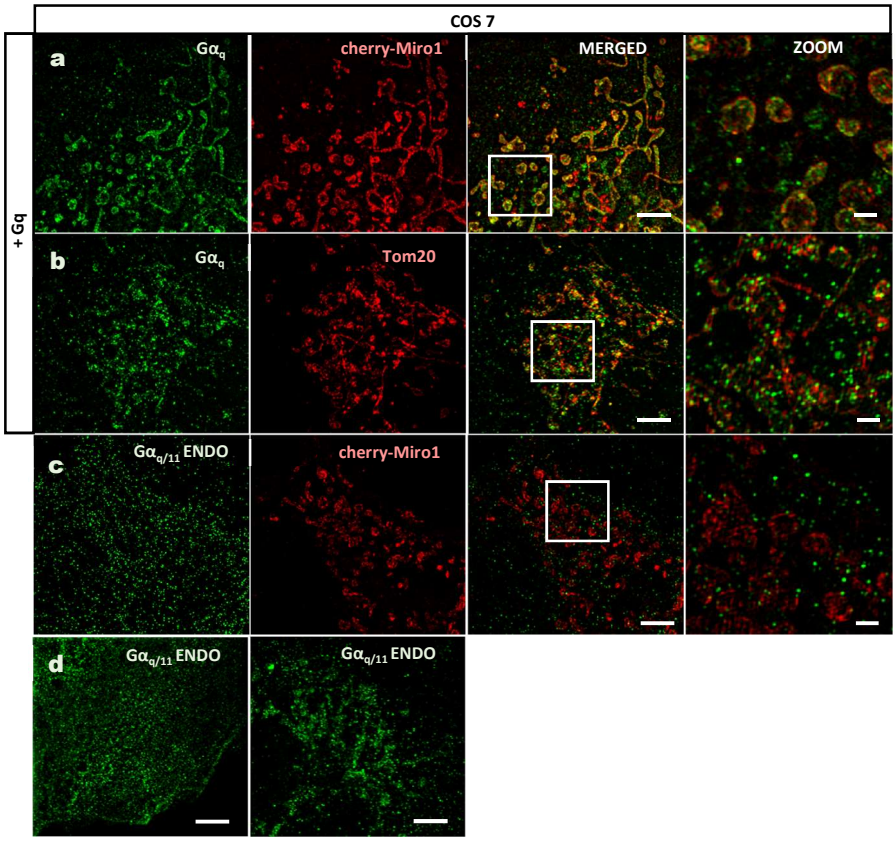

Figure R12. Superresolution images of $G\alpha_q$ and Miro1 at the outer mitochondrial membrane. Superresolution images of Cos7 cells expressing cherry-Miro1 and $G\alpha_q$ (**a**), cherry-Tom20 and $G\alpha_q$ (**b**), cherry-Miro1 alone (**c**) or none of them (**d**, control cells). Immunofluorescence was performed using anti-$G\alpha_q$ (Sta. Cruz®) and Alexa-Fluor-488 antibodies. Images were taken using a N-SIM microscope system (Nikon) equipped with a SR Apo TIRF 100× objective and are representative of the majority of the cells of at least 2 independent experiments. Images are overlays from 0.15 µm slides. Magnified images corresponding to the small box are shown on the right. Scale bars, 5 µm and 1 µm (magnification).

4. Alex3 expression induces fusion at the outer mitochondrial membrane

4.1. Alex3 induces fusion at the outer mitochondrial membrane in HeLa and MEF cells

It was previously described that Alex3 overexpression induces mitochondrial aggregation around the perinuclear region (López-Doménech et al. 2012; Serrat et al. 2013). To evaluate that phenotype, MEF and HeLa cells were transfected with GFP-Alex3 and mtDsRed, a fusion protein containing *Discosoma* red fluorescent protein and the mitochondrial targeting sequence from

subunit VIII of human cytochrome c oxidase. The first impression from MEF cells expressing GFP-Alex3 is a clear hyperfusion of the mitochondrial network. Fused mitochondria seem to collapse in a point close to the nucleus, generating a mitochondrial cluster (Fig.R13a). Looking in depth those clustered mitochondria we realized there is no colocalization between Alex3 (which locates at the outer mitochondrial membrane) and mtDsRed (that localizes inside the mitochondrial matrix). Mitochondrial clusters seem to have a fusion phenotype of the outer mitochondrial membrane (shown in green) while keeping unaltered their mitochondrial matrixes (Fig.R13b). Interestingly, Miro1 overexpression alters mitochondrial network in a similar manner, inducing hyper fusion and perinuclear aggregation (Yamaoka, Nakajima, Fujimoto, & Tsutsumi, 2011). Although this phenotype has been linked to an interaction with mitofusins (Misko et al., 2010), we cannot rule out the involvement of alternative pathways regulating mitochondrial morphology. It can also imply that the phenotype promoted by Alex3 is linked to Mfn1 or 2.

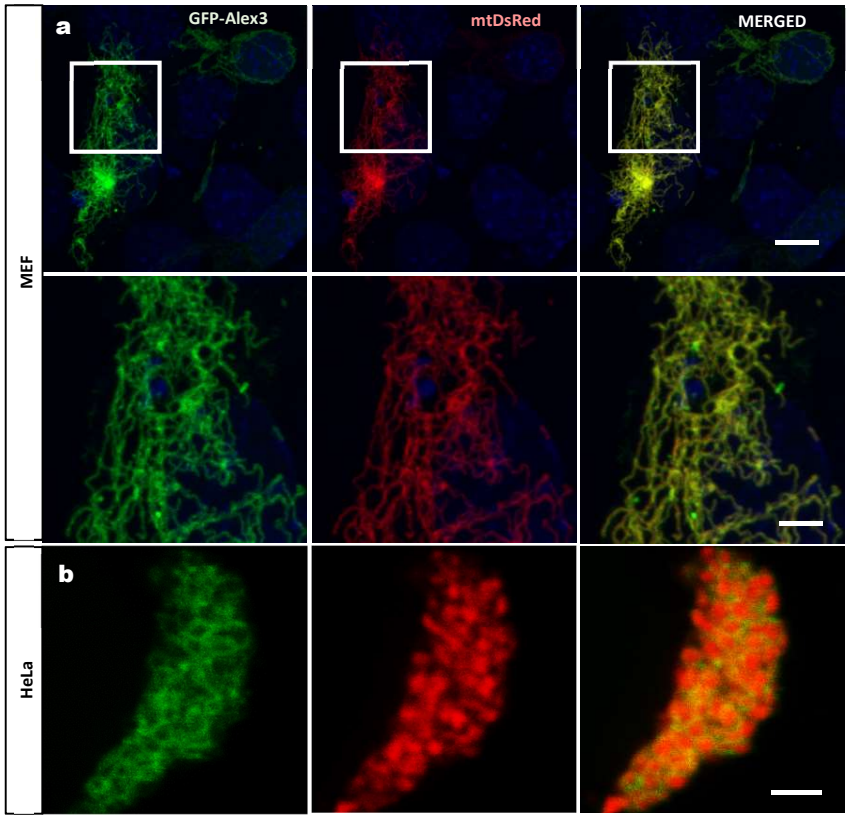

Figure R13. Alex3 overexpression induces fusion of the outer mitochondrial membrane and perinuclear aggregation. a, Confocal micrographs of MEF cells expressing mtDsRed and GFP-Alex3. Magnified images corresponding to the small box are shown below. **b,** Confocal micrographs of HeLa cells expressing mtDsRed and GFP-Alex3. Images are maximum intensity projections of 6 stacks (0.3 µm per stack) and were acquired using Zeiss LSM780 confocal microscope using a 63x1.3NA oil immersion lens. All images are representative of the majority of the cells from 3 independent experiments. Images are maximum intensity projections. Scale bars, 10 µm (upper panels), 3 µm (middle and lower panels).

4.2. Alex3 induces mitochondrial clustering and fusion of the outer mitochondrial membrane in the absence of mitofusins

Our previous images suggest a possible role of Alex3 regulating fusion of the outer mitochondrial membrane. Since fusion is primarily mediated by mitofusins 1 or 2 (Hsiuchen Chen et al., 2003; Filadi, Pendin, & Pizzo, 2018; Ansgar Santel et al., 2003), we wondered if Alex3 could be affecting somehow their function.

To address that question, MEF cells depleted for Mfn1 or Mfn2 were transfected with plasmids expressing the mitochondrial marker mtDsRed and GFP-Alex3. It is widely documented that depletion of either Mfn1 or Mf2 results in a totally fragmented mitochondrial network (Santel & Fuller, 2001; Santel et al., 2003). Indeed, in our experiments we also noticed that those cells expressing mtDsRed but not Alex3 show completely fragmented mitochondria (FigR14a,c white arrowheads). However, expression of Alex3 (detected by the GFP signal) was sufficient to induce perinuclear aggregation of mitochondria (FigR14a,c yellow arrowheads). Because Alex3-induced mitochondrial clustering depends on the expression levels of the protein, we also looked for cells with milder levels of Alex3 to see whether it could also rescue the fragmentation phenotype. Indeed, cells expressing Alex3 displayed longer mitochondria than would be expected for either Mfn1 or Mfn2-deficient cells (FigR14b,d). With that, we demonstrate that Alex3 can induce mitochondrial aggregation and, more impressively, prevent mitochondrial fragmentation in a Mfn1- or Mfn2-deficient background.

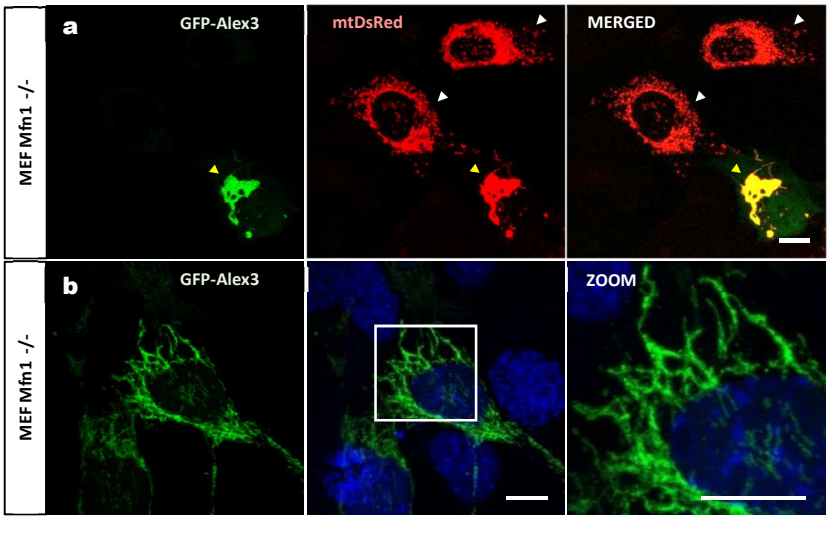

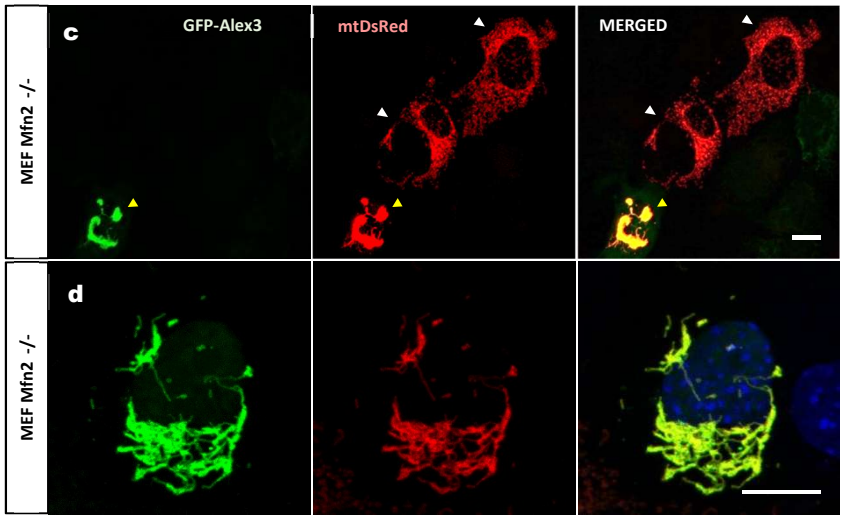

Figure R14. Alex3 expression induces mitochondrial fusion and perinuclear aggregation even in the absence of Mfn1 or Mfn2. a, Confocal micrographs of MEF Mfn1(-/-) transfected with mtDsRed and GFP-Alex3. Cells that do not express GFP-Alex3 show fragmented mitochondrial network, whereas expression Alex3 induces mitochondrial fusion. Box corresponds to the magnified image shown at a side. **b,** Confocal micrographs of a Mfn1(-/-) cell expressing GFP-Alex3. **c,** Example of MEF cells Mfn2(-/-) transfected with mtDsRed and GFP-Alex3. Again, only cells that express GFP-Alex3 show clustered mitochondria. **d,** Confocal micrographs of a Mfn2(-/-) cell expressing GFP-Alex3. Images are maximum intensity projections of 6 stacks and were acquired using a Zeiss LSM780 confocal microscope using a 63x1.3NA oil immersion lens. All images are representative of the majority of the cells from 3 independent experiments. Scale bars, 10µm.

4.3. Depletion of $G\alpha_q$ increases Alex3-induced mitochondrial clustering

Previous results from our group revealed important alterations in the mitochondrial network of MEF cells depleted for $G\alpha_q$ (Benincá et al., 2014), so we asked if those effects could be related with the mitochondrial clustering induced by Alex3. To address the putative implication of $G\alpha_q$ pathway in those aggregates, Alex3 was co-expressed with the mitochondrial marker mtDsRed in MEF wt and MEF $G\alpha_{q/11}$ (-/-) cells.

As previously reported, cells expressing Alex3 display mitochondrial aggregates that are absent in those only expressing mtDsRed (**Fig.R15a**). Strikingly, this phenotype was enhanced in cells lacking $G\alpha_q$, thus suggesting a possible inhibitory effect of $G\alpha_q$ on Alex3 phenotype. The number of cells with clustered mitochondria (**Fig.R15c**) as well as the aggregation degree (**Fig.15d**) was quantified and demonstrates the impact of $G\alpha_q$ regulating mitochondrial positioning.

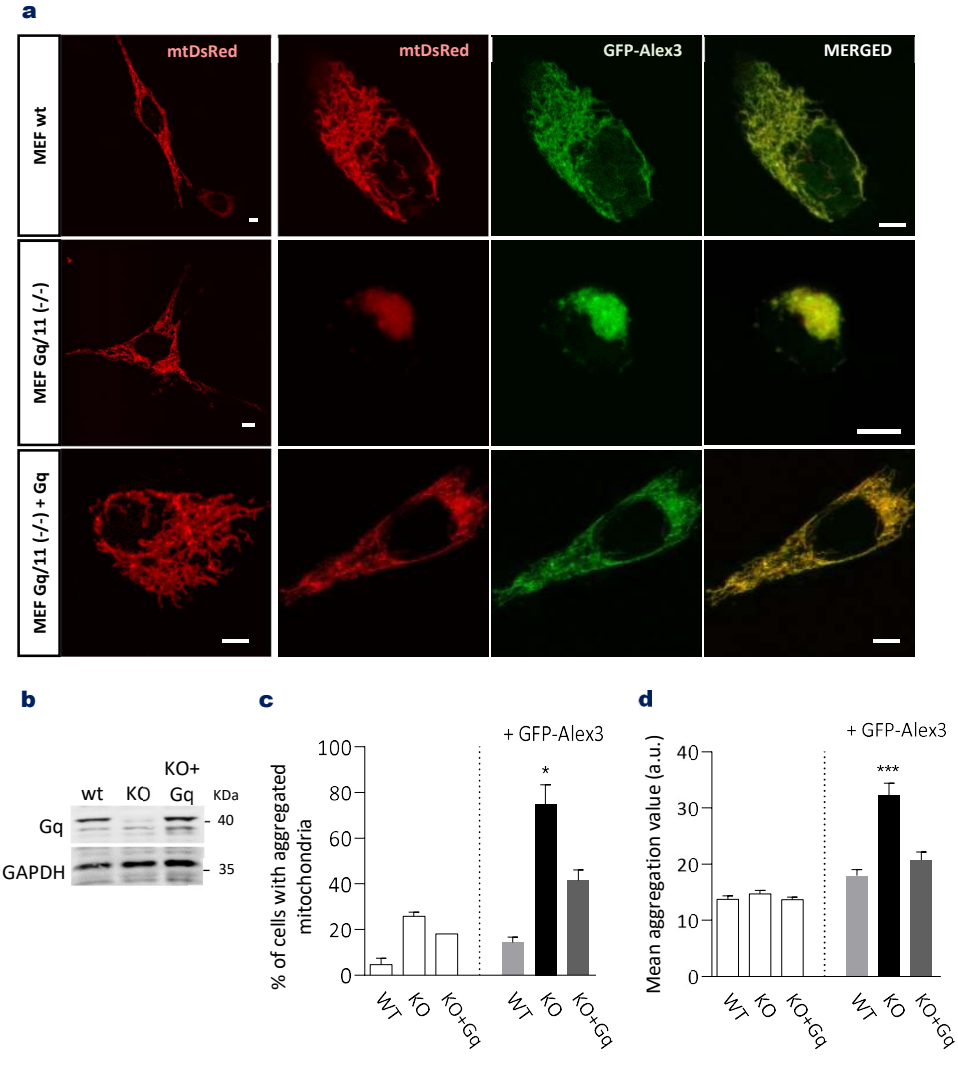

Figure R15. Alex3-mediated mitochondrial aggregation is enhanced in MEF $G\alpha_{q/11}$ (-/-) cells. a, MEF wt, MEF $G\alpha_{q/11}$ (-/-) and MEF $G\alpha_{q/11}$ (-/-) cells stably expressing $G\alpha_q$ were transfected with plasmids containing the mitochondrial marker mtDsRed along with pEGFP-Alex3. Images are maximum intensity projections of 6 stacks (0.4 µm per stack) and were acquired with a Leica SP5 confocal microscope using a 63x1.3NA oil immersion lens. All images are representative of the majority of transfected cells from 3 independent experiments. Scale bars, 5 µm. **b,** Expression of $G\alpha_q$ on MEF and MEF $G\alpha_{q/11}$ (-/-)(KO) cells was analyzed by western blot using a $G\alpha_q$ specific antibody (BD biosciences®). GAPDH was used as a loading control **c,** Quantification of the average number of cells containing mitochondrial aggregates in MEF wt, MEF $G\alpha_{q/11}$ (-/-)(KO) or MEF $G\alpha_{q/11}$ (-/-) stably expressing $G\alpha_q$ (KO+ $G\alpha_q$) in the presence or absence of GFP-Alex3. **d,** The degree of mitochondrial aggregation was inferred from the mean aggregation value of mtDsred-labeled mitochondria using the LAS AF software (Leica). For each experimental condition, n≥25 cells were quantified. Error bars represent SEM. Statistical analysis was carried out using a one-way ANOVA. *p<0.05 ,***p<0.001.

Miro1 overexpression also enhances mitochondrial clustering, although in a lesser extend when compared with Alex3 (**Fig.R16**).

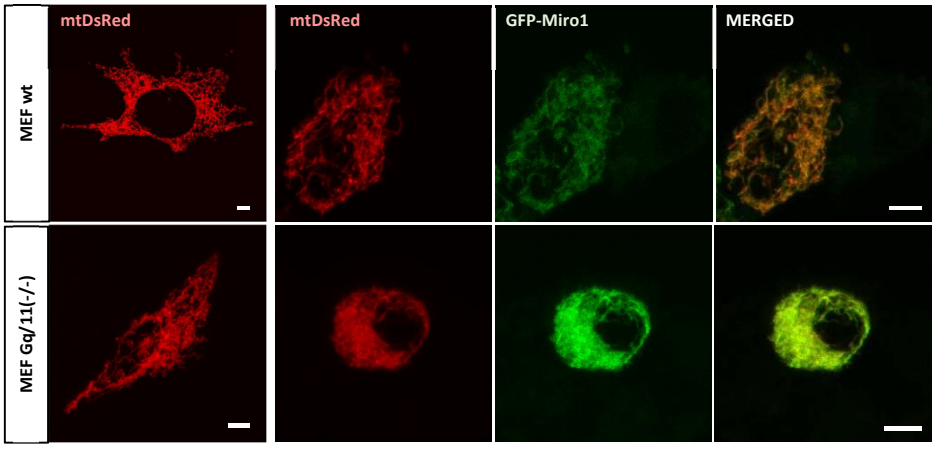

Figure R16. Mitochondrial aggregation induced by Miro1 overexpression is increased in MEF $G\alpha_{q/11}$ (-/-) cells. MEF wt and MEF $G\alpha_{q/11}$(-/-) cells were transfected with plasmids containing the mitochondrial marker mtDsRed along with pEGFP-Miro1. Images are maximum intensity projections of 6 stacks and were acquired using a Leica SP5 confocal microscope using a 63x1.3NA oil immersion lens. Confocal micrographs are representative of the majority of transfected cells from 3 independent experiments. Scale bar, 5µm.

4.4. Alex3-containing mitochondrial clusters are surrounded by ER

To further investigate the origin of Alex3-containing mitochondrial aggregates and the specificity of those clusters for mitochondria (but no other endomembranes), we looked at the ER localization of cells expressing GFP-Alex3. Because ER-mitochondria contact sites are often related with alterations in mitochondrial dynamics (Friedman et al., 2011; Lee et al., 2016), we looked at the ER network using the MEF $G\alpha_{q/11}$ (-/-) cells as a cellular model with increased Alex3-induced mitochondrial aggregation. Unlike mitochondria, no important alterations were found in ER-network besides a slight enrichment in the region surrounding mitochondrial clusters, where ERMES are usually located (**Fig.R17**). Alex3 then does not aggregate ER as it does with mitochondria, but may be involved in the formation of those ER-mitochondria contact sites.

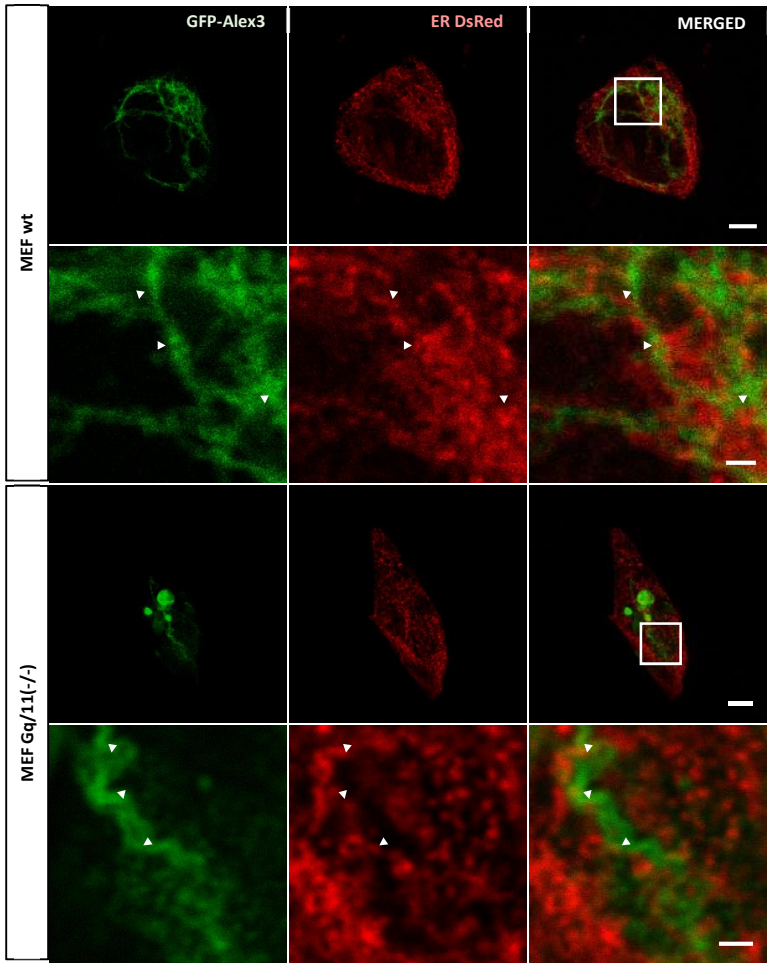

Figure R17. Alex3-induced mitochondrial clusters are close to ER structures. MEF wt (panels above) and MEF $G\alpha_{q/11}$ (-/-) (panels below) were co-transfected with plasmids containing the endoplasmic reticulum marker ER-DsRed and GFP-Alex3. Images are single stacks and were acquired using a Zeiss LSM780 confocal microscope with a 63x oil immersion lens. Arrowheads point to putative ER-mitochondria contact sites. Confocal micrographs are representative of the majority of transfected cells from 3 independent experiments. Magnified images corresponding to the small box are shown below. Scale bars, 5 μm and 1 μm (magnifications).

5. Live imaging of axonal mitochondria in mouse hippocampal neurons

Considering $G\alpha_q$ depletion has an impact on Alex3-induced mitochondrial aggregation, we hypothesized $G\alpha_q$ could also play a role on mitochondrial motility, as occurs with Alex3 and Miro1 (Birsa et al. 2013; López-Doménech et al. 2012). To adress the possible regulation of mitochondrial trafficking by $G\alpha_q$, we switched from cell lines to primary cultures of mouse hippocampal neurons and performed live imaging of axonal-labeled mitochondria.

Figure R18 shows a representative control neuron imaged in our experiments. In that example, neurons were co-transfected with GFP to fill the cell and mtDsRed to label mitochondria. An axonal region located around 6-fold the soma diameter (white rectangle) was imaged during 10 or 15 minutes. From the time-lapse recordings, kymographs were generated using a plug-in from Fiji software and analyzed according to several motility parameters.

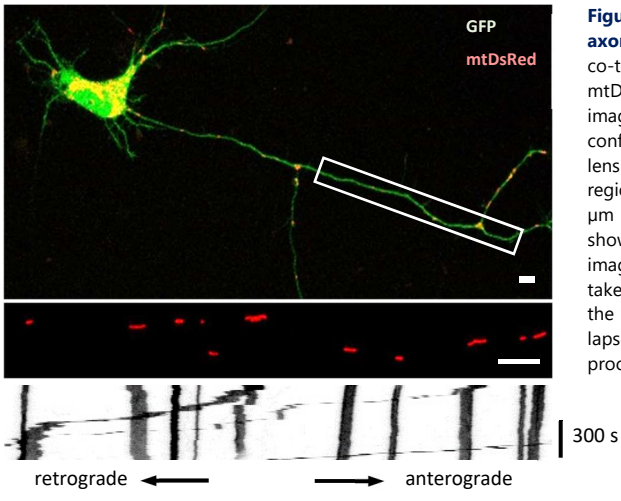

Figure R18. Example of time-lapse imaged axonal section. DIV 4 hippocampal neurons were co-transfected with pEGFP to fill the cell and mtDsRed to label mitochondria. Time-lapse imaging was performed using a Zeiss LSM780 confocal microscope with a 63x oil immersion lens 1 and 2 days post-transfection. Imaged region was determined approximately 90 to 160 µm away from the soma. The white rectangle shows the axonal region selected for time-lapse imaging. Images of labeled mitochondria were taken every 6 s during 10 or 15 min. Images above the kymograph show the first frame of the time-lapse imaging. Kymographs were generated and processed using Fiji software. Scale bars, 5 µm.

5.1. Depletion of $G\alpha_q$ increases retrograde motility and bidirectional speed

To find out a possible involvement of $G\alpha_q$ in mitochondrial trafficking, we first knocked-down $G\alpha_q$ expression using specific short hairpin RNAs that was known to be effective on MEFs cells analyzed in parallel (**Fig.R19a**). As shown in the quantification analysis (**Fig.R19b**), $G\alpha_q$ expression levels were reduced over 60% in cells expressing the short-hairpin RNA, thus confirming their specificity. Immunofluorescence staining with anti-$G\alpha_q$ antibodies in neurons expressing the specific shRNAs also revealed a decrease in $G\alpha_q$ signal (**Fig.R19c**, white arrowheads). In contrast, neurons expressing the control shRNAs and non-transfected neurons displayed increased signal when immunolabeled with the $G\alpha_q$-specific antibody (**Fig.R19c**, yellow arrowheads), further reinforcing the specificity of the shRNAs.

Having demonstrated the efficiency and specificity of the $G\alpha_q$-targeted shRNA, hippocampal neurons were either co-transfected with mtDsRed, GFP and a $G\alpha_q$ specific shRNA (sh1) or with mtDsRed and a GFP-containing shRNA (sh2). Although only a small set of neurons were transfected, that set was enough to perform the time-lapse experiments.

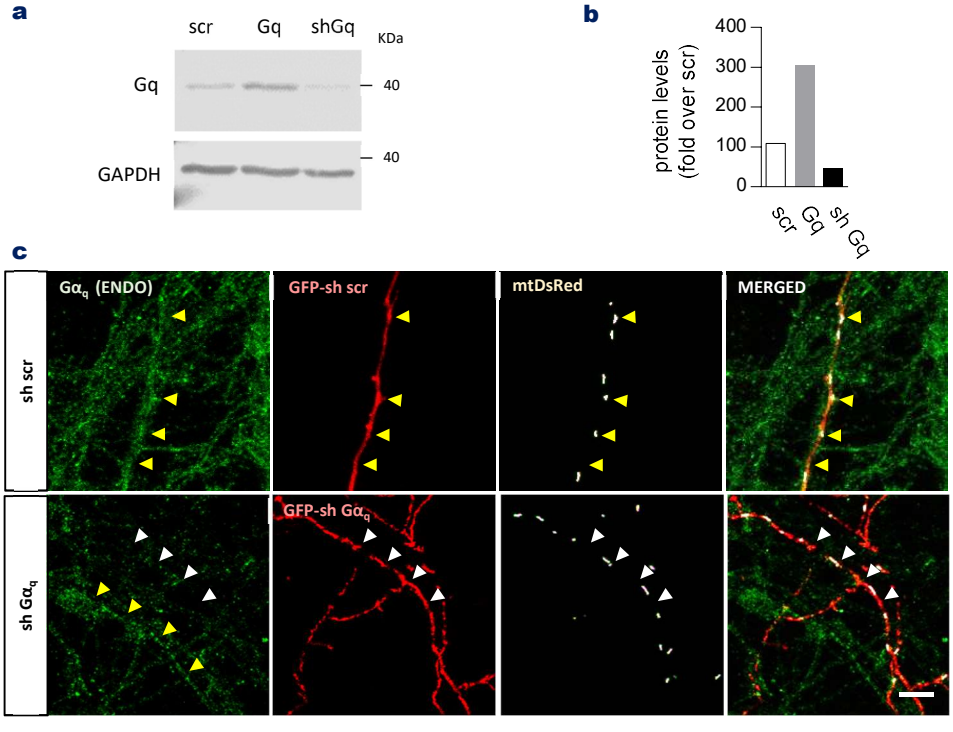

Figure R19 shRNAs specifically knock-down $G\alpha_q$ expression in neuronal axons. a, MEF cells were transfected with plasmids containing a shRNA scramble (sh scr) or a shRNA targeting $G\alpha_q$ mRNA (sh Gq). For each condition, 15 µg of protein extracts from cell lysates were analyzed by western blot with $G\alpha_q$-specific antibody. GAPDH was used as a loading control. **b,** Band intensity from western blots as in (a) was quantified using ImageStudio® software. **c,** Immunofluorescence against $G\alpha_q$ was carried out in 6 DIV hippocampal neurons expressing GFP-containing control shRNAs (scr) or shRNAs specific for $G\alpha_q$. Neurons were stained with anti-$G\alpha_q$ (E-17, Sta. Cruz®) and Alexa-Fluor-647 anti-mouse (color has been changed to facilitate visualization of endogenous $G\alpha_q$). Arrowheads point to the axon of a shRNA-expressing neuron. Notice that in the case of control neurons (yellow arrowheads), $G\alpha_q$ expression is detected along the axon, whereas axons expressing the $G\alpha_q$-specific shRNA (white arrowheads) barely show $G\alpha_q$ signal. Non-transfected neurons in the same plate express the endogenous protein (yellow arrowheads). Images are maximum intensity projections of 6 stacks, were acquired using a Zeiss LSM780 confocal microscope equipped with a 63x oil immersion lens and are representative of the majority of neurons from 3 independent experiments. Scale bar, 10 µm.

As overview of mitochondrial motility, we determined the percentage of time that mitochondria spent in motion (Fig.R20b). It was selected as the primary parameter for quantifying motility, rather than percent of moving mitochondria (Fig.R20c), because the former distinguishes mitochondria that move for only a fraction of the imaging period from those that move continuously (Wang et al., 2011). In any case, the percentage of mitochondria that move relative to the amount of axonal mitochondria (Fig.R20c) and their frequency of stopping (Fig.R20e) were also quantified. Average velocity (Fig.R20d) reflects the mean velocity of individual mitochondria, taking into account the time they spend arrested. Finally, we also determined the number of times a moving mitochondria reaches velocities over 2 µm/sec (Fig.R20f) and the mean velocity of the runs from moving mitochondria (Fig.R20g). As documented in previous studies (Wang et al. 2011), we observed a similar fraction of anterograde and retrograde movement in control

neurons. The percentage of mitochondria in movement (around 20%) and the average velocity (between 0.3 and 0.7 μm/sec) also agreed with previous studies (Schwarz, 2013), which is an indication that the neuron preparation and treatment produced healthy neurons.

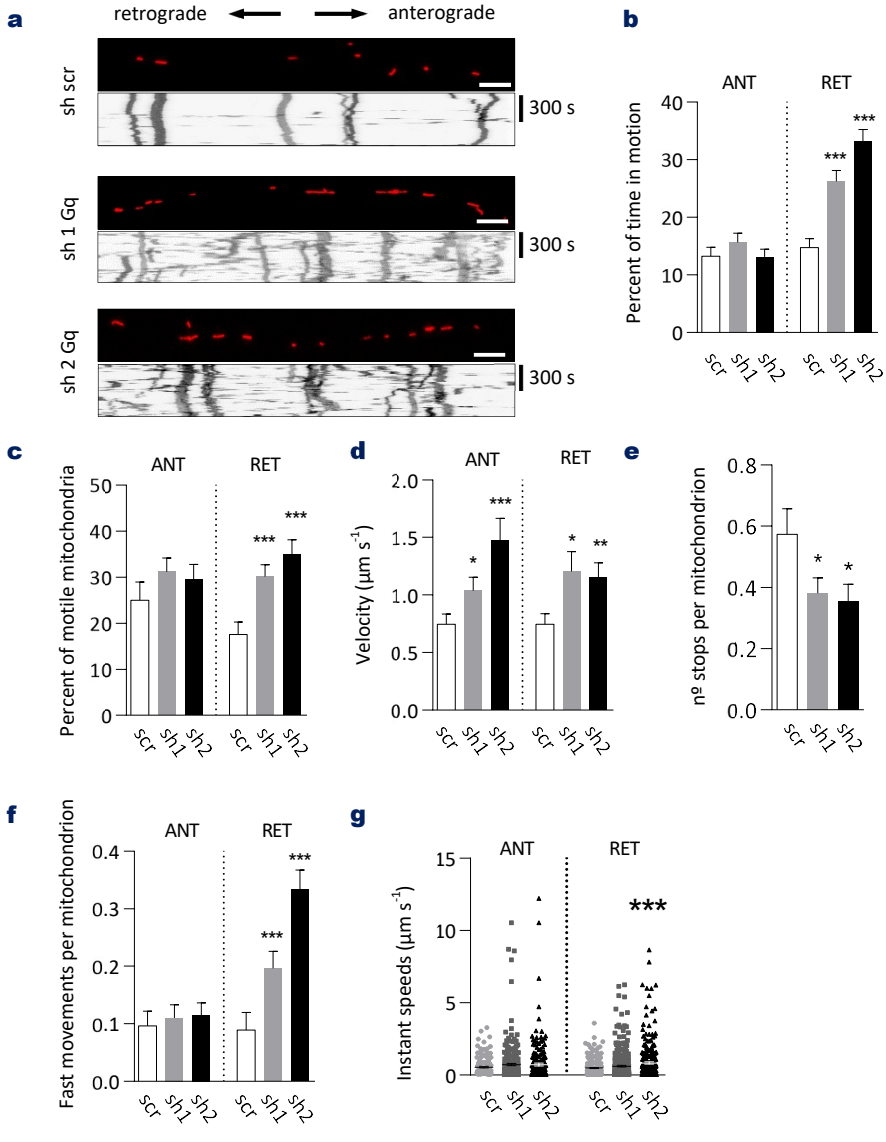

Figure R20. Gα$_q$ depletion increases mitochondrial speed and promotes retrograde trafficking. DIV 4 hippocampal neurons were co-transfected with mtDsRed and a GFP-containing scramble shRNA (scr), GFP and a Gα$_q$-specific shRNA (sh1) or a Gα$_q$-specific GFP-bound shRNA (sh2). Time-lapse imaging was performed 1 and 2 days post-transfection as explained in Figure R18. **a,** Representative images of mtDsRed-labelled mitochondria on axons and corresponding kymographs. For each condition, the first frame of the live-imaging series appears above the kymograph. Scale bars, 5 μm. **b,** From kymographs as in (a), the percent of time each mitochondrion spent in motion was determined, averaged, and compared with control for the anterograde (ANT) and retrograde (RET) direction. **c,** Mitochondrial motility expressed as percentage of total mitochondria within axons. **d,** Average velocity of moving mitochondria. **e,** Average number of

times a moving mitochondria reduced its velocity below a threshold (0,0083 μm/s). **f,** Average number of times a moving mitochondria increased its velocity over 2 μm/s. **g,** Dot chart of all velocities reached by mitochondria in each experimental condition. For each condition, 20 to 28 axons were analyzed from 4 independent experiments. Error bars represent SEM. Statistical analysis was carried out using a one-way ANOVA and two-tailed Student's t-test. *p<0.05,**p<0.01,***p<0.001.

After kymograph analysis, axonal mitochondria from neurons knocked-down for the expression of $G\alpha_q$ revealed a significant increase in the percentage of movement towards the retrograde direction (from 14.8±1.6% to 26.2±1.9% and 33.3±2%, depending on the utilized shRNA) (Fig.R20b). The number of motile mitochondria that move back to the soma was also increased (from 17.4±2.7% to 30.2±2.6% and 35±3.2%, depending on the shRNA) (Fig.R20c). Both parameters are therefore consistent with an increase on the movement towards the soma. A bit more surprising was to find that the overall speed of mitochondria in both directions was increased (Fig.R20d). Not only increased the amount of mitochondria that move, but also mitochondria moved faster, and in that case in both directions (from 0.75±0.1 until 1.0±0.1 and 1.5±0.2 μm/sec in the anterograde direction and from 0.75±0.1 until 1.2±0.2 and 1.2±0.1 μm/sec in the retrograde direction). This is an important observation since only a few proteins can affect the speed of mitochondria. On the other hand, mitochondrial velocity can be directly linked with the decrease in the frequency of stopping (from 0.57±0.08 to 0.38±0.05 and 0.35±0.06) (Fig.R20e). Therefore, the reduction of $G\alpha_q$ levels produces a gain in anterograde movement and an increase in the velocity of the mitochondria besides a reduction in the number of stops. As a consequence of absence or reduction of $G\alpha_q$, mitochondria returns to the soma. We also observed an increase in the number of times a mitochondria reaches velocities over 2 μm/sec (Fig.R20f) and instantaneous speeds over average (Fig.R20g), indicating that other mechanisms besides the ability to bind microtubule adaptors may regulate mitochondrial speed in the absence of $G\alpha_q$.

Together, this data confirms the involvement of $G\alpha_q$ not only in the regulation of mitochondrial morphology, but also in the axonal trafficking, which is directly dependent on Alex3 and Miro1.

5.2. Depletion of $G\alpha_q$ increases mitochondrial motility in an Alex3-dependent manner

Because MEF $G\alpha_{q/11}$ (-/-) cells expressing exogenous Alex3 showed increased mitochondrial aggregation and our previous results demonstrate a specific binding between Alex3 and $G\alpha_q$, we hypothesized that $G\alpha_q$ could have an inhibitory effect over Alex3 function. It was previously demonstrated that expression or reduction (by siRNA) of Alex3 protein levels in hippocampal neurons stop mitochondrial movement (López-Doménech et al. 2012). Thanks to the availability

of the Alex3 knockout mice (Prof. Soriano's group), we were now able to determine the impact that low levels of $G\alpha_q$ would have on Alex3 functionality. Hippocampal neurons from Alex3 KO mice embryos were transfected with specific shRNAs to knock-down $G\alpha_q$ expression. First, neurons were fixed and immunostained with specific antibodies against Alex3 to check the depletion of the protein as well as Tuj1 and MAP2 to determine the integrity of neuronal cytoskeleton. Images in **Figure R21** show the absence of signal in Alex3 KO neurons stained with Alex3 specific antibody (lower middle panel), thus validating our approach. Besides, no major alterations in dendritic cytoskeleton structure (shown with MAP2) or axonal tubulin cytoskeleton (shown by Tuj1 staining) were visible in Alex3 KO neurons.

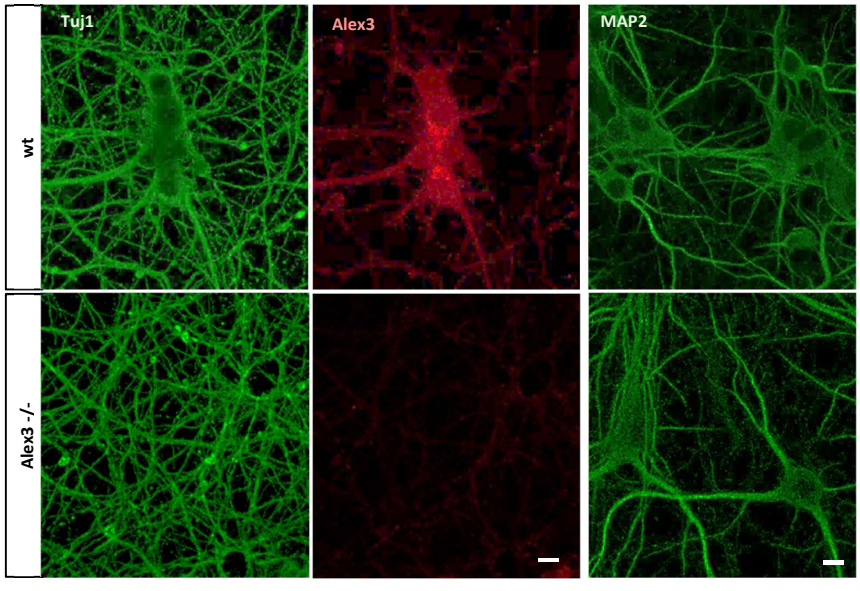

Figure R21. Alex3 KO neurons show no visible alterations in axonal and dendritic cytoskeleton. Confocal micrographs of hippocampal neurons stained with anti-Tuj1 (**a,** axonal tubulin) or MAP2 (**b,** dendritic tubulin) and Alexa-Fluor-488-conjugated anti-mouse antibodies and anti-Alex3 and Alexa-Fluor-568 anti-rabbit antibodies. DIV 5-6 hippocampal neurons from wild-type and Alex3 (-/-) mice embryos 48 h after seeding. Images are maximum intensity projections of 6 stacks, were acquired using a using Zeiss LSM780 confocal microscope equipped with a 63x oil immersion lens and are representative of the majority of neurons from 3 independent experiments. Scale bars, 10μm

Live imaging of axonal mitochondria confirmed the previously observed increase in mitochondrial motility towards the soma knocking-down $G\alpha_q$. In this case, the time mitochondria spend in motion increased from 10.1±2% to 16.4±4% (**Fig.R22c,** white bars), whereas the percentage of motile mitochondria raised from 17.9±3% to 39.9±7.3% (**Fig.R22d,** white bars). However, that increase in the number of motile mitochondria and the time they move towards the soma was absent or significantly reduced in Alex3 KO neurons (**R22c,d** black bars). Hence, these results support the hypothesis that $G\alpha_q$ function on mitochondria motility requires Alex3.

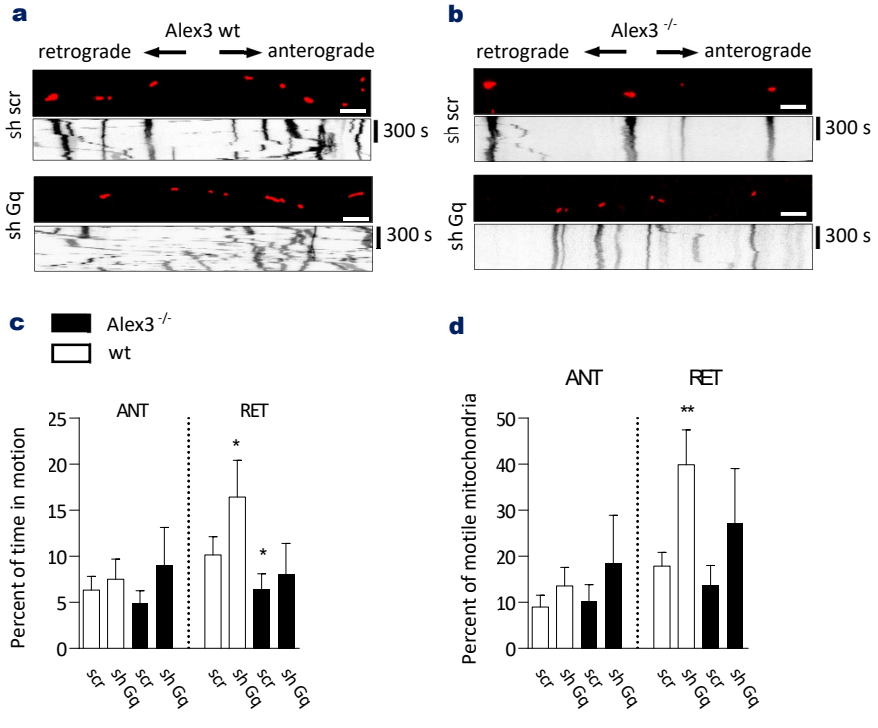

Figure R22 $G\alpha_q$ depletion increases mitochondria retrograde trafficking in a mechanism dependent on Alex3. Alex3 wt and Alex3 KO hippocampal neurons (DIV 5) were co-transfected with mtDsRed and either a GFP-containing scramble short-hairpin RNA (scr), or a $G\alpha_q$-specific short hairpin RNA containing GFP (Gq). Time-lapse imaging was performed 1 and 2 days post-transfection as explained in Figure R18. **a,** Representative confocal images of mtDsRed-labeled mitochondria on axons and respective kymographs. For each condition, the first frame of the live-imaging series appears above the kymograph. Scale bars, 5 μm. **b,** From kymographs as in (a), the percent of time each mitochondrion spent in motion was determined, averaged, and compared with control for the anterograde (ANT) and retrograde (RET) direction. **c,** Mitochondrial motility expressed as percentage of total mitochondria within axons. For each condition, 10 to 15 axons were analyzed from 3 independent experiments. Error bars represent SEM. Statistical analysis was carried out using a one-way ANOVA. *p<0.05,**p<0.01.

5.3. $G\alpha_q$ overexpression increases anterograde mitochondrial transport

The data presented so far strongly suggest that $G\alpha_q$ could be regulating mitochondrial trafficking. Depletion of $G\alpha_q$ significantly increases axonal mitochondrial motility especially towards the soma, but not in the absence of Alex3. To further study this phenotype, neurons were transfected with untagged $G\alpha_q$ and live imaging of axonal mitochondria was carried out as before.

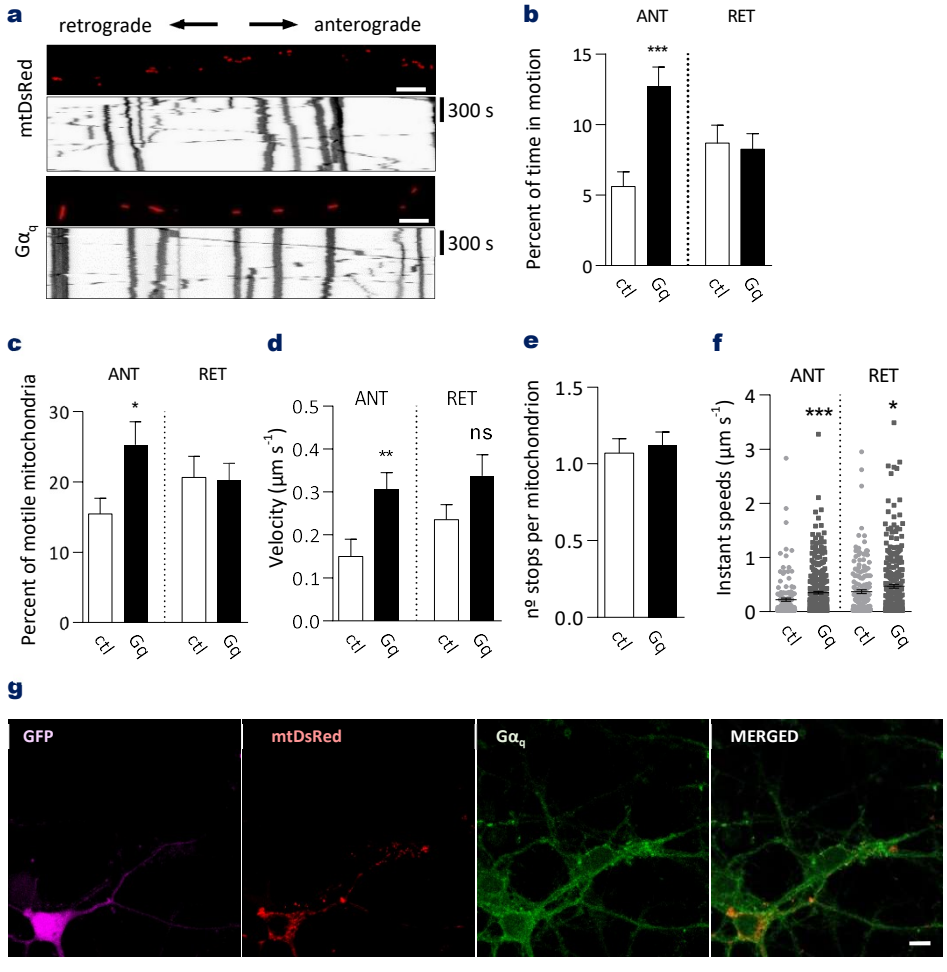

Figure R23. Gα$_q$ promotes anterograde mitochondrial transport. DIV 4 hippocampal neurons were transfected with GFP, mtDsRed and either an empty vector or containing Gα$_q$. Time-lapse imaging was performed 1 and 2 days post-transfection as explained in Figure R18. **a,** Representative images of axonal mitochondria in neurons and corresponding kymographs. For each condition, the first frame of the live-imaging series appears above the kymograph. Scale bars, 5 μm. **b,** From kymographs as in (a), the percent of time each mitochondrion was in motion was determined, averaged, and compared with control for the anterograde (ANT) and retrograde (RET) direction. **c,** Mitochondrial motility expressed as percentage of total mitochondria within axons. **d,** Average velocity of moving mitochondria **e,** number of times a moving mitochondria reduced its velocity below a threshold (0,0083μm/s). **f,** Dot chart of all velocities reached by mitochondria in each experimental condition. For each condition, 30 to 32 axons were analyzed from 4 independent experiments. Error bars represent SEM. Statistical analysis was carried out using a two-tailed Student's t-test followed by Mann-Whitney's test. *p<0.05,**p<0.01,***p<0.001. **g,** Immunostaining of Gα$_q$-transfected neurons. DIV 6 hippocampal neurons analyzed in (a) where fixed and stained using a specific anti-Gα$_q$ (BD-biosciences®) and Alexa-Fluor-647 anti-mouse (colors have been switched to improve visualization of Gα$_q$ at the mitochondria). Images on the right are merged channels of Gα$_q$ and mtDsRed. Images were taken using Zeiss LSM780 confocal microscope with a 63x oil immersion lens and are representative of most neurons from 3 independent experiments. Scale bar, 10 μm.

Kymograph analysis from time-lapse videos unveiled interesting results: overexpression of $G\alpha_q$ increased mitochondrial motility towards the anterograde direction from 5.6±1% to 12.7±1.4 %, as reflected in the percentage of time in motion (**Fig.R23b**). Besides, the number of mitochondria that moved towards the axonal tips increased from 15.5±2.2% to 25.3±3.3% (**Fig.R23c**) and the mean anterograde velocity raised from 0.15±0.04 to 0.31±0.04 µm/sec (**Fig.R23d**). This time, no significant changes were observed in the number of stops per mitochondria (**Fig.R23e**) or the instantaneous mitochondrial speeds (**Fig.R23f**). The expression of $G\alpha_q$ in the neurons analyzed was confirmed by retrospective immunostaining with anti-$G\alpha_q$ antibodies (**Fig.R23g**). These results further confirm the importance of $G\alpha_q$ regulating mitochondrial motility and suggest its involvement in anterograde transport.

5.4. $G\alpha_q$ promotes Miro1 interaction with kif5c

The increment in anterograde mitochondrial transport induced by $G\alpha_q$ prompted us to investigate whether it could have an impact on Miro1 association with the main mediator of anterograde transport, the microtubule motor protein kif5c. To address the putative link between kif5c and $G\alpha_q$, myc-Kif5c was immunoprecipitated from HEK293 cells overexpressing $G\alpha_q$, GFP-Miro1 or both. Surprisingly, a band at 40 KDa appeared in immunoprecipitates when developed with anti-$G\alpha_q$ antibody, indicating a specific interaction between the small GTPase and the kinesin motor (**Fig.R24a,** track 4). As expected, Miro1 also co-immunoprecipitated with myc-kif5c (**Fig.R24a,** track 6). More interestingly, co-expression of $G\alpha_q$ increased Miro1 co-IP with kif5c (**Fig.R24a,** track 7), suggesting it may stabilize the interaction of the mitochondrial GTPase with the anterograde motor, thus supporting our live-imaging results. In aggrement with our previous experiment, IP of GFP-Alex3 also revealed a faint band corresponding to Kif5c when precipitated in the presence of exogenous Kif5c, Miro1 and $G\alpha_q$ (**Fig.R24b,** track 7), reinforcing the notion of a putative complex containing the four partners when $G\alpha_q$ is present.

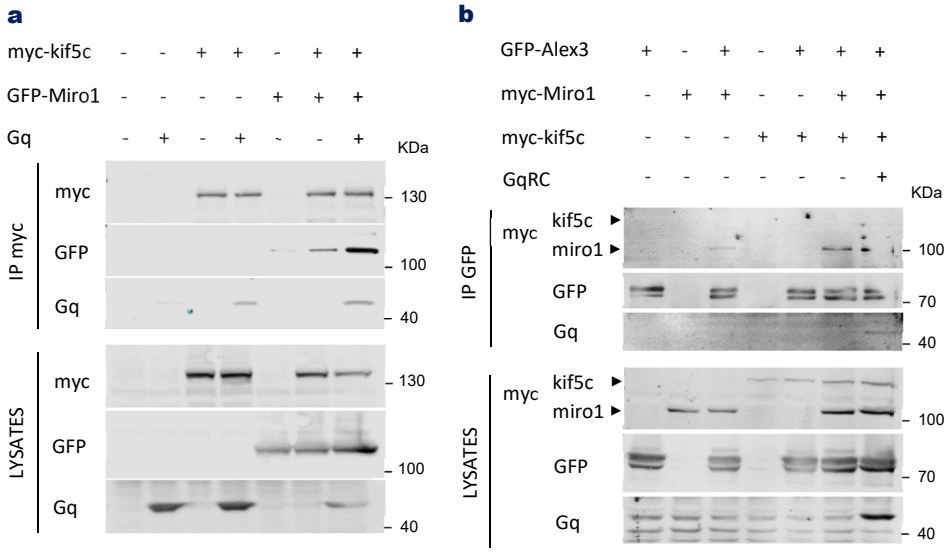

Figure R24. Gα$_q$ promotes Miro1 association to kif5c. **a,** Immunoprecipitation of myc-Kif5c from HEK293 cells expressing myc-Kif5c, GFP-Miro1 and Gα$_q$. Cell lysates (700 µg) were immunoprecipitated with myc-trap antibody previous to SDS-PAGE analysis. **b,** Immunoprecipitation of GFP-Alex3 from HEK293 cells expressing GFP-Alex3, myc-Miro1, myc-Kif5c and Gα$_q$. Cell lysates (700 µg) were immunoprecipitated with GFP-trap antibody previous to SDS-PAGE analysis. In both cases, western blots were analyzed with the corresponding antibodies: anti-myc (Millipore®), anti-GFP (Invitrogen®) and anti-Gα$_q$ (BD biosciences®). Data are representative of at least 2 independent experiments.

5.5. Active Gα$_q$ decreases mitochondrial motility and speed

According to the presented data, Gα$_q$ would not only be involved in the regulation of mitochondrial morphology, but also in the molecular mechanisms controlling mitochondrial trafficking. To further address the involvement of Gα$_q$ activity in axonal mitochondrial transport, we took advantage of the previously tested GFP-containing Gα$_q$ chimeric proteins (Benincá et al., 2014; Hughes, Zhang, Logothetis, & Berlot, 2001). We used the wild-type Gα$_q$, the GTPase deficient Gα$_q$R183C (Hughes et al., 2001), the mitochondria-targeted Gα$_q$MAS70 and the N-terminal peptide of Gα$_q$. In Gα$_q$MAS70, the first 30 residues of the Gα$_q$ are replaced by the 30 initial amino acids of MAS70, a protein that is fully targeted to the mitochondria. On the other hand, the N-terminal region of Gα$_q$ comprises the first 124 residues and contains the predicted mitochondrial targeting sequence of Gα$_q$, but lacks the nucleotide-binding region. Those GFP-chimeric proteins were previously utilized by our group as a tool to better detect the amount of G protein that localizes at the mitochondria (around 10-15% of the total Gα$_q$ protein) (Benincá et al., 2014).

In contrast with the previous observations, the results revealed an overall decrease in bidirectional mitochondrial motility when expressing GFP-Gα_q as well as GFP-Gα_qMAS70 and was accentuated in the case of GFP-Gα_qR183C. The percentage of time in motion revealed a significant decrease in anterograde (from 10.0±1.2% to 4.5±1.0%, 3.1±1.4% and 1.7±0.7% in the wild-type, MAS70 and R183C proteins, respectively) and retrograde motility (from 12.4±1.4% to 5.4±1.0%, 3.4±0.7% and 1.6±0.6%) when expressing the chimeric proteins (**Fig.R25b**). In the same direction, the percentage of moving mitochondria was reduced in the anterograde direction from 20.8±2.8% to 9.3±2.2%, 6.9±4.5% 4.1±3.1% and in the retrograde direction from 26.6±3.7% to 14.6±4.1%, 15.2±6.4% and 5.2±2.3% in the wild-type, MAS70, R183C chimeras, respectively (**Fig.R25c**). Average mitochondrial speed showed no significant changes when expressing the wild-type Gα_q, but was reduced in both directions when expressing GFP-Gα_qR183C (from 0.45±0.05 to 0.14±0.04 and from 0.45±0.06 to 0.13±0.03 μm/sec in anterograde and retrograde directions, respectively), and when expressing GFP-Gα_qMAS70 in the retrograde direction (from 0.45±0.06 to 0.16±0.04 μm/sec) (**Fig.R25d**). The increase on the number of stops per mitochondria when expressing the active mutant may explain those differences (**Fig.R25e**), since no significant alterations in instantaneous velocities were observed (**Fig.R25f**). Expression of the GFP-Nt region showed no significant changes on mitochondrial motility parameters, even though it perfectly localizes at the mitochondria (**Fig.R25a**). It thus serves as a useful control and reinforces the dependence of the GTP-binding domain and Gα_q activity to alter mitochondrial motility and decrease their speed.

On the other hand, the reduction on the percentage of time in motion and number of motile mitochondria induced by GFP-Gα_q are likely to be due to an increased activity and/or mitochondrial localization due to the inclusion of a GFP molecule in the central hinge. This peptide may increase the dimerization of the Gα_q molecule and induce differential effects as the previously observed expressing the untagged protein. Thus, these experiments provide a first impression on the importance of the GTPase domain of Gα_q to induce mitochondrial arrest, but require additional experiments to address the specific function of both the wild-type and the Gα_qR183C proteins.

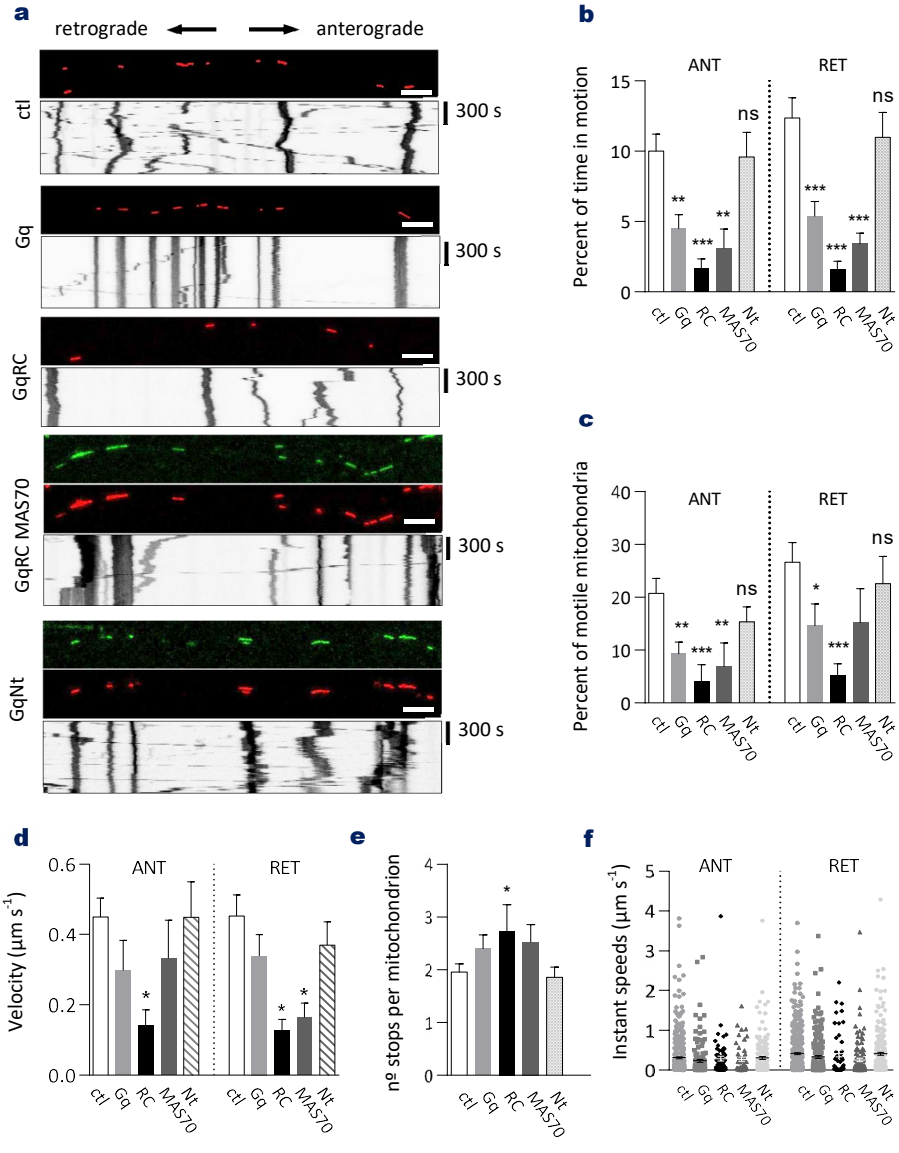

Figure R25. Gα$_q$ activation promotes mitochondrial arrest. DIV 4 hippocampal neurons were transfected with mtDsRed and either GFP (ctl), GFP-Gα$_q$ (Gq) the constitutive-active mutant GFP-Gα$_q$R183C (RC), the mitochondrial-targeted GFP-Gα$_q$ MAS70 (MAS70) or the GFP-Gα$_q$ N-terminal (Nt) containing the mitochondrial targeting sequence. Time-lapse imaging was performed 1 and 2 days post-transfection as described in Figure R18. **a,** Representative images of axonal mitochondria in neurons and corresponding kymographs. For each condition, the first frame of the live-imaging series appears above the kymograph. Scale bars, 5 µm. **b,** From kymographs as in (a), the percent of time each mitochondrion was in motion was determined, averaged, and compared with control for the anterograde (ANT) and retrograde (RET) direction. **c,** Motile mitochondria expressed as percentage of total mitochondria within axons. **d,** Average velocity of moving mitochondria **e,** number of times a moving mitochondria reduced its velocity below a threshold (0,0083µm/s). **f,** Dot chart of all velocities reached by mitochondria in each experimental condition. For each condition, 10 to 26 axons were analyzed from 4 independent experiments. Error bars represent SEM. Statistical analysis was carried out using a Student's t-test followed by Mann-Whitney's test. *p<0.05,**p<0.01,***p<0.001.

5.6. GFP-Gα$_q$ and GFP-Gα$_q$R183C do not alter tubulin cytoskeleton in axons and dendrites

Our previous data suggested a role of Gα$_q$ promoting mitochondrial arrest. Since mitochondria move through tubulin tracks, one of the reasons of the reduced mitochondrial motility could be a dysfunctional tubulin cytoskeleton. To address whether Gα$_q$ could be altering tubulin cytoskeleton, neurons were next co-transfected with mtDsRed and GFP-Gα$_q$ or GFP-Gα$_q$R183C and immunostained with specific antibodies for MAP2 and Tuj1, which are widely used markers of dendritic and axonal tubulin, respectively. No major alterations in cytoskeletal structure were observed in either the dendritic arbor (Fig.R26a) or axons (Fig. R26b) in those neurons selected for time-lapse imaging, thus demonstrating that the observed alterations in mitochondrial movement are not caused by a dysfunctional tubulin cytoskeleton.

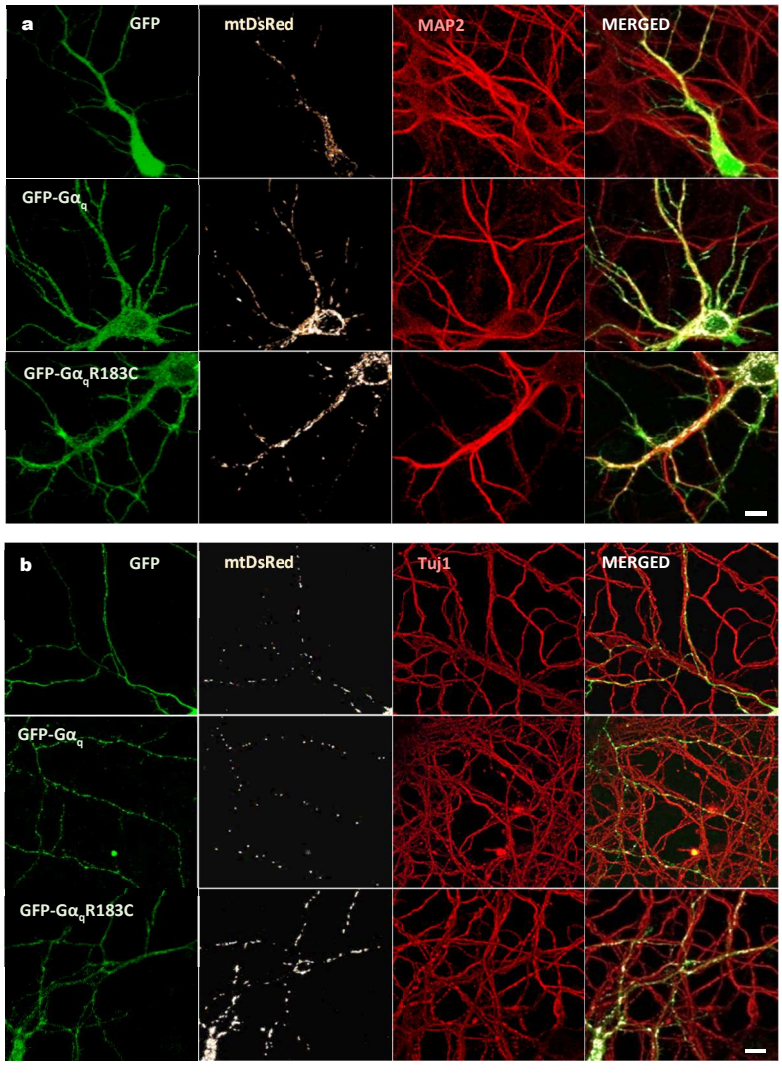

Figure R26. Expression of GFP-Gα$_q$ or GFP-Gα$_q$R183C does not alter microtubule cytoskeleton in axons and dendrites. DIV 4 hippocampal neurons were transfected with plasmids containing mtDsRed and GFP, GFP-Gα$_q$ or Gα$_q$R183C 24 h after seeding. Neurons were fixed 48 h after transfection and analyzed with anti-MAP2 (**a,** used to label dendritic tubulin) or anti-Tuj1 (**b,** used to label axonal tubulin) and Alexa-Fluor-568 anti-mouse. Images are z-projections of 7 stacks, were acquired using a using Zeiss LSM780 confocal microscope equipped with a 63x oil immersion lens and are representative of the majority of neurons from 3 independent experiments. Scale bars, 10µm.

5.7. GFP-Gα$_q$ and GFP-Gα$_q$R183C localize at the mitochondria

The previously utilized GFP-containing Gα$_q$ chimeras allow a rapid identification of those neurons that express the protein, but more interestingly, they are an important tool to overcome the lack of specific antibodies against endogenous Gα$_q$ for immunofluorescence techniques. A closer look at the intracellular localization of GFP-Gα$_q$ or GFP-Gα$_q$R183C revealed a dual localization pattern of the G proteins: they are found at the plasma membrane, where they interact with GPCRs, Gβγ subunits and canonical effectors, but also show a strong co-localization with mitochondrial markers (Fig.R27), suggesting that they may play important roles in these organelles. Another observation that grabbed our attention was to find that active-Gα$_q$ chimera tended to induce mitochondrial fragmentation, which suggests it may also regulate fusion and fission.

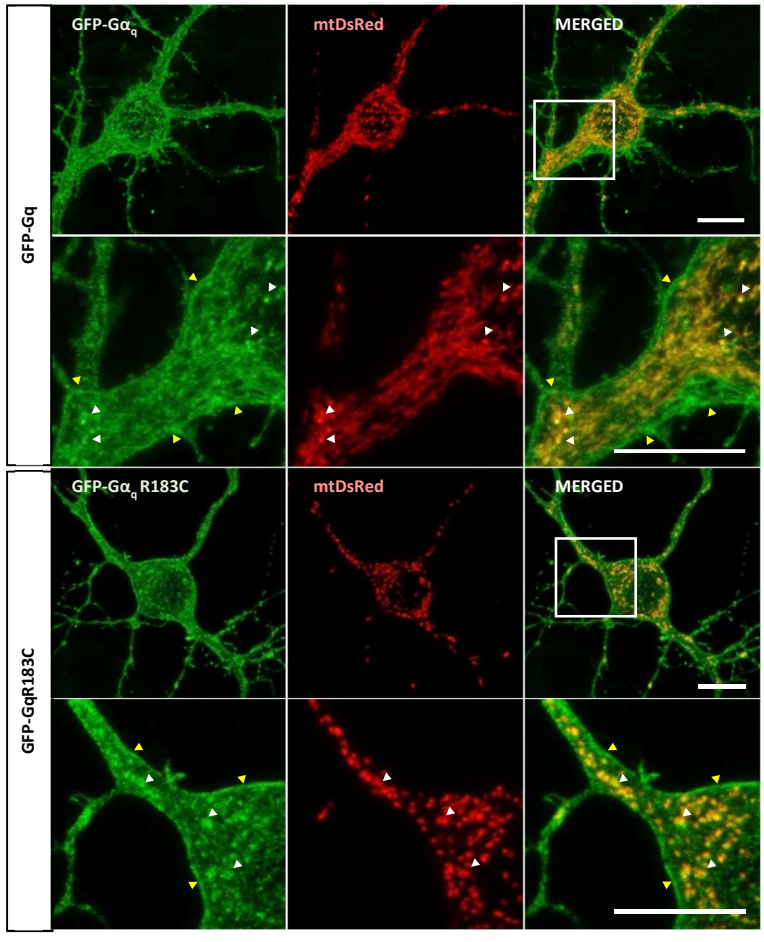

Figure R27. $G\alpha_q$ localizes at the plasma membrane and the mitochondria in hippocampal neurons. Confocal micrographs of hippocampal neuron at 6 DIV expressing mtDsRed and either GFP-$G\alpha_q$ (panels above) or GFP-$G\alpha_q$R183C (panels below). Magnified images (3X optical zoom) corresponding to small box are shown below. Notice that $G\alpha_q$ localizes both at the plasma membrane (yellow arrowheads) and the mitochondria (white arrowheads). Neurons expressing GFP-$G\alpha_q$R183C also tend to display a more fragmented mitochondrial network. Images are z-projections of 7 stacks, were acquired using a using Zeiss LSM780 confocal microscope equipped with a 63x oil immersion lens and are representative of the majority of neurons from 3 independent experiments. Scale bars, 10 µm.

5.8. GFP-$G\alpha_q$ and GFP-$G\alpha_q$R183C immunoprecipitate with Alex3 and Miro1

The binding capacity of the GFP-containing $G\alpha_q$ proteins to both Alex3 and Miro1 was also addressed by immunoprecipitation experiments. Indeed, immunoprecipitation of myc-Miro1 from HEK293 lysates precipitates both GFP-$G\alpha_q$ and GFP-$G\alpha_q$R183C (**Fig.R28a,** upper panels). Consistently, immunoprecipitation of either of the two GFP-$G\alpha_q$ proteins also precipitate Miro1, with a more prominent band in the case of the active mutant (**Fig.R28a,** middle panels). In the same direction, IP of Alex3 also co-IPs GFP-$G\alpha_q$ and GFP-$G\alpha_q$R183C (**Fig.R28b,** upper panels), and in the other way around, bands corresponding to the molecular weight of Alex3 were observed when immunoprecipitating the G proteins (**Fig.R28b,** middle panels). The N-terminal region of $G\alpha_q$ also precipitated with either Miro1 or Alex3, though in a lesser extent, which suggests that the nucleotide-binding domain could be necessary to interact with both mitochondrial proteins.

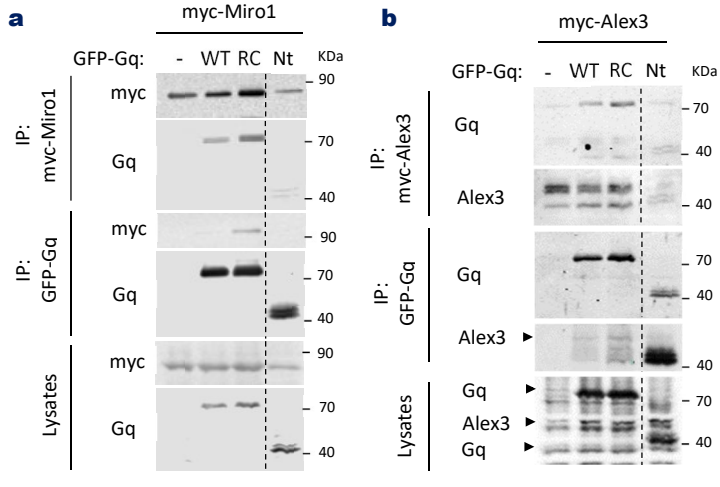

Figure R28. GFP-$G\alpha_q$, GFP-$G\alpha_q$R183C and GFP-$G\alpha_q$Nt precipitate with Alex3 and Miro1 as seen with the untagged $G\alpha_q$ proteins. a, Immunoprecipitation with anti-myc (upper panels) or anti-GFP (middle panels) from HEK293 cells expressing GFP-$G\alpha_q$ (WT) GFP-$G\alpha_q$R183C (RC) or GFP-Nt (first 124 amino acids of $G\alpha_q$) in the presence of myc-Miro1. Cell lysates (700 µg) were incubated with myc-trap antibodies or with anti-$G\alpha_q$ antibody (BD biosciences®) and protein G-Sepharose previous to SDS-PAGE analysis. **b,** Immunoprecipitation with anti-myc (upper panels) or anti-GFP (middle panels) of from HEK293 cells expressing myc-Alex3 in the presence of GFP-$G\alpha_q$ (WT), GFP-$G\alpha_q$R183C (RC) or GFP-Nt (Nt). The position of GFP-$G\alpha_q$, GFP-$G\alpha_q$Nt and the bands corresponding to Alex3 are indicated by arrowheads. For both experiments, immunoprecipitated proteins and total cell lysates were analyzed by western blot with specific antibodies for $G\alpha_q$ (BD biosciences®), Alex3 (Proteintech®) and myc (Millipore®). Data are representative of 2 independent experiments.

5.9. Expression of $G\alpha_q$ or $G\alpha_q$R183C using bicistroic vectors leads to significant alterations in mitochondrial motility

To overcome the difficulties to detect the expression of $G\alpha_q$ in live neurons and address effects of expressing a non-chimeric $G\alpha_q$ protein, we generated polycistronic vectors containing mtDsRed and $G\alpha_q$ or $G\alpha_q$R183C sequences under the same promoter (**Fig.R29a**). Using IRES-containing vectors, $G\alpha_q$ expression levels can be inferred from the intensity of the mtDsRed marker. Western blot analysis of HEK293 cells transfected with these plasmids revealed similar levels of expression of the $G\alpha_q$ protein than the initially utilized pcDNA3.1 vectors (**Fig.R29b,c**).

Neurons were then co-transfected with GFP and bicistronic vectors expressing mtDsred alone or co-expressing either $G\alpha_q$ or $G\alpha_q$R183C in the same vector. Consistent with our initial data, exogenous expression of $G\alpha_q$ increased the percentage of time in motion in the anterograde direction (from 6.5±1% to 12.3±1.4%). Besides, a significant decrease in the movement towards the soma was also observed upon $G\alpha_q$ expression (from 8.0±1.1% to 4.2±0.9%) (**Fig.R29e**). Data also showed a significant decrease in the percentage of mitochondria that moved towards the soma, from 22.3±2.2% to 14.5±2.4% (**Fig.R29f**), even though their speed and number of times they stop was not significantly altered (**Fig.R29g,h**). Expression of the constitutive active mutant, however, induced a strong mitochondrial arrest as previously seen using the GFP-tagged $G\alpha_q$ proteins (from 6.5±1% to 2.2±0.6% in the anterograde direction and from 8.0±1.1% to 3.5±0.9% in the retrograde) (**Fig.R29e**). This phenotype is not only reflected by the low amount of motile mitochondria (only 6.6±2.3% and 7.4±2% in the anterograde and retrograde direction, respectively) (**Fig.R29f**), but also by their slower average speed (**Fig.R29g**). Once again, the number of stops per mitochondrion is significantly higher (**Fig.R29h**), but no significant changes were observed in instantaneous speeds (**Fig.R29i**).

Overall, these experiments demonstrate the importance of $G\alpha_q$ in the regulation of mitochondrial motility, which plays differential roles depending on the nucleotide-bound conformation; whereas $G\alpha_q$ expression promotes mitochondrial motility towards the axonal tips, its activation (mimetized by the expression of $G\alpha_q$R183C mutant) is able to arrest mitochondrial movement.

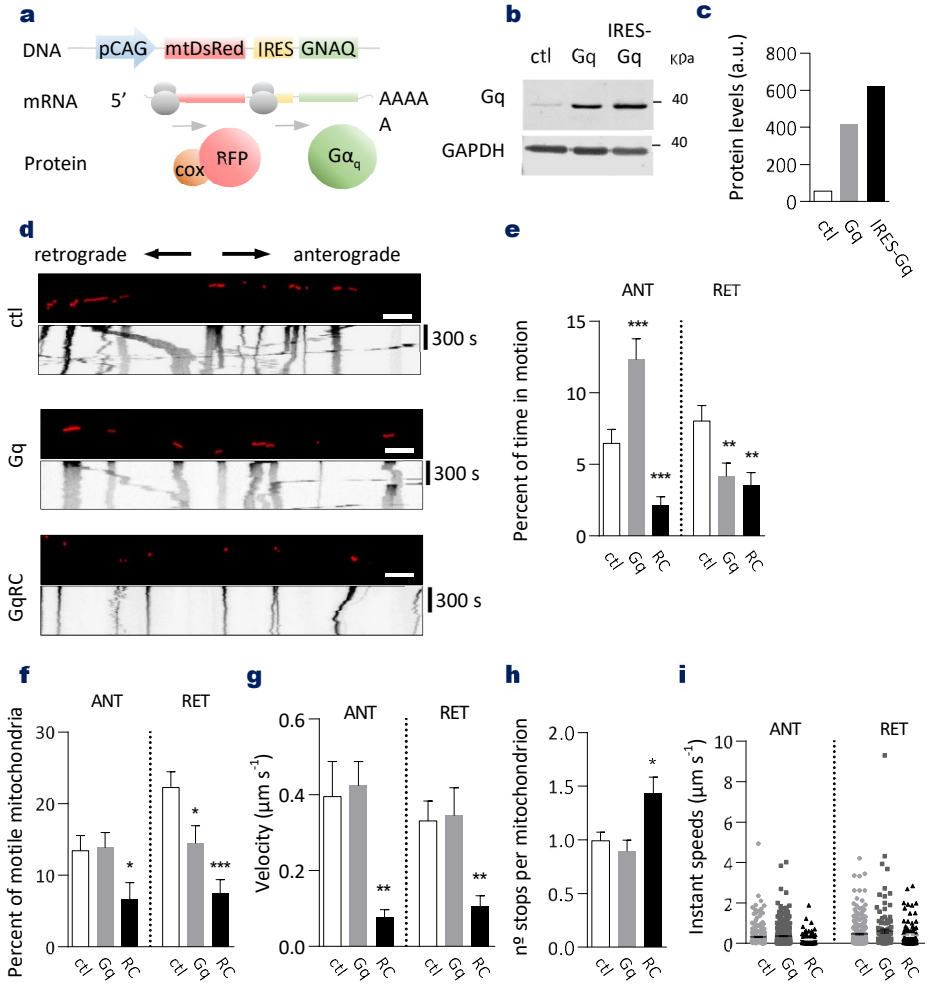

Figure R29. $G\alpha_q$R183C reduces mitochondrial motility. a, Diagram of the IRES vector, which enables bicistronic expression of MtDsRed and $G\alpha_q$. **b,** HEK293 cells were transfected with pcDNA3.1 empty vector (ctl), pcDNA3.1-$G\alpha_q$ (Gq) or the pIRES-mtDsRed $G\alpha_q$. Cell lysates (20 µg each) were separated by SDS-PAGE previous to western blot analysis with anti-$G\alpha_q$ antibody (BD biosciences®). GAPDH was used as a loading control. **c,** Band intensity from (b) was quantified using ImageStudio® software and normalized with GAPDH intensity. **d,** DIV 4 hippocampal neurons were co-transfected with GFP and IRES vectors containing mtDsRed (ctl), mtDsRed and $G\alpha_q$ (Gq) or mtDsRed and $G\alpha_q$R183C (RC). Time-lapse imaging was performed 1 and 2 days post-transfection as explained in Figure 18. Representative images of axonal mitochondria in neurons and corresponding kymographs. For each condition, the first frame of the live-imaging series appears above the kymograph. Scale bars, 5 µm. **e,** From kymographs as in (a), the percent of time each mitochondrion was in motion was determined, averaged, and compared with control for the anterograde (ANT) and retrograde (RET) direction. **f,** Mitochondrial motility expressed as percentage of total mitochondria within axons. **g,** Average velocity of moving mitochondria **h,** Average number of times a moving mitochondria reduced its velocity below a threshold (0,0083µm/s). **i,** Dot chart of all velocities reached by mitochondria in each experimental condition. Error bars represent SEM. For each condition, 33 to 42 axons were analyzed from 4 independent experiments. Statistical analysis was carried out using a one-way ANOVA *p<0.05,**p<0.01,***p<0.001.

5.10. The YM-254890 specific inhibitor impairs $G\alpha_q$R183C-induced mitochondrial arrest

Besides the experiments using bicistronic vectors, the ability of $G\alpha_q$ to arrest mitochondrial motility was tested using the YM-254890 specific $G\alpha_q$ inhibitor. This molecule is predicted to bind to a hinge between the α-helical domain and the Ras-like domain of the $G\alpha_q$ subunit, thus keeping the $G\alpha_q$ subunit in a closed conformation and impairing the release of GDP and the binding of GTP (Campbell & Smrcka, 2018). It therefore represents a useful tool to study $G\alpha_{q/11}$-coupled receptor signaling and their physiological roles (Uemura et al., 2006).

In accordance with our previous results, $G\alpha_q$ overexpression increased the anterograde movement without significantly affecting the retrograde transport or the number of stops per mitochondria (**Fig.R30b,c** white bars). Conversely, expressing active $G\alpha_q$ decreases mitochondrial motility in both directions and increases the number of times they stop (**Fig.R30b,c** white bars).

Though the presence of $G\alpha_q$-inhibitor did not significantly alter mitochondrial motility parameters when acting on endogenous $G\alpha_q$ protein (**Fig.R30b,c**), we detected significant changes when overexpressing $G\alpha_q$ or expressing its active mutant. $G\alpha_q$ no longer increased anterograde mitochondrial movement when overexpressed in the presence of the inhibitor (**Fig.R30b,c**). Besides, the molecule abrogated mitochondrial arrest induced by $G\alpha_q$R183C expression, as shown with the increase in the presence of time in motion and the reduction in the number of times mitochondria stop (**Fig.R30b,c** black bars).

5.11. $G\alpha_q$ does not significantly alter the trafficking of synaptophysin-containing vesicles

$G\alpha_q$ modulates axonal mitochondrial motility, so we asked whether this regulation was specific for mitochondria or could be extended to vesicle trafficking. To evaluate axonal vesicle trafficking, neurons were co-transfected with the vesicle marker GFP-synaptophysin and the previously utilized IRES vectors, which co-express mtDsRed and either $G\alpha_q$ or $G\alpha_q$R183C. Live-imaging of axonal vesicles and kymograph analysis was performed as for mitochondria. In contrast with mtDsRed, GFP- synaptophysin is also present along the axonal cytoplasm, though it concentrates on small vesicles (**Fig.R31a**). This fact, besides the smaller and highly variable size of synaptophysin-containing vesicles, results in fuzzier kymographs from which fewer motility parameter can be obtained.

Vesicle quantification showed no significant differences in neurons transfected with $G\alpha_q$ or its active mutant from those of the control condition. In the three cases, the percentage of moving vesicles stays from 35 to 40% (**Fig.R31b**), which are similar values as the reported in other studies using the same vesicle marker in control neurons (Norkett et al., 2016). These results indicate therefore that the previous alterations in axonal mitochondrial trafficking do not apply to synaptophysin-containing vesicles, which suggests they may be mitochondria-specific.

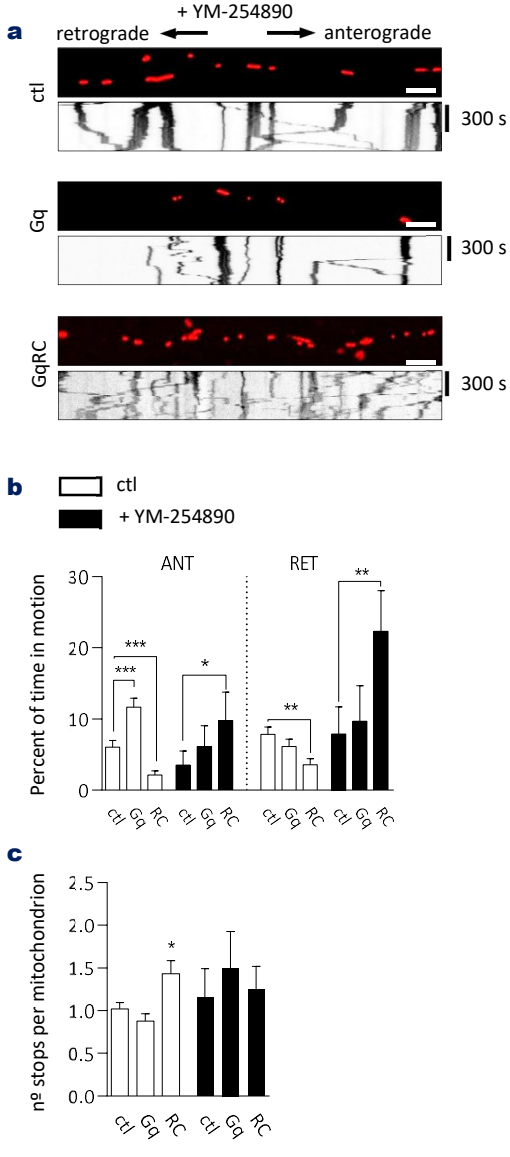

Figure R30. $G\alpha_q$ inhibition partially reverts $G\alpha_q$R183C-induced mitochondrial arrest. DIV 4 hippocampal neurons were co-transfected with GFP and IRES vectors containing mtDsRed (ctl), mtDsRed and $G\alpha_q$ (Gq) or mtDsRed and $G\alpha_q$R183C (RC). Time-lapse imaging was performed 1 and 2 days post-transfection in the presence or absence of 10 μM of YM-254890 in the medium, as indicated. **a,** Representative images of axonal mitochondria in neurons and corresponding kymographs. For each condition, the first frame of the live-imaging series appears above the kymograph. Scale bars, 5 μm. **b,** From kymographs as in (a), the percent of time each mitochondrion was in motion was determined, averaged, and compared with control for the anterograde (ANT) and retrograde (RET) direction **c,** Average number of times a moving mitochondria reduced its velocity below a threshold (0,0083μm/s). For each condition, 10 to 20 axons were analyzed from 2 independent experiments. Error bars represent SEM. Statistical analysis was carried out using a two-tailed Student's t-test followed by Mann-Whitney test. *p<0.05,**p<0.01,***p<0.001.

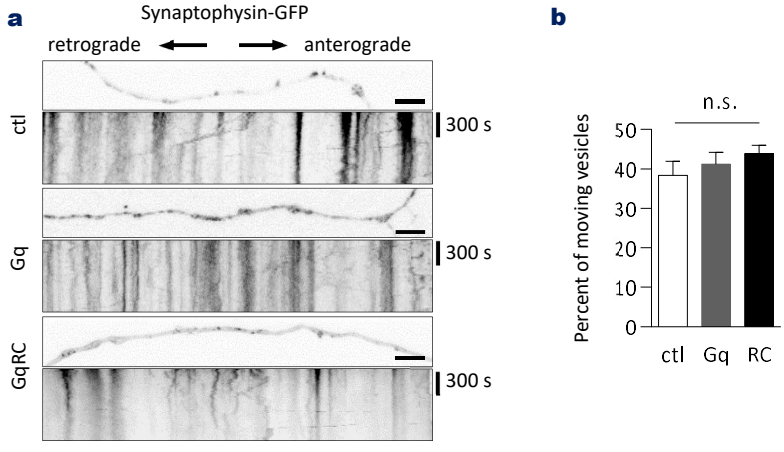

Figure R31. $G\alpha_q$ or $G\alpha_q$R183C overexpression does not alter axonal vesicular transport. DIV 4 hippocampal neurons were co-transfected with GFP-synaptophysin and IRES vectors containing mtDsRed (ctl), mtDsRed and $G\alpha_q$ (Gq) or mtDsRed and $G\alpha_q$R183C (RC). Time-lapse imaging was performed 1 and 2 days post-transfection. **a,** Representative images of synaptophysin vesicles in axons and corresponding kymographs. For each condition, the first frame of the live-imaging series appears above the kymograph. Scale bars, 5 µm. **b,** From kymographs as in (a), the percent of moving vesicles containing GFP-synaptophysin was determined, averaged, and compared with control. For each condition, 5 to 7 axons were analyzed from 2 independent experiments. Error bars represent SEM. Statistical analysis was carried out using a one-way ANOVA. n.s., not significant.

5.12. Stimulation of $G\alpha_q$-specific GPCRs arrests mitochondrial movement

Our results demonstrating the ability of active $G\alpha_q$ to arrest mitochondrial trafficking promted us to test whether $G\alpha_q$-dependent signaling from GPCR activation would have a similar outcome. In this regard, Designer Receptors Exclusively Activated by Designer Drugs (DREADD) were used as a chemogenetic tool to demonstrate the impact of $G\alpha_q$ signaling in axonal mitochondrial movement.

Neurons were co-transfected with the previously characterized DsRed-tagged hM3Dq DREADD receptor (Hu et al., 2016; Roth, 2016) and mito-GFP, a marker containing the mitochondrial localization signal of COX VIII bound to GFP. Axons from neurons expressing both DREADD receptor and mito-GFP were imaged for 10 minutes in the absence of clozapine N-oxide, the hM3Dq-specific ligand (CNO -). Then, the same axons were imaged once more 15 minutes after addition of 1 µM CNO (CNO +) to evaluate the effects of GPCR activation over mitochondrial transport.

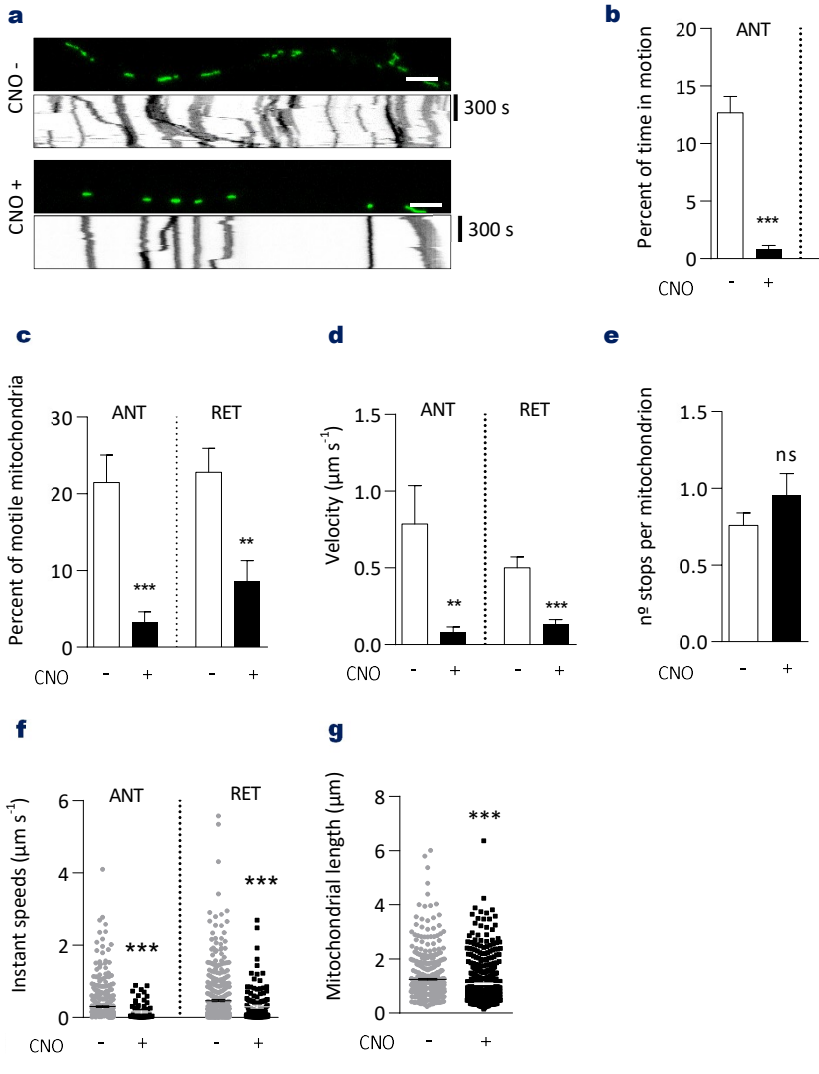

Figure R32. $G\alpha_q$ signaling from GPCRs induces mitochondrial arrest. DIV 4-5 hippocampal neurons were co-transfected with mito-GFP and the $G\alpha_q$-specific hM_3D DREADD receptor. Time-lapse imaging was performed 1 and 2 days post-transfection before (CNO-) and 15 min after (CNO +) the addition of 1 µM clozapine-N-oxide. **a,** Representative images of axonal mitochondria from neurons and corresponding kymographs. For each condition, the first frame of the live-imaging series appears above the kymograph. Scale bars, 5 µm. **b,** From kymographs as in (a), the percent of time each mitochondrion was in motion was determined, averaged, and compared with control for the anterograde (ANT) and retrograde (RET) direction. **c,** Mitochondrial motility expressed as percentage of total mitochondria within axons. **d,** Average velocity of moving mitochondria **e,** Number of times a moving mitochondria reduced its velocity below a threshold (0,0083 µm/s). **f,** Representation of all velocities reached by mitochondria in each experimental condition. **g,** Average mitochondrial length from axonal images as in (a) was calculated using the NeuronJ plugin from the Fiji software. n= 572 (CNO-) and 570 (CNO+) mitochondria from at least 15 different neurons from 3 different preparations. Error bars represent SEM. Statistical analysis was carried out using a two-tailed Student's t-test followed by Mann-Whitney test. n.s., not significant,**p<0.01,***p<0.001.

Consistent with the phenotype of $G\alpha_qR183C$ expression, GPCR stimulation strongly reduced bidirectional mitochondrial motility upon ligand stimulation, as reflected in the percentage of time in motion (**Fig.R32b**) (from 12.7±1.3% to 0.85±0.3% in the anterograde direction and from 13.2±1.5% to 2.3±0.6% in the retrograde). The number of motile mitochondria was also significantly decreased (**Fig.R32c**) (from 21.5±3.6% to 3.2±1.4% and from 22.8±3.2% to 8.6±2.8% in the anterograde and retrograde directions, respectively). Further, the overall speed of the few mitochondria that still moved was reduced (**Fig.R32d**) (from 0.79±0.25 to 0.08±0.03 µm/sec and from 0.5±0.07 to 0.13±0.03 µm/sec in the anterograde and retrograde directions, respectively) as well as the instantaneous speed (**Fig.R32f**). Conversely, the number of stops per mitochondria showed a tendency towards the increase upon receptor stimulation, through this increase did not reach significance (**Fig.R32e**). As observed with $G\alpha_qR183C$ expression, activation of $G\alpha_q$ signaling also reduced mitochondrial length (**Fig.R32g**).

5.13. Summary of $G\alpha_q$ impact on mitochondrial motility

Experiment	Condition	TIM (%±SEM)		Mobile mito (%±SEM)		Mean velocity		n
		A	R	A	R	A	R	
sh RNAs	sh scr	13,3±1,5	16,4±1,7	25,1±4	17,6±2,7	0,75±0,09	0,75±0,09	347
	sh Gq 1	15,6±1,6	29±2,1***	31,3±3	30,2±2,6***	1,04±0,12*	1,21±0,17*	375
	sh Gq 2	14,4±1,5	36,5±2,2***	29,5±3,3	35±3,2***	1,48±0,19***	1,15±0,13**	396
sh RNA-Alex3 KO	sh scr	6,3±1,5	10,1±2,0	9±2,6	17,9±3,0			166
	sh Gq	7,5±2,2	16,4±4,0*	13,6±4,0	39,9±7,6**			64
	sh scr- A3 KO	4,9±1,3	6,5±1,6*	10,3±3,6	13,7±4,3			187
	sh Gq- A3 KO	9,0±4,1,0	8,0±3,4	18,6±10,3	27,1±11,9			25
GFP-Gq proteins	GFP	10±1,2	12,4±1,4	20,8±2,8	26,6±3,7	0,45±0,05	0,45±0,06	390
	GqRC-GFP	1,7±0,7***	1,6±0,6***	4,1±3,1***	5,2±2,3***	0,14±0,04***	0,12±0,03***	261
	GqMAS70GFP	3,1±1,4**	3,4±0,7**	6,9±4,5*	15,2±6,4	0,33±0,11	0,16±0,04***	470
	Gq-Nt-GFP	9,6±1,7	11±1,8	15,4±2,8	22,6±5,2	0,45±0,10	0,37±0,07	211
Co-transfection	ctl	5,6±1,0	8,7±1,3	16,6±2,4	20,6±3,1	0,15±0,04	0,24±0,03	343
	Gq	12,7±1,4***	8,3±1,1	24,5±3,6**	20,0±2,5	0,30±0,04*	0,34±0,05	430
IRES vectors	ctl	6,47±0,98	8,0±1,1	13,4±2,2	22,3±2,2	0,40±0,09	0,33±0,05	470
	Gq	12,3±1,4***	4,19±0,9**	13,9±2,1	14,5±2,4*	0,42±0,06	0,35±0,07	390
	GqRC	2,2±0,6***	3,5±0,9**	6,6±2,3*	7,4±2,0***	0,08±0,02***	0,11±0,03***	305
DREADD -Gq	-cno	12,7±1,4	13,2±1,5	21,5±3,6	22,8±3,2	0,79±0,25	0,50±0,07	387
	+cno	0,90±0,3***	2,4±0,6***	3,2±1,4***	8,6±2,8**	0,08±0,03**	0,13±0,03***	429
Gq-inhibitor	Ctl	6,1±0,9	7,9±1,0					510
	Gq	11,7±1,3***	6,2±1,0					452
	GqRC	2,2±0,6***	3,5±0,9**					305
	Ctl+inh	3,5±2,0	7,9±3,8					29
	Gq+inh	6,1±2,9	9,7±5					28
	GqRC+inh	9,8±4*	22,3±5,8**					26

Table R3. Summary of the key data from the different analysis of mitochondrial motility related with $G\alpha_q$. Table shows the mean±SEM obtained for the analysis of the percentage of time in motion (TIM), the percentage of moving mitochondria (Mobile mito) and the mean velocity for the anterograde (A) and retrograde (R) directions, for each condition of the previously described live-imaging experiments. n=number of analyzed mitochondria. Statistical significance: *p<0.05**, p<0.01, ***p<0.001.

As an overview of the previous results, three major changes were observed regarding the impact of $G\alpha_q$ on mitochondrial trafficking. First, we observed that $G\alpha_q$ depletion increased the overall mitochondrial speed, including the instantaneous speed, and promoted mitochondrial transport towards the neuronal soma. Second, expression of $G\alpha_q$ promoted mitochondrial trafficking towards the opposite direction, that is, towards the axonal tips. And third, expression of a $G\alpha_q$ mutant that mimics its GTP-bound stage or activation of $G\alpha_q$ pathway from the level of GPCRs induced mitochondrial arrest. The most relevant data obtained is summarized in **table R3**, whereas the most important alterations in mitochondrial transport promoted by $G\alpha_q$ or Alex3 are summarized in **table R4**.

Condition	Experiment	Effects	
↓ $G\alpha_q$	$G\alpha_q$-specific shRNAs $G\alpha_q$-specific shRNAs in Alex3KO neurons	↑ retrograde movement ↑ bidirectional speed ↓ stops per mitochondria	+ motility
↑ $G\alpha_q$	Co-transfection IRES-containing vectors	↑ anterograde movement	
↓ $G\alpha_q$/Alex3 KO	$G\alpha_q$-specific shRNAs in Alex3KO neurons	-Alex3 KO avoids $G\alpha_q$-induced increase in anterograde motility and overall speed	
↓ $G\alpha_q$ activity	$G\alpha_q$ GTPase inhibitor	-Avoids $G\alpha_q$R183C-induced mitochondrial arrest in both directions -Reduces $G\alpha_q$-induced increase in anterograde movement	
↑ Alex3	GFP tagged protein (López-Doménech et al. 2012)	↓ bidirectional motility and speed	
↓ Alex3	Alex3-specific siRNAs (López-Doménech et al. 2012)	↓ bidirectional motility	+ mitochondrial arrest
↑ $G\alpha_q$R183C	GFP-tagged protein IRES-containing vectors $G\alpha_q$ GTPase inhibitor	↓ bidirectional motility and speed ↑ stops per mitochondria	
↑ $G\alpha_q$ activity	DREADD- $G\alpha_q$ receptors	↓ bidirectional motility and speed	

Table R4. Summary of the key data from the different analysis of mitochondrial motility related with $G\alpha_q$ and Alex3. Table shows the experimental condition in which mitochondrial motility was evaluated, the experiments performed to demonstrate the impact of the tested condition and the effects observed after kymograph processing. Conditions highlighted in green represent a tendency to increase mitochondrial motility, those in blue show no impact or alter a previous phenotype, and those in red arrest mitochondrial motility in different degrees. Conditions increasing or reducing Alex3 expression were performed in López-Doménech et al. 2012 and have been included to better understand the effects of $G\alpha_q$ in Alex3(-/-) neurons.

6. Involvement of $G\alpha_q$ in mitochondrial morphology and neuronal physiology

6.1. $G\alpha_q$ is necessary to maintain mitochondrial length and complexity

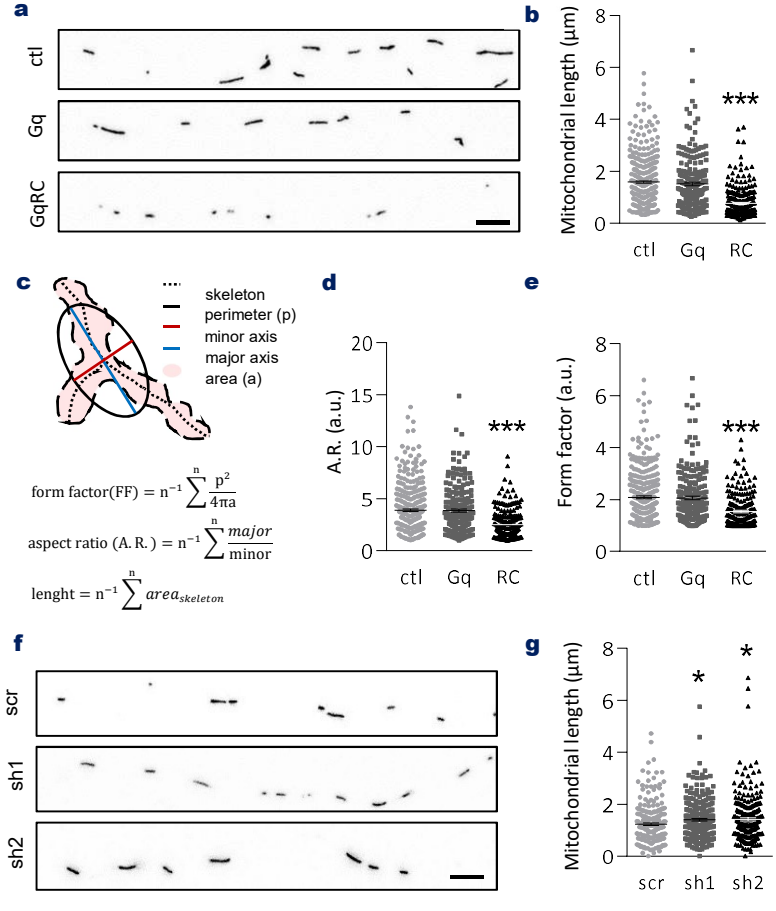

Figure R33. $G\alpha_qR183C$ reduces mitochondrial length and shape complexity, whereas $G\alpha_q$ knock-down increases mitochondrial length. a, Axonal mitochondria from neurons co-transfected with GFP and IRES vectors containing mtDsRed (ctl), mtDsRed and $G\alpha_q$ (Gq) or mtDsRed and $G\alpha_qR183C$ (RC). Scale bar, 5 µm. **b,** Average mitochondrial length from axonal images as in (a) was calculated using the NeuronJ plugin from the Fiji software. n= 347 ctl, n=227 $G\alpha_q$ and n=248 $G\alpha_qR183C$ mitochondria from at least 20 different neurons from 3 different preparations **c,** Representation of the formulas used to calculate the morphological parameters. **d,** Average aspect ratio (AR, the ratio between the major and minor axis of the ellipse equivalent to the mitochondrion) and **e,** Average degree of branching or form factor (FF, defined as (Pm2)/(4πAm), where Pm is the length of mitochondrial outline and Am is the area of mitochondrion) were calculated using mitochondrial morphology macro for Fiji software. n= 342 ctl, 220 $G\alpha_q$ and 204 $G\alpha_qR183C$ mitochondria from at least 20 different neurons from 3 different preparations. **f,** Axonal mitochondria from neurons co-transfected with mtDsRed and a GFP-containing scramble short-hairpin RNA (scr), GFP and a $G\alpha_q$-specific short hairpin RNA (sh1) or a $G\alpha_q$-specific GFP-bound short hairpin RNA (sh2). Scale bar, 5 µm. **g,** Average mitochondrial length from axonal images as in (f) was calculated using the NeuronJ plugin from the Fiji software. n= 252 control (ctl), 249 sh1 and 247 sh2 mitochondria from at least 15 different neurons from 3 different preparations. Statistical significance was calculated using one-way ANOVA.*p<0.05,***p<0.001.

During the time-lapse imaging of axonal mitochondria, we realized that most of the mitochondria from neurons expressing $G\alpha_q$R183C were shorter and round-shaped, compared with those from neurons expressing only fluorescent markers or expressing the wild type form (**Fig.R33a**). The quantitative analysis of mitochondrial length confirmed our previous thoughts: neurons expressing active $G\alpha_q$ had shorter mitochondria (**Fig.R33b**). The roundness and morphological complexity was also quantified by means of a program based on the formulas in **Fig.R33c**. Both mitochondrial aspect ratio (**Fig.R33d**) and form factor (**Fig.R33e**) were significantly reduced in mitochondria from neurons expressing $G\alpha_q$R183C compared with the other two conditions, indicating the circular shape and low number of protrusions in those mitochondria. Moreover, during the knock-down experiments using shRNAs we observed that mitochondria from neurons with low levels of $G\alpha_q$, and especially those moving at high speeds seemed longer that those that remained still. Consistent with data of $G\alpha_q$R183C expression, depletion of the $G\alpha_q$ leaded to a small but significant increase in mitochondrial length (**Fig.R33f,g**), which suggests $G\alpha_q$ may not only be involved in mitochondrial motility, but also regulating important processes of mitochondrial dynamics, including fusion and fission.

6.2. Expression of active $G\alpha_q$ affects morphological parameters of neurons

On the basis of the above data, it is likely that reducing mitochondrial motility would affect the overall physiology of the neuron. Indeed, during the imaging experiments we observed that several of the neurons and most specially those expressing $G\alpha_q$R183C showed alterations in their morphology, with less branching and shorter dendrites (**Fig.R34a**). Neurite length quantification confirmed a significant shortening of dendrites arising directly from the soma in cells overexpressing $G\alpha_q$, a phenotype that was more distinguishable in cells expressing active $G\alpha_q$ (**Fig.R34b**). Dendrites arising from other dendrites as a result from branching, when present, were not significantly altered in cells overexpressing $G\alpha_q$, although they decreased their length after $G\alpha_q$R183C expression (**Fig.R34c**).

To evaluate the overall dendritic arborization, we carried out sholl analysis from neurons co-transfected with GFP and IRES vectors containing $G\alpha_q$ or $G\alpha_q$R183C. This method is based on the plot of dendrite intersections against the radial distance from the soma center (Binley, Ng, Tribble, Song, & Morgan, 2014). Neurons overexpressing $G\alpha_q$ showed a similar sholl profile as those in the control condition. Conversely, expression of active $G\alpha_q$ reduced the number of intersections at 70, 110, 130 and 190 µm from the soma, thus demonstrating the lower degree in dendritic arborization (**Fig.R34d**).

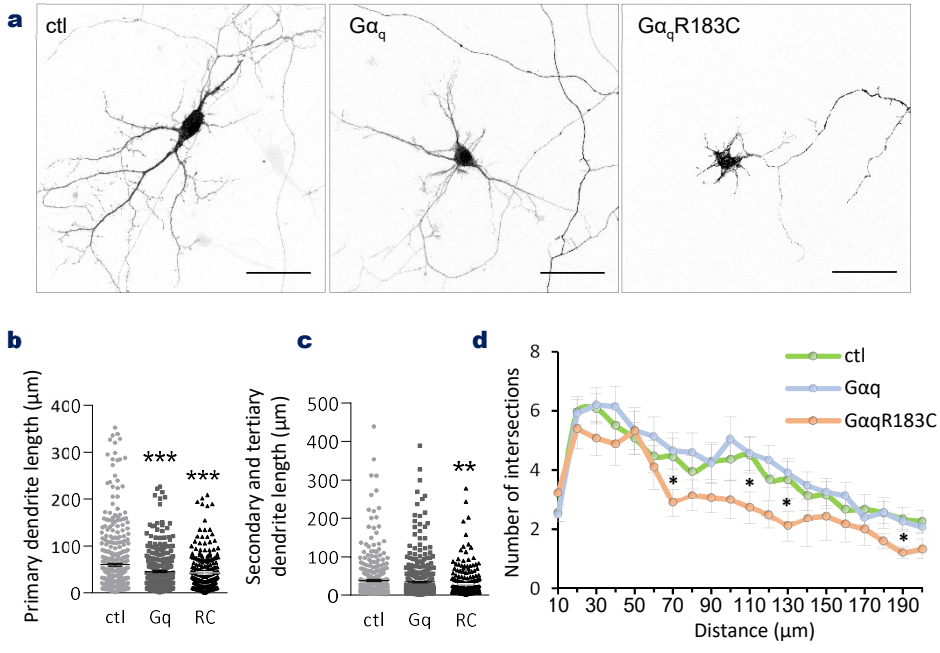

Figure R34. $G\alpha_q$R183C reduces dendritic length and branching. DIV 4-5 hippocampal neurons were co-transfected with GFP and IRES vectors containing mtDsRed as control (ctl), mtDsRed and $G\alpha_q$ (Gq) or mtDsRed and $G\alpha_q$R183C (RC). Live imaging was performed 2 days post-transfection. **a,** Neuronal morphology under the different conditions is shown by the GFP used to fill the cell. Scale bars, 50 µm. **b,c,** Average length of primary (b) or secondary and tertiary (c) dendrites. n=407 control (ctl), 308 $G\alpha_q$ and 243 $G\alpha_q$R183C dendrites from 3 independent preparations of neurons. Statistical analysis was carried out using a one-way ANOVA. **d,** Sholl analysis was performed from images as in (a) using the NeuronJ plugin from the Fiji software. n= 45 control (ctl), 35 $G\alpha_q$ and 32 $G\alpha_q$R183C neurons from 3 different preparations. Data were analyzed by two-tailed Student's t-test *p<0.05,**p<0.005,***p<0.001.

7. $G\alpha_q$ regulates TRAK proteins

The previous results demonstrate a clear involvement of $G\alpha_q$ regulating mitochondrial transport. Depletion of the protein increases the overall speed and movement especially towards the neuronal soma, whereas expression of its wild type form enhances the transport towards the axonal tips. Consistently, expression of the constitutive active $G\alpha_q$ or activation of $G\alpha_q$ signaling from the GPCRs induces an arrest in mitochondrial movement. The degree of arborization of neurons expressing active $G\alpha_q$ is also clearly altered. Besides Miro1 and Alex3, alteration in dendrite arborization has been reported by modification of the TRAK adaptor proteins (Brickley and Stephenson 2011; Granatiero et al. 2019; López-Doménech et al. 2012; MacAskill et al. 2009; van Spronsen et al. 2013). Since TRAK proteins are part of the same multi-protein complex that regulate mitochondrial motility, we considered $G\alpha_q$ could also be affecting their function.

TRAK1 and TRAK2 couple mitochondria to microtubule-based motor proteins and have Miro1 as their main receptor (López-Doménech et al., 2018). Whereas TRAK1/OIP106 has been reported to interact mainly with Kif5C and mediate the anterograde transport in axons, TRAK2/GRIF2 is able to bind kinesin and dynein motor proteins and promote both anterograde and retrograde movement (López-Doménech et al., 2018; van Spronsen et al., 2013). Due to their impact on mitochondrial dynamics, overexpression of TRAK proteins has been previously used as method to study mitochondrial redistribution in cell lines (López-Doménech et al., 2018). High levels of TRAK1 induce mitochondrial redistribution towards the cell periphery. Conversely, expression of TRAK2 leads to the accumulation of mitochondria around the perinuclear region in a similar manner as Miro1 or Alex3 (López-Doménech et al., 2018).

7.1. $G\alpha_q$ alters mitochondrial redistribution induced by TRAK proteins

To evaluate the impact of $G\alpha_q$ expression on TRAK-induced mitochondrial distribution, we used HeLa and MEF cells as a model to express HA-tagged TRAK 1 or TRAK 2 either alone or in the presence of $G\alpha_q$ or $G\alpha_q$R183C. As previously documented (López-Doménech et al., 2018), TRAK1 strongly localizes at the mitochondria and its expression induces mitochondrial redistribution at the periphery (**Fig.R35a**). Co-expression of TRAK1 with $G\alpha_q$, however, impairs mitochondrial localization close to the plasma membrane and induces the formation of mitochondrial aggregates at the perinuclear region. Besides, TRAK1 no longer shows a fully mitochondrial localization, but rather localizes in patches mainly concentrated at the mitochondrial aggregates (**Fig.R35b**). $G\alpha_q$R183C seemed to concentrate slightly more at regions where mitochondria and TRAK1 were present and allowed in a higher degree the scattering of mitochondria towards the cell periphery induced by TRAK1 overexpression (**fig.R35c**). Both wild-type $G\alpha_q$ and the active mutant showed a punctate staining mostly scattered through the cytoplasm with only mild co-localization at the mitochondria.

Expression of $G\alpha_q$ and $G\alpha_q$R183C was also evaluated in the presence of HA-TRAK2. In contrast with TRAK1, TRAK2 localizes at the mitochondria and the cytoplasm and its expression greatly promotes mitochondrial redistribution around the nuclei (Smith, Pozo, Brickley, & Stephenson, 2006) (**Fig.R35d**). Interestingly, co-expression of TRAK2 with $G\alpha_q$, again, enhanced the formation of perinuclear aggregates (**Fig.R35e**). When co-expressed with $G\alpha_q$R183C, though, we observed a mitochondrial redistribution towards the cell periphery and a marked localization of TRAK2 in some patches closed to the cell edges (**Fig.R35f**). Besides, active $G\alpha_q$ co-localized in some of those patches with TRAK2, suggesting a possible role of the active G protein removing the adaptor from perinuclear aggregates and taking it to the periphery.

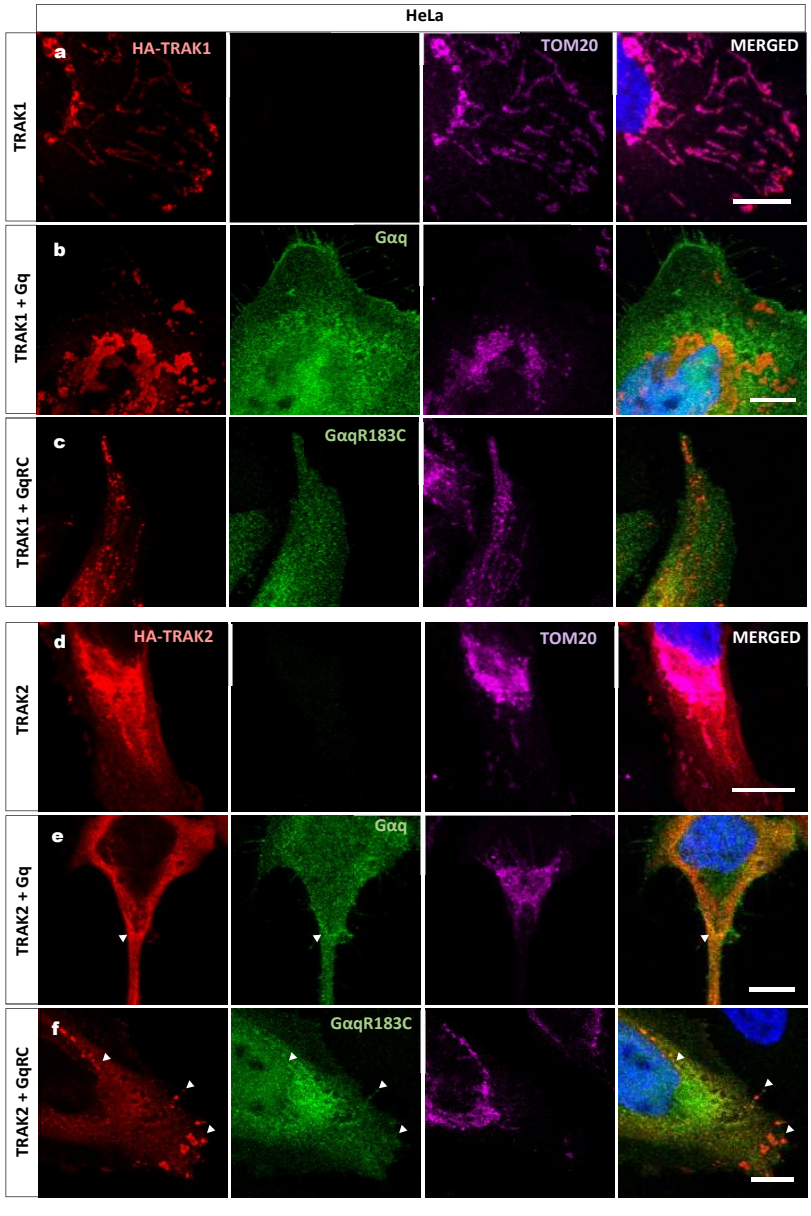

Figure R35. $G\alpha_qR183C$ expression induces TRAK2 localization near the plasma membrane. HeLa cells were transfected with plasmids containing HA-TRAK1 (panels above) or HA-TRAK2 (panels below) along with pcDNA3 empty vector or containing $G\alpha_q$ or $G\alpha_qR183C$. Confocal micrographs of MEF cells stained with anti-HA and Alexa-Fluor-568 anti-rat; anti- $G\alpha_q$ (BD biosciences®) and Alexa-fluor-488 anti-mouse; and anti-Tom20 and Alexa-Fluor-647 anti-rabbit and mounted on ProlongDiamond-DAPI. White arrowheads point to co-localization points of TRAK2 with $G\alpha_q$ or $G\alpha_qR183C$. Tom20 immunostaining was excluded from merged panels for a better visualization of $G\alpha_q$ localization with TRAK proteins. Images are z-projections of 7 stacks, were acquired using a using Zeiss LSM780 confocal microscope equipped with a 63x oil immersion lens and are representative of the majority of cells from 3 independent experiments.

7.2. $G\alpha_qR183C$ induces TRAK2 localization at the cell periphery in MEF cells

The atypical distribution of TRAK2 in Hela cells expressing active-$G\alpha_q$ prompted us to investigate the intracellular localization of the mitochondrial adaptor. With that end, MEF cells were transfected with HA-TRAK2 alone or in the presence of $G\alpha_qR183C$. Surprisingly, in this model expression of active-$G\alpha_q$ leaded to a marked redistribution of TRAK2 from the cytoplasm towards the cell periphery (**Fig.R36**), even in a clearer manner as previously seen in HeLa cells. Thus, this data further supports the involvement of $G\alpha_q$ regulating the subcellular localization of TRAK2.

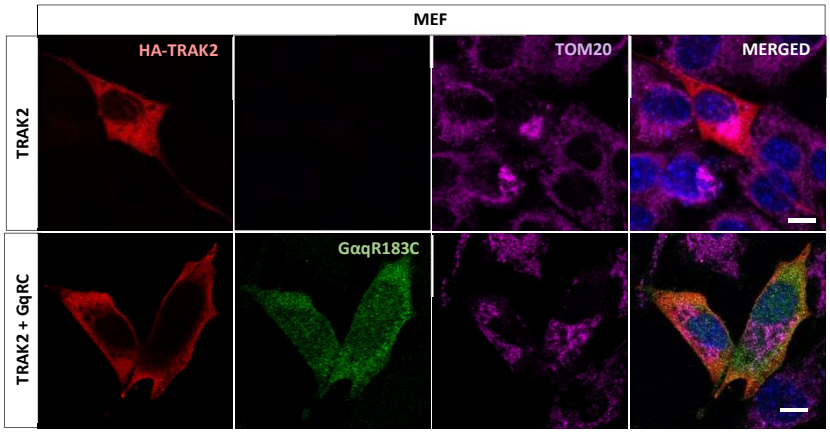

Figure R36. $G\alpha_qR183C$ promotes TRAK2 localization at the cell periphery. MEF cells were transfected with plasmids containing HA-TRAK2 along with pcDNA3 empty vector or containing $G\alpha_qR183C$. Confocal micrographs of MEF cells were stained with anti-HA and Alexa-Fluor-568 anti-rat; anti-$G\alpha_q$ (BD biosciences®) and Alexa-Fluor-488 anti-mouse; and anti-Tom20 and Alexa-Fluor-647 anti-rabbit and mounted on ProlongDiamond-DAPI. Images are z-projections of 7 stacks, were acquired using a using Zeiss LSM780 confocal microscope equipped with a 63x oil immersion lens and are representative of the majority of cells from 3 independent experiments. Scale bars: 10 µm.

7.3. Co-expression of $G\alpha_q$ with TRAK proteins does not alter actin cytoskeleton

To address whether the previously observed changes in mitochondrial aggregates where induced by alterations in actin cytoskeleton, HeLa cells were, again, co-transfected with $G\alpha_q$ or $G\alpha_qR183C$ and TRAK proteins. This time though, we expressed Lifeact-DsRed plasmids (adenoviral vectors, Ibidi ®) to evaluate the structure of actin filaments.

Figure R37a clearly shows an arranged structure of actin filaments in cells expressing TRAK1, which still remains intact when co-expressing $G\alpha_q$ or $G\alpha_qR183C$. In the same direction, co-expression of TRAK2 with either the wild-type or the active $G\alpha_q$ did not apparently altered the filamentous structures of actin cytoskeleton (**Fig.R37b**). This data indicates that those aggregates are not caused by dysfunctional F-actin structures.

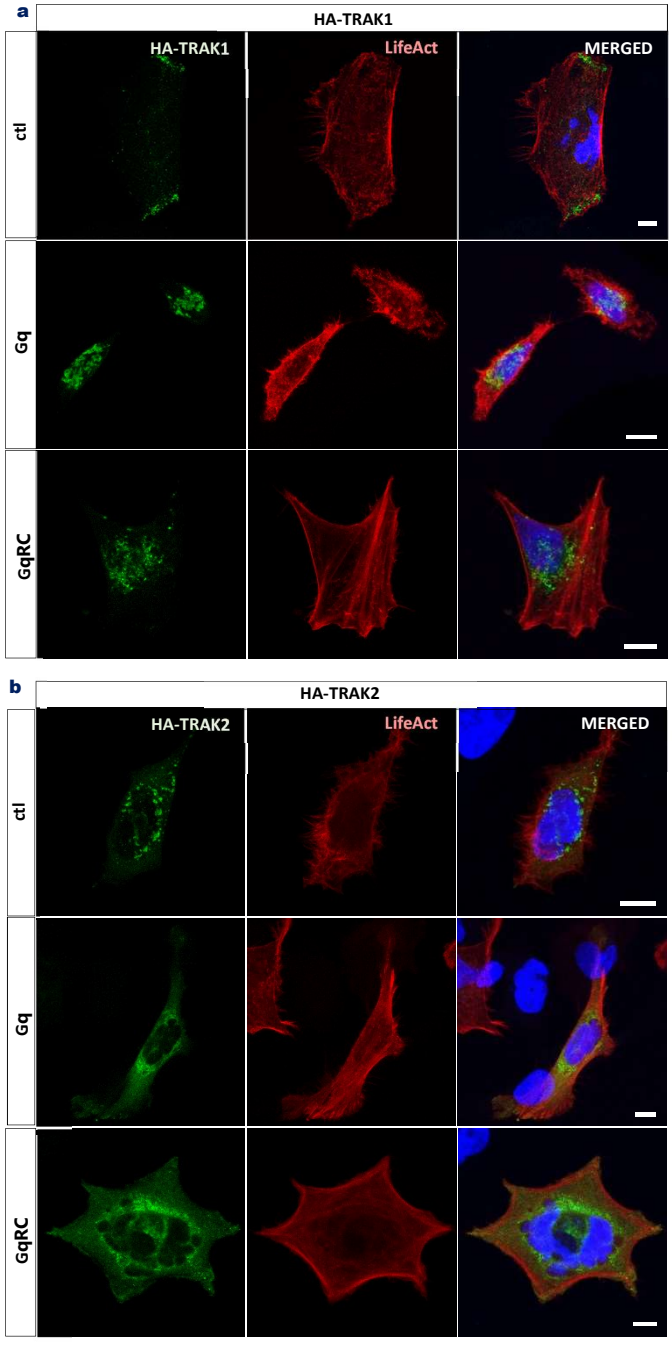

Figure R37. Labeling actin cytoskeleton in the presence of TRAK proteins and $G\alpha_q$ or $G\alpha_q$R183C in Hela cells. HeLa cells were co-transfected with plasmids containing HA-TRAK1 (**a**) or HA-TRAK2 (**b**), LifeAct (to label actin cytoskeleton) and pcDNA3 empty vector or containing $G\alpha_q$ or $G\alpha_q$R183C. Confocal micrographs of HeLa cells stained with anti-HA and Alexa-Fluor-488 mounted on ProlongDiamond-DAPI. $G\alpha_q$ was not immunolabeled. Images are z-projections of 7 stacks, were acquired using a using Zeiss LSM780 confocal microscope equipped with a 63x oil immersion lens and are representative of the majority of cells from 3 independent experiments. Scale bars: 10 µm.

7.4. $G\alpha_q$ immunoprecipitates with TRAK proteins and precipitates more with TRAK2

The fact that $G\alpha_q$ localized at specific points with TRAK2 prompted us to investigate if it could interact with TRAK proteins. With that end, HA-tagged TRAK1 and TRAK2 were immunoprecipitated from HEK293 cells co-expressing $G\alpha_q$ or $G\alpha_q$R183C (**Fig.R38a**). Because both TRAK adaptors and specially TRAK1 are well-described kinesin-binding proteins, an additional condition expressing myc-tagged Kif5C was tested as a positive control.

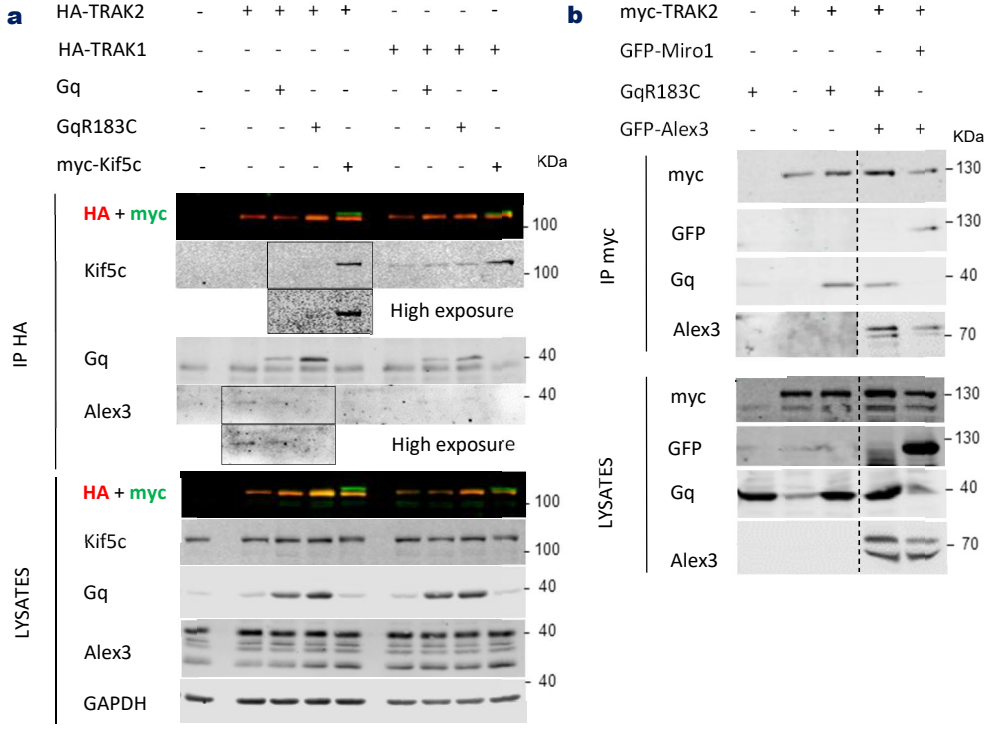

Figure R38. $G\alpha_q$ co-immunoprecipitation with TRAK2 and TRAK1. a, Immunoprecipitation of HA-tagged TRAK1 and TRAK2 from HEK293 cells transfected with vectors containing HA-TRAK1 or HA-TRAK2 and $G\alpha_q$, $G\alpha_q$R183C or myc-Kif5c (used as a control) as indicated above. For each condition, 700 µg of lysates were incubated with HA-agarose beads (Sigma®) and analyzed by western blot with specific antibodies for HA (Roche®), myc (Millipore®), $G\alpha_q$ (BD biosciences®), GAPDH (Cell signaling®, used as a loading control), Alex3 (Proteintech®) and Kif5c (F-5, Sta. Cruz®), as indicated. Western blot analysis of Kif5c and Alex3 immunoprecipitates are shown with higher exposure for a better visualization of faint bands (panels below). **b,** Immunoprecipitation of myc-tagged TRAK2 from HEK293 cells transfected with vectors containing myc-TRAK2, GFP-Miro1, $G\alpha_q$ R183C and/or GFP-Alex3, as indicated above. For each condition, 700 µg of lysates were incubated with myc-trap (Chromotek®) and analyzed by western blot with specific antibodies for myc (Millipore®), GFP (Invitrogen®), $G\alpha_q$ (BD biosciences®) and Alex3 (Proteintech®), as indicated. Data are representative of 3 independent experiments.

In accordance with the observed co-localization, the western blot analysis using a $G\alpha_q$ specific antibody revealed a more prominent co-immunoprecipitation of the constitutive-active mutant with both TRAK adaptors than that of the wild-type form. $G\alpha_qR183C$ precipitated more with TRAK2 than TRAK1 (**Fig.R38a**, fourth panel). Western blot using myc antibody revealed similar interaction of transfected Kif5C with both adaptors (**Fig.R38a**, first panel in green), but only TRAK1 interacted clearly with the endogenous Kif5C in the other conditions (**Fig.R38a**, second panel). This result supports a previous report of TRAK1 showing higher affinity for endogenous kinesin that TRAK2, which shows stronger affinity for endogenous dynein instead (van Spronsen et al., 2013). Even so, a faint band corresponding to endogenous Kif5C co-immunoprecipitated with TRAK2 in the presence of $G\alpha_qR183C$ but not with wild type $G\alpha_q$, suggesting that active $G\alpha_q$ could stabilize somehow a TRAK2-kinesin complex (**Fig.R38a**, third panel). We also performed western blot analysis using Alex3 specific antibody to check whether the endogenous protein could interact with HA-TRAK2, as previously reported (López-Doménech et al. 2012). Indeed, endogenous Alex3 co-immunoprecipitated with TRAK2 (**Fig.R38a**, fifth and sixth panels) but that interaction became weaker upon $G\alpha_q$ expression and almost undetectable when expressing its active mutant. That could be due to the previously observed changes in TRAK2 localization in the presence of $G\alpha_q$. Since Alex3 is primarily present at the outer mitochondrial membrane, localization of TRAK2 at the cell edges would difficult Alex3-TRAK2 interaction.

To evaluate once more $G\alpha_q$ interaction with the motor adaptor, a myc-tagged TRAK2 was immunoprecipitated from HEK293 cells co-expressing $G\alpha_qR183C$ (**Fig.38b**). Consistent with the previous report (López-Doménech et al., 2012), Alex3 co-immunoprecipitated with TRAK2 in the presence of Miro1 or $G\alpha_q$ (**Fig.38b**). $G\alpha_q$, in turn, co-immunoprecipitated with TRAK2 when expressed alone or in the presence of Alex3, suggesting that Alex3 and $G\alpha_q$ may bind the molecular adaptor in a putative protein complex with Miro1.

8. A novel interaction of $G\alpha_q$ with myosin X

The results from time-lapse imaging experiments unveiled important changes in mitochondrial motility when expressing or depleting $G\alpha_q$, in both its wild type and its constitutive-active forms. Low levels of $G\alpha_q$ not only increased retrograde motility and overall speed, but also the instantaneous speed at which mitochondria moved and the number of times mitochondria reached velocities over 2 μm/sec. Besides, expression of wild-type $G\alpha_q$ increased mitochondrial speed in the anterograde direction with no significant alterations in the number of stops per mitochondria.

It is well known that the overall speed can be modulated by the coupling and detaching of mitochondrial protein complexes to kinesin and dynein motors. As mentioned, this coupling is

mainly promoted by the TRAK adaptors, and necessarily results in an increase in the number of stops per mitochondria when the protein complexes are disassembled and a reduction when the complexes are stabilized. For this reason, such alterations of instantaneous speed promoted by $G\alpha_q$ will probably require the involvement of additional molecular mechanisms.

8.1. $G\alpha_q$ interacts specifically with the atypical myosin X

One of the mechanisms that regulates the speed at which mitochondria move (when they are moving) is the coupling to actin filaments through myosin motors. Several myosins have been described to mediate mitochondrial motility, including myosin XIX and myosin VI (Kruppa et al., 2018; Lu et al., 2014; Rohn et al., 2014; Ropars et al., 2016). Looking again at our mass-spectrometry analysis, we found that the atypical myosin X co-immunoprecipitated specifically with $G\alpha_q$ in NIH3T3 fibroblasts and MEF KO recovered for $G\alpha_q$ expression with both E17 and C19 antibodies, and suggests the presence of Myosin X in $G\alpha_q$-containing mitochondrial complexes.

	Cell line	Antibody	Number of peptides	coverage	Peptides found
Myosin X	NIH3T3	E17	1	100%	SADLLGLDPTQLTDALTQR
	MEF KO+Gq	E17	4	100%	NLALPDDIR SADLLGLDPTQLTDALTQR VEGQEFIVR WSSAIQNVTDTK
	NIH 3T3	C19	1	98%	WSSAIQNVTDTK
	MEF KO+Gq	C19	2	100%	DETFLWFR WSSAIQNVTDTK
	MEF WT	C19	1	95%	LQYLQGDYTPHTSIPPLEEVYSVQR

Table R5. Representation of the peptides found for Myosin X in the mass spectrometry analysis.

8.2. $G\alpha_q$ localizes at specific points with Myosin X

To address if $G\alpha_q$ localized with Myosin X in axonal mitochondria, DIV4-5 hippocampal neurons were immunostained with specific antibodies for $G\alpha_q$ and Myosin X. Interestingly, Myosin X concentrates at specific spots close to endogenous $G\alpha_q$, suggesting they may localize within the same protein complexes (**Fig.39,** upper pannels). Additional immunostaining with the mitochondrial marker Tom20 determined that those spots where myosin X concentrates localize within the mitochondria (**Fig.39,** lower pannels). In fact, those points may be the regions where mitochondria binds to actin cytoskeleton.

Together, this preliminary data opens a new range of possibilities to study $G\alpha_q$ involvement in mitochondrial motility not only from the regulation of microtubule-base transport, but also through the coupling to novel actin-based motors, as is the case of Myosin X.

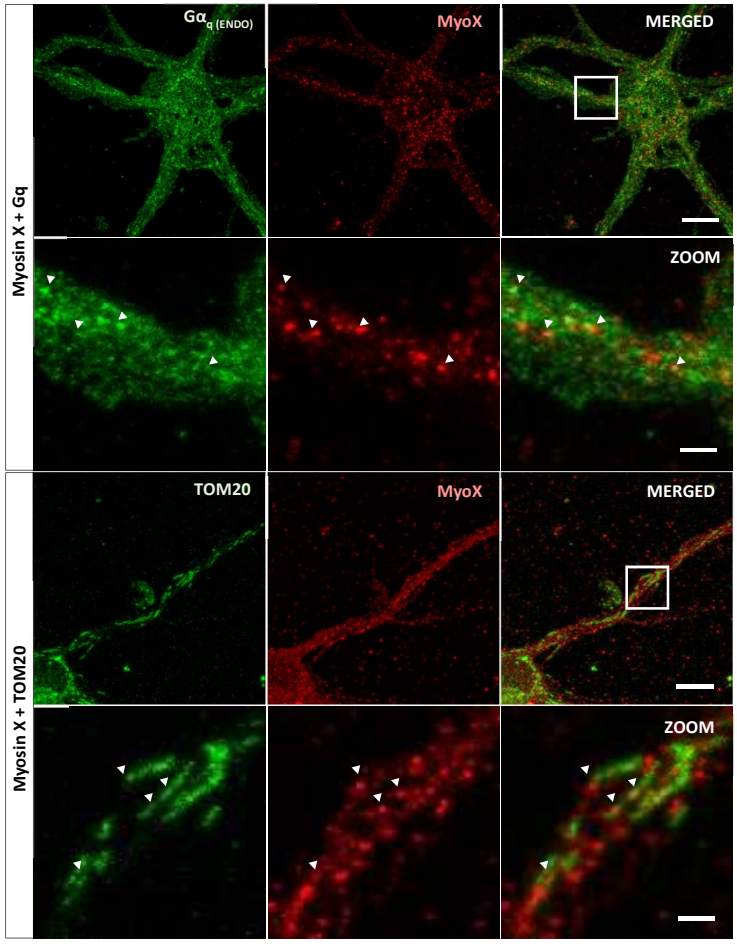

Figure R39. Endogenous Myosin X localizes at specific dotty areas with $G\alpha_q$ and the mitochondria in mouse hippocampal neurons. Immunofluorescence was performed in 5 DIV hippocampal neurons with anti-myosin X (C1, Sta. Cruz®) and Alexa-Fluor-568 and anti-$G\alpha_q$ (E17, Sta. Cruz®) or anti-Tom20 (FL145, Sta. Cruz®, used as a mitochondrial marker) and Alexa-Fluor-488. Magnified images (5X) corresponding to the white box are shown below and arrowheads indicate co-localization or putative interaction points. Images are z-projections of 7 stacks, were acquired using a using Zeiss LSM780 confocal microscope equipped with a 63x oil immersion lens and are representative of the majority of neurons from 3 independent experiments. Scale bar, 10 µm and 2 µm (magnification).

DISCUSSION

Mitochondrial receptors for kinesin and dynein motor proteins along with their adaptors and regulators play a crucial role regulating mitochondrial motility by allowing microtubule-based transport in response to internal or external stimuli. Such processes are essential to place mitochondria at the sites where energy demands are high and to substitute old damaged mitochondria for newly generated ones. In the present work, we identified a previously uncharacterized role of $G\alpha_q$ as a key regulator of the mitochondrial movement machinery. In contrast with previous assumptions, $G\alpha_q$ not only localizes close to the plasma membrane or cytoplasm, but also at the mitochondria and other endomembranes where it regulates the physiology of these organelles (Sánchez-Fernández et al., 2014). In particular, the $G\alpha_q$ subfamily is required to keep the proper balance between mitochondrial fusion and fission acting at both outer and inner membrane. $G\alpha_q$ is also necessary for cristae formation and its absence impairs the organization of complexes at the electron transport chain, which in turn decreases oxidative rate, ATP production and mitochondrial functionality (Benincá et al., 2014). A mass-spectrometry analysis based on $G\alpha_q$ immunoprecipitates from cellular endomembranes allowed us to identify Alex3 as a putative $G\alpha_q$ effector at the mitochondria. A series of immunoprecipitation and pull-down studies revealed a specific interaction of endogenous $G\alpha_q$ with Alex3 in lysates from MEF, HEK293 and SHSY5Y, as well as mouse brain homogenates. $G\alpha_q$ binds directly to the C-terminal arm-containing region of Alex3. Subsequent immunoprecipitation and pull-down studies demonstrated a specific interaction of $G\alpha_q$ with the mitochondrial Rho GTPase 1 (Miro1) and the milton adaptor protein TRAK2, which couple mitochondria to kinesin and dynein. Together, those proteins constitute the main mediators of mitochondrial transport in neurons and some of the most relevant regulators of mitochondrial physiology. Consequently, life-cell imaging of mitochondria revealed that $G\alpha_q$ is necessary for the regulation of the anterograde and retrograde movement of mitochondria along the axons of hippocampal neurons. Its absence or its activation modifies the dynamic pattern of mitochondria and the dendritic arborization of neurons. Therefore, a better understanding of the link between their function and $G\alpha_q$ signaling could be of foremost importance to modulate their responses in the many neuropathological disorders that compromise neuronal viability and neurotransmission.

1. Alex3 as a novel downstream effector of $G\alpha_q$

The comparative study of our mass-spectrometry analysis based on $G\alpha_q$ immunoprecipitates from mitochondria-enriched cell lysates unveiled Alex3 and Armc10 as putative candidates to interact with $G\alpha_q$ at the mitochondria. Such results were subsequently validated though a series of immunoprecipitation and pull-down experiments using Alex3 as a model, but considering the high sequence similarity shared between both proteins, most of the phenotypic alterations described herein for Alex3 could also apply to Armc10 (López-Doménech et al. 2012). Because Alex3 cluster was originally generated by retrotransposition of the Armc10 gene (Serrat et al., 2013), it is not surprising that the ancestor protein leads to similar phenotypic alterations and regulates mitochondrial dynamics through the same binding partners as Alex3, including Miro1 and TRAK2 (Mirra et al., 2016; Serrat et al., 2014).

The number and the origin of the peptides obtained in the MS-analysis shows that Alex3 interacted with endogenous $G\alpha_q$ in two of the cell lines, MEF and NIH cells. Moreover, endogenous Alex3 co-precipitated with $G\alpha_q$ in brain homogenates and SHSY5Y lysates. Together with the results from IP and pull-down experiments in cell lines, our data demonstrates that Alex3 is a novel binding partner of $G\alpha_q$. In fact the definitive prove that Alex3 interacts with $G\alpha_q$ came from experiments with purified $G\alpha_q$ and histidine-tagged purified Alex3 proteins. As additional support, an independent proteomic analysis identified two other G protein alpha subunits, $G\alpha_s$ and $G\alpha_t$, as binding partners of Alex3 (Huttlin et al., 2015), although no functional analysis were reported. Alex3 could then function as a binding partner for other $G\alpha$ subunits besides $G\alpha_q$, although we have not explored this possibility in this work.

The identification of Alex3/Armc10 proteins as putative $G\alpha_q$-binding partners was of special interest to our group after previous studies that provided evidence of the specific interaction between $G\alpha$ subunits and other armadillo domain-containing proteins. One of the best characterized is p120catenin (p120ctn), a negative regulator of Rho small GTPases that mediates cell adhesion and migration (Ardawatia et al., 2011). p120ctn co-immunoprecipitates the two members of the $G\alpha_{12}$ subfamily, $G\alpha_{12}$ and $G\alpha_{13}$, and this association abrogates p120ctn-induced RhoA inhibition (Ardawatia et al., 2011; Krakstad et al., 2004). Similar to the immunoprecipitation experiments presented with $G\alpha_q$ and Alex3, the p120ctn protein shows preferential interaction with the active form of the $G\alpha$ proteins (Krakstad et al., 2004). In that case, $G\alpha$ proteins can associate to the N-terminal region and the armadillo domains (Krakstad et al., 2004). Besides p120ctn, $G\alpha_{12}$ was found to immunoprecipitate with the arm-containing proteins ARVCF and p0071 (unpublished results from our group). It is especially interesting that ARVCF is present in

the mitoproteome analysis in two of the cell lines, MEF and NIN3T3, and the group has some preliminary data pointing to the interaction with $G\alpha_q$, suggesting it could constitute a functional effector for $G\alpha_q$. In addition to that, the armadillo repeat containing protein 6 (Armcx6) was also present in NIH3T3 samples of the mitoproteome study. None of those proteins was present in the KO cell lines.

	Cell line	Antibody	Peptides	Coverage	Peptides spectra
Alex3	MEF WT	C-19	13	41%	**1-** YNDWSDDDDDSNESKSIVWYPPWAR **2-** RASPNSDDTVLSPQELQK
	MEF WT	E-17	7	24%	**3-** DLGGLPIVAKILNTRDPIVK **4-** ALIVLNNLSVNAENQR
	NIH 3T3	E-17	2	7,9%	**5-**LNSSVQLAGLRLLTNMTVTNEYQHILAN SISDFFRLFSAGNEETKLQVLKLLLNLAENPAMTR **6-** AQVPSSLGSLFNKK
Armc10	MEF WT	C-19	7	33%	**1-**SAEDLTDGSYDDILNAEQLKKLLYLLESTDDPVITEK ALVTLGNNAAFSTNQAIIRELGGIPIVGNKINSLNQSIK **2-** ALNALNNLSVNVENQTK **3-** ANEILLRALTLFQNINNCLK **4-** LANQIPFAK
	MEF KO+ Gq	C-19	1	3,6%	
	MEF WT	E-17	6	28%	
	MEF KO+ Gq	E-17	2	5,9%	
ARVCF	MEF WT	E-17	2	3,1%	**1-** GLPLLVALLDHPR
	MEF WT	C-19	2	3,1%	**2-** ELVTGTLWNLSSYEPLK
Alex6	NIH3T3	E-17	3	10%	**1-** EAVEQFESQGVDLSNIVK **2-** AGGTESIVAAmTR **3-** VIIEGGGALAALQAMK

Table D 1 Summary of the armadillo domain-containing proteins identified in our mitoprorteome study as binding partners of $G\alpha_q$

An interesting protein partner of Gα subunits that contains armadillo-like domains is Ric8 (Figueroa et al., 2009). The interaction between Ric8 and $G\alpha_q$ is well reported and studied (Tall, 2013). Ric8 is considered an activator of heterotrimeric G-protein signaling (AGS). It binds to $G\alpha_q$, $G\alpha_{i1}$ and $G\alpha_{o1}$ and functions as a GEF to induce a GTP-bound conformation in the Gα either in the absence of GPCR signaling or in the presence of it to serve as signal amplificator. (Tall et al., 2003). It is also well-documented that Ric8 interacts (via C-terminus) with RGS14; the interaction stimulates the dissociation of the complex between RGS14 and releases the GTP-bound form of $G\alpha_{i1}$ promoting its activation (Vellano et al., 2011). Moreover, it has also been demonstrated that Ric8 is required to inhibit the degradation of the nascent G protein acting as chaperone (Chan, Thomas, Sprang, & Tall, 2013; Gabay et al., 2011). In *C. Elegans* and *Drosophila*, Ric8 is present in a complex with the G protein. In that case, the $G\alpha_i$ subunit binds to a GDI protein and the Gα-GDI complex is necessary for orienting the mitotic spindle together with other proteins that couple to microtubules (Couwenbergs, Spilker, & Gotta, 2004; Tall & Gilman, 2005). The mechanism is controlled by Ric8 and impeaches in the interactions between the cell membrane

and microtubules, affecting spindle orientation and the generation of pulling force (Hinrichs, Torrejón, Montecino, & Olate, 2012).

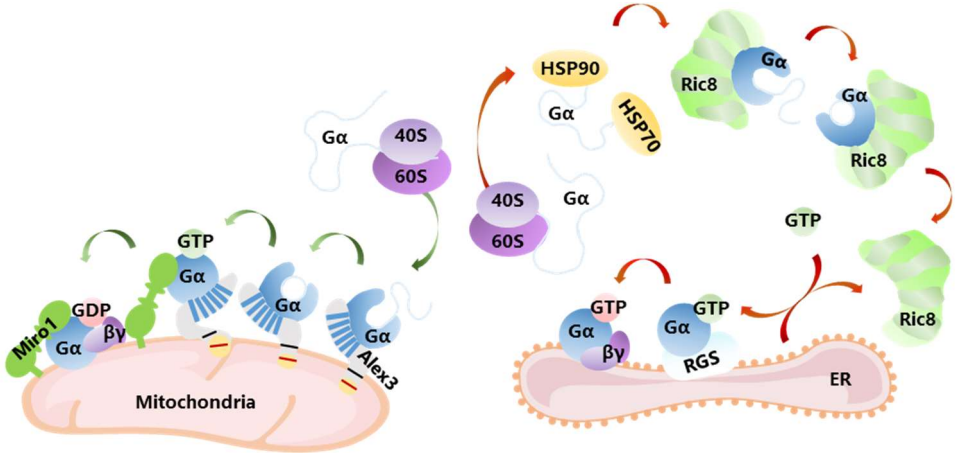

Figure D1. Schematic representation of Ric-8-stimulated Gα nucleotide exchange cycle (ER, right) and analogy with Alex3-Gα_q association at the mitochondrion (mitochondria, left). Like Ric-8, Alex3 would function as a chaperone for Gα_q. Ric-8/Alex3 would bind to a nucleotide-free Gα_q and promote the incorporation of GTP. Sufficient GTP would dissociate the Ric-8/Alex3 from Gα_q-GTP and would either allow its interaction with other mitochondrial partners, including Miro1, to transduce the signal. Association with RGS effectors would promote GTP hydrolysis within the Gα and association with Gβγ. Adapted from Tall 2013.

Taken as a whole, the studies in the bibliography relating G protein signaling and arm-containing proteins besides the previous and current data from our group provide a compelling evidence of a new family of Gα_q-binding proteins with the characteristic to possess armadillo repeats in their structure (Fig D1).

This novel family of proteins could work as non-canonical GEF or as molecular chaperons. Considering this, it is possible that Alex3 also works as a GEF for Gα_q. Our results demonstrate that Alex3 predominantly associates with the Gα_qR183C active mutant, which would argue against of a conserved mechanism for the novel family. Nevertheless, we should be cautious about that since Alex3 shows weak association with the fully active mutant Gα_qQ209L. The only known difference between these two mutants is that the R183C form is still able to bind to RGS and as consequence, it is not considered fully active. Therefore, Alex3 could be acting as a mitochondrial GEF for Gα proteins binding to the GDP form and/or to the R183C mutant. It could also bind to the GTP form bound to RGS (as Ric8), although the presence of RGS proteins in the complex reminds to be analyzed.

Figure D2. Sequence alignment of Alex3 and Ric8A murine sequences performed using ClustalW and BLOSUM62 matrix.

The capacity of $G\alpha_q$ to bind Alex3 not only depends on its nucleotide-bound stage, but also on the conformation of the arm-containing protein due to post-translational modifications. Previous computational studies predicted the presence of phosphorylation sties for many kinases within the arm-like domains of Alex3 (Serrat et al., 2013). Among them, several phosphorylation sites for CKII and PKC leading to different outcomes. Whereas CKII phosphorylation promotes Alex3 degradation at proteasome, phosphorylation by PKC increases its stability and avoids ubiquitination (Serrat et al., 2013). Other phosphorylable residues have been identified in Alex3 through large-scale quantitative phosphoproteomic analysis coupled to mass spectrometry (Lumpkin et al., 2017; Lundby et al., 2012; Wiśniewski, Nagaraj, Zougman, Gnad, & Mann, 2010). Alex3 could thus acquire different conformations leading to increased affinity towards chaperones and other signaling proteins to promote or prevent its degradation at the proteasome. In this regard, it is interesting that GTP-bound $G\alpha_q$ activates downstream PKC, which would presumably lead to phosphorylation of the arm domains similar as proposed for the Wnt pathway (Serrat et al., 2013). On the other hand, $G\alpha_q$ binding along with other molecular interactors could also stabilize the protein to prevent its degradation.

An unexpected finding of $G\alpha_q$ association with Alex3 came from a mutant lacking the most distal 16 residues. Since the mutant lacking a putative target region for post-translational modifications shows better capacity to precipitate $G\alpha_q$, it is tempting to consider that some post-translational modifications within those residues would have a negative impact on $G\alpha_q$ association. According

to a proposed computational model (Serrat et al., 2013), within the missing residues is predicted to locate a PKC phosphorylation site. Signaling from PKC and other kinases could then constitute a mechanism for $G\alpha_q$ to self-regulate its binding and each pathway would be more prevalent depending on the expression levels of PKC isoforms or the phosphatases that release Alex3 from PKC phosphorylation. In the same direction, Alex3 is target of numerous SUMOylations and acetylations that regulate its stability and conformation. Indeed, an acetylation of Lysine 364 (Lundby et al., 2012) is a good example of how different post-translational modifications of the arm-domains can regulate its binding partners, and in our case the interaction with $G\alpha_q$. Overall, those changes in Alex3 phosphorylation could represent a feedback regulation mechanism, important to subsequent transfer of the signal through new protein interactions.

To date, the molecular mechanisms by which Alex3 regulates mitochondrial transport are still elusive and do not allow to distinguish an active or an inactive state of the protein. The only known facts are that it interacts directly with Miro1, as we have proven here, and its expression in cells seems to phenocopy the mitochondrial aggregation induced by Miro1 and TRAK2. The new results provide a novel hypothesis by which the interplay between the G protein and Alex3 regulates the motility of mitochondria through the link between Miro1 proteins and TRAKs.

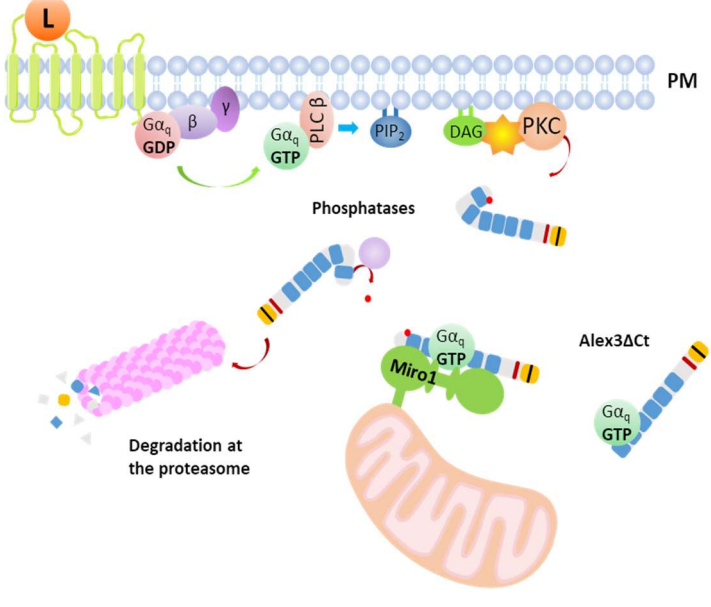

Figure D 3 Schematic representation of PKC regulation of Alex3 through $G\alpha_q$ signaling. Stimulation of $G\alpha_q$-coupled receptors induce PLCβ activation, which leads to IP_3 and DAG production. DAG is a potent activator of several PKC isoforms. PKC, in turn, phosphorylates Alex3 and prevents its degradation at the proteasome. Several phosphatases can revert this process, leading to reduced levels of Alex3 protein. An Alex3 mutant lacking the last 16 C-terminal residues (Alex3ΔCt) shows increased affinity towards $G\alpha_q$. We hypothesize this mutant may acquire a similar conformation as the PKC-phosphorylated Alex, making it more resistant to degradation and with higher capacity to complex Miro1.

1.1. Alex3 is detected as at least 2 independent bands by western blot

Several lines of evidence support that Alex3 appears as at least two independent bands after SDS-PAGE and western blot analysis. Two distinguishable bands usually appear when detecting the exogenous protein using the anti-myc or anti-GFP, but also by using a specific antibody against the endogenous protein previously tested using Alex3 KO mice as a control (Prof. Soriano's laboratory). The molecular significance of each band has never been addressed, but considering that Alex3 protein is translated from a single exon (López-Doménech et al. 2012) the possibility of having different splicing variants can be dismissed. A variety of isoforms, however, can be distinguished within the armc10 gene (Huang et al., 2003) or other proteins with armadillo domains, such as p120ctn (Keirsebilck et al., 1998). In the case of Alex3, a small peptide at the N-terminal or C-terminal region of the protein could be cleaved during a putative posttranslational processing. Each resulting peptide could be directed to a different location or play an independent (but complementary) role, although their relevance remains to be experimentally determined. Immunoprecipitates from mouse brain homogenates showed that the upper molecular weight precipitated more with endogenous $G\alpha_q$ despite appearing in relative lesser amount in total homogenates (**Fig.R2c**). Again, the upper molecular weight band was more prominent in $G\alpha_q$ precipitates from SHSY5Y lysates (**Fig.R2b**). In MEF lysates, $G\alpha_q$ precipitated both bands of Alex3, although again with a slight prevalence of the upper molecular weight band (**Fig.R2a**). Those results contrast with the IPs of endogenous $G\alpha_q$ and exogenous $G\alpha_q$R183C from HEK293 lysates, as $G\alpha_q$ seemed to precipitate the lower molecular weight band instead (**Fig.R3a**). It is possible then that differential signaling and expression of proteins that promote Alex3 post-translational modification between the different cell lines could affect the relative capacity of each form to associate to other partners, such as $G\alpha_q$. However, the same effect could be applied to previously described partners, as showed for myc-Miro1 when immunoprecipitating GFP-Alex3 from HEK293 lysates (**Fig.R7a**). In this particular case, the upper molecular weight band prevails when Alex3 is expressed alone, whereas co-expression of Miro1 balances the intensity of both bands and addition of $G\alpha_q$R183C increases the relative amounts of the lower molecular weight band. Such results are very consistent among the different experiments carried out and also match the western blots shown in the literature (López-Doménech et al. 2012). Whether and how Miro1 or $G\alpha_q$ expression affect Alex3 cleavage pattern is still unknown, but seems an important step to understand the function and physiological relevance of the protein. Further studies will though be needed to fully understand the signals that regulate Alex3 processing and subcellular localization.

1.2. Subcellular localization of Alex3- $G\alpha_q$ complex

Through immunofluorescence techniques in neurons and cell lines, Alex3 was found in three distinguished localizations: the mitochondria, the cytoplasm and the nucleus (López-Doménech et al. 2012). Although the mitochondrial functions have been the focus of most studies, its nuclear function, which is shared with other armadillo-domain proteins, is still elusive. An early report demonstrated that Alex3 localizes into the nucleus and regulates the transcription factor Sox10 (Mou et al., 2009), but so far no mechanistic information has been provided to explain its translocation, nor indeed if the transcriptional regulation is related with its role in mitochondrial transport. In our experiments using MEF cells we could not find clear differences on Alex3 subcellular localization between MEF wt and MEF $G\alpha_{q/11}$ (-/-) (data not shown). Nonetheless, this does not exclude a possible regulation of nuclear localization of Alex3 by $G\alpha_q$ interaction. In fact, it is interesting to notice that Alex3 regulates gene transcription acting as an adaptor for Sox10, which can localize at the mitochondria besides the nucleus (Mou et al., 2009). Sox10 interacts with the proximal ARM-containing region of Alex3, comprising the residues 109-200. Deletion of that sequence impairs Sox10 association, but truncating the C-terminal ARM domains away from amino acid 200 has no significant impact for the binding (Mou et al., 2009). $G\alpha_q$ binds preferentially to the residues 107-273, though it still shows a slight affinity for the N-terminal and the distal C-terminal region of Alex3 sequence. Hence, $G\alpha_q$ might compete with Sox10 for the same Alex3 binding region, thus allowing it to release the nuclei and modifying the transcription pattern. In this regard, high levels of Sox10 were found in all samples of a screening of uveal melanocytes, a tumor commonly caused by activating mutations in the GNAQ/GNA11 genes, suggesting that Sox10 expression and Alex3 nuclear localization could be related with $G\alpha_q$ activity (Mori et al., 2017). Since our mitoproteome analysis was directed towards endomembranes and not nuclei, we did not find evidence of Sox10 co-immunoprecipitating with endogenous $G\alpha_q$, though this does not rule out a possible link between both proteins.

1.3. $G\alpha_q$ regulation of mitochondrial aggregation

Alex3 overexpression results in perinuclear clustering of mitochondria, both in neurons and HEK293 cells (López-Doménech et al. 2012). A similar phenotype (although in a lesser degree) was also reported when altering the levels or functionality of other proteins involved in mitochondrial transport, such as Miro1, TRAK1 and 2 adaptors or kinesin motor proteins. (López-Doménech et al., 2018; Nguyen et al., 2014; Stowers et al., 2002). Here, we used MEF cells as a model to evaluate the effects of Alex3 overexpression in a $G\alpha_{q/11}$-deficient background. Because MEF cells express milder levels of protein when transfected than HEK293, we were able to

determine that Alex3 overexpression further increases perinuclear aggregation of mitochondria in the absence of $G\alpha_q$ and $G\alpha_{11}$, suggesting an inhibitory role of the $G\alpha$ over Alex3 function. This phenotype was also perceptible, though in a lesser extent, when expressing Miro1. We propose that endogenous $G\alpha_q$ would reduce Alex3-mediated perinuclear clustering of mitochondria by direct interaction with its arm-domains and/or linking the protein to other cytoplasmic machinery. The absence of $G\alpha_q$ would then affect Alex3 signaling rather than its stability, since similar levels of Alex3 protein were detected in MEF KO cells by western-blot or immunofluorescence analysis.

Confocal images of Hela and HEK293 cells expressing GFP-Alex3 also revealed that Alex3-induced mitochondrial aggregation was associated with fusion of the outer mitochondrial membrane (OMM) with no perceptible alterations in the mitochondrial matrix. Previous reports proposed that Alex3-induced alterations in mitochondrial distribution were not associated with changes in mitochondrial fusion (López-Doménech et al. 2012). However, such finding was supported by experimental approaches based on photobleaching and recovery of the fluorescence of the matrix-targeted protein mito-PAGFP, which are compatible with the absence of fusion at the inner-membrane observed in cells expressing GFP-Alex3 and do not rule out a possible fusion of the OMM.

Fusion of the OMM is primarily mediated by mitofusins 1 and 2 (Hsiuchen Chen et al., 2003; Filadi et al., 2018; Santel et al., 2003), two multifunctional GTPases whose roles in mitochondrial physiology are no longer considered restricted to fusion. A good example of side-function came from Mfn2 interaction with Miro1. As observed in neurons expressing Alex3-directed siRNAs (López-Doménech et al. 2012), depletion of Mfn2 also results in mitochondrial arrest (Misko et al., 2010). This suggests that Mfn2 could exert a similar regulation of Miro1 function as proposed for Alex3, or even be part of the same molecular complex. Indeed, Mfn2 overexpression increases fusion leading to interconnected mitochondrial networks, but also induces mitochondrial aggregation around the perinuclear area in mouse fibroblasts comparable to the ones induced by Alex3 (Santel & Fuller, 2001). In the same direction, Fis1, another binding partner of $G\alpha_q$ at the mitochondria (proteomic table and unpublished results) was recently proposed to induce mitochondrial fragmentation by interacting with and inhibiting the GTPase activity of both mitofusins and Opa1 (Yu, Jin, Lendahl, Nistér, & Zhao, 2019). With that, it is tempting to consider that both Alex3 and Mfn2 could play complementary roles on mitochondrial dynamics when associated with Miro1 and those complexes could be regulated by $G\alpha_q$. This hypothesis is consistent with our the preliminary results showing that Alex3 expression overcomes mitochondrial fragmentation inducing fusion of the OMM in MEF Mfn2 (-/-) cells and, in a lesser extent, in MEF Mfn1 (-/-).

2. $G\alpha_q$ interacts with Miro1

The experiments presented not only unveiled Alex3 as novel $G\alpha_q$ effector at the mitochondria, but also provided evidence of the association with the mitochondrial RhoGTPase Miro1. Miro1 was originally identified in mammals as an atypical RhoA-like small GTPase (Fransson et al., 2003). Unlike RhoA, it is featured by the presence of two GTPase domains flanking the EF-hand calcium-binding domains at the central region (Devine, Birsa, and Kittler 2016; Hajnóczky et al. 2014; MacAskill et al. 2009). Such domains not only allow Miro1 to function as a key regulator of mitochondrial transport, but also as a sensor to maintain calcium homeostasis (Bagur & Hajnóczky, 2017). Its function is tightly regulated by multiple posttranslational modifications and binding partners (Birsa et al. 2014; Kalinski et al. 2019; Niescier et al. 2018; Ogawa et al. 2014), but its concrete role in mitochondrial transport is still controversial. Initial studies carried out in cortical neurons demonstrated that the absence of Miro1 decreases retrograde transport rather than bidirectional mitochondrial movement (Nguyen et al., 2014). However, an independent study claimed that low levels of Miro1 caused by the ALS-associated mutant SOD G91A specifically decrease anterograde motility (Moller, Bauer, Cohen, Webster, & De Vos, 2017). Such disagreements are likely to be caused by the usage of different experimental models, since the mitochondrial GTPase is able to couple both kinesin and dynein/dynactin motors to drive bidirectional movement (Devine et al., 2016; Las & Shirihai, 2014; Schwarz, 2013).

Many authors have proposed Miro1 as the foremost regulator of mitochondrial motility and the most prevalent linker between mitochondria and kinesin/dynein motors (Ahmad et al. 2014; Birsa et al. 2013; Devine, Birsa, and Kittler 2016; Fransson, Ruusala, and Aspenström 2003; Fransson, Ruusala, and Aspenström 2006; Granatiero et al. 2019; Las and Shirihai 2014; MacAskill et al. 2009). We have demonstrated the direct interaction between Alex3 and Miro1 and also have provided evidence for a direct interaction between $G\alpha_q$ and Miro1, suggesting a putative regulation of mitochondrial transport by $G\alpha_q$ through both proteins.

IP experiments evidence that Miro1 can efficiently precipitate GDP-bound $G\alpha_q$ besides $G\alpha_q$R183C, so we propose that Miro1 could be acting as a GDI for the $G\alpha$ in absence of GTP (Jordens et al., 2001; Ma et al., 2018). In addition to that, a Miro1 with point mutations within its EF hand domains unable to be regulated by calcium (Fransson, Ruusala, and Aspenström 2006) showed stronger affinity towards $G\alpha_q$, indicating that, unlike Alex3, Miro1 could bind $G\alpha_q$ independently from calcium regulation. Miro1 immunoprecipitations only revealed a slight reduction in $G\alpha_q$ precipitation in the presence of high calcium concentrations (2 mM Ca^{2+}), contrary than observed for Alex3 in previous studies (López-Doménech et al. 2012) or our assays with purified components (**Fig.R6d**) or detecting the endogenous protein (**Fig.R10d**). Therefore, $G\alpha_q$ is more likely to bind Miro1 through a mechanism independent of calcium and different from Alex3,

which, together with our assays with purified components, rules out Alex3 as the only possible connection between Miro1 and $G\alpha_q$.

These results were a bit surprising taking into account that $G\alpha_q$ signaling evokes the release of calcium from intracellular stores through IP_3-induced channels. The $G\alpha_q$-Miro1-Alex3 complex at the mitochondria could then play and independent (may be parallel) role than the $G\alpha_q$-canonical pathway at the plasma membrane. The fact that $G\alpha_q$ has higher affinity for the N-terminal peptide that the wild type Miro1 form (as well as for the Miro EE-mutant) suggests a possible mechanism in which Miro1 may exist in two conformations and the presence of calcium would release the constrain. $G\alpha_q$ may be bound to Miro1 and Alex3. $G\alpha_q$ would not be active in its GDP form or else in its active state but bound to an RGS protein. This complex may facilitate mitochondrial dynamics. Then the presence of calcium would release Alex3, $G\alpha_q$ would be activated by Alex3 and then de-activated back to GDP by RGSs and bound at the N-terminal region of Miro1 that will act as GDI. The tandem Miro1-$G\alpha_q$ would then regulate the dynamic state of the mitochondria blocking interaction with TRAK proteins or changing the direction of movement by switching between TRAK adaptors.

To date many proteins have been proposed to link mitochondrial dynamics with specific cellular processes by interacting with and regulating Miro1. For example, PINK1 phosphorylates Miro1 and promotes the recruitment of Parkin to target Miro1 for degradation (Birsa et al., 2014; Lahiri & Klionsky, 2017; Wang et al., 2011). Thus, PINK1 and Parkin couple mitophagy with mitochondrial arrest. A second example comes from DISC1, a protein often mutated in cases of dementia and schizophrenia that couples to Miro1 and TRAK1 adaptor to promote anterograde movement of mitochondria (Ogawa et al. 2014). Third, the N-terminus of MCU (mitochondrial calcium uniporter) binds Miro1 and couples mitochondrial positioning with calcium influx towards the organelle (Niescier et al., 2018). As a fourth example, the armadillo domain-containing protein vimar also associates with Miro to promote mitochondrial fission under high calcium concentrations (Ding et al., 2016). Finally, Mitofusin2 also interacts in a complex with Miro and TRAK proteins and is essential for bidirectional motility (Misko et al., 2010). Considering those data, $G\alpha_q$ could be considered a novel piece of the Miro1-containing macromolecular complexes that drive and control the movement of mitochondria.

3. TRAK adaptors and dendritic regression

The results reported herein demonstrate that $G\alpha_q$ is an essential regulator of mitochondrial dynamics in neurons. $G\alpha_q$ can fine-tune the motility of mitochondria in axons and modulate the balance between fusion and fission. Besides, its activation induces dendritic regression in neurons, as shown by the reduction in dendritic length and the number of branch points in the sholl analysis. Dendritic regression was previously documented in neurons expressing either a

dominant-negative form of TRAK2 or a specific shRNA to knock down the expression of the endogenous protein (Brickley & Stephenson, 2011). Here we provide evidence that active $G\alpha_q$ phenocopies such effects. A comparative study between both TRAK homologues suggested potentially distinct roles in mitochondrial transport since TRAK1 and TRAK2 localize in different neuronal regions (van Spronsen et al., 2013). The study indicated that TRAK2 is more abundant in dendrites whereas TRAK1 concentrates in axons and exerts a stronger impact in the regulation of axonal motility (van Spronsen et al., 2013). Neurons knocked-down for TRAK1 show decreased axonal length and mitochondrial motility, whereas those with low levels of TRAK2 displayed shorter dendrites and reduced motility of dendritic mitochondria (Brickley & Stephenson, 2011; van Spronsen et al., 2013). The observed alterations on dendritic length and mitochondrial motility upon $G\alpha_q$R183C expression could be a result of an increased TRAK2 association, which may promote an uncoupling from mitochondria of the molecular adaptor. The fact that $G\alpha_q$ and $G\alpha_q$R183C interact with both TRAK adaptors (although with higher binding to TRAK2 complexes) also supports this hypothesis. Interestingly, the presence of $G\alpha_q$ increases the capacity of both TRAKs to co-immunoprecipitate kinesin. Images from HeLa and MEF cells expressing $G\alpha_q$ or $G\alpha_q$R183C along with TRAK2 show a trend in the mitochondrial distribution pattern and subcellular localization of the molecular adaptor, which moves towards the cell periphery. Such observations reinforce the notion that $G\alpha_q$-induced morphological alterations are the result of impairing TRAK2 localization at the mitochondria.

Van Spronsen and collaborators proposed that conformational changes in TRAK proteins would modulate their affinities towards kinesin motors, thus affecting their axonal and dendritic localizations (van Spronsen et al., 2013). In the case of TRAK2, a suggested "closed" conformation in which the N-terminal and the C-terminal regions are close to each other would impair it from binding kinesins, whereas an "open" conformation would enhance their association. TRAK2 has 2 coiled-coil domains within its sequence that could be used for protein-protein interactions, yet other Gα proteins have been found to interact with similar domains (Masià et al., 2015). As mentioned, increased complex formation between TRAKs and kinesin is observed in the presence of $G\alpha_q$, so in analogy with other coiled-coil containing proteins, $G\alpha_q$ would stabilize the "closed" conformation, in which TRAK2 has lower affinity towards kinesin motors, thus promoting mitochondrial arrest.

A similar example of that regulation takes place with NuMa protein. As mentioned, in *Drosophila* a complex between Gα subunit and a GDI protein (LGN) together with the GEF protein (Ric8) binds NuMa. Like TRAK adaptors, NuMA is a large coiled-coil protein that contains a microtubule-binding domain at its C-terminus, but is unable to bind LGN and microtubules simultaneously (Du & Macara, 2004). It is possible then that a similar regulation for the capacity of TRAK2 to bind

microtubules and Miro1 (through kinesin and dynein adaptors) takes place when Alex3 and active $G\alpha_q$ are present. Whether $G\alpha_q$ binds directly to TRAKs and the existence of a similar regulation mechanism as proposed for NuMa still reminds to be experimentally determined and will require further research.

What is clear is that depletion of $G\alpha_q$ induces an increase in mitochondrial movement towards the soma whereas increasing $G\alpha_q$ levels promotes anterograde transport. Instead, active $G\alpha_q$ induces mitochondrial arrest. On the other hand, active $G\alpha_q$ induces peripheral movement of TRAK2 in HeLa and MEF cells, which could be the result of uncoupling of TRAK2 from mitochondria or a switch from dynein to kinesin. Looking for a link to motor proteins, in the proteomic analysis it was found $G\alpha_q$ association to dynein heavy chain 5 and 17 and to Kif5C, although no further experimental work has been made. This would be compatible with the idea that $G\alpha_q$-TRAK2 association could promote dendritic regression, as shown by the decrease in dendritic length and the reduced branch points in neurons expressing $G\alpha_q$R183C.
However, since TRAK2 expression is lower in axonal compartments, it would be unlikely that $G\alpha_q$ induces mitochondrial arrest by interacting with and regulating only the subcellular localization of TRAK2. A recent study has help to understand these results (Loss & Stephenson, 2017). The authors mentioned that the localization of TRAK proteins depends on the developmental stage of the neurons. The study indicates that in young developing neurons as the ones we used in our experiments (DIV 2 to 5), TRAK1 and TRAK2 would contribute similarly to mitochondrial transport in both axons and dendrites, but as the neuron matures (DIV 14), expression of TRAK2 in axonal compartment would decrease, thus reducing its impact in axonal transport (Loss & Stephenson, 2017). Therefore, it may be possible that the arrest induced by $G\alpha_q$R183C expression is caused by TRAK2 re-localization at points close to the plasma membrane.

It was recently shown that TRAK2 is able to couple mitochondria to kinesin and dynein motors in the absence of Miro1 and Miro2, suggesting the presence of novel adaptors at the mitochondria (López-Doménech et al., 2018). In this direction, mitofusin1 interacts with TRAK2 and has been proposed as alternative mitochondrial receptor. As mentioned, mitofusin1 interacts with and is regulated by $G\beta_2$, and depletion of the Gβ results in mitochondrial fragmentation and, on the contrary, expression of Gβ induces perinuclear aggregation, as does Alex3 (Zhang et al. 2010). Thus, it is possible that $G\alpha_q$ binding to GDI proteins (as could be for instance a role for Miro1) induces dissociation of the Gβγ dimmer. TRAK2 could compete with the Gβ to bind mitofusin1, thus decreasing the fusion rates and leading to fragmented mitochondria and mitochondrial aggregation. On the contrary, $G\alpha_q$ through Miro1 could allow interaction with TRAK1 or TRAK2 and induce movement along the microtubules towards cell periphery. Again, future experiments analyzing the effect of Gβγ expression along with TRAK1 and 2 will help to clarify this hypothesis.

4. Mitochondrial motility in hippocampal neurons

After determining the molecular association of $G\alpha_q$ with Alex3, Miro1 and TRAK proteins through biochemistry studies, the link of $G\alpha_q$ with mitochondrial transport was addressed in mouse neurons. Live cell imaging and tracking of mitochondria was performed in axons of hippocampal neurons, that are known to be a reliable model for this type of studies (Devine, Birsa, and Kittler 2016; Glater et al. 2006; Schwarz 2013; Wang et al. 2011). The experiment set up was done in a way that images of moving mitochondria are captured in an area located approximately from six to ten times the size of the nuclei from the soma (around 90 to 160 µm). In the literature, values reported for the percentage of mobile mitochondria in axons at any given time vary between 10%–50%. Their velocities range from 0.2 to 0.8 µm/s, with some variations depending on the neuronal type (MacAskill & Kittler, 2010; MacAskill, Rinholm, et al., 2009; Miller & Sheetz, 2006). The values reported herein fall within this range, which support the viability of our experiments. Nevertheless, some differences between control conditions of independent experiments were still present. Such differences could be a consequence of variations in sample preparation and image acquisition. For example, variations in neurite size between conditions affected the relative distance of the imaged area to the axonal tips. Additional differences may arise in Alex3 knockout experiments as neurons were transfected at 5 days in vitro instead of 4 to allow genotypic of the embryos before transfection. As reported for TRAK adaptors (Loss & Stephenson, 2017), mature neurons tend to have lower mitochondrial velocities than those embryonic, so differences in the schedule may account for the slower speed observed in the knockout experiments.

Although the number of motile mitochondria and their velocities are often considered the main parameters to represent mitochondrial motility (López-Doménech et al. 2012), we selected the percentage of time in motion as the primary indicator of mitochondrial movement because the former distinguishes mitochondria that move for only a fraction of the observation period from those that move continuously. This parameter was previously described by Wang and collaborators (Wang et al. 2011) and allows a more precise sorting of mitochondrial movement into anterograde and retrograde directions. Data relative to velocities or percentage of moving mitochondria necessarily require sorting each mitochondrion into moving or not moving, and in the case of moving mitochondria, into anterograde- or retrograde-moving mitochondria, according to the direction towards they ran longer distance. Thus, the analysis of the percentage of time in motion prevents the loss of information of those mitochondria that change their directionality or only move for a fraction of time.

4.1. $G\alpha_q$ regulation of mitochondrial motility

Following the methods described before, we found a significant increase in bidirectional mitochondrial speed in neurons knocked-down for $G\alpha_q$ besides a decrease in the number of stops per mitochondrion. Analysis of the percentage of time in motion also revealed that moving mitochondria spent more time moving towards the soma. Such data was quite surprising since just a small set of proteins are known to increase the instantaneous speed (Quintero et al., 2009). However, our data is consistent with a previous report indicating an increase in mitochondrial motility upon depletion of endogenous $G\alpha_{12}$ in fibroblasts (Andreeva, Kutuzov, & Voyno-Yasenetskaya, 2008). Data also revealed that the increase observed by $G\alpha_q$ depletion was dependent on Alex3 expression, indicating that Alex3 must participate in the same pathway of $G\alpha_q$ for the control of mitochondrial motility. Together with Miro1 and TRAK adaptors, $G\alpha_q$ and Alex are both essential to control the anterograde and retrograde movement of mitochondria along the axons and alterations of the novel $G\alpha_q$-Alex3 pathway will result in defective transport of mitochondria.

Increasing the levels of $G\alpha_q$ by the expression of wild-type $G\alpha_q$ leaded to a selective increase in anterograde motility, both in experiments co-expressing $G\alpha_q$ and mtDsRed or using bicistronic vectors to express both proteins. On the contrary, expression of the constitutive-active mutant $G\alpha_q$R183C decreased bidirectional mitochondrial motility and increased the number of stops per mitochondria either in the experiments expressing GFP-containing proteins or co-expressing an untagged protein with the mtDsRed marker using bicistronic vectors. In this case, expression of GTP-bound $G\alpha_q$ mimics somehow the effects of Alex3 expression (López-Doménech et al. 2012). Consistently, activation of endogenous $G\alpha_q$ through stimulation of a synthetic DREADD receptor drastically abrogated the motility of those mitochondria that previously moved, further reinforcing the role of a GTP-bound stage of the $G\alpha_q$ to induce mitochondrial arrest. As a control we utilized the N-terminal region of $G\alpha_q$ that contains the mitochondrial-localization sequence but no other protein binding structures (Benincá et al., 2014). This peptide fully co-localized with the mitochondrial marker, yet it showed no significant impact on the tested motility parameters. Previous reports indicated that $G\alpha_s$ and $G\alpha_i$ could destabilize microtubules by interacting with their plus ends and promoting GTP hydrolysis (Dave, Saengsawang, Yu, Donati, & Rasenick, 2009; Wang, Yan, & Rasenick, 1990). That results in a general arrest of microtubule trafficking and could lead us to think that $G\alpha_q$ may act in a similar manner. However, we did not detect differences in the transport of synaptophysin-containing vesicles in neurons expressing $G\alpha_q$R183C, which are also transported along microtubule tracks; we neither detected substantial alterations in the microtubule network in neurons inmmunolabeled with MAP2 or Tuj1 antibodies, a commonly used markers for dendritic and axonal microtubules, respectively. Thus, we can infer that $G\alpha_q$

alterations in microtubule transport are specific for mitochondria. Active $G\alpha_q$ would then arrest mitochondrial transport through a dual signaling event, probably involving both PKC stimulation and calcium release from the ER stores and also by direct interaction with Alex3, Miro1 and TRAK2 proteins.

5. Molecular mechanisms to regulate mitochondrial transport

Like other small GTPases such as Rho or Ras, $G\alpha_q$ switches between a GDP-bound inactive and a GTP-bound active conformation. As show in many of the results herein, both conformations show different binding capacities and display distinctive phenotypes regarding mitochondrial aggregation and motility. The wild-type $G\alpha_q$ showed lesser capacity to bind some proteins of the transport machinery, including Alex3 and TRAK2, as reflected in the co-immunoprecipitation experiments. One possible explanation might be that in its GDP-bound state, $G\alpha_q$ is mainly associated with **Gβγ** subunits and the heterotrimeric complex displays lesser capacity to bind mitochondrial effectors. In a hypothetical non-canonical signaling at the mitochondria, only a small part of $G\alpha_q$ would be bound to Miro1 and Alex3. In the case of Miro1, it could be acting as a GDI binding partner for $G\alpha_q$. Our experiments confirmed that Miro1 precipitates the wild-type form of $G\alpha_q$. Analogous to Ric8, which modulates the complex between Gα and GDI-NuMa proteins, we propose that Alex3 can have a similar function with the Miro1-TRAK-$G\alpha_q$ complex. Interestingly, Zhang and coworkers reported the presence of Gβ2 subunit at the outer mitochondrial membrane, where it interacts with mitofusin1 to promote mitochondrial fusion in absence of the Gα subunit (Zhang et al. 2010). This suggests that a mitochondrial-pull of $G\alpha_q$ could be sequestered by **Gβγ** after GTP hydrolysis, thus representing a mechanism to modulate its signal. Predictably, the GDP-bound $G\alpha_q$ would keep associated to Miro1 to promote anterograde movement. Activation of $G\alpha_q$ by Alex3 or release of a putative RGS would disassemble the complex from the motor proteins and in turn impair mitochondrial movement.
On the other hand, stimulation of $G\alpha_q$ signaling through DREADD receptors was sufficient to abrogate mitochondrial motility in a short period, indicating that upstream signaling through $G\alpha_q$ is also able to stop mitochondria. In this case, either the canonical PLC**β**-Ca^{2+} increase or a non-canonical signaling converging at the mitochondria could mediate the effects. Many of the endogenous $G\alpha_q$-associated receptors are predominantly expressed at specific points through the axonal membrane, including the nodes of Ranvier, axonal tips and synaptic buttons. Most $G\alpha_q$-coupled GPCRs including the muscarinic, opioid-like and glutamatergic receptors (Felder, 1995; Jeon, Dean, Scarr, & Gibbons, 2015; Nasrallah et al., 2018; Toll, Bruchas, Caló, Cox, & Zaveri, 2016) can also couple to other G proteins like $G\alpha_i$ or $G\alpha_s$ to trigger different signaling responses (de Oliveira, Ramos, Amaro, Dias, & Vieira, 2019). Thus, the use of genetic-engineered tools like the DREADD receptors allows a more specific assessment of the $G\alpha_q$ signaling than stimulating

endogenous GPCRs. However, receptor overexpression makes it to localize all along the axonal membrane and even scattered through the cytoplasm, making it difficult to discern whether its activation with CNO only stimulates the pull of $G\alpha_q$ that remains located at the plasma membrane or also activates other pulls of the Gα protein, including the mitochondria-localized $G\alpha_q$.

Stimulation of DREADD receptors decreased mitochondrial motility to 7.2% of the basal levels in those mitochondria moving towards the axonal tips, and to 18.9 % in those moving towards the soma, as reflected in the percentage of time in motion (**Fig.R32b**). This reduction was more pronounced than expressing the constitutive-active mutant either using IRES-containing vectors or GFP-tagged chimeras, particularly in those mitochondria moving towards the anterograde direction. Such differences are likely to be caused by a stronger calcium mobilization from intracellular stores after GPCR-stimulation. Calcium-based responses usually appear from seconds to a few minutes after the stimuli; in the experiments expressing the constitutive active mutant, mitochondrial motility was quantified 24 to 48 hours after transfection, so the neuron has enough time to restore cytoplasmic calcium concentrations to levels close to the basal. Even so, we cannot rule out that $G\alpha_q$R183C expression cyclically mobilizes calcium stores through PLCβ activation as long as it is present in the cell.

We propose that $G\alpha_q$ activation would play a dual role by enabling both canonical calcium mobilization and interaction with its mitochondrial binding partners: Alex3, Miro1 and TRAK2. In case both signals come from GPCRs located at the plasma membrane, this dual signaling would promote a stronger mitochondrial arrest than a calcium-based response on its own. However, it is possible that interaction with the mitochondrial binding partners is primarily mediated by the mitochondrial pull of $G\alpha_q$ (Benincá et al., 2014), which implies that the pull of $G\alpha_q$ located at the plasma membrane does not move towards the mitochondria. That means endogenous stimuli would trigger the activation and dissociation of $G\alpha_q$ form mitochondrial Gβγ or Gβγ-like subunits, allowing the Gα to bind and uncouple TRAK2 from the mitochondria and arrest their movement. The possibility of an induced disassemble of the mitochondrial motor complex, comprising Alex3, Miro1 and TRAK2 by GTP-bound $G\alpha_q$ is supported by the increased number of times a mitochondria stops when expressing $G\alpha_q$R183C with either GFP chimeras or bicistronic vectors. Besides, it is supported by images showing that TRAK2 localizes with $G\alpha_q$R183C on cell edges when both proteins are expressed on HeLa or MEF cells. A possible molecular mechanism to abrogate motility could be a disruption of Alex3-TRAK2 interaction upon binding of active $G\alpha_q$ based on a competitive mechanism, or even a delocalization of TRAK2 adaptor at distal points of the cell, thus impairing the binding of Miro1 and Alex3 to microtubule-based motors.

As shown in HA-TRAK2 immunoprecipitation experiments (**Fig.R38a**), TRAK2 binding to endogenous Alex3 decreases upon $G\alpha_q$ expression and it becomes undetectable when expressing its active form. Concomitantly, TRAK2 increases its binding to endogenous KIF5c,

indicating a possible association with the anterograde-directed motor presumably in the absence of mitochondria, where Alex3 localizes.

In the same direction, depletion of $G\alpha_q$ using short-hairpin RNAs could facilitate the complex formation or release Alex3 from a putative inhibition, thus decreasing the number of times mitochondria stops and increasing thereby mitochondrial motility and speed.

The fact that $G\alpha_q$ may inhibit Alex3 is supported by the increased mitochondrial aggregation that occurs in $G\alpha_{q/11}$ (-/-) MEF cells overexpressing the armadillo-protein, but also by the fact that down-regulating $G\alpha_q$ expression in an Alex3-defitient background cannot revert mitochondrial arrest. In this regard, we can also state that $G\alpha_q$-mediated effects in mitochondrial movement are partially, if not totally, dependent on Alex3 expression. The analysis of the percentage of time in motion unveiled a predominant increase in the retrograde movement rather than the anterograde, even though it increases mitochondrial speed bidirectionally. This leads us to infer an increased tendency towards the formation of a dynein-based complex in the absence of $G\alpha_q$. TRAK2 is precisely the main mediator of retrograde transport rather than TRAK1 (van Spronsen et al., 2013), which indicates a higher efficiency of this adaptor to bind dynein-dynactin complex in the absence of $G\alpha_q$. This is consistent with our immunoprecipitation results showing an increased uncoupling of TRAK2 from kinesin after $G\alpha_q$ binding and supported by our confocal data showing $G\alpha_q$ and TRAK2 at cell edges. Thus, we can hypothesize the absence of $G\alpha_q$ would favor the formation of a dynein/dynactin-TRAK2 complex and the retrograde transport.

5.2. Impact for neuronal physiology

Expression of the GTPase deficient mutant $G\alpha_q$R183C results in neurons having shorter and round-shaped axonal mitochondria, as reflects the reduction in the aspect ratio and form factor. A recent report related GPCR activation and calcium mobilization with mitochondrial fragmentation and swelling, a process called mitochondrial shape transition (MiST) that involves the mitochondrial GTPase Miro1 (Nemani et al., 2018). Thus, the fragmented mitochondria displayed in axons expressing $G\alpha_q$R183C could be a result of calcium mobilization and Miro1 binding. Interestingly, the GTP-bound mutant $G\alpha_q$Q209L, but not other Gα subfamilies, induces Golgi fragmentation in a PKC-dependent manner and modulates vesicle trafficking (Coria, Masseroni, & Díaz Añel, 2014). In this regard, several reports indicate that activation of PKC kinases downstream of $G\alpha_q$ can also cause fragmentation of the mitochondrial network (Baines et al., 2002; Sugawara et al., 2007; Yajima et al., 2011).

Classically, the canonical $G\alpha_q$ signaling induces PLCβ activity, which in turn hydrolyzes PIP_3 into PIP_2 and IP_3. IP_3 acts as a second messenger to open calcium channels mainly located at the ER, which increases cytoplasmic Ca^{2+}. Both PIP_2 and Ca^{2+} activate several PKC isoforms, including the

novel PKCδ and PKCε, both of which localize in endomembranes, including Golgi and mitochondria. PKCε interacts with MAPKs and forms functional signaling modules in cardiac mitochondria that include ERKs, JNKs and p38 MAPK. PKCε activation triggers phosphorylation of MAPKs proteins, which phosphorylate and inactivate Bad, thus inducing cardiac protection (Baines et al., 2002). Curiously, $G\alpha_q$ also mediates p38 MAPK activation at the plasma membrane by interacting with and regulating flotillins, the major protein components of lipid rafts (Sugawara et al., 2007; Yajima et al., 2011). Concomitant to p38 activation, active PKCδ triggers Ser579 phosphorylation of Drp1, which promotes its translocation to the mitochondria and induces mitochondrial fission (Qi, Disatnik, Shen, Sobel, & Mochly-Rosen, 2011). Besides, mitochondrial fragmentation has also been linked with low levels of Miro1 in lung epithelial cells, suggesting that additional signaling at the mitochondria might mediate such fragmentation. Since diverse $G\alpha_q$-downstream pathways can lead to mitochondrial fragmentation, the prevalence of one or another will depend on the relative expression of each effector.

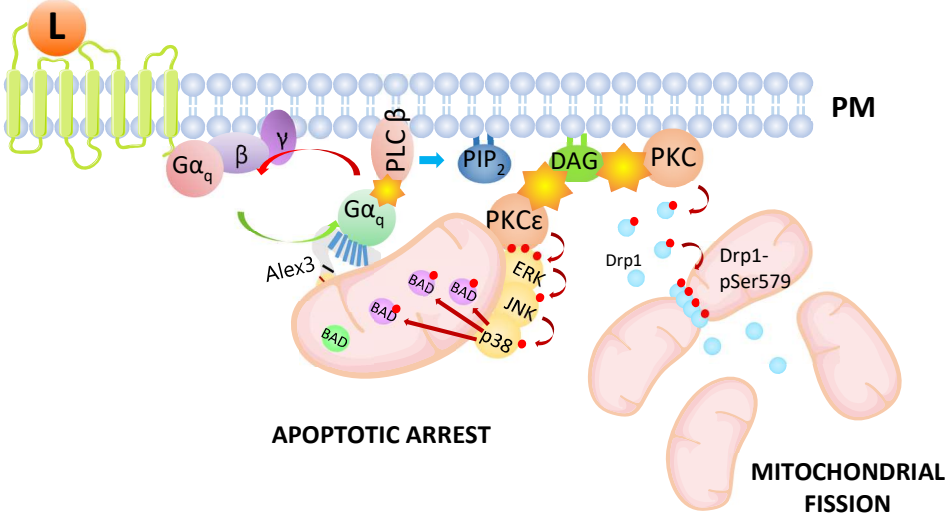

Figure D4 $G\alpha_q$ signaling leads to the activation of PKCδ and PKCε, inducing cardio-protective responses. Stimulation of PKCε induces phosphorylation and activation of ERK kinases, leading to subsequent phosphorylation of JNK and p38, which phosphorylates BAD preventing the apoptotic response. In turn, PKCδ phosphorylates Drp1 at Ser579, enhancing its recruitment at the mitochondria and promoting fission.

6. Through actin cytoskeleton

Despite the classical models point to a microtubule-based mitochondrial motility powered by kinesin and dynein, recent reports indicate that Miro1 also interacts and drives motility through actin filaments by associating with unconventional myosins (López-Doménech et al., 2018). In contrast with microtubule-based transport, in which motor proteins show a constant speed and the overall trafficking depends on the coupling and uncoupling of mitochondria from microtubule tracks, myosins allow fine tune regulation of mitochondrial speed during the runs, as described for Myo19 (Oeding et al., 2018; Quintero et al., 2009). In our studies expressing shRNAs to knockdown the expression of $G\alpha_q$, we not only noticed an increase in the overall mitochondrial speed, but also in the number of times a moving mitochondria reached velocities over 2 µm/sec. Although the overall velocity is directly dependent on the number of times mitochondria release from microtubule adaptors, an increase in the speed during the movement cannot be accounted for by microtubule coupling and requires the involvement of side-mechanisms that modulate motility. In that sense, $G\alpha_q$ signaling could also be regulating the coupling of mitochondria to actin filaments through myosin motors (Moore & Holzbaur, 2018), as was proposed for the transport in dendritic spines and synaptic buttons (Cai & Sheng, 2009). Similarly, the increase in mitochondrial length observed in neurons with low levels of $G\alpha_q$ could be linked with myosin regulation, as knockdown of myosin V has a similar impact on mitochondrial morphology (Pathak et al., 2010).

In this regard, our mass spectrometry analysis identified myosin X as a putative $G\alpha_q$-binding partner at the mitochondria. Myosin X, like Myo19, is an unconventional Myosin initially related with filopodia formation in non-neuronal cells (Li, Lu, & Zhang, 2016). Myo X also plays important roles in the development of dendritic spines and synaptic buttons of hippocampal neurons, where it mediates actin-based transport of vesicles and organelles (Lin, Hurley, Raines, Cheney, & Webb, 2013). However, its implications in mitochondrial transport are still unknown. Immunofluorescence studies using myosin X-specific antibodies detected a punctuated localization of this myosin at specific points of the mitochondria in hippocampal neurons. Nevertheless, those studies are still in a preliminary stage so future experiments will be needed to elucidate whether Myosin X or other unconventional myosins are involved in $G\alpha_q$ regulation of mitochondrial transport.

7. Proposed Model

With the results herein, we propose a model in which GDP-bound $G\alpha_q$ would favor the formation of a kinesin-mediated complex to promote anterograde movement, whereas a GTP-bound $G\alpha_q$ would uncouple mitochondria from microtubule tracks and cease their movement. GDP-bound

$G\alpha_q$ would allow the association of either TRAK1 or TRAK2 to kinesin or dynein motors, as reported for other Gα proteins in GDP form involved in vesicle traffic (Lambert, 2008; Tall, 2013). $G\alpha_q$ activation would mainly occur at places with high signaling activity and/or where calcium levels would increase. Those sites include Ranvier nodes, growing cones and synaptic buttons, and mitochondrial arrest would allow a better energy supply where energy demands are high. Since a pull of $G\alpha_q$ protein is located at the mitochondria (Benincá et al., 2014; Sánchez-Fernández et al., 2014), a local activation of $G\alpha_q$ in a GPCR-independent mechanism at the OMM would also be possible. For example, through arm-containing proteins with similar function than Ric8 towards $G\alpha_q$, as could be the case for Alex3. At that stage, the $G\alpha_q$ subunit may be bound to Miro1 in a GDP form and Alex3 could partially activate the $G\alpha_q$. High levels of calcium would disrupt Alex3-Miro1 association, which would release $G\alpha_q$ from Alex3 after activation. A pull of GTP-bound $G\alpha_q$ would then associate to TRAK2 and lead the adaptor towards the cell periphery, thus reducing the association of Miro1 to dynein/kinesin motors. Dissociation of TRAK2 from the mitochondria would then stop their motility. GTP hydrolysis would return $G\alpha_q$ to its basal stage, allowing TRAK2 to cycle back to the mitochondria and associate with Miro1. Alex3 could function as an adaptor to assemble TRAK2 and Miro1 at the motor complex.

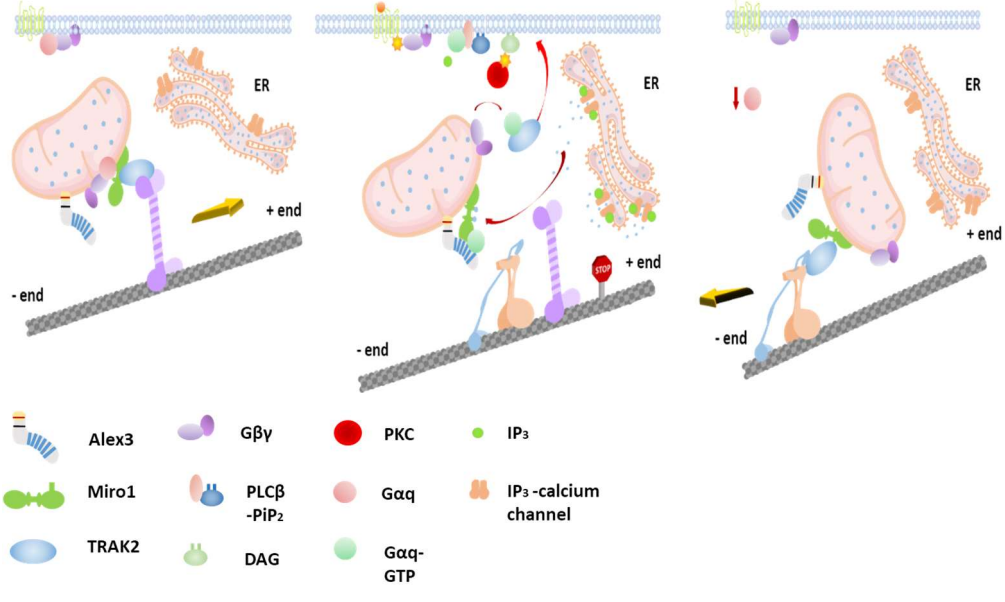

Figure D 3 Proposed model of $G\alpha_q$-mediated regulation of mitochondrial transport. Representation of the suggested mechanisms mediated by $G\alpha_q$ to allow or arrest mitochondrial motility. In the absence of stimuli, the mitochondrial pull of $G\alpha_q$ would remain associated with Gβγ at the outer mitochondrial membrane. This pull could be activated by endogenous stimuli and interact with Miro1. Miro1 would bind Alex3 to couple TRAK2 and promote anterograde movement (first picture). $G\alpha_q$ activation at the level of GPCRs at the plasma membrane would activate PLCβ and trigger calcium movilization. Concomitantly, the mitochondrial pull of $G\alpha_q$ would promote the disociation of TRAK2 from the mitochondria and relocate the adaptor to the cell peryphery, thus arresting mitochondrial movement (second picture). In the absence of $G\alpha_q$, TRAK adaptors would better couple its microtubule-motor proteins, enhancing mitochondrial motility and speed (third picture).

8. Relevance of $G\alpha_{q/11}$: a link with its mitochondrial localization

A variety of data support that $G\alpha_q$ is key for the maintenance of neuronal physiology and the proper development of neuronal and glial progenitors. Studies using $G\alpha_q$-deficient mice demonstrated the implication of the G protein in the regression of climbing fibers of cerebellar Purkinje cells during development (Offermanns et al., 1997). Those deficiencies were previously documented in mice depleted from the $G\alpha_q$-associated metabotropic glutamate receptor 1 (mGluR1) and lead to animals showing ataxic gait, loss of balance and motor coordination deficiencies (Kano et al., 1997). Conditional $G\alpha_{q/11}$ null mice in heart fail to reach cardiac hypertrophy, display craniofacial abnormalities and dye at mid-gestational stage due to inability to keep the blood pressure (Offermanns et al., 1998). Although cardiac hypertrophy is canonically induced by calcium mobilization though stimulation of $G\alpha_q$-associated GPCRs, such as angiotensin II and endotelin-1 receptors, the implication of alternative pathways involving specific organelles cannot be dismissed. Interestingly, both neurons and cardiac myocytes rely on mitochondria to develop and maintain their physiology more than other cell types. The fact that depletion of $G\alpha_q$ produces alterations in mitochondria morphology and dynamics as well as in mitochondria energy efficiency suggest that some of the effects could be at least partially explained by the lack of $G\alpha_q$ signaling at the mitochondria. However, it is still unknown whether those alterations are caused by the mitochondrial pull of $G\alpha_{q/11}$, the $G\alpha_{q/11}$ localized at the plasma membrane or a combination of both.

Specially exciting is that most of the phenotypic alterations of the conditional $G\alpha_{q/11}$ mice in neuronal and glial cells are partially, if not totally, shared with the conditional Alex3 KO mice in brain (Prof. Soriano's laboratory, unpublished results). Among those dysfunctions stand out the ataxic movement, loss of balance, decreased size, and premature death of the knockout animals.

In sum, in this work we have proposed $G\alpha_q$ as an essential regulator of the mitochondrial transport complex in neurons, able to match synaptic activity with energy supply through its interaction with Alex3, Miro1 and TRAK2 by a mechanism independent of a GPCR. The data obtained combining immunoprecipitation, pull down and live imaging of axonal mitochondria from wild type and Alex3 KO embryos provide a compelling evidence of a common signaling involving Alex3 and $G\alpha_q$ at the mitochondria. In-depth study of the molecular mechanisms of this novel pathway will be key in the future to better understand the basis of the neurological diseases in which they may be involved. Further work will help to elucidate the molecular interplay between $G\alpha_q$, mitochondrial receptors, motor proteins and adaptors in mitochondrial transport and advance our understanding of neurodegenerative disorders, including Alzheimer and Parkinson's disease.

CONCLUSIONS

1. A mass spectrometry analysis based on immunoprecipitates from endomembrane enriched cell lysates identified Alex3 as putative binding partner of $G\alpha_q$ at the mitochondria
2. $G\alpha_q$ interacts directly with the proximal arm-containing region of Alex3; it shows higher binding capacity in its GTP-bound conformation, and its binding is likely to stabilize the formation of a Miro1-Alex3 complex.
3. $G\alpha_q$ binds directly to Miro1 and unlike Alex3, it interacts in the presence of high calcium concentrations.
4. $G\alpha_q$ interaction with Miro1 is enhanced upon depletion of the C-terminal GTPase or disruption of the calcium-binding domains.
5. Alex3-induced mitochondrial aggregation leads to fusionated outer mitochondrial membrane without appreciable alterations in the mitochondrial matrix in the absence of Mfn1 and Mfn2.
6. Alex3 ability to induce perinuclear clustering of mitochondria is enhanced in the absence of $G\alpha_q$.
7. Low levels of $G\alpha_q$ increase mitochondrial motility and speed and promote the retrograde transport.
8. $G\alpha_q$ overexpression increases mitochondrial transport towards the axonal tips.
9. Expression of the constitutive active mutant $G\alpha_q$R183C or activation of $G\alpha_q$ signal using DREADD specific receptors decreases mitochondrial motility.
10. $G\alpha_q$ co-immunoprecipitates with TRAK proteins and shows higher binding capacity with TRAK2 in its GTP-bound conformation.
11. $G\alpha_q$ promotes mitochondrial clustering in the perinuclear region when co-expressed with TRAK proteins.
12. $G\alpha_q$R183C increases TRAK2 localization at the cell periphery

REFERENCES

Abu-Helo, Alaa and Frédéric Simonin. 2010. "Identification and Biological Significance of G Protein-Coupled Receptor Associated Sorting Proteins (GASPs)." *Pharmacology & Therapeutics* 126(3):244–50.

Ahmad, Tanveer, Shravani Mukherjee, Bijay Pattnaik, Manish Kumar, Suchita Singh, Manish Kumar, Rakhshinda Rehman, Brijendra K. Tiwari, Kumar A. Jha, Amruta P. Barhanpurkar, Mohan R. Wani, Soumya S. Roy, Ulaganathan Mabalirajan, Balaram Ghosh, and Anurag Agrawal. 2014. "Miro1 Regulates Intercellular Mitochondrial Transport & Enhances Mesenchymal Stem Cell Rescue Efficacy." *The EMBO Journal* 33(9):994–1010.

Ahmad, Tanveer, Shravani Mukherjee, Bijay Pattnaik, Manish Kumar, Suchita Singh, Rakhshinda Rehman, Brijendra K. Tiwari, Kumar A. Jha, Amruta P. Barhanpurkar, Mohan R. Wani, Soumya S. Roy, Ulaganathan Mabalirajan, Balaram Ghosh, and Anurag Agrawal. 2014. "Miro1 Regulates Intercellular Mitochondrial Transport & Enhances Mesenchymal Stem Cell Rescue Efficacy." *EMBO Journal* 33(9):994–1010.

Aizawa, Hiroyuki, Yasuhiko Sekine, Reiko Takemura, Zhao Zhang, M.asaomi Nangaku, and Nobutaka Hirokawa. 1992. "Kinesin Family in Murine Central Nervous System." *The Journal of Cell Biology* 119(5):1287–96.

Alexander, Christiane, Marcela Votruba, Ulrike E. A. Pesch, Dawn L. Thiselton, Simone Mayer, Anthony Moore, Miguel Rodriguez, Ulrich Kellner, Beate Leo-Kottler, Georg Auburger, Shomi S. Bhattacharya, and Bernd Wissinger. 2000. "OPA1, Encoding a Dynamin-Related GTPase, Is Mutated in Autosomal Dominant Optic Atrophy Linked to Chromosome 3q28." *Nature Genetics* 26(2):211–15.

Alexander, Steve PH, Alistair Mathie, and John A. Peters. 2011. "G Protein-Coupled Receptors" *British Journal of Pharmacology* 164(supplement s1):S5–113.

Amiri, Mandana and Peter J. Hollenbeck. 2008. "Mitochondrial Biogenesis in the Axons of Vertebrate Peripheral Neurons." *Developmental Neurobiology* 68(11):1348–61.

Andreeva, Alexandra V., Mikhail A. Kutuzov, and Tatyana A. Voyno-Yasenetskaya. 2008. "Gα12 Is Targeted to the Mitochondria and Affects Mitochondrial Morphology and Motility." *The FASEB Journal* 22(8):2821–31.

Andrus, Paula K., Timothy J. Fleck, Mark E. Gurney, and Edward D. Hall. 1998. "Protein Oxidative Damage in a Transgenic Mouse Model of Familial Amyotrophic Lateral Sclerosis." *Journal of Neurochemistry* 71(5):2041–48.

Añel, Alberto Marcelo Díaz and Vivek Malhotra. 2005. "PKCη Is Required for β1γ2/β3γ2- and PKD-Mediated Transport to the Cell Surface and the Organization of the Golgi Apparatus." *The Journal of Cell Biology* 169(1):83.

Angers, Stephane, Ali Salahpour, and Michel Bouvier. 2002. " Dimerization : An Emerging Concept for G Protein–Coupled Receptor Ontogeny and Function ." *Annual Review of Pharmacology and Toxicology* 42(1):409–35.

Ardawatia, Vandana V., Miriam Masià-Balagué, Beate F. Krakstad, Bente B. Johansson, Kelly M. Kreitzburg, Endy Spriet, Aurélia E. Lewis, Thomas E. Meigs, and Anna M. Aragay. 2011. "Gα12 Binds to the N-Terminal Regulatory Domain of P120ctn, and Downregulates P120ctn Tyrosine Phosphorylation Induced by Src Family Kinases via a RhoA Independent Mechanism." *Experimental Cell Research* 317(3):293–306.

Armbruster, Blaine N., Xiang Li, Mark H. Pausch, Stefan Herlitze, and Bryan L. Roth. 2007. "Evolving the Lock to Fit the Key to Create a Family of G Protein-Coupled Receptors Potently Activated by an Inert Ligand." *Proceedings of the National Academy of Sciences of the United States of America* 104(12):5163–68.

Auer, Thomas O., Tong Xiao, Valerie Bercier, Christoph Gebhardt, Karine Duroure, Jean-Paul Concordet, Claire Wyart, Maximiliano Suster, Koichi Kawakami, Joachim Wittbrodt, Herwig Baier, and Filippo Del Bene. 2015. "Deletion of a Kinesin I Motor Unmasks a Mechanism of Homeostatic Branching Control by Neurotrophin-3." *ELife* 4.

Avisar, Dror, Mohamad Abu-Abied, Eduard Belausov, Einat Sadot, Chris Hawes, and Imogen A. Sparkes. 2009. "A Comparative Study of the Involvement of 17 Arabidopsis Myosin Family Members on the Motility of Golgi and Other Organelles." *Plant Physiology* 150(2):700–709.

Avisar, Dror, Alexey I. Prokhnevsky, Kira S. Makarova, Eugene V Koonin, and Valerian V Dolja. 2008. "Myosin XI-K Is Required for Rapid Trafficking of Golgi Stacks, Peroxisomes, and Mitochondria in Leaf Cells of Nicotiana Benthamiana." *Plant Physiology* 146(3):1098–1108.

Babenko, Valentina A., Denis N. Silachev, Vasily A. Popkov, Ljubava D. Zorova, Irina B. Pevzner, Egor Y. Plotnikov, Gennady T. Sukhikh, and Dmitry B. Zorov. 2018. "Miro1 Enhances Mitochondria Transfer from Multipotent Mesenchymal Stem Cells (MMSC) to Neural Cells and Improves the Efficacy of Cell Recovery." *Molecules (Basel, Switzerland)* 23(3).

Babic, Milos, Gary J. Russo, Andrea J. Wellington, Ryan M. Sangston, Migdalia Gonzalez, and Konrad E. Zinsmaier. 2015. "Miro's N-Terminal GTPase Domain Is Required for Transport of Mitochondria into Axons and Dendrites." *The Journal of Neuroscience : The Official Journal of the Society for Neuroscience*.

Bagur, Rafaela and György Hajnóczky. 2017. "Intracellular Ca^{2+} Sensing: Its Role in Calcium Homeostasis and Signaling." *Molecular Cell* 66(6):780–88.

Baines, Christopher P., Jun Zhang, Guang-Wu Wang, Yu-Ting Zheng, Joanne X. Xiu, Ernest M. Cardwell, Roberto Bolli, and Peipei Ping. 2002. "Mitochondrial PKC and MAPK Form Signaling Modules in the Murine Heart Enhanced Mitochondrial PKC-MAPK Interactions and Differential MAPK Activation in PKC-Induced Cardioprotection."

Bajetto, Adriana, Rudy Bonavia, Simone Barbero, Tullio Florio, and Gennaro Schettini. 2001. "Chemokines and Their Receptors in the Central Nervous System." *Frontiers in Neuroendocrinology* 22(3):147–84.

Baloh, Robert H. 2008. "Mitochondrial Dynamics and Peripheral Neuropathy." *The Neuroscientist* 14(1):12–18.

Behl, Christian. 1999. "Alzheimer's Disease and Oxidative Stress: Implications for Novel Therapeutic Approaches." *Prog Neurobiol*. 301-23.

Benincá, Cristiane, Jesús Planagumà, Adriana de Freitas Shuck, Rebeca Acín-Perez, Juan Pablo Muñoz, Marina Mateus de Almeida, Joan H. Brown, Anne N. Murphy, Antonio Zorzano, Jose Antonio Enríquez, and Anna M. Aragay. 2014. "A New Non-Canonical Pathway of Gαq Protein Regulating Mitochondrial Dynamics and Bioenergetics." *Cellular Signalling* 26(5):1135–46.

Berman, David M., Thomas M. Wilkie, and Alfred G. Gilman. 1996. "GAIP and RGS4 Are GTPase-Activating Proteins for the Gi Subfamily of G Protein α Subunits." *Cell* 86(3):445–52.

Bhatnagar, Anushree, Douglas J. Sheffler, Wesley K. Kroeze, BethAnn Compton-Toth, and Bryan L. Roth. 2004. "Caveolin-1 Interacts with 5-HT2A Serotonin Receptors and Profoundly Modulates the Signaling of Selected Galphaq-Coupled Protein Receptors." *The Journal of Biological Chemistry* 279(33):34614–23.

Biliński, Tomasz, Jadwiga Litwińska, Mieczysław Błaszczyński, and Andrzej Bajus. 1989. "Superoxide Dismutase Deficiency and the Toxicity of the Products of Autooxidation of Polyunsaturated Fatty Acids in Yeast." *Biochimica et Biophysica Acta* 1001(1):102–6.

Binley, Kate E., Wai S. Ng, James R. Tribble, Bing Song, and James E. Morgan. 2014. "Sholl Analysis: A Quantitative Comparison of Semi-Automated Methods." *Journal of Neuroscience Methods* 225:65–70.

Bird, Thomas D. 1993. *Charcot-Marie-Tooth (CMT) Hereditary Neuropathy Overview*. University of Washington, Seattle.

Birsa, Nicol, Rosalind Norkett, Nathalie Higgs, Guillermo Lopez-Domenech, and Josef T. Kittler. 2013. "Mitochondrial Trafficking in Neurons and the Role of the Miro Family of GTPase Proteins." *Biochemical Society Transactions* 41(6):1525–31.

Birsa, Nicol, Rosalind Norkett, Tobias Wauer, Tycho E. T. Mevissen, Hsiu-Chuan Wu, Thomas Foltynie, Kailash Bhatia, Warren D. Hirst, David Komander, Helene Plun-Favreau, and Josef T. Kittler. 2014. "Lysine 27 Ubiquitination of the Mitochondrial Transport Protein Miro Is Dependent on Serine 65 of the Parkin Ubiquitin Ligase." *The Journal of Biological Chemistry* 289(21):14569–82.

Blasius, T. Lynne, Dawen Cai, Gloria T. Jih, Christopher P. Toret, and Kristen J. Verhey. 2007. "Two Binding Partners Cooperate to Activate the Molecular Motor Kinesin-1." *The Journal of Cell Biology* 176(1):11–17.

van der Bliek, Alexander M., Qinfang Shen, and Sumihiro Kawajiri. 2013. "Mechanisms of Mitochondrial Fission and Fusion." *Cold Spring Harbor Perspectives in Biology* 5(6).

Blumer, Joe B., Mary J. Cismowski, Motohiko Sato, and Stephen M. Lanier. 2005. "AGS Proteins: Receptor-Independent Activators of G-Protein Signaling." *Trends in Pharmacological Sciences* 26(9):470–76.

Bockaert, Joël. 2012. "Les Récepteurs Couplés Aux Protéines G." *Médecine/Sciences* 28(12):1133–37.

Boeuf, Julien, José Manuel Trigo, Pierre-Henri Moreau, Lucas Lecourtier, Elise Vogel, Jean-Cristophe Cassel, Chantal Mathis, Paul Klosen, Rafael Maldonado, and Frédéric Simonin. 2009. "Attenuated Behavioural Responses to Acute and Chronic Cocaine in GASP-1-Deficient Mice." *European Journal of Neuroscience* 30(5):860–68.

Boitier, Eric, Ruth Rea, and Michael R. Duchen. 1999. "Mitochondria Exert a Negative Feedback on the Propagation of Intracellular Ca2+ Waves in Rat Cortical Astrocytes." *The Journal of Cell Biology* 145(4):795–808.

Bose, Poulomee, Elsa Tremblay, Claudia Maois, Vijay Narasimhan, Gary A. B. Armstrong, Meijiang Liao, J. Alex Parker, Richard Robitaille, Xiao Yan Wen, Christopher Barden, and Pierre Drapeau. 2019. "The Novel Small Molecule TRVA242 Stabilizes Neuromuscular Junction Defects in Multiple Animal Models of Amyotrophic Lateral Sclerosis." *Neurotherapeutics*. 10.1007[Epub Ahead of print]

Boukelmoune, Nabila, Gabriel S. Chiu, Annemieke Kavelaars, and Cobi J. Heijnen. 2018. "Mitochondrial Transfer from Mesenchymal Stem Cells to Neural Stem Cells Protects against the Neurotoxic Effects of Cisplatin." *Acta Neuropathologica Communications* 6(1):139.

Brandon, Nicholas J. and Akira Sawa. 2011. "Linking Neurodevelopmental and Synaptic Theories of Mental Illness through DISC1." *Nature Reviews Neuroscience* 12(12):707–22.

Brickley, Kieran, Miriam J. Smith, Mike Beck, and F. Anne Stephenson. 2005. "GRIF-1 and OIP106, Members of a Novel Gene Family of Coiled-Coil Domain Proteins: Association in Vivo and in Vitro with Kinesin." *The Journal of Biological Chemistry* 280(15):14723–32.

Brickley, Kieran and F. Anne Stephenson. 2011. "Trafficking Kinesin Protein (TRAK)-Mediated Transport of Mitochondria in Axons of Hippocampal Neurons." *Journal of Biological Chemistry* 286(20):18079–92.

de Brito, Olga Martins and Luca Scorrano. 2008. "Mitofusin 2 Tethers Endoplasmic Reticulum to Mitochondria." *Nature* 456(7222):605–10.

de Brito, Olga Martins and Luca Scorrano. 2009. "Mitofusin-2 Regulates Mitochondrial and Endoplasmic Reticulum Morphology and Tethering: The Role of Ras." *Mitochondrion* 9(3):222–26.

Bruijn, Lucie I., Timothy M. Miller, and Don W. Cleveland. 2004. "Unraveling the mechanisms involved in motor neuron degeneration in ALS." *Annual Review of Neuroscience* 27(1):723–49.

Cabiscol, E., E. Piulats, P. Echave, E. Herrero, and J. Ros. 2000. "Oxidative Stress Promotes Specific Protein Damage in Saccharomyces Cerevisiae." *Journal of Biological Chemistry* 275(35):27393–98.

Cai, Qian, Claudia Gerwin, and Zu-Hang Sheng. 2005. "Syntabulin-Mediated Anterograde Transport of Mitochondria along Neuronal Processes." *The Journal of Cell Biology* 170(6):959–69.

Cai, Qian and Zu-Hang Sheng. 2009. "Mitochondrial Transport and Docking in Axons." *Experimental Neurology* 218(2):257–67.

Calizo, Rhodora Cristina and Suzanne Scarlata. 2012. "A Role for G-Proteins in Directing G-Protein-Coupled Receptor-Caveolae Localization." *Biochemistry* 51(47):9513–23.

Calogero, Alessandra M., Samanta Mazzetti, Gianni Pezzoli, and Graziella Cappelletti. 2019. "Neuronal Microtubules and Proteins Linked to Parkinson's Disease: A Relevant Interaction?" *Biological Chemistry* 0(0).

Campbell, Adrian P. and Alan V Smrcka. 2018. "Targeting G Protein-Coupled Receptor Signalling by Blocking G Proteins." *Nature Reviews. Drug Discovery* 17(11):789–803.

Campbell, Philip D., Kimberle Shen, Matthew R. Sapio, Thomas D. Glenn, William S. Talbot, and Florence L. Marlow. 2014. "Unique Function of Kinesin Kif5A in Localization of Mitochondria in Axons." *The Journal of Neuroscience : The Official Journal of the Society for Neuroscience* 34(44):14717–32.

Cartier, Andréane, Audrey Parent, Pascale Labrecque, Geneviève Laroche, and Jean-Luc Parent. 2011. "WDR36 Acts as a Scaffold Protein Tethering a G-Protein-Coupled Receptor, Gαq and Phospholipase Cβ in a Signalling Complex." *Journal of Cell Science* 124(Pt 19):3292–3304.

Castellanos, Ernesto and Nathan James Lanning. 2019. "Phosphorylation of OXPHOS Machinery Subunits: Functional Implications in Cell Biology and Disease." *The Yale Journal of Biology and Medicine* 92(3):523–31.

Castro, Inês G. and Michael Schrader. 2018. "Miro1 - the Missing Link to Peroxisome Motility." *Communicative & Integrative Biology* 11(4):e1526573.

Cavalli, Valeria, Pekka Kujala, Judith Klumperman, and Lawrence S. B. Goldstein. 2005. "Sunday Driver Links Axonal Transport to Damage Signaling." *The Journal of Cell Biology* 168(5):775–87.

Chan, Puiyee, Celestine J. Thomas, Stephen R. Sprang, and Gregory G. Tall. 2013. "Molecular Chaperoning Function of Ric-8 Is to Fold Nascent Heterotrimeric G Protein α Subunits." *Proceedings of the National Academy of Sciences of the United States of America* 110(10):3794–99.

Chang, Chuang-Rung and Craig Blackstone. 2007. "Cyclic AMP-Dependent Protein Kinase Phosphorylation of Drp1 Regulates Its GTPase Activity and Mitochondrial Morphology." *The Journal of Biological Chemistry* 282(30):21583–87.

Chang, Karen T., Robert F. Niescier, and Kyung-Tai Min. 2011. "Mitochondrial Matrix Ca^{2+} as an Intrinsic Signal Regulating Mitochondrial Motility in Axons." *Proceedings of the National Academy of Sciences of the United States of America* 108(37):15456–61.

Chen, H. and D. C. Chan. 2009. "Mitochondrial Dynamics-Fusion, Fission, Movement, and Mitophagy-in Neurodegenerative Diseases." *Human Molecular Genetics* 18(R2):R169–76.

Chen, Hsiuchen and David C. Chan. 2004. "Mitochondrial Dynamics in Mammals." *Current Topics in Developmental Biology* 59:119–44.

Chen, Hsiuchen, Scott A. Detmer, Andrew J. Ewald, Erik E. Griffin, Scott E. Fraser, and David C. Chan. 2003. "Mitofusins Mfn1 and Mfn2 Coordinately Regulate Mitochondrial Fusion and Are Essential for Embryonic Development." *The Journal of Cell Biology* 160(2):189–200.

Chen, Y. M., C. Gerwin, and Z. H. Sheng. 2009. "Dynein Light Chain LC8 Regulates Syntaphilin-Mediated Mitochondrial Docking in Axons." *Journal of Neuroscience* 29(30):9429–38.

Chen, Yanmin and Zu-Hang Sheng. 2013a. "Kinesin-1-Syntaphilin Coupling Mediates Activity-Dependent Regulation of Axonal Mitochondrial Transport." *The Journal of Cell Biology* 202(2):351–64.

Cherok, Edward, Shan Xu, Sunan Li, Shweta Das, W. Alex Meltzer, Michal Zalzman, Chunxin Wang, and Mariusz Karbowski. 2017. "Novel Regulatory Roles of Mff and Drp1 in E3 Ubiquitin Ligase MARCH5-Dependent Degradation of MiD49 and Mcl1 and Control of Mitochondrial Dynamics." *Molecular Biology of the Cell* 28(3):396–410.

Chi, Zai Long, Fumie Yasumoto, Yuri Sergeev, Masayoshi Minami, Minoru Obazawa, Itaru Kimura, Yuichiro Takada, and Takeshi Iwata. 2010. "Mutant WDR36 Directly Affects Axon Growth of Retinal Ganglion Cells Leading to Progressive Retinal Degeneration in Mice." *Human Molecular Genetics* 19(19):3806–15.

Cho, Joon-Ho, Deepak Kumar Saini, W. K. Ajith Karunarathne, Vani Kalyanaraman, and N. Gautam. 2011. "Alteration of Golgi Structure in Senescent Cells and Its Regulation by a G Protein γ Subunit." *Cellular Signalling* 23(5):785–93.

Cho, Kyoung-in, Yunfei Cai, Haiqing Yi, Andrew Yeh, Azamat Aslanukov, and Paulo A. Ferreira. 2007. "Association of the Kinesin-Binding Domain of RanBP2 to KIF5B and KIF5C Determines Mitochondria Localization and Function." *Traffic* 8(12):1722–35.

Cho, Kyoung-in, Dosuk Yoon, Minzhong Yu, Neal S. Peachey, and Paulo A. Ferreira. 2019. "Microglial Activation in an Amyotrophic Lateral Sclerosis-like Model Caused by Ranbp2 Loss and Nucleocytoplasmic Transport Impairment in Retinal Ganglion Neurons." *Cellular and Molecular Life Sciences* 1–26.

Chubb, Jennifer, Nicholas J. Bradshaw, Dinesh C. Soares, David J. Porteous, and J. Kirsty Millar. 2008. "The DISC Locus in Psychiatric Illness." *Molecular Psychiatry* 13(1):36–64.

Cohen, Mickael M. and David Tareste. 2018. "Recent Insights into the Structure and Function of Mitofusins in Mitochondrial Fusion." *F1000Research* 7.

Coleman, Brantley D., Arthur Marivin, Kshitij Parag-Sharma, Vincent Digiacomo, Seongseop Kim, Judy S. Pepper, Jason Casler, Lien T. Nguyen, Michael R. Koelle, and Mikel Garcia-Marcos. 2016. "Evolutionary Conservation of a GPCR-Independent Mechanism of Trimeric g Protein Activation." *Molecular Biology and Evolution* 33(3):820–37.

Coleman, Brantley, Irini Topalidou, and Michael Ailion. 2018. "Modulation of Gq-Rho Signaling by the ERK MAPK Pathway Controls Locomotion in *Caenorhabditis Elegans*." *Genetics* 209(2):523–35.

Comi, Anne. 2015. "Current Therapeutic Options in Sturge-Weber Syndrome." *Seminars in Pediatric Neurology* 22(4):295–301.

Coria, A. Soledad, M. Luján Masseroni, and Alberto M. Díaz Añel. 2014. "Regulation of PKD1-Mediated Golgi to Cell Surface Trafficking by Gαq Subunits." *Biology of the Cell* 106(1):30–43.

Couwenbergs, Claudia, Annina C. Spilker, and Monica Gotta. 2004. "Control of Embryonic Spindle Positioning and Gα Activity by C. Elegans RIC-8." *Current Biology* 14(20):1871–76.

Cribbs, J. Thomas and Stefan Strack. 2007. "Reversible Phosphorylation of Drp1 by Cyclic AMP-Dependent Protein Kinase and Calcineurin Regulates Mitochondrial Fission and Cell Death." *EMBO Reports* 8(10):939–44.

Danial, Nika N. and Stanley J. Korsmeyer. 2004. "Cell Death: Critical Control Points." *Cell* 116(2):205–19.

Das, Joydeep and Parames C. Sil. 2012. "Taurine Ameliorates Alloxan-Induced Diabetic Renal Injury, Oxidative Stress-Related Signaling Pathways and Apoptosis in Rats." *Amino Acids* 43(4):1509–23.

Dave, Rahul H., Witchuda Saengsawang, Jiang-Zhou Yu, Robert Donati, and Mark M. Rasenick. 2009. "Heterotrimeric G-Proteins Interact Directly with Cytoskeletal Components to Modify Microtubule-Dependent Cellular Processes." *Neuro-Signals* 17(1):100–108.

Deas, Emma, Helene Plun-Favreau, Sonia Gandhi, Howard Desmond, Svend Kjaer, Samantha H. Y. Loh, Alan E. M. Renton, Robert J. Harvey, Alexander J. Whitworth, L. Miguel Martins, Andrey Y. Abramov, and Nicholas W. Wood. 2011. "PINK1 Cleavage at Position A103 by the Mitochondrial Protease PARL." *Human Molecular Genetics* 20(5):867–79.

Delettre, Cécile, Guy Lenaers, Jean-Michel Griffoin, Nadine Gigarel, Corinne Lorenzo, Pascale Belenguer, Laetitia Pelloquin, Josiane Grosgeorge, Claude Turc-Carel, Eric Perret, Catherine Astarie-Dequeker, Laetitia Lasquellec, Bernard Arnaud, Bernard Ducommun, Josseline Kaplan, and Christian P. Hamel. 2000. "Nuclear Gene OPA1, Encoding a Mitochondrial Dynamin-Related Protein, Is Mutated in Dominant Optic Atrophy." *Nature Genetics* 26(2):207–10.

Delphin, Christian, Tinglu Guan, Frauke Melchior, and Larry Gerace. 1997. "RanGTP Targets P97 to RanBP2, a Filamentous Protein Localized at the Cytoplasmic Periphery of the Nuclear Pore Complex." *Molecular Biology of the Cell* 8(12):2379–90.

Devine, Michael J., Nicol Birsa, and Josef T. Kittler. 2016. "Miro Sculpts Mitochondrial Dynamics in Neuronal Health and Disease." *Neurobiology of Disease* 90:27–34.

Ding, Lianggong, Ye Lei, Yanping Han, Yuhong Li, Xunming Ji, and Lei Liu. 2016. "Vimar Is a Novel Regulator of Mitochondrial Fission through Miro." *PLoS Genetics* 12(10):e1006359.

Drerup, Catherine M., Amy L. Herbert, Kelly R. Monk, and Alex V Nechiporuk. 2017. "Regulation of Mitochondria-Dynactin Interaction and Mitochondrial Retrograde Transport in Axons." *ELife* 6.

Du, Jiang, Xiupeng Zhang, Haijing Zhou, Yuan Miao, Yong Han, Qiang Han, and Enhua Wang. 2017. "Alex3 Suppresses Non–Small Cell Lung Cancer Invasion via AKT/Slug/E-Cadherin Pathway." *Tumor Biology* 39(7):101042831770144.

Du, Quansheng and Ian G. Macara. 2004. "Mammalian Pins Is a Conformational Switch That Links NuMA to Heterotrimeric G Proteins." *Cell* 119(4):503–16.

Duchen, Michael R. 2004. "Mitochondria in Health and Disease: Perspectives on a New Mitochondrial Biology." *Molecular Aspects of Medicine* 25(4):365–451.

Ehses, Sarah, Ines Raschke, Giuseppe Mancuso, Andrea Bernacchia, Stefan Geimer, Daniel Tondera, Jean-Claude Martinou, Benedikt Westermann, Elena I. Rugarli, and Thomas Langer. 2009. "Regulation of OPA1 Processing and Mitochondrial Fusion by M-AAA Protease Isoenzymes and OMA1." *The Journal of Cell Biology* 187(7):1023–36.

Eisen, Andrew and Markus Weber. 2001. "The Motor Cortex and Amyotrophic Lateral Sclerosis." *Muscle & Nerve* 24(4):564–73.

Emery, Alan E. and Susan M. Holloway. 1982. "Familial Motor Neuron Diseases." *Advances in Neurology* 36:139–47.

Esser, Karlheinz, Baris Tursun, Martin Ingenhoven, Georg Michaelis, and Elke Pratje. 2002. "A Novel Two-Step Mechanism for Removal of a Mitochondrial Signal Sequence Involves the MAAA Complex and the Putative Rhomboid Protease Pcp1." *Journal of Molecular Biology* 323(5):835–43.

Fang, Yanshan, Lorena Soares, Xiuyin Teng, Melissa Geary, and Nancy M. Bonini. 2012. "A Novel Drosophila Model of Nerve Injury Reveals an Essential Role of Nmnat in Maintaining Axonal Integrity." *Current Biology* 22(7):590–95.

Felder, Christian C. 1995. "Muscarinic Acetylcholine Receptors: Signal Transduction through Multiple Effectors." *FASEB Journal : Official Publication of the Federation of American Societies for Experimental Biology* 9(8):619–25.

Feng, Xiaodong, Nadia Arang, Damiano Cosimo Rigiracciolo, Joo Sang Lee, Huwate Yeerna, Zhiyong Wang, Simone Lubrano, Ayush Kishore, Jonathan A. Pachter, Gabriele M. König, Marcello Maggiolini, Evi Kostenis, David D. Schlaepfer, Pablo Tamayo, Qianming Chen, Eytan Ruppin, and J. Silvio Gutkind. 2019. "A Platform of Synthetic Lethal Gene Interaction Networks Reveals That the GNAQ Uveal Melanoma Oncogene Controls the Hippo Pathway through FAK." *Cancer Cell* 35(3):457-472.e5.

Feng, Xiaodong, Maria Sol Degese, Ramiro Iglesias-Bartolome, Jose P. Vaque, Alfredo A. Molinolo, Murilo Rodrigues, M. Raza Zaidi, Bruce R. Ksander, Glenn Merlino, Akrit Sodhi, Qianming Chen, and J. Silvio Gutkind. 2014. "Hippo-Independent Activation of YAP by the GNAQ Uveal Melanoma Oncogene through a Trio-Regulated Rho GTPase Signaling Circuitry." *Cancer Cell* 25(6):831–45.

Ferré, Marc, Dominique Bonneau, Dan Milea, Arnaud Chevrollier, Christophe Verny, Hélène Dollfus, Carmen Ayuso, Sabine Defoort, Catherine Vignal, Xavier Zanlonghi, Jean-Francois Charlin, Josseline Kaplan, Sylvie Odent, Christian P. Hamel, Vincent Procaccio, Pascal Reynier, and Patrizia Amati-Bonneau. 2009. "Molecular Screening of 980 Cases of Suspected Hereditary Optic Neuropathy with a Report on 77 Novel *OPA1* Mutations." *Human Mutation* 30(7):E692–705.

Figueroa, Maximiliano, María Victoria Hinrichs, Marta Bunster, Patricia Babbitt, José Martinez-Oyanedel, and Juan Olate. 2009. "Biophysical Studies Support a Predicted Superhelical Structure with Armadillo Repeats for Ric-8." *Protein Science* 18(6):1139–45.

Filadi, Riccardo, Diana Pendin, and Paola Pizzo. 2018. "Mitofusin 2: From Functions to Disease." *Cell Death & Disease* 9(3):330.

Fischer, Lindsey R., Deborah G. Culver, Philip Tennant, Albert A. Davis, Minsheng Wang, Amilcar Castellano-Sanchez, Jaffar Khan, Meraida A. Polak, and Jonathan D. Glass. 2004. "Amyotrophic Lateral Sclerosis Is a Distal Axonopathy: Evidence in Mice and Man." *Experimental Neurology* 185(2):232–40.

Forno, Lysia S. 1996. "Neuropathology of Parkinson's Disease." *Journal of Neuropathology and Experimental Neurology* 55(3):259–72.

Fransson, Åsa, Aino Ruusala, and Pontus Aspenström. 2003. "Atypical Rho GTPases Have Roles in Mitochondrial Homeostasis and Apoptosis." *The Journal of Biological Chemistry* 278(8):6495–6502.

Fransson, Åsa, Aino Ruusala, and Pontus Aspenström. 2006. "The Atypical Rho GTPases Miro-1 and Miro-2 Have Essential Roles in Mitochondrial Trafficking." *Biochemical and Biophysical Research Communications* 344(2):500–510.

Frederick, Rebecca L., J. Michael McCaffery, Kyle W. Cunningham, Koji Okamoto, and Janet M. Shaw. 2004. "Yeast Miro GTPase, Gem1p, Regulates Mitochondrial Morphology via a Novel Pathway." *The Journal of Cell Biology* 167(1):87–98.

Fredriksson, Robert, Malin C. Lagerström, Lars-Gustav Lundin, and Helgi B. Schiöth. 2003. "The G-Protein-Coupled Receptors in the Human Genome Form Five Main Families. Phylogenetic Analysis, Paralogon Groups, and Fingerprints." *Molecular Pharmacology* 63(6):1256–72.

Friedman, Jonathan R, Laura L. Lackner, Matthew West, Jared R. DiBenedetto, Jodi Nunnari, and Gia K. Voeltz. 2011. "ER Tubules Mark Sites of Mitochondrial Division." *Science* 334(6054):358–62.

Fritz, Stefan, Doron Rapaport, Elisabeth Klanner, Walter Neupert, Benedikt Westerman. 2001. "Connection of the Mitochondrial Outer and Inner Membranes by Fzo1 Is Critical for Organellar Fusion." *The Journal of Cell Biology* 152(4):683–92.

Gabay, Meital, Mary E. Pinter, Forrest A. Wright, Pui Yee Chan, Andrew J. Murphy, David M. Valenzuela, George D. Yancopoulos, and Gregory G. Tall. 2011. "Ric-8 Proteins Are Molecular Chaperones That Direct Nascent G Protein α Subunit Membrane Association." *Science Signaling* 4(200).

Gahbauer, Stefan and Rainer A. Böckmann. 2016. "Membrane-Mediated Oligomerization of G Protein Coupled Receptors and Its Implications for GPCR Function." *Frontiers in Physiology* 7(OCT).

Gama, José B., Cláudia Pereira, Patrícia A. Simões, Ricardo Celestino, Rita M. Reis, Daniel J. Barbosa, Helena R. Pires, Cátia Carvalho, João Amorim, Ana X. Carvalho, Dhanya K. Cheerambathur, and Reto Gassmann. 2017. "Molecular Mechanism of Dynein Recruitment to Kinetochores by the Rod-Zw10-Zwilch Complex and Spindly." *The Journal of Cell Biology* 216(4):943–60.

García-Hoz, Carlota, Guzmán Sánchez-Fernández, Maria Teresa Díaz-Meco, Jorge Moscat, Federico Mayor, and Catalina Ribas. 2010. "G Alpha(q) Acts as an Adaptor Protein in Protein Kinase C Zeta (PKCzeta)-Mediated ERK5 Activation by G Protein-Coupled Receptors (GPCR)." *The Journal of Biological Chemistry* 285(18):13480–89.

García-Regalado, Alejandro, María Luisa Guzmán-Hernández, Iliana Ramírez-Rangel, Evelyn Robles-Molina, Tamas Balla, José Vázquez-Prado, and Guadalupe Reyes-Cruz. 2008. "G Protein-Coupled Receptor-Promoted Trafficking of Gbeta1gamma2 Leads to AKT Activation at Endosomes via a Mechanism Mediated by Gbeta1gamma2-Rab11a Interaction." *Molecular Biology of the Cell* 19(10):4188–4200.

García-Frigola, Cristina, Ferran Burgaya, Marta Calbet, Guillermo López-Domènech, Luis de Lecea, and Eduardo Soriano. 2004. "A Collection of CDNAs Enriched in Upper Cortical Layers of the Embryonic Mouse Brain." *Molecular Brain Research* 122(2):133–50.

Gauthier, Laurent R., Bénédicte C. Charrin, Maria Borrell-Pagès, Jim P. Dompierre, Hélène Rangone, Fabrice P. Cordelières, Jan De Mey, Marcy E. MacDonald, Volkmar Lessmann, Sandrine Humbert, and Frédéric Saudou. 2004. "Huntingtin Controls Neurotrophic Support and Survival of Neurons by Enhancing BDNF Vesicular Transport along Microtubules." *Cell* 118(1):127–38.

Geisler, Sven, Kira M. Holmström, Diana Skujat, Fabienne C. Fiesel, Oliver C. Rothfuss, Philipp J. Kahle, and Wolfdieter Springer. 2010. "PINK1/Parkin-Mediated Mitophagy Is Dependent on VDAC1 and P62/SQSTM1." *Nature Cell Biology* 12(2):119–31.

Gibbons, Ian R. and Arthur J. Rowe. 1965. "Dynein: A Protein with Adenosine Triphosphatase Activity from Cilia." *Science* 149(3682):424–26.

Gindhart, Joseph G., Jinyun Chen, Melissa Faulkner, Rita Gandhi, Karl Doerner, Tiffany Wisniewski, and Aline Nandlestadt. 2003. "The Kinesin-Associated Protein UNC-76 Is Required for Axonal Transport in the *Drosophila* Nervous System." *Molecular Biology of the Cell* 14(8):3356–65.

Glater, Elizabeth E, Laura J. Megeath, R. Steven Stowers, and Thomas L. Schwarz. 2006. "Axonal Transport of Mitochondria Requires Milton to Recruit Kinesin Heavy Chain and Is Light Chain Independent." *The Journal of Cell Biology* 173(4):545–57.

Górska-Andrzejak, J., R. S. Stowers, J. Borycz, R. Kostyleva, T. L. Schwarz, and I. A. Meinertzhagen. 2003. "Mitochondria Are Redistributed in *Drosophila* Photoreceptors Lacking Milton, a Kinesin-Associated Protein." *Journal of Comparative Neurology* 463(4):372–88.

Granatiero, Veronica and Giovanni Manfredi. 2019. "Mitochondrial Transport and Turnover in the Pathogenesis of Amyotrophic Lateral Sclerosis." *Biology* 8(2):36.

Griparic, Lorena, Takayuki Kanazawa, and Alexander M. van der Bliek. 2007. "Regulation of the Mitochondrial Dynamin-like Protein Opa1 by Proteolytic Cleavage." *The Journal of Cell Biology* 178(5):757–64.

Grishin, Anatoly, Hui Li, Edwin S. Levitan, and Elena Zaks-Makhina. 2006. "Identification of Gamma-Aminobutyric Acid Receptor-Interacting Factor 1 (TRAK2) as a Trafficking Factor for the K+ Channel Kir2.1." *The Journal of Biological Chemistry* 281(40):30104–11.

Guillaud, Laurent, Mitsutoshi Setou, and Nobutaka Hirokawa. 2003. "KIF17 Dynamics and Regulation of NR2B Trafficking in Hippocampal Neurons." *The Journal of Neuroscience : The Official Journal of the Society for Neuroscience* 23(1):131–40.

Guo, Chun, Kevin A. Wilkinson, Ashley J. Evans, Philip P. Rubin, and Jeremy M. Henley. 2017. "SENP3-Mediated DeSUMOylation of Drp1 Facilitates Interaction with Mff to Promote Cell Death." *Scientific Reports 2017 7*:43811.

Guo, Xiufang, Greg T. Macleod, Andrea Wellington, Fangle Hu, Sarvari Panchumarthi, Miriam Schoenfield, Leo Marin, Milton P. Charlton, Harold L. Atwood, and Konrad E. Zinsmaier. 2005. "The GTPase DMiro Is Required for Axonal Transport of Mitochondria to Drosophila Synapses." *Neuron* 47(3):379–93.

Guo, Yuanjian, Urszula Golebiewska, and Suzanne Scarlata. 2011. "Modulation of Ca^{2+} Activity in Cardiomyocytes through Caveolae-Gαq Interactions." *Biophysical Journal* 100(7):1599–1607.

Gurevich, Vsevolod V. and Eugenia V. Gurevich. 2019. "GPCR Signaling Regulation: The Role of GRKs and Arrestins." *Frontiers in Pharmacology* 10:125.

Haghnia, Marjan, Valeria Cavalli, Sameer B. Shah, Kristina Schimmelpfeng, Richard Brusch, Ge Yang, Cheryl Herrera, Aaron Pilling, and Lawrence S. B. Goldstein. 2007. "Dynactin Is Required for Coordinated Bidirectional Motility, but Not for Dynein Membrane Attachment" edited by Y. Zheng. *Molecular Biology of the Cell* 18(6):2081–89.

Hajnóczky, György, David Booth, György Csordás, Valentina Debattisti, Tünde Golenár, Shamim Naghdi, Nima Niknejad, Melanie Paillard, Erin L. Seifert, and David Weaver. 2014. "Reliance of ER–Mitochondrial Calcium Signaling on Mitochondrial EF-Hand Ca2+ Binding Proteins: Miros, MICUs, LETM1 and Solute Carriers." *Current Opinion in Cell Biology* 29:133–41.

Hales, Karen G. and Margaret T. Fuller. 1997. "Developmentally Regulated Mitochondrial Fusion Mediated by a Conserved, Novel, Predicted GTPase." *Cell* 90(1):121–29.

Harder, Zdena, Rodolfo Zunino, and Heidi McBride. 2004. "Sumo1 Conjugates Mitochondrial Substrates and Participates in Mitochondrial Fission." *Current Biology : CB* 14(4):340–45.

Hardiman, Orla, Leonard H. van den Berg, and Matthew C. Kiernan. 2011. "Clinical Diagnosis and Management of Amyotrophic Lateral Sclerosis." *Nature Reviews Neurology* 7(11):639–49.

Harwig, Megan C., Matheus P. Viana, John M. Egner, Jason J. Harwig, Michael E. Widlansky, Susanne M. Rafelski, and R. Blake Hill. 2018. "Methods for Imaging Mammalian Mitochondrial Morphology: A Prospective on MitoGraph." *Analytical Biochemistry* 552:81–99.

Hatzfeld, M. 1999. "The Armadillo Family of Structural Proteins." *International Review of Cytology* 186:179–224.

He, Yan, Xiaoqing Yuan, Yan Li, Chunlian Zhong, Yuan Liu, Hongyan Qian, Jingxiu Xuan, Lihua Duan, and Guixiu Shi. 2018. "Loss of Gαq Impairs Regulatory B-Cell Function." *Arthritis Research & Therapy* 20(1):186.

Head, Brian, Lorena Griparic, Mandana Amiri, Shilpa Gandre-Babbe, and Alexander M. van der Bliek. 2009. "Inducible Proteolytic Inactivation of OPA1 Mediated by the OMA1 Protease in Mammalian Cells." *The Journal of Cell Biology* 187(7):959–66.

Hennah, W., Teppo Varilo, Marjo Kestilä, Tiina Paunio, Ritva Arajärvi, Jari Haukka, Alex Parker, Rory Martin, Steve Levitzky, Timo Partonen, Joanne Meyer, Jouko Lönnqvist, Leena Peltonen, and Jesper Ekelund. 2003. "Haplotype Transmission Analysis Provides Evidence of Association for DISC1 to Schizophrenia and Suggests Sex-Dependent Effects." *Human Molecular Genetics* 12(23):3151–59.

Herlan, Mark, Carsten Bornhövd, Kai Hell, Walter Neupert, and Andreas S. Reichert. 2004. "Alternative Topogenesis of Mgm1 and Mitochondrial Morphology Depend on ATP and a Functional Import Motor." *The Journal of Cell Biology* 165(2):167–73.

Herlan, Mark, Frank Vogel, Carsten Bornhovd, Walter Neupert, and Andreas S. Reichert. 2003. "Processing of Mgm1 by the Rhomboid-Type Protease Pcp1 Is Required for Maintenance of Mitochondrial Morphology and of Mitochondrial DNA." *The Journal of Biological Chemistry* 278(30):27781–88.

Hermann, Greg J., John W. Thatcher, John P. Mills, Karen G. Hales, Margaret T. Fuller, Jodi Nunnari, and Janet M. Shaw. 1998. "Mitochondrial Fusion in Yeast Requires the Transmembrane GTPase Fzo1p." *The Journal of Cell Biology* 143(2):359.

Hewavitharana, Thamara and Philip B. Wedegaertner. 2012. "Non-Canonical Signaling and Localizations of Heterotrimeric G Proteins." *Cellular Signalling* 24(1):25–34.

Hinrichs, María Victoria, Marcela Torrejón, Martín Montecino, and Juan Olate. 2012. "Ric-8: Different Cellular Roles for a Heterotrimeric G-Protein GEF." *Journal of Cellular Biochemistry* 113(9):2797–2805.

Hirokawa, Nobutaka, Reiko Sato-Yoshitake, Naoto Kobayashi, K. Kevin Pfister, George S. Bloom, and Scott Brady. 1991. "Kinesin Associates with Anterogradely Transported Membranous Organelles in Vivo." *The Journal of Cell Biology* 114(2):295–302.

Hirokawa, Nobutaka and Reiko Takemura. 2004. "Kinesin Superfamily Proteins and Their Various Functions and Dynamics." *Experimental Cell Research* 301(1):50–59.

Etienne Hirsch. 1993. "Does Oxidative Stress Participate in Nerve Cell Death in Parkinson's Disease?" *European Neurology* 33(1):52–59.

Hollenbeck, Peter J. and William M. Saxton. 2005. "The Axonal Transport of Mitochondria." *Journal of Cell Science* 118(23):5411–19.

Holzbaur, Erika L. F. and Richard Vallee. 1994. "Dyneins: Molecular Structure and Cellular Function." *Annual Review of Cell Biology* 10(1):339–72.

Horn, Sarah R., Michael J. Thomenius, Erika Segear Johnson, Christopher D. Freel, Judy Q. Wu, Jonathan L. Coloff, Chih-Sheng Yang, Wanli Tang, Jie An, Olga R. Ilkayeva, Jeffrey C. Rathmell, Christopher B. Newgard, and Sally Kornbluth. 2011. "Regulation of Mitochondrial Morphology by APC/C Cdh1-Mediated Control of Drp1 Stability." 22.

Hu, Jianxin, Matthew Stern, Luis E. Gimenez, Lizzy Wanka, Lu Zhu, Mario Rossi, Jaroslawna Meister, Asuka Inoue, Annette G. Beck-Sickinger, Vsevolod V Gurevich, and Jürgen Wess. 2016. "A G Protein-Biased Designer G Protein-Coupled Receptor Useful for Studying the Physiological Relevance of Gq/11-Dependent Signaling Pathways." *The Journal of Biological Chemistry* 291(15):7809–20.

Huang, Ruimin, Zhigang Xing, Zhidong Luan, Tangming Wu, Xin Wu, and Gengxi Hu. 2003. "A Specific Splicing Variant of SVH, a Novel Human Armadillo Repeat Protein, Is up-Regulated in Hepatocellular Carcinomas." *Cancer Research* 63(13):3775–82.

Hughes, Thomas E., Hailin Zhang, Diomedes E. Logothetis, and Catherine H. Berlot. 2001. "Visualization of a Functional Gαq-Green Fluorescent Protein Fusion in Living Cells." *Journal of Biological Chemistry* 276(6):4227–35.

Hurd, Daryl D. and William M. Saxton. 1996. "Kinesin Mutations Cause Motor Neuron Disease Phenotypes by Disrupting Fast Axonal Transport in *Drosophila*." *Genetics* 144(3).

Huttlin, Edward L., Lily Ting, Raphael J. Bruckner, Fana Gebreab, Melanie P. Gygi, John Szpyt, Stanley Tam, Gabriela Zarraga, Greg Colby, Kurt Baltier, Rui Dong, Virginia Guarani, Laura Pontano Vaites, Alban Ordureau, Ramin Rad, Brian K. Erickson, Martin Wühr, Joel Chick, Bo Zhai, Deepak Kolippakkam, Julian Mintseris, Robert A. Obar, Tim Harris, Spyros Artavanis-Tsakonas, Mathew E. Sowa, Pietro De Camilli, Joao A. Paulo, J. Wade Harper, and Steven P. Gygi. 2015. "The BioPlex Network: A Systematic Exploration of the Human Interactome." *Cell* 162(2):425–40.

Hwang, Michael J., Kelly G. Bryant, Jae H. Seo, Qin Liu, Peter A. Humphrey, Mary Ann C. Melnick, Dario C. Altieri, and Marie E. Robert. 2019. "Syntaphilin Is a Novel Biphasic Biomarker of Aggressive Prostate Cancer and a Metastasis Predictor." *The American Journal of Pathology* 189(6):1180–89.

Iijima-Ando, Kanae, Michiko Sekiya, Akiko Maruko-Otake, Yosuke Ohtake, Emiko Suzuki, Bingwei Lu, and Koichi M. Iijima. 2012. "Loss of Axonal Mitochondria Promotes Tau-Mediated Neurodegeneration and Alzheimer's Disease–Related Tau Phosphorylation Via PAR-1" edited by M. K. Lee. *PLoS Genetics* 8(8):e1002918.

Irannejad, Roshanak, Jin C. Tomshine, Jon R. Tomshine, Michael Chevalier, Jacob P. Mahoney, Jan Steyaert, Søren G. F. Rasmussen, Roger K. Sunahara, Hana El-Samad, Bo Huang, and Mark von Zastrow. 2013. "Conformational Biosensors Reveal GPCR Signalling from Endosomes." *Nature* 495(7442):534–38.

Irannejad, Roshanak and Philip B. Wedegaertner. 2010. "Regulation of Constitutive Cargo Transport from the Trans-Golgi Network to Plasma Membrane by Golgi-Localized G Protein Betagamma Subunits." *The Journal of Biological Chemistry* 285(42):32393–404.

Iseki, Hiroyoshi, Akihiko Takeda, Toshiwo Andoh, Koki Kuwabara, Norio Takahashi, Igor V. Kurochkin, Hideyuki Ishida, Yasushi Okazaki, and Isamu Koyama. 2012. "ALEX1 Suppresses Colony Formation Ability of Human Colorectal Carcinoma Cell Lines." *Cancer Science* 103(7):1267–71.

Ishihara, Naotada, Yuka Eura, and Katsuyoshi Mihara. 2004. "Mitofusin 1 and 2 Play Distinct Roles in Mitochondrial Fusion Reactions via GTPase Activity." *Journal of Cell Science* 117(Pt 26):6535–46.

Iwata, Keiko and Luca Scorrano. 2019. "Finding a New Balance to Cure Charcot-Marie-Tooth 2A." *The Journal of Clinical Investigation* 129(4):1533–35.

Jaaro-Peled, Hanna, Minae Niwa, Catherine A. Foss, Rina Murai, Samantha de los Reyes, Atsushi Kamiya, Yolanda Mateo, Patricio O'Donnell, Nicola G. Cascella, Toshitaka Nabeshima, Tomás R. Guilarte, Martin G. Pomper, and Akira Sawa. 2013. "Subcortical Dopaminergic Deficits in a DISC1 Mutant Model: A Study in Direct Reference to Human Molecular Brain Imaging." *Human Molecular Genetics* 22(8):1574–80.

James, Rachel, Richard R. Adams, Sheila Christie, Sebastienne R. Buchanan, David J. Porteous, and J. Kirsty Millar. 2004. "Disrupted in Schizophrenia 1 (DISC1) Is a Multicompartmentalized Protein That Predominantly Localizes to Mitochondria." *Molecular and Cellular Neuroscience* 26(1):112–22.

Jamora, Colin, Peter A. Takizawa, Rania F. Zaarour, Caroline Denesvre, D.John Faulkner, and Vivek Malhotra. 1997. "Regulation of Golgi Structure through Heterotrimeric G Proteins." *Cell* 91(5):617–26.

Jamora, Colin, Norma Yamanouye, Johan Van Lint, John Laudenslager, Jackie R. Vandenheede, D. Joh. Faulkner, and Vivek Malhotra. 1999. "Gβγ-Mediated Regulation of Golgi Organization Is through the Direct Activation of Protein Kinase D." *Cell* 98(1):59–68.

Jeon, Won Je, Brian Dean, Elizabeth Scarr, and Andrew Gibbons. 2015. "The Role of Muscarinic Receptors in the Pathophysiology of Mood Disorders: A Potential Novel Treatment?" *Current Neuropharmacology* 13(6):739–49.

Jia, Nannan, Guoping Li, Pu Huang, Jiazhi Guo, Lugang Wei, Di Lu, and Shaochun Chen. 2017. "Protective Role and Related Mechanism of Gnaq in Neural Cells Damaged by Oxidative Stress." *Acta Biochimica et Biophysica Sinica* 49(5):428–34.

Jin, Seok Min, Michael Lazarou, Chunxin Wang, Lesley A. Kane, Derek P. Narendra, and Richard J. Youle. 2010. "Mitochondrial Membrane Potential Regulates PINK1 Import and Proteolytic Destabilization by PARL." *The Journal of Cell Biology* 191(5):933–42.

Johri, Ashu, Abhishek Chandra, and M. Flint Beal. 2013. "PGC-1α, Mitochondrial Dysfunction, and Huntington's Disease." *Free Radical Biology & Medicine* 62:37–46.

Jones, Bryan A. and Walton L. Fangman. 1992. "Mitochondrial DNA Maintenance in Yeast Requires a Protein Containing a Region Related to the GTP-Binding Domain of Dynamin." *Genes & Development* 6(3):380–89.

Jordens, Ingrid, Mar Fernandez-Borja, Marije Marsman, Simone Dusseljee, Lennert Janssen, Jero Calafat, Hans Janssen, Richard Wubbolts, and Jacques Neefjes. 2001. "The Rab7 Effector Protein RILP Controls Lysosomal Transport by Inducing the Recruitment of Dynein-Dynactin Motors." *Current Biology* 11(21):1680–85.

Kalinski, Ashley L., Amar N. Kar, John Craver, Andrew P. Tosolini, James N. Sleigh, Seung Joon Lee, Alicia Hawthorne, Paul Brito-Vargas, Sharmina Miller-Randolph, Ryan Passino, Liang Shi, Victor S. C. Wong, Cristina Picci, Deanna S. Smith, Dianna E. Willis, Leif A. Havton, Giampietro Schiavo, Roman J. Giger, Brett Langley, and Jeffery L. Twiss. 2019. "Deacetylation of Miro1 by HDAC6 Blocks Mitochondrial Transport and Mediates Axon Growth Inhibition." *The Journal of Cell Biology* 218(6):1871–90.

Kamal, Adeela, Gorazd B. Stokin, Zhaohaui Yang, Chun-Hong Xia, and Lawrence S. .. Goldstein. 2000. "Axonal Transport of Amyloid Precursor Protein Is Mediated by Direct Binding to the Kinesin Light Chain Subunit of Kinesin-I." *Neuron* 28(2):449–59.

Kanai, Yoshimitsu, Naoshi Dohmae, and Nobutaka Hirokawa. 2004. "Kinesin Transports RNA: Isolation and Characterization of an RNA-Transporting Granule." *Neuron* 43(4):513–25.

Kane, Lesley A. and Richard J. Youle. 2011. "PINK1 and Parkin Flag Miro to Direct Mitochondrial Traffic." *Cell* 147(4):721–23.

Kang, Eunchai, Katherine E. Burdick, Ju Young Kim, Xin Duan, Junjie U. Guo, Kurt A. Sailor, Dhong-Eun Jung, Sundar Ganesan, Sungkyung Choi, Dennis Pradhan, Bai Lu, Dimitrios Avramopoulos, Kimberly Christian, Anil K. Malhotra, Hongjun Song, and Guo-li Ming. 2011. "Interaction between FEZ1 and DISC1 in Regulation of Neuronal Development and Risk for Schizophrenia." *Neuron* 72(4):559–71.

Kang, Jian-Sheng, Jin-Hua Tian, Ping-Yue Pan, Philip Zald, Cuiling Li, Chuxia Deng, and Zu-Hang Sheng. 2008. "Docking of Axonal Mitochondria by Syntaphilin Controls Their Mobility and Affects Short-Term Facilitation." *Cell* 132(1):137–48.

Kano, Masanobu, Kouichi Hashimoto, Hideo Kurihara, Masahiko Watanabe, Yoshiro Inoue, Atsu Aiba, and Susumu Tonegawa. 1997. "Persistent Multiple Climbing Fiber Innervation of Cerebellar Purkinje Cells in Mice Lacking MGluR1." *Neuron* 18(1):71–79.

Kargl, Julia, Nariman Balenga, Wolfgang Platzer, Leonardo Martini, Jennifer L. Whistler, and Maria Waldhoer. 2012. "The GPCR-Associated Sorting Protein 1 Regulates Ligand-Induced down-Regulation of GPR55." *British Journal of Pharmacology* 165(8):2611–19.

Karki, Sher and Erika LF Holzbaur. 1999. "Cytoplasmic Dynein and Dynactin in Cell Division and Intracellular Transport." *Current Opinion in Cell Biology* 11(1):45–53.

Karle, Kathrin N., Diana Möckel, Evan Reid, and Ludger Schöls. 2012. "Axonal Transport Deficit in a KIF5A –/– Mouse Model." *Neurogenetics* 13(2):169–79.

Kask, Keiu, Katrin Ruisu, Laura Tikker, Kirstin Karis, Merly Saare, Riho Meier, Alar Karis, Tambet Tõnissoo, and Margus Pooga. 2015. "Deletion of RIC8A in Neural Precursor Cells Leads to Altered Neurogenesis and Neonatal Lethality of Mouse." *Developmental Neurobiology* 75(9):984–1002.

Kask, Keiu, Laura Tikker, Katrin Ruisu, Sirje Lulla, Eva-Maria Oja, Riho Meier, Raivo Raid, Teet Velling, Tambet Tõnissoo, and Margus Pooga. 2018. "Targeted Deletion of RIC8A in Mouse Neural Precursor Cells Interferes with the Development of the Brain, Eyes, and Muscles." *Developmental Neurobiology* 78(4):374–90.

Kasom, Mohammad, Samia Gharra, Isra Sadiya, Meirav Avital-Shacham, and Mickey Kosloff. 2018. "Interplay between Negative and Positive Design Elements in Gα Helical Domains of G Proteins Determines Interaction Specificity toward RGS2." *The Biochemical Journal* 475(14):2293–2304.

Katritch, Vsevolod, Vadim Cherezov, and Raymond C. Stevens. 2012. "Diversity and Modularity of G Protein-Coupled Receptor Structures." *Trends in Pharmacological Sciences* 33(1):17–27.

Keirsebilck, Annick, Stefan Bonné, Katrien Staes, Jolanda Van Hengel, Friedel Nollet, Albert Reynolds, and Frans Van Roy. 1998. "Molecular Cloning of the Human P120(Ctn) Catenin Gene (CTNND1): Expression of Multiple Alternatively Spliced Isoforms." *Genomics* 50(2):129–46.

Kenakin, Terry. 2015. "Gaddum Memorial Lecture 2014: Receptors as an Evolving Concept: From Switches to Biased Microprocessors." *British Journal of Pharmacology* 172(17):4238–53.

Kiernan, Matthew C., Steve Vucic, Benjamin C. Cheah, Martin R. Turner, Andrew Eisen, Orla Hardiman, James R. Burrell, and Margaret C. Zoing. 2011. "Amyotrophic Lateral Sclerosis." *Lancet (London, England)* 377(9769):942–55.

Kijima, Kazuki, Chikahiko Numakura, Hiroko Izumino, Kazuo Umetsu, Atsuo Nezu, Toshihide Shiiki, Masafumi Ogawa, Yoshito Ishizaki, Takeshi Kitamura, Yasunobu Shozawa, and Kiyoshi Hayasaka. 2005. "Mitochondrial GTPase Mitofusin 2 Mutation in Charcot Marie Tooth Neuropathy Type 2A." *Human Genetics* 116(1–2):23–27.

Kimura, Toshiya and Fujio Murakami. 2014. "Evidence That Dendritic Mitochondria Negatively Regulate Dendritic Branching in Pyramidal Neurons in the Neocortex." *Journal of Neuroscience* 34(20):6938–51.

Kino, Tomoshige, Tohru Kozasa, and George P. Chrousos. 2005. "Statin-Induced Blockade of Prenylation Alters Nucleocytoplasmic Shuttling of GTP-Binding Proteins Gamma2 and Beta2 and Enhances Their Suppressive Effect on Glucocorticoid Receptor Transcriptional Activity." *European Journal of Clinical Investigation* 35(8):508–13.

Kino, Tomoshige, Anatoly Tiulpakov, Takamasa Ichijo, Ly Chheng, Tohru Kozasa, and George P. Chrousos. 2005. "G Protein Beta Interacts with the Glucocorticoid Receptor and Suppresses Its Transcriptional Activity in the Nucleus." *The Journal of Cell Biology* 169(6):885–96.

Kirk, Elizabeth, Lih-Shen Chin, and Lian Li. 2006. "GRIF1 Binds Hrs and Is a New Regulator of Endosomal Trafficking." *Journal of Cell Science* 119(22):4689–4701.

Kiyama, Atsuko, Yasushi Isojima, and Katsuya Nagai. 2006. "Role of Per1-Interacting Protein of the Suprachiasmatic Nucleus in NGF Mediated Neuronal Survival." *Biochemical and Biophysical Research Communications* 339(2):514–19.

Kobayashi, Masanobu, Teruki Honma, Yuichi Matsuda, Yoji Suzuki, Riuchi Narisawa, Yoichi Ajioka, and Hiroyuki Asakura. 2000. "True." *British Journal of Cancer* 82(10):1689–93.

Kon, Takahide, Takuji Oyama, Rieko Shimo-Kon, Kenji Imamula, Tomohiro Shima, Kazuo Sutoh, and Genji Kurisu. 2012. "The 2.8 Å Crystal Structure of the Dynein Motor Domain." *Nature* 484(7394):345–50.

Koopman, Werner J. H., Henk-Jan Visch, Jan A. M. Smeitink, and Peter H. G. M. Willems. 2006. "Simultaneous Quantitative Measurement and Automated Analysis of Mitochondrial Morphology, Mass, Potential, and Motility in Living Human Skin Fibroblasts." *Cytometry Part A* 69A(1):1–12.

Kornmann, Benoît, Christof Osman, and Peter Walter. 2011. "The Conserved GTPase Gem1 Regulates Endoplasmic Reticulum-Mitochondria Connections." *Proceedings of the National Academy of Sciences* 108(34):14151–56.

Koshiba, Takumi, Scott A. Detmer, Jens T. Kaiser, Hsiuchen Chen, J. Michael McCaffery, and David C. Chan. 2004. "Structural Basis of Mitochondrial Tethering by Mitofusin Complexes." *Science* 305(5685):858–62.

Krakstad, Beate F., Vandana V. Ardawatia, and Anna M. Aragay. 2004. "A Role for G 12/G 13 in P120ctn Regulation." *Proceedings of the National Academy of Sciences* 101(28):10314–19.

Krig, Sheryl R., Victor X. Jin, Mark C. Bieda, Henriette O'Geen, Paul Yaswen, Roland Green, and Peggy J. Farnham. 2007. "Identification of Genes Directly Regulated by the Oncogene ZNF217 Using Chromatin Immunoprecipitation (ChIP)-Chip Assays." *The Journal of Biological Chemistry* 282(13):9703–12.

Kruppa, Antonina J., Chieko Kishi-Itakura, Thomas A. Masters, Joanna E. Rorbach, Guinevere L. Grice, John Kendrick-Jones, James A. Nathan, Michal Minczuk, and Folma Buss. 2018. "Myosin VI-Dependent Actin Cages Encapsulate Parkin-Positive Damaged Mitochondria." *Developmental Cell* 44(4):484-499.e6.

Kurochkin, Igor V, Natsumi Yonemitsu, Shin-ichi Funahashi, and Hitoshi Nomura. 2001. "ALEX1, a Novel Human Armadillo Repeat Protein That Is Expressed Differentially in Normal Tissues and Carcinomas." *Biochemical and Biophysical Research Communications* 280(1):340–47.

Kuroda, Shun'ichi, Noritaka Nakagawa, Chiharu Tokunaga, Kenji Tatematsu, and Katsuyuki Tanizawa. 1999. "Mammalian Homologue of the Caenorhabditis Elegans UNC-76 Protein Involved in Axonal Outgrowth Is a Protein Kinase C Zeta-Interacting Protein." *The Journal of Cell Biology* 144(3):403–11.

Kuyznierewicz, Ileana and Murray Thomson. 2002. "GTP-binding proteins Gsα, Giα, and Ran identified in mitochondria of human placenta." *Cell Biology International* 26(1):99–108.

Labbé, Katherine, Andrew Murley, and Jodi Nunnari. 2014. "Determinants and Functions of Mitochondrial Behavior." *Annual Review of Cell and Developmental Biology* 30(1):357–91.

Laemmli, Ulrich K. 1970. "Cleavage of Structural Proteins during the Assembly of the Head of Bacteriophage T4." *Nature* 227(5259):680–85.

Lahiri, Vikramjit and Daniel J. Klionsky. 2017. "Functional Impairment in RHOT1/Miro1 Degradation and Mitophagy Is a Shared Feature in Familial and Sporadic Parkinson Disease." *Autophagy* 13(8):1259–61.

Lambert, Nevin A. 2008. "Dissociation of Heterotrimeric G Proteins in Cells." *Sci. Signal.* 1(25):re5–re5.

Lao, Guifang, Volker Scheuss, Claudia M. Gerwin, Qingning Su, Sumiko Mochida, Jens Rettig, and Zu-Hang Sheng. 2000. "Syntaphilin: A Syntaxin-1 Clamp That Controls SNARE Assembly." *Neuron* 25(1):191–201.

Las, Guy and Orian S. Shirihai. 2014. "Miro1: New Wheels for Transferring Mitochondria." *The EMBO Journal* 33(9):939–41.

Lazarou, Michael, Seok Min Jin, Lesley A. Kane, and Richard J. Youle. 2012. "Role of PINK1 Binding to the TOM Complex and Alternate Intracellular Membranes in Recruitment and Activation of the E3 Ligase Parkin." *Developmental Cell* 22(2):320–33.

Lazarou, Michael, Danielle A. Sliter, Lesley A. Kane, Shireen A. Sarraf, Chunxin Wang, Jonathon L. Burman, Dionisia P. Sideris, Adam I. Fogel, and Richard J. Youle. 2015. "The Ubiquitin Kinase PINK1 Recruits Autophagy Receptors to Induce Mitophagy." *Nature* 524(7565):309–14.

Lee, Seongsoo, Kyu-Sun Lee, Sungun Huh, Song Liu, Do-Yeon Lee, Seung Hyun Hong, Kweon Yu, and Bingwei Lu. 2016. "Polo Kinase Phosphorylates Miro to Control ER-Mitochondria Contact Sites and Mitochondrial Ca2+ Homeostasis in Neural Stem Cell Development." *Developmental Cell* 37(2):174–89.

Lee, Syann, Christine L. Walker, Barbara Karten, Sharee L. Kuny, Alysa A. Tennese, Megan A. O'Neill, and Rachel Wevrick. 2005. "Essential Role for the Prader–Willi Syndrome Protein Necdin in Axonal Outgrowth." *Human Molecular Genetics* 14(5):627–37.

Lefkowitz, Robert J. and Sudha K. Shenoy. 2005. "Transduction of Receptor Signals by β-Arrestins." *Science* 308(5721):512–17.

Lenaers, Guy, Christian Hamel, Cécile Delettre, Patrizia Amati-Bonneau, Vincent Procaccio, Dominique Bonneau, Pascal Reynier, and Dan Milea. 2012. "Dominant Optic Atrophy." *Orphanet Journal of Rare Diseases* 7:46.

Li, Hongyan and Rong Wang. 2017. "A Focus on CXCR4 in Alzheimer's Disease." *Brain Circulation* 3(4):199–203.

Li, Jianchao, Qing Lu, and Mingjie Zhang. 2016. "Structural Basis of Cargo Recognition by Unconventional Myosins in Cellular Trafficking." *Traffic* 17(8):822–38.

Lin, Ping, Thierry Fischer, Christine Lavoie, Haining Huang, and Marilyn Gist Farquhar. 2009. "Calnuc Plays a Role in Dynamic Distribution of Galphai but Not Gbeta Subunits and Modulates ACTH Secretion in AtT-20 Neuroendocrine Secretory Cells." *Molecular Neurodegeneration* 4:15.

Lin, Wan-Hsin, Joshua T. Hurley, Alexander N. Raines, Richard E. Cheney, and Donna J. Webb. 2013. "Myosin X and Its Motorless Isoform Differentially Modulate Dendritic Spine Development by Regulating Trafficking and Retention of Vasodilator-Stimulated Phosphoprotein." *Journal of Cell Science* 126(20):4756.

Litosch, Irene. 2016. "Decoding Gαq Signaling." *Life Sciences* 152:99–106.

Little, Kevin D., Martin E. Hemler, and Christopher S. Stipp. 2004. "Dynamic Regulation of a GPCR-Tetraspanin-G Protein Complex on Intact Cells: Central Role of CD81 in Facilitating GPR56-Gαq/11 Association." *Molecular Biology of the Cell* 15(5):2375–87.

Liu, Song, Tomoyo Sawada, Seongsoo Lee, Wendou Yu, George Silverio, Philomena Alapatt, Ivan Millan, Alice Shen, William Saxton, Tomoko Kanao, Ryosuke Takahashi, Nobutaka Hattori, Yuzuru Imai, and Bingwei Lu. 2012. "Parkinson's Disease–Associated Kinase PINK1 Regulates Miro Protein Level and Axonal Transport of Mitochondria" edited by G. P. Copenhaver. *PLoS Genetics* 8(3):e1002537.

López-Doménech, Guillermo, Román Serrat, Serena Mirra, Salvatore D'Aniello, Ildiko Somorjai, Alba Abad, Nathalia Vitureira, Elena García-Arumí, María Teresa Alonso, Macarena Rodriguez-Prados, Ferran Burgaya, Antoni L. Andreu, Javier García-Sancho, Ramón Trullas, Jordi Garcia-Fernàndez, and Eduardo Soriano. 2012. "The Eutherian Armcx Genes Regulate Mitochondrial Trafficking in Neurons and Interact with Miro and Trak2." *Nature Communications* 3:814.

López-Doménech, Guillermo, Christian Covill-Cooke, Davor Ivankovic, Els F. Halff, David F. Sheehan, Rosalind Norkett, Nicol Birsa, and Josef T. Kittler. 2018. "Miro Proteins Coordinate Microtubule- and Actin-dependent Mitochondrial Transport and Distribution." *The EMBO Journal* 37(3):e96380.

Loss, Omar and F. Anne Stephenson. 2015. "Localization of the Kinesin Adaptor Proteins Trafficking Kinesin Proteins 1 and 2 in Primary Cultures of Hippocampal Pyramidal and Cortical Neurons." *Journal of Neuroscience Research* 93(7):1056–66.

Loss, Omar and F. Anne Stephenson. 2017. "Developmental Changes in Trak-Mediated Mitochondrial Transport in Neurons." *Molecular and Cellular Neuroscience* 80:134–47.

Lu, Zekuan, Xiao-Nan Ma, Hai-Man Zhang, Huan-Hong Ji, Hao Ding, Jie Zhang, Dan Luo, Yujie Sun, and Xiang-Dong Li. 2014. "Mouse Myosin-19 Is a plus-End-Directed, High-Duty Ratio Molecular Motor." *The Journal of Biological Chemistry* 289(26):18535–48.

Lumpkin, Ryan J., Hongbo Gu, Yiying Zhu, Marilyn Leonard, Alla S. Ahmad, Karl R. Clauser, Jesse G. Meyer, Eric J. Bennett, and Elizabeth A. Komives. 2017. "Site-Specific Identification and Quantitation of Endogenous SUMO Modifications under Native Conditions." *Nature Communications* 8(1).

Lundby, Alicia, Kasper Lage, Brian T. Weinert, Dorte B. Bekker-Jensen, Anna Secher, Tine Skovgaard, Christian D. Kelstrup, Anatoliy Dmytriyev, Chunaram Choudhary, Carsten Lundby, and Jesper V. Olsen. 2012. "Proteomic Analysis of Lysine Acetylation Sites in Rat Tissues Reveals Organ Specificity and Subcellular Patterns." *Cell Reports* 2(2):419–31.

Lutz, Susanne, Aruna Shankaranarayanan, Cassandra Coco, Marc Ridilla, Mark R. Nance, Christiane Vettel, Doris Baltus, Chris R. Evelyn, Richard R. Neubig, Thomas Wieland, and John J. G. Tesmer. 2007. "Structure of Gαq-P63RhoGEF-RhoA Complex Reveals a Pathway for the Activation of RhoA by GPCRs." *Science* 318(5858):1923–27.

Lyssand, John S. and Sandra M. Bajjalieh. 2007. "The Heretotrimeric G Protein Subunit Gαi Is Present on Mitochondria." *FEBS Letters* 581(30):5765–68.

Ma, Xinli, Kai Liu, Jian Li, Huanhuan Li, Jun Li, Yingfang Liu, Chonglin Yang, and Huanhuan Liang. 2018. "A Non-Canonical GTPase Interaction Enables ORP1L-Rab7-RILP Complex Formation and Late Endosome Positioning." *Journal of Biological Chemistry* 293(36):14155–64.

MacAskill, Andrew F., Kieran Brickley, F. Anne Stephenson, and Josef T. Kittler. 2009. "GTPase Dependent Recruitment of Grif-1 by Miro1 Regulates Mitochondrial Trafficking in Hippocampal Neurons." *Molecular and Cellular Neuroscience* 40(3):301–12.

MacAskill, Andrew F. and Josef T. Kittler. 2010. "Control of Mitochondrial Transport and Localization in Neurons." *Trends in Cell Biology* 20(2):102–12.

MacAskill, Andrew F., Johanne E. Rinholm, Alison E. Twelvetrees, I. Lorena Arancibia-Carcamo, James Muir, Asa Fransson, Pontus Aspenstrom, David Attwell, and Josef T. Kittler. 2009. "Miro1 Is a Calcium Sensor for Glutamate Receptor-Dependent Localization of Mitochondria at Synapses." *Neuron* 61(4):541–55.

Mahoney, Jacob P. and Roger K. Sunahara. 2016. "Mechanistic Insights into GPCR–G Protein Interactions." *Current Opinion in Structural Biology* 41:247–54.

Manna, Prasenjit and Parames C. Sil. 2012a. "Arjunolic Acid: Beneficial Role in Type 1 Diabetes and Its Associated Organ Pathophysiology." *Free Radical Research* 46(7):815–30.

Manna, Prasenjit and Parames C. Sil. 2012b. "Impaired Redox Signaling and Mitochondrial Uncoupling Contributes Vascular Inflammation and Cardiac Dysfunction in Type 1 Diabetes: Protective Role of Arjunolic Acid." *Biochimie* 94(3):786–97.

Masià, Miriam, Ismael Izquierdo, Georgina Garrido, Arnau Cordomí, Laura Perez, Nichol L. G. Miller, David D. Schlaepfer, Véronique Gigoux, and Anna M. Aragay. 2015. "Gastrin-Stimulated Galpha13 Activation of Rgnef (ArhGEF28) in DLD-1 Colon Carcinoma Cells." *Journal of Biological Chemistry* 290(24):jbc.M114.628164.

Matamoros, Andrew J. and Peter W. Baas. 2016. "Microtubules in Health and Degenerative Disease of the Nervous System." *Brain Research Bulletin* 126(Pt 3):217–25.

Mathis, Chantal, Jean-Bastien Bott, Marie-Pierre Candusso, Frédéric Simonin, and Jean-Christophe Cassel 2011. "Impaired Striatum-Dependent Behavior in GASP-1-Knock-out Mice." *Genes, Brain and Behavior* 10(3):299–308.

Meissner, Cathrin, Holger Lorenz, Andreas Weihofen, Dennis J. Selkoe, and Marius K. Lemberg. 2011. "The Mitochondrial Intramembrane Protease PARL Cleaves Human Pink1 to Regulate Pink1 Trafficking." *Journal of Neurochemistry* 117(5):856–67.

Melkov, Anna and Uri Abdu. 2018. "Regulation of Long-Distance Transport of Mitochondria along Microtubules." *Cellular and Molecular Life Sciences* 75(2):163–76.

Meyer, Etienne H., Elina Welchen, and Chris Carrie. 2019. "Assembly of the Complexes of the Oxidative Phosphorylation System in Land Plant Mitochondria." *Annual Review of Plant Biology* 70(1):23–50.

Millar, J. Kirsty, Julie C. Wilson-Annan, Susan Anderson, Sheila Christie, Martin S. Taylor, Colin A. M. Semple, Rebecca S. Devon, David M. St Clair, Walter J. Muir, Douglas H. R. Blackwood, and David J. Porteous. 2000. "Disruption of Two Novel Genes by a Translocation Co-Segregating with Schizophrenia." *Human Molecular Genetics* 9(9):1415–23.

Miller, Kyle E. and Michael P. Sheetz. 2004. "Axonal Mitochondrial Transport and Potential Are Correlated." *Journal of Cell Science* 117(Pt 13):2791–2804.

Miller, Kyle E. and Michael P. Sheetz. 2006. "Direct Evidence for Coherent Low Velocity Axonal Transport of Mitochondria." *The Journal of Cell Biology* 173(3):373–81.

Milligan, Graeme. 1993. "Regional Distribution and Quantitative Measurement of the Phosphoinositidase C-Linked Guanine Nucleotide Binding Proteins $G\alpha_1$ and $G\alpha_q$? In Rat Brain." *Journal of Neurochemistry* 61(3):845–51.

Milligan, Graeme and Evi Kostenis. 2006. "Heterotrimeric G-Proteins: A Short History." *British Journal of Pharmacology* 147 Suppl 1(Suppl 1):S46-55.

Mirra, Serena, Fausto Ulloa, Irene Gutierrez-Vallejo, Elisa Martì, and Eduardo Soriano. 2016. "Function of Armcx3 and Armc10/SVH Genes in the Regulation of Progenitor Proliferation and Neural Differentiation in the Chicken Spinal Cord." *Frontiers in Cellular Neuroscience* 10:47.

Misgeld, Thomas, Martin Kerschensteiner, Florence M. Bareyre, Robert W. Burgess, and Jeff W. Lichtman. 2007. "Imaging Axonal Transport of Mitochondria in Vivo." *Nature Methods* 4(7):559–61.

Misko, Albert, Sirui Jiang, Iga Wegorzewska, Jeffrey Milbrandt, and Robert H. Baloh. 2010. "Mitofusin 2 Is Necessary for Transport of Axonal Mitochondria and Interacts with the Miro/Milton Complex." *Journal of Neuroscience* 30(12):4232–40.

Moller, Annekathrin, Claudia S. Bauer, Rebecca N. Cohen, Christopher P. Webster, and Kurt J. De Vos. 2017. "Amyotrophic Lateral Sclerosis-Associated Mutant SOD1 Inhibits Anterograde Axonal Transport of Mitochondria by Reducing Miro1 Levels." *Human Molecular Genetics* 26(23):4668–79.

Moore, Andrew S. and Erika LF Holzbaur. 2018. "Mitochondrial-Cytoskeletal Interactions: Dynamic Associations That Facilitate Network Function and Remodeling." *Current Opinion in Physiology* 3:94–100.

Moore, Catherine A. C., Shawn K. Milano, and Jeffrey L. Benovic. 2007. "Regulation of Receptor Trafficking by GRKs and Arrestins." *Annual Review of Physiology* 69(1):451–82.

Morena, Jonathan, Anirudh Gupta, J. Chad Hoyle, Jonathan Morena, Anirudh Gupta, and J. Chad Hoyle. 2019. "Charcot-Marie-Tooth: From Molecules to Therapy." *International Journal of Molecular Sciences* 20(14):3419.

Mori, Taisuke, Aoi Sukeda, Shigeki Sekine, Shinsuke Shibata, Eijitsu Ryo, Hideyuki Okano, Shigenobu Suzuki, and Nobuyoshi Hiraoka. 2017. "SOX10 Expression as Well as *BRAF* and *GNAQ/11* Mutations Distinguish Pigmented Ciliary Epithelium Neoplasms From Uveal Melanomas." *Investigative Opthalmology & Visual Science* 58(12):5445.

Mortiboys, Heather, Kelly Jean Thomas, Werner J. H. Koopman, Stefanie Klaffke, Patrick Abou-Sleiman, Simon Olpin, Nicholas W. Wood, Peter H. G. M. Willems, Jan A. M. Smeitink, Mark R. Cookson, and Oliver Bandmann. 2008. "Mitochondrial Function and Morphology Are Impaired in Parkin-Mutant Fibroblasts." *Annals of Neurology* 64(5):555–65.

Mou, Z., a. R. Tapper, and P. D. Gardner. 2009. "The Armadillo Repeat-Containing Protein, ARMCX3, Physically and Functionally Interacts with the Developmental Regulatory Factor Sox10." *Journal of Biological Chemistry* 284(20):13629–40.

Murley, Andrew, Laura L. Lackner, Christof Osman, Matthew West, Gia K. Voeltz, Peter Walter, and Jodi Nunnari. 2013. "ER-Associated Mitochondrial Division Links the Distribution of Mitochondria and Mitochondrial DNA in Yeast." *ELife* 2.

Nagai, Makiko, Diane B. Re, Tetsuya Nagata, Alcmène Chalazonitis, Thomas M. Jessell, Hynek Wichterle, and Serge Przedborski. 2007. "Astrocytes Expressing ALS-Linked Mutated SOD1 Release Factors Selectively Toxic to Motor Neurons." *Nature Neuroscience* 10(5):615–22.

Nakagawa, Hiroshi, Haruka Umadome, Shuichi Miyazaki, Katsuhiro Tanaka, Kazuhiko Nishimura, Masayuki Komori, and Saburo Matsuo. 2011. "ER-Resident $G\alpha_{i2}$ Protein Controls Sar1 Translocation onto the ER during Budding of Transport Vesicles." *Journal of Cellular Biochemistry* 112(9):2250–56.

Nangaku, Masaomi, Reiko Sato-Yoshitake, Yasushi Okada, Yasuko Noda, Reiko Takemura, Hiroto Yamazaki, and Nobutaka Hirokawa. 1994. "KIF1B, a Novel Microtubule plus End-Directed Monomeric Motor Protein for Transport of Mitochondria." *Cell* 79(7):1209–20.

Nasrallah, Chady, Karine Rottier, Romain Marcellin, Vincent Compan, Joan Font, Amadeu Llebaria, Jean-Philippe Pin, Jean-Louis Banères, and Guillaume Lebon. 2018. "Direct Coupling of Detergent Purified Human MGlu5 Receptor to the Heterotrimeric G Proteins Gq and Gs." *Scientific Reports* 8(1):4407.

Nelson, Melanie R., Eva Thulin, Patricia A. Fagan, Sture Forsén, and Walter J. Chazin. 2009. "The EF-Hand Domain: A Globally Cooperative Structural Unit." *Protein Science* 11(2):198–205.

Nemani, Neeharika, Edmund Carvalho, Dhanendra Tomar, Zhiwei Dong, Andrea Ketschek, Sarah L. Breves, Fabián Jaña, Alison M. Worth, Julie Heffler, Palaniappan Palaniappan, Aparna Tripathi, Ramasamy Subbiah, Massimo F. Riitano, Ajay Seelam, Thomas Manfred, Kie Itoh, Shuxia Meng, Hiromi Sesaki, William J. Craigen, Sudarsan Rajan, Santhanam Shanmughapriya, Jeffrey Caplan, Benjamin L. Prosser, Donald L. Gill, Peter B. Stathopulos, Gianluca Gallo, David C. Chan, Prashant Mishra, and Muniswamy Madesh. 2018. "MIRO-1 Determines Mitochondrial Shape Transition upon GPCR Activation and Ca2+Stress." *Cell Reports* 1005–19.

Nguyen, Tammy T., Sang S. Oh, David Weaver, Agnieszka Lewandowska, Dane Maxfield, Max-Hinderk Schuler, Nathan K. Smith, Jane Macfarlane, Gerald Saunders, Cheryl A. Palmer, Valentina Debattisti, Takumi Koshiba, Stefan Pulst, Eva L. Feldman, György Hajnóczky, and Janet M. Shaw. 2014. "Loss of Miro1-Directed Mitochondrial Movement Results in a Novel Murine Model for Neuron Disease." *Proceedings of the National Academy of Sciences of the United States of America* 111(35):E3631-40.

Niescier, Robert F., Kido Hong, Dongkeun Park, and Kyung-Tai Min. 2018. "MCU Interacts with Miro1 to Modulate Mitochondrial Functions in Neurons." *The Journal of Neuroscience : The Official Journal of the Society for Neuroscience* 38(20):4666–77.

Norkett, Rosalind, Souvik Modi, Nicol Birsa, Talia A. Atkin, Davor Ivankovic, Manav Pathania, Svenja V. Trossbach, Carsten Korth, Warren D. Hirst, and Josef T. Kittler. 2016. "DISC1-Dependent Regulation of Mitochondrial Dynamics Controls the Morphogenesis of Complex Neuronal Dendrites." *Journal of Biological Chemistry* 291(2):613–29.

Oeding, Stefanie J., Katarzyna Majstrowicz, Xiao-Ping Hu, Vera Schwarz, Angelika Freitag, Ulrike Honnert, Petra Nikolaus, and Martin Bähler. 2018. "Identification of Miro1 and Miro2 as Mitochondrial Receptors for Myosin XIX." *Journal of Cell Science* 131(17):jcs219469.

Offermanns, Steffan, Kouichi Hashimoto, Masahiko Watanabe, William Sun, Hideo Kurihara, Richard F. Thompson, Yoshiro Inoue, Masanobu Kano, and Melvin I. Simon. 1997. "Impaired Motor Coordination and Persistent Multiple Climbing Fiber Innervation of Cerebellar Purkinje Cells in Mice Lacking Galphaq." *Proceedings of the National Academy of Sciences of the United States of America* 94(25):14089–94.

Offermanns, Steffan, Li-Ping Zhao, Antje Gohla, Ildiko Sarosi, Melvin I. Simon, and Thomas M. Wilkie. 1998. "Embryonic Cardiomyocyte Hypoplasia and Craniofacial Defects in Galpha q/Galpha 11-Mutant Mice." *The EMBO Journal* 17(15):4304–12.

Offermanns, Stefan, Christopher F. Toombs, Yi-Hui Hu, and Melvin I. Simon. 1997. "Defective Platelet Activation in Gαq-Deficient Mice." *Nature* 389(6647):183–86.

Ogawa, Fumiaki, Elise L. V. Malavasi, Darragh K. Crummie, Jennifer E. Eykelenboom, Dinesh C. Soares, Shaun Mackie, David J. Porteous, and J. Kirsty Millar. 2014. "DISC1 Complexes with TRAK1 and Miro1 to Modulate Anterograde Axonal Mitochondrial Trafficking." *Human Molecular Genetics* 23(4):906–19.

Oh, Phil and Jan E. Schnitzer. 2001. "Segregation of Heterotrimeric G Proteins in Cell Surface Microdomains. G(q) Binds Caveolin to Concentrate in Caveolae, Whereas G(i) and G(s) Target Lipid Rafts by Default." *Molecular Biology of the Cell* 12(3):685–98.

Ohno, Nobuhiko, Hao Chiang, Don J. Mahad, Grahame J. Kidd, LiPing Liu, Richard M. Ransohoff, Zu-Hang Sheng, Hitoshi Komuro, and Bruce D. Trapp. 2014. "Mitochondrial Immobilization Mediated by Syntaphilin Facilitates Survival of Demyelinated Axons." *Proceedings of the National Academy of Sciences of the United States of America* 111(27):9953–58.

Okada, Yasushi, Hiroto Yamazaki, Yoko Sekine-Aizawa, and Nobutaka Hirokawa. 1995. "The Neuron-Specific Kinesin Superfamily Protein KIF1A Is a Uniqye Monomeric Motor for Anterograde Axonal Transport of Synaptic Vesicle Precursors." *Cell* 81(5):769–80.

Okatsu, Kei, Midori Uno, Fumika Koyano, Etsu Go, Mayumi Kimura, Toshihiko Oka, Keiji Tanaka, and Noriyuki Matsuda. 2013. "A Dimeric PINK1-Containing Complex on Depolarized Mitochondria Stimulates Parkin Recruitment." *The Journal of Biological Chemistry* 288(51):36372–84.

Okumoto, Kanji, Tatsuaki Ono, Ryusuke Toyama, Ayako Shimomura, Aiko Nagata, and Yukio Fujiki. 2018. "New Splicing Variants of Mitochondrial Rho GTPase-1 (Miro1) Transport Peroxisomes." *The Journal of Cell Biology* 217(2):619–33.

Olichon, A., G. ElAchouri, L. Baricault, C. Delettre, P. Belenguer, and G. Lenaers. 2007. "OPA1 Alternate Splicing Uncouples an Evolutionary Conserved Function in Mitochondrial Fusion from a Vertebrate Restricted Function in Apoptosis." *Cell Death & Differentiation* 14(4):682–92.

Olichon, Aurélien, Laurent J. Emorine, Eric Descoins, Laetitia Pelloquin, Laetitia Brichese, Nicole Gas, Emmanuelle Guillou, Cécile Delettre, Annie Valette, Christian P. Hamel, Bernard Ducommun, Guy Lenaers, and Pascale Belenguer. 2002. "The Human Dynamin-Related Protein OPA1 Is Anchored to the Mitochondrial Inner Membrane Facing the Inter-Membrane Space." *FEBS Letters* 523(1–3):171–76.

de Oliveira, Patrícia G., Marta L. S. Ramos, António J. Amaro, Roberto A. Dias, and Sandra I. Vieira. 2019. "Gi/o-Protein Coupled Receptors in the Aging Brain." *Frontiers in Aging Neuroscience* 11:89.

Osellame, Laura D., Abeer P. Singh, David A. Stroud, Catherine S. Palmer, Diana Stojanovski, Rajesh Ramachandran, and Michael T. Ryan. 2016. "Cooperative and Independent Roles of the Drp1 Adaptors Mff, MiD49 and MiD51 in Mitochondrial Fission." *Journal of Cell Science* 129(11):2170–81.

Park, Cana, Seol-Ae Lee, Ji-Ho Hong, Yeongjun Suh, Sung Jin Park, Bo Kyoung Suh, Youngsik Woo, Jinhyuk Choi, Ji-Won Huh, You-Me Kim, and Sang Ki Park. 2016. "Disrupted-in-Schizophrenia 1 (DISC1) and Syntaphilin Collaborate to Modulate Axonal Mitochondrial Anchoring." *Molecular Brain* 9(1):69.

Park, Jin-Gyoon, Aleixo Muise, Gong-Ping He, Sung-Woo Kim, and Hyo-Sung Ro. 1999. "Transcriptional Regulation by the Gamma5 Subunit of a Heterotrimeric G Protein during Adipogenesis." *The EMBO Journal* 18(14):4004–12.

Park, Young-Un, Jaehoon Jeong, Haeryun Lee, Ji Young Mun, Joung-Hun Kim, Jong Seo Lee, Minh Dang Nguyen, Sung Sik Han, Pann-Ghill Suh, and Sang Ki Park. 2010. "Disrupted-in-Schizophrenia 1 (DISC1) Plays Essential Roles in Mitochondria in Collaboration with Mitofilin." *Proceedings of the National Academy of Sciences of the United States of America* 107(41):17785–90.

Paschal, Bryce M. and Richard B. Vallee. 1987. "Retrograde Transport by the Microtubule-Associated Protein MAP 1C." *Nature* 330(6144):181–83.

Pathak, Divya, Katharine J. Sepp, and Peter J. Hollenbeck. 2010. "Evidence That Myosin Activity Opposes Microtubule-Based Axonal Transport of Mitochondria." *The Journal of Neuroscience : The Official Journal of the Society for Neuroscience* 30(26):8984–92.

Patil, Hemangi, Kyoung-in Cho, James Lee, Yi Yang, Andrew Orry, and Paulo A. Ferreira. 2013. "Kinesin-1 and Mitochondrial Motility Control by Discrimination of Structurally Equivalent but Distinct Subdomains in Ran-GTP-Binding Domains of Ran-Binding Protein 2." *Open Biology* 3(3):120183.

Pazour, Gregory J., Bethany L. Dickert, and George B. Witman. 1999. "The DHC1b (DHC2) Isoform of Cytoplasmic Dynein Is Required for Flagellar Assembly." *The Journal of Cell Biology* 144(3):473–81.

Pilling, Aaron D, Dai Horiuchi, Curtis M. Lively, and William M. Saxton. 2006. "Kinesin-1 and Dynein Are the Primary Motors for Fast Transport of Mitochondria in *Drosophila* Motor Axons." *Molecular Biology of the Cell* 17(4):2057–68.

Pin, Jean-Philippe, Julie Kniazeff, Laurent Prézeau, Jiang-Feng Liu, and Philippe Rondard. 2019. "GPCR Interaction as a Possible Way for Allosteric Control between Receptors." *Molecular and Cellular Endocrinology* 486:89–95.

Pinto, Anna, Mustafa Sahin, and Phillip L. Pearl. 2016. "Epileptogenesis in Neurocutaneous Disorders with Focus in Sturge Weber Syndrome." *F1000Research* 5.

Popova, Juliana S. and Mark M. Rasenick. 2000. "Muscarinic Receptor Activation Promotes the Membrane Association of Tubulin for the Regulation of Gq-Mediated Phospholipase Cβ1signaling." *Journal of Neuroscience* 20(8):2774–82.

Porter, Mary E., Raqual Bower, Julie A. Knott, Pamela Byrd, and William Dentler. 1999. "Cytoplasmic Dynein Heavy Chain 1b Is Required for Flagellar Assembly in *Chlamydomonas*" edited by J. R. McIntosh. *Molecular Biology of the Cell* 10(3):693–712.

Preuß, Inga, Barbara Kurig, Bernd Nürnberg, Joachim H. C. Orth, and Klaus Aktories. 2009. "Pasteurella Multocida Toxin Activates Gβγ Dimers of Heterotrimeric G Proteins." *Cellular Signalling* 21(4):551–58.

Prudent, Julien, Rodolfo Zunino, Ayumu Sugiura, Sevan Mattie, Gordon C. Shore, and Heidi M. McBride. 2015. "MAPL SUMOylation of Drp1 Stabilizes an ER/Mitochondrial Platform Required for Cell Death." *Molecular Cell* 59(6):941–55.

Qi, Xin, Marie-Helene Disatnik, Ning Shen, Raymond A. Sobel, and Daria Mochly-Rosen. 2011. "Aberrant Mitochondrial Fission in Neurons Induced by Protein Kinase Cδ under Oxidative Stress Conditions in Vivo" edited by P. Forscher. *Molecular Biology of the Cell* 22(2):256–65.

Quintero, Omar A., Melinda M. DiVito, Rebecca C. Adikes, Melisa B. Kortan, Lindsay B. Case, Audun J. Lier, Niki S. Panaretos, Stephanie Q. Slater, Michelle Rengarajan, Marianela Feliu, and Richard E. Cheney. 2009. "Human Myo19 Is a Novel Myosin That Associates with Mitochondria." *Current Biology : CB* 19(23):2008–13.

Van Raamsdonk, Catherine D., Vladimir Bezrookove, Gary Green, Jürgen Bauer, Lona Gaugler, Joan M. O'Brien, Elizabeth M. Simpson, Gregory S. Barsh, and Boris C. Bastian. 2009. "Frequent Somatic Mutations of GNAQ in Uveal Melanoma and Blue Naevi." *Nature* 457(7229):599–602.

Rahimi-Balaei, Maryam, Hugo Bergen, Jiming Kong, and Hassan Marzban. 2018. "Neuronal Migration during Development of the Cerebellum." *Frontiers in Cellular Neuroscience* 12.

Rajagopal, Sudarshan and Sudha K. Shenoy. 2018. "GPCR Desensitization: Acute and Prolonged Phases." *Cellular Signalling* 41:9–16.

Rashid, Kahkashan, Joydeep Das, and Parames C. Sil. 2013. "Taurine Ameliorate Alloxan Induced Oxidative Stress and Intrinsic Apoptotic Pathway in the Hepatic Tissue of Diabetic Rats." *Food and Chemical Toxicology* 51:317–29.

Ratnaparkhi, Anuradha. 2013. "Signaling by Folded Gastrulation Is Modulated by Mitochondrial Fusion and Fission." *Journal of Cell Science* 126(Pt 23):5369–76.

Rawson, Randi L., Lung Yam, Robby M. Weimer, Eric G. Bend, Erika Hartwieg, H. Robert Horvitz, Scott G. Clark, and Erik M. Jorgensen. 2014. "Axons Degenerate in the Absence of Mitochondria in C. Elegans." *Current Biology* 24(7):760–65.

Rhee, Sue Goo. 2001. *Regulation of phosphoinositide-specific phospholipase C*.

Rizzuto, Rosario, Marisa Brini, Marta Murgia, and Tullio Pozzan. 1993. "Microdomains with High Ca2+ Close to IP3-Sensitive Channels That Are Sensed by Neighboring Mitochondria." *Science (New York, N.Y.)* 262(5134):744–47.

Robb-Gaspers, Lawrence D., Paul Burnett, Guy A. Rutter, Richard M. Denton, Rosario Rizzuto, and Andrew P. Thomas. 1998. "Integrating Cytosolic Calcium Signals into Mitochondrial Metabolic Responses." *The EMBO Journal* 17(17):4987–5000.

Robitaille, Mélanie, Sarah Gora, Ying Wang, Eugénie Goupil, Darlaine Pétrin, Danny Del Duca, Louis R. Villeneuve, Bruce G. Allen, Stéphane A. Laporte, Daniel J. Bernard, and Terence E. Hébert. 2010. "Gβγ Is a Negative Regulator of AP-1 Mediated Transcription." *Cellular Signalling* 22(8):1254–66.

Rochdi, Moulay Driss and Jean Luc Parent. 2003. "Gαq-Coupled Receptor Internalization Specifically Induced by Gαq Signaling. Regulation by EBP50." *Journal of Biological Chemistry* 278(20):17827–37.

Rochdi, Moulay Driss, Valérie Watier, Carole La Madeleine, Hiroko Nakata, Tohru Kozasa, and Jean Luc Parent. 2002. "Regulation of GTP-Binding Protein α q (Gα q) Signaling by the Ezrin-Radixin-Moesin-Binding Phosphoprotein-50 (EBP50)." *Journal of Biological Chemistry* 277(43):40751–59.

Roger, Andrew J., Sergio A. Muñoz-Gómez, and Ryoma Kamikawa. 2017. "The Origin and Diversification of Mitochondria." *Current Biology* 27(21):R1177–92.

Rohn, Jennifer L., Jigna V Patel, Beate Neumann, Jutta Bulkescher, Nunu Mchedlishvili, Rachel C. McMullan, Omar A. Quintero, Jan Ellenberg, and Buzz Baum. 2014. "Myo19 Ensures Symmetric Partitioning of Mitochondria and Coupling of Mitochondrial Segregation to Cell Division." *Current Biology : CB* 24(21):2598–2605.

Ropars, Virginie, Zhaohui Yang, Tatiana Isabet, Florian Blanc, Kaifeng Zhou, Tianming Lin, Xiaoyan Liu, Pascale Hissier, Frédéric Samazan, Béatrice Amigues, Eric D. Yang, Hyokeun Park, Olena Pylypenko, Marco Cecchini, Charles V Sindelar, H. Lee Sweeney, and Anne Houdusse. 2016. "The Myosin X Motor Is Optimized for Movement on Actin Bundles." *Nature Communications* 7:12456.

Roth, Bryan L. 2016. "DREADDs for Neuroscientists." *Neuron* 89(4):683–94.

Roychowdhury, Sukla and Mark M. Rasenick. 1994. "Tubulin-G Protein Association Stabilizes GTP Binding and Activates GTPase: Cytoskeletal Participation in Neuronal Signal Transduction." *Biochemistry* 33(32):9800–9805.

Rozengurt, Enrique. 1998. "Signal Transduction Pathways in the Mitogenic Response to G Protein-Coupled Neuropeptide Receptor Agonists." *Journal of Cellular Physiology* 177(4):507–17.

Runnels, Loren W. and Suzanne F. Scarlata. 1999. "Determination of the Affinities between Heterotrimeric G Protein Subunits and Their Phospholipase C-β Effectors †." *Biochemistry* 38(5):1488–96.

Russo, Gary J., Kathryn Louie, Andrea Wellington, Greg T. Macleod, Fangle Hu, Sarvari Panchumarthi, and Konrad E. Zinsmaier. 2009. "*Drosophila* Miro Is Required for Both Anterograde and Retrograde Axonal Mitochondrial Transport." *The Journal of Neuroscience : The Official Journal of the Society for Neuroscience* 29(17):5443–55.

Sack, Michael N. 2011. "Mitofusin Function Is Dependent on the Distinct Tissue and Organ Specific Roles of Mitochondria." *Journal of Molecular and Cellular Cardiology* 51(6):881–82.

Saini, Deepak Kumar, W. K. Ajith Karunarathne, Nataraju Angaswamy, Deepti Saini, Joon-Ho Cho, Vani Kalyanaraman, and Narasimhan Gautam. 2010. "Regulation of Golgi Structure and Secretion by Receptor-Induced G Protein βγ Complex Translocation." *Proceedings of the National Academy of Sciences of the United States of America* 107(25):11417–22.

Saito, Nobuhito, Yasushi Okada, Yasuko Noda, Yoshihiro Kinoshita, Satoru Kondo, and Nobutaka Hirokawa. 1997. "KIFC2 Is a Novel Neuron-Specific C-Terminal Type Kinesin Superfamily Motor for Dendritic Transport of Multivesicular Body-Like Organelles." *Neuron* 18(3):425–38.

Sala, Luca, Giovanni Cirillo, Gabriele Riva, Gabriele Romano, Carlo Giussani, Annamaria Cialdella, Antonio Todisco, Assunta Virtuoso, Maria Grazia Cerrito, Angela Bentivegna, Emanuela Grassilli, Antonio Ardizzoia, Emanuela Bonoldi, Roberto Giovannoni, Michele Papa, and Marialuisa Lavitrano. 2019. "Specific Expression of a New Bruton Tyrosine Kinase Isoform (P65BTK) in the Glioblastoma Gemistocytic Histotype." *Frontiers in Molecular Neuroscience* 12:2.

Sánchez-Fernández, Guzmán, Sofía Cabezudo, Carlota García-Hoz, Cristiane Benincá, Anna M. Aragay, Federico Mayor, and Catalina Ribas. 2014a. "Gαq Signalling: The New and the Old." *Cellular Signalling* 26(5):833–48.

Sánchez-Fernández, Guzmán, Sofía Cabezudo, Carlota García-Hoz, Andrew B. Tobin, Federico Mayor, and Catalina Ribas. 2013. "ERK5 Activation by Gq-Coupled Muscarinic Receptors Is Independent of Receptor Internalization and β-Arrestin Recruitment." *PloS One* 8(12):e84174.

Santel, Ansgar and Margaret T. Fuller. 2001. "Control of Mitochondrial Morphology by a Human Mitofusin." *Journal of Cell Science* 114(Pt 5):867–74.

Santel, Ansgar, Stephan Frank, Brigitte Gaume, Michael Herrler, Richard J. Youle, and Margaret T. Fuller. 2003. "Mitofusin-1 Protein Is a Generally Expressed Mediator of Mitochondrial Fusion in Mammalian Cells." *Journal of Cell Science* 116(Pt 13):2763–74.

Saotome, Masao, Dzhamilja Safiulina, György Szabadkai, Sudipto Das, Åsa Fransson, Pontus Aspenstrom, Rosario Rizzuto, and György Hajnóczky. 2008. "Bidirectional Ca2+-Dependent Control of Mitochondrial Dynamics by the Miro GTPase." *Proceedings of the National Academy of Sciences* 105(52):20728–33.

Sato, Motohiko, Masahiro Hiraoka, Hiroko Suzuki, Yunzhe Bai, Reiko Kurotani, Utako Yokoyama, Satoshi Okumura, Mary J. Cismowski, Stephen M. Lanier, and Yoshihiro Ishikawa. 2011. "Identification of Transcription Factor E3 (TFE3) as a Receptor-Independent Activator of Gα16: Gene Regulation by Nuclear Gα Subunit and Its Activator." *The Journal of Biological Chemistry* 286(20):17766–76.

Satoh, Akiko K., Bingbing X. Li, Hongai Xia, and Donald F. Ready. 2008. "Calcium-Activated Myosin V Closes the *Drosophila* Pupil." *Current Biology : CB* 18(13):951–55.

Satoh, Daisuke, Daichi Sato, Taiichi Tsuyama, Motoki Saito, Hiroyuki Ohkura, Melissa M. Rolls, Fuyuki Ishikawa, and Tadashi Uemura. 2008. "Spatial Control of Branching within Dendritic Arbors by Dynein-Dependent Transport of Rab5-Endosomes." *Nature Cell Biology* 10(10):1164–71.

Sawa, Akira, Koko Ishizuka, and Nicholas Katsanis. 2016. "The Potential of DISC1 Protein as a Therapeutic Target for Mental Illness." *Expert Opinion on Therapeutic Targets* 20(6):641–43.

Schmidt, Helgo, Emma S. Gleave, and Andrew P. Carter. 2012. "Insights into Dynein Motor Domain Function from a 3.3-Å Crystal Structure." *Nature Structural & Molecular Biology* 19(5):492–97.

Schmidt, Helgo, Ruta Zalyte, Linas Urnavicius, and Andrew P. Carter. 2015. "Structure of Human Cytoplasmic Dynein-2 Primed for Its Power Stroke." *Nature* 518(7539):435–38.

Schroeder, Courtney M., Jonathan ML Ostrem, Nicholas T. Hertz, and Ronald D. Vale. 2014. "A Ras-like Domain in the Light Intermediate Chain Bridges the Dynein Motor to a Cargo-Binding Region." *ELife* 3.

Schwarz, Thomas L. 2013. "Mitochondrial Trafficking in Neurons." *Cold Spring Harbor Perspectives in Medicine* 3(1):a011304.

Selkoe, Dennis J. 2002. "Deciphering the Genesis and Fate of Amyloid Beta-Protein Yields Novel Therapies for Alzheimer Disease." *The Journal of Clinical Investigation* 110(10):1375–81.

Senese, Nicolas B., Mark M. Rasenick, and John R. Traynor. 2018. "The Role of G-Proteins and G-Protein Regulating Proteins in Depressive Disorders." *Frontiers in Pharmacology* 9:1289.

Sengupta, Parijat, Finly Philip, and Suzanne Scarlata. 2008. "Caveolin-1 Alters Ca(2+) Signal Duration through Specific Interaction with the G Alpha q Family of G Proteins." *Journal of Cell Science* 121(Pt 9):1363–72.

Sepulveda-Falla, Diego, Alvaro Barrera-Ocampo, Christian Hagel, Anne Korwitz, Maria Fernanda Vinueza-Veloz, Kuikui Zhou, Martijn Schonewille, Haibo Zhou, Luis Velazquez-Perez, Roberto Rodriguez-Labrada, Andres Villegas, Isidro Ferrer, Francisco Lopera, Thomas Langer, Chris I. De Zeeuw, and Markus Glatzel. 2014. "Familial Alzheimer's Disease–Associated Presenilin-1 Alters Cerebellar Activity and Calcium Homeostasis." *The Journal of Clinical Investigation* 124(4):1552–67.

Serrat, Román, Serena Mirra, Joana Figueiro-Silva, Enrique Navas-Pérez, Martí Quevedo, Guillermo López-Doménech, Petar Podlesniy, Fausto Ulloa, Jordi Garcia-Fernàndez, Ramón Trullas, and Eduardo Soriano. 2014. "The Armc10/SVH Gene: Genome Context, Regulation of Mitochondrial Dynamics and Protection against Aβ-Induced Mitochondrial Fragmentation." *Cell Death & Disease* 5:e1163.

Serrat, Román, Guillermo López-Doménech, Serena Mirra, Martí Quevedo, Jordi Garcia-Fernàndez, Fausto Ulloa, Ferrán Burgaya, and Eduardo Soriano. 2013. "The Non-Canonical Wnt/PKC Pathway Regulates Mitochondrial Dynamics through Degradation of the Arm-Like Domain-Containing Protein Alex3." *PLoS ONE* 8(7):e67773.

Sesaki, Hiromi, Sheryl M. Southard, Alyson E. Aike. Hobbs, and Robert E. Jensen. 2003. "Cells Lacking Pcp1p/Ugo2p, a Rhomboid-like Protease Required for Mgm1p Processing, Lose MtDNA and Mitochondrial Structure in a Dnm1p-Dependent Manner, but Remain Competent for Mitochondrial Fusion." *Biochemical and Biophysical Research Communications* 308(2):276–83.

Setou, Mitsutoshi, Dae-Hyung Seog, Yosuke Tanaka, Yoshimitsu Kanai, Yosuke Takei, Masahiko Kawagishi, and Nobutaka Hirokawa. 2002. "Glutamate-Receptor-Interacting Protein GRIP1 Directly Steers Kinesin to Dendrites." *Nature* 417(6884):83–87.

Shang, Shuang, Fang Hua, and Zhuo-Wei Hu. 2017. "The Regulation of β-Catenin Activity and Function in Cancer: Therapeutic Opportunities." *Oncotarget* 8(20):33972–89.

Shankaranarayanan, Aruna, Cassandra A. Boguth, Susanne Lutz, Christiane Vettel, Franca Uhlemann, Mohamed Aittaleb, Thomas Wieland, and John J. G. Tesmer. 2010. "Gαq Allosterically Activates and Relieves Autoinhibition of P63RhoGEF." *Cellular Signalling* 22(7):1114–23.

Sharma, Virendra K., Venkat Ramesh, Clara Franzini-Armstrong, and Shey-Shing Sheu. 2000. "Transport of Ca2+ from Sarcoplasmic Reticulum to Mitochondria in Rat Ventricular Myocytes." *Journal of Bioenergetics and Biomembranes* 32(1):97–104.

Shaw, Pamela J. 2005. "Molecular and Cellular Pathways of Neurodegeneration in Motor Neurone Disease." *Journal of Neurology, Neurosurgery, and Psychiatry* 76(8):1046–57.

Sheng, Zu-Hang and Qian Cai. 2012. "Mitochondrial Transport in Neurons: Impact on Synaptic Homeostasis and Neurodegeneration." *Nature Reviews Neuroscience* 13(2):77–93.

Siderovski, David P. and Francis S. Willard. 2005. "The GAPs, GEFs, and GDIs of Heterotrimeric G-Protein Alpha Subunits." *International Journal of Biological Sciences* 1(2):51–66.

Simonin, Frederic, Pascale Karcher, Julien J. M. Boeuf, Audrey Matifas, and Brigitte L. Kieffer. 2004. "Identification of a Novel Family of G Protein-Coupled Receptor Associated Sorting Proteins." *Journal of Neurochemistry* 89(3):766–75.

Sinha, Krishnendu, Joydeep Das, Pabitra Bikash Pal, and Parames C. Sil. 2013. "Oxidative Stress: The Mitochondria-Dependent and Mitochondria-Independent Pathways of Apoptosis." *Archives of Toxicology* 87(7):1157–80.

Slessareva, Janna E., Sheri M. Routt, Brenda Temple, Vytas A. Bankaitis, and Henrik G. Dohlman. 2006. "Activation of the Phosphatidylinositol 3-Kinase Vps34 by a G Protein α Subunit at the Endosome." *Cell* 126(1):191–203.

Smith, Jeffrey S., Robert J. Lefkowitz, and Sudarshan Rajagopal. 2018. "Biased Signalling: From Simple Switches to Allosteric Microprocessors." *Nature Reviews Drug Discovery* 17(4):243–60.

Smith, Jeffrey S. and Sudarshan Rajagopal. 2016. "The β-Arrestins: Multifunctional Regulators of G Protein-Coupled Receptors." *The Journal of Biological Chemistry* 291(17):8969–77.

Smith, Miriam J., Karine Pozo, Kieran Brickley, and F. Anne Stephenson. 2006. "Mapping the GRIF-1 Binding Domain of the Kinesin, KIF5C, Substantiates a Role for GRIF-1 as an Adaptor Protein in the Anterograde Trafficking of Cargoes." *Journal of Biological Chemistry* 281(37):27216–28.

Song, Zhiyin, Hsiuchen Chen, Maja Fiket, Christiane Alexander, and David C. Chan. 2007. "OPA1 Processing Controls Mitochondrial Fusion and Is Regulated by MRNA Splicing, Membrane Potential, and Yme1L." *The Journal of Cell Biology* 178(5):749–55.

Sorkin, Alexander and Mark von Zastrow. 2009. "Endocytosis and Signalling: Intertwining Molecular Networks." *Nature Reviews Molecular Cell Biology* 10(9):609–22.

Spangler, Skylar M. and Michael R. Bruchas. 2017. "Optogenetic Approaches for Dissecting Neuromodulation and GPCR Signaling in Neural Circuits." *Current Opinion in Pharmacology* 32:56–70.

Spiegelberg, Bryan D. and Heidi E. Hamm. 2005. "Gβγ Binds Histone Deacetylase 5 (HDAC5) and Inhibits Its Transcriptional Co-Repression Activity." *Journal of Biological Chemistry* 280(50):41769–76.

van Spronsen, Myrrhe, Marina Mikhaylova, Joanna Lipka, Max A. Schlager, Dave J. van den Heuvel, Marijn Kuijpers, Phebe S. Wulf, Nanda Keijzer, Jeroen Demmers, Lukas C. Kapitein, Dick Jaarsma, Hans C. Gerritsen, Anna Akhmanova, and Casper C. Hoogenraad. 2013. "TRAK/Milton Motor-Adaptor Proteins Steer Mitochondrial Trafficking to Axons and Dendrites." *Neuron* 77(3):485–502.

Srivastava, Ashish, Bhagyashri Gupta, Charu Gupta, and Arun K. Shukla. 2015. "Emerging Functional Divergence of β-Arrestin Isoforms in GPCR Function." *Trends in Endocrinology and Metabolism: TEM* 26(11):628–42.

Stokin, Gorazd B., Concepción Lillo, Tomás L. Falzone, Richard G. Brusch, Edward Rockenstein, Stephanie L. Mount, Rema Raman, Peter Davies, Eliezer Masliah, David S. Williams, and Lawrence S. B. Goldstein. 2005. "Axonopathy and Transport Deficits Early in the Pathogenesis of Alzheimer's Disease." *Science (New York, N.Y.)* 307(5713):1282–88.

Stolz, Alexandra, Andreas Ernst, and Ivan Dikic. 2014. "Cargo Recognition and Trafficking in Selective Autophagy." *Nature Cell Biology* 16(6):495–501.

Stow, Jennifer L., J. Brunno de Almeida, Navneet Narula, Eliezer J. Holtzman, Louis Ercolani, and Dennis A. Ausiello. 1991. "A Heterotrimeric G Protein, G Alpha i-3, on Golgi Membranes Regulates the Secretion of a Heparan Sulfate Proteoglycan in LLC-PK1 Epithelial Cells." *The Journal of Cell Biology* 114(6):1113–24.

Stowers, R. Steve., Laura J. Megeath, Jolanta Górska-Andrzejak, Ian A. Meinertzhagen, and Thomas L. Schwarz. 2002. "Axonal Transport of Mitochondria to Synapses Depends on Milton, a Novel *Drosophila* Protein." *Neuron* 36(6):1063–77.

Su, Bo, Xinglong Wang, Ling Zheng, George Perry, Mark A. Smith, and Xiongwei Zhu. 2010. "Abnormal Mitochondrial Dynamics and Neurodegenerative Diseases." *Biochimica et Biophysica Acta* 1802(1):135–42.

Su, Ping, Shupeng Li, Sheng Chen, Tatiana V. Lipina, Min Wang, Terence K. Y. Lai, Frankie H. F. Lee, Hailong Zhang, Dongxu Zhai, Stephen S. G. Ferguson, José N. Nobrega, Albert H. C. Wong, John C. Roder, Paul J. Fletcher, and Fang Liu. 2014. "A Dopamine D2 Receptor-DISC1 Protein Complex May Contribute to Antipsychotic-Like Effects." *Neuron* 84(6):1302–16.

Sugawara, Yo, Hiroko Nishii, Tomoko Takahashi, Junji Yamauchi, Norikazu Mizuno, Kenji Tago, and Hiroshi Itoh. 2007. "The Lipid Raft Proteins Flotillins/Reggies Interact with Gαq and Are Involved in Gq-Mediated P38 Mitogen-Activated Protein Kinase Activation through Tyrosine Kinase." *Cellular Signalling* 19(6):1301–8.

Suh, Yeongjun, Su-Jin Noh, Saebom Lee, Bo Kyoung Suh, Su Been Lee, Jinhyuk Choi, Jaehoon Jeong, Sangjune Kim, and Sang Ki Park. 2019. "Dopamine D1 Receptor (D1R) Expression Is Controlled by a Transcriptional Repressor Complex Containing DISC1." *Molecular Neurobiology* 1–11.

Sundaram, Senthil K., Sharon K. Michelhaugh, Neil V Klinger, William J. Kupsky, Sandeep Sood, Harry T. Chugani, Sandeep Mittal, and Csaba Juhász. 2017. "GNAQ Mutation in the Venous Vascular Malformation and Underlying Brain Tissue in Sturge-Weber Syndrome." *Neuropediatrics* 48(5):385–89.

Syrovatkina, Viktoriya, Kamela O. Alegre, Raja Dey, and Xin-Yun Huang. 2016. "Regulation, Signaling, and Physiological Functions of G-Proteins." *Journal of Molecular Biology* 428(19):3850–68.

Taguchi, Naoko, Naotada Ishihara, Akihiro Jofuku, Toshihiko Oka, and Katsuyoshi Mihara. 2007. "Mitotic Phosphorylation of Dynamin-Related GTPase Drp1 Participates in Mitochondrial Fission." *Journal of Biological Chemistry* 282(15):11521–29.

Takahashi-Iwanaga, Hiromi and Toshihiko Iwanaga. 2012. "Accumulated Caveolae Constitute Subcellular Compartments for Glial Calcium Signaling in Lanceolate Sensory Endings Innervating Rat Vibrissae." *The Journal of Comparative Neurology* 520(9):2053–66.

Takahide Kon, Masaya Nishiura, Reiko Ohkura, and Yoko Y. Toyoshima, and Kazuo Sutoh. 2004. "Distinct Functions of Nucleotide-Binding/Hydrolysis Sites in the Four AAA Modules of Cytoplasmic Dynein."

Takasaki, Jun, Tetsu Saito, Masatoshi Taniguchi, Tomihisa Kawasaki, Yumiko Moritani, Kazumi Hayashi, and Masato Kobori. 2004. "A Novel Galphaq/11-Selective Inhibitor." *The Journal of Biological Chemistry* 279(46):47438–45.

Tall, Gregory G. 2013. "Ric-8 Regulation of Heterotrimeric G Proteins." *Journal of Receptors and Signal Transduction* 33(3):139–43.

Tall, Gregory G. and Alfred G. Gilman. 2005. "Resistance to Inhibitors of Cholinesterase 8A Catalyzes Release of Gαi-GTP and Nuclear Mitotic Apparatus Protein (NuMA) from NuMA/LGN/Gαi-GDP Complexes." *Proceedings of the National Academy of Sciences of the United States of America* 102(46):16584–89.

Tall, Gregory G., Andrejs M. Krumins, and Alfred G. Gilman. 2003. "Mammalian Ric-8A (Synembryn) Is a Heterotrimeric Gα Protein Guanine Nucleotide Exchange Factor." *Journal of Biological Chemistry* 278(10):8356–62.

Tanaka, Yosuke and Nobutaka Hirokawa. 2002. "Mouse Models of Charcot-Marie-Tooth Disease." *Trends in Genetics* 18(12):S39–44.

Tanaka, Yosuke, Yoshimitsu Kanai, Yasushi Okada, Shigenori Nonaka, Sen Takeda, Akihiro Harada, and Nobutaka Hirokawa. 1998. "Targeted Disruption of Mouse Conventional Kinesin Heavy Chain Kif5B, Results in Abnormal Perinuclear Clustering of Mitochondria." *Cell* 93(7):1147–58.

Tang, Bor, Tang, and Bor Luen. 2015. "MIRO GTPases in Mitochondrial Transport, Homeostasis and Pathology." *Cells* 5(1):1.

Teixeira, Mariana Bertini, Marcos Rodrigo Alborghetti, and Jörg Kobarg. 2019. "Fasciculation and Elongation Zeta Proteins 1 and 2: From Structural Flexibility to Functional Diversity." *World Journal of Biological Chemistry* 10(2):28–43.

Thomas, Bobby. and M. Flint Beal. 2007. "Parkinson's Disease." *Human Molecular Genetics* 16(R2):R183–94.

Thompson, Dawn, Margareta Pusch, and Jennifer L. Whistler. 2007. "Changes in G Protein-Coupled Receptor Sorting Protein Affinity Regulate Postendocytic Targeting of G Protein-Coupled Receptors." *The Journal of Biological Chemistry* 282(40):29178–85.

Thornberry, Nancy A. and Yuri Lazebnik. 1998. "Caspases: Enemies Within." *Science (New York, N.Y.)* 281(5381):1312–16.

Toll, Lawrence, Michael R. Bruchas, Girolamo Caló, Brian M. Cox, and Nurulain T. Zaveri. 2016. "Nociceptin/Orphanin FQ Receptor Structure, Signaling, Ligands, Functions, and Interactions with Opioid Systems." *Pharmacological Reviews* 68(2):419–57.

Toyama, Erin Quan, Sébastien Herzig, Julien Courchet, Tommy L. Lewis, Oliver C. Losón, Kristina Hellberg, Nathan P. Young, Hsiuchen Chen, Franck Polleux, David C. Chan, and Reuben J. Shaw. 2016. "Metabolism. AMP-Activated Protein Kinase Mediates Mitochondrial Fission in Response to Energy Stress." *Science (New York, N.Y.)* 351(6270):275–81.

Traut, Thomas W. 1994. "Physiological Concentrations of Purines and Pyrimidines." *Molecular and Cellular Biochemistry* 140(1):1–22.

Trokter, Martina, Norbert Mücke, and Thomas Surrey. 2012. "Reconstitution of the Human Cytoplasmic Dynein Complex." *Proceedings of the National Academy of Sciences of the United States of America* 109(51):20895–900.

Tsai, Pei-I., Meredith M. Course, Jonathan R. Lovas, Chung-Han Hsieh, Milos Babic, Konrad E. Zinsmaier, and Xinnan Wang. 2015. "PINK1-Mediated Phosphorylation of Miro Inhibits Synaptic Growth and Protects Dopaminergic Neurons in *Drosophila*." *Scientific Reports* 4(1):6962.

Uemura, Toshio, Tomihisa Kawasaki, Masatoshi Taniguchi, Yumiko Moritani, Kazumi Hayashi, Tetsu Saito, Jun Takasaki, Wataru Uchida, and Keiji Miyata. 2006. "Biological Properties of a Specific Galpha q/11 Inhibitor, YM-254890, on Platelet Functions and Thrombus Formation under High-Shear Stress." *British Journal of Pharmacology* 148(1):61–69.

Urnavicius, Linas, Clinton K. Lau, Mohamed M. Elshenawy, Edgar Morales-Rios, Carina Motz, Ahmet Yildiz, and Andrew P. Carter. 2018. "Cryo-EM Shows How Dynactin Recruits Two Dyneins for Faster Movement." *Nature* 554(7691):202–6.

Urnavicius, Linas, Kai Zhang, Aristides G. Diamant, Carina Motz, Max A. Schlager, Minmin Yu, Nisha A. Patel, Carol V Robinson, and Andrew P. Carter. 2015. "The Structure of the Dynactin Complex and Its Interaction with Dynein." *Science (New York, N.Y.)* 347(6229):1441–46.

Vagnoni, Alessio, Patrick C. Hoffmann, and Simon L. Bullock. 2016. "Reducing Lissencephaly-1 Levels Augments Mitochondrial Transport and Has a Protective Effect in Adult *Drosophila* Neurons." *Journal of Cell Science* 129(1):178–90.

Vale, Ronald D., Thomas S. Reese, and Michael P. Sheetz. 1985. "Identification of a Novel Force-Generating Protein, Kinesin, Involved in Microtubule-Based Motility." *Cell* 42(1):39–50.

Valkenburg, Kenneth C., Carrie R. Graveel, Cassandra R. Zylstra-Diegel, Zhendong Zhong, Bart O. Williams, Kenneth C. Valkenburg, Carrie R. Graveel, Cassandra R. Zylstra-Diegel, Zhendong Zhong, and Bart O. Williams. 2011. "Wnt/β-Catenin Signaling in Normal and Cancer Stem Cells." *Cancers* 3(2):2050–79.

Vellano, Christopher P., Feng Jue Shu, Suneela Ramineni, Cindee K. Yates, Gregory G. Tall, and John R. Hepler. 2011. "Activation of the Regulator of G Protein Signaling 14-Gαi1-GDP Signaling Complex Is Regulated by Resistance to Inhibitors of Cholinesterase-8A." *Biochemistry* 50(5):752–62.

Verburg, Jessica and Peter J. Hollenbeck. 2008. "Mitochondrial Membrane Potential in Axons Increases with Local Nerve Growth Factor or Semaphorin Signaling." *The Journal of Neuroscience : The Official Journal of the Society for Neuroscience* 28(33):8306–15.

De Vos, Kurt J., Anna L. Chapman, Maria E. Tennant, Catherine Manser, Elizabeth L. Tudor, Kwok-Fai Lau, Janet Brownlees, Steven Ackerley, Pamela J. Shaw, Declan M. McLoughlin, Christopher E. Shaw, P. Nigel Leigh, Christopher C. J. Miller, and Andrew J. Grierson. 2007. "Familial Amyotrophic Lateral Sclerosis-Linked SOD1 Mutants Perturb Fast Axonal Transport to Reduce Axonal Mitochondria Content." *Human Molecular Genetics* 16(22):2720–28.

De Vos, Kurt J., Andrew J. Grierson, Steven Ackerley, and Christopher C. J. Miller. 2008. "Role of Axonal Transport in Neurodegenerative Diseases." *Annual Review of Neuroscience* 31(1):151–73.

Wai, Timothy and Thomas Langer. 2016. "Mitochondrial Dynamics and Metabolic Regulation." *Trends in Endocrinology & Metabolism* 27(2):105–17.

Wallace, Douglas C. 2005. "A Mitochondrial Paradigm of Metabolic and Degenerative Diseases, Aging, and Cancer: A Dawn for Evolutionary Medicine." *Annual Review of Genetics* 39(1):359–407.

Wang, Hongxia, Pingping Song, Lei Du, Weili Tian, Wen Yue, Min Liu, Dengwen Li, Bin Wang, Yushan Zhu, Cheng Cao, Jun Zhou, and Quan Chen. 2011. "Parkin Ubiquitinates Drp1 for Proteasome-Dependent Degradation: Implication of Dysregulated Mitochondrial Dynamics in Parkinson Disease." *The Journal of Biological Chemistry* 286(13):11649–58.

Wang, Limin, Dagang Guo, Bowen Xing, J. Jillian Zhang, Hong-Bing Shu, Lin Guo, and Xin-Yun Huang. 2011. "Resistance to Inhibitors of Cholinesterase-8A (Ric-8A) Is Critical for Growth Factor Receptor-Induced Actin Cytoskeletal Reorganization." *The Journal of Biological Chemistry* 286(35):31055–61.

Wang, Nan, Kun Yan, and Mark M. Rasenick. 1990. "Tubulin Binds Specifically to the Signal-Transducing Proteins, Gs Alpha and Gi Alpha 1." *The Journal of Biological Chemistry* 265(3):1239–42.

Wang, Shiyu, Savitha Narendra, and Nina Fedoroff. 2007. "Heterotrimeric G Protein Signaling in the Arabidopsis Unfolded Protein Response." *Proceedings of the National Academy of Sciences of the United States of America* 104(10):3817–22.

Wang, Xinglong, Bo Su, Hyoung-gon Lee, Xinyi Li, George Perry, Mark A. Smith, and Xiongwei Zhu. 2009. "Impaired Balance of Mitochondrial Fission and Fusion in Alzheimer's Disease." *The Journal of Neuroscience : The Official Journal of the Society for Neuroscience* 29(28):9090–9103.

Wang, Xinglong, Bo Su, Sandra L. Siedlak, Paula I. Moreira, Hisashi Fujioka, Yang Wang, Gemma Casadesus, and Xiongwei Zhu. 2008. "Amyloid-Beta Overproduction Causes Abnormal Mitochondrial Dynamics via Differential Modulation of Mitochondrial Fission/Fusion Proteins." *Proceedings of the National Academy of Sciences of the United States of America* 105(49):19318–23.

Wang, Xinnan and Thomas L. Schwarz. 2009. "The Mechanism of Ca2+-Dependent Regulation of Kinesin-Mediated Mitochondrial Motility." *Cell* 136(1):163–74.

Wang, Xinnan, Dominic Winter, Ghazaleh Ashrafi, Julia Schlehe, Yao Liang Wong, Dennis Selkoe, Sarah Rice, Judith Steen, Matthew J. LaVoie, and Thomas L. Schwarz. 2011. "PINK1 and Parkin Target Miro for Phosphorylation and Degradation to Arrest Mitochondrial Motility." *Cell* 147(4):893–906.

Waring, Stephen C. and Roger N. Rosenberg. 2008. "Genome-Wide Association Studies in Alzheimer Disease." *Archives of Neurology* 65(3):329–34.

Wasiak, Sylwia, Rodolfo Zunino, and Heidi M. McBride. 2007. "Bax/Bak Promote Sumoylation of DRP1 and Its Stable Association with Mitochondria during Apoptotic Cell Death." *The Journal of Cell Biology* 177(3):439–50.

Waterman-Storer, C. M., S. Karki, and E. L. Holzbaur. 1995. "The P150Glued Component of the Dynactin Complex Binds to Both Microtubules and the Actin-Related Protein Centractin (Arp-1)." *Proceedings of the National Academy of Sciences of the United States of America* 92(5):1634–38.

Wegner, Michael. 1999. "From Head to Toes: The Multiple Facets of Sox Proteins." *Nucleic Acids Research* 27(6):1409–20.

Weihofen, Andreas, Kelly Jean Thomas, Beth L. Ostaszewski, Mark R. Cookson, and Dennis J. Selkoe. 2009. "Pink1 Forms a Multiprotein Complex with Miro and Milton, Linking Pink1 Function to Mitochondrial Trafficking." *Biochemistry* 48(9):2045–52.

Weiss, Catherine A., Elyssa White, Hai Huang, and Hong Ma. 1997. "The G Protein α Subunit (GPα1) Is Associated with the ER and the Plasma Membrane in Meristematic Cells of *Arabidopsis* and Cauliflower." *FEBS Letters* 407(3):361–67.

Weiss, Thomas S., Chester E. Chamberlain, Tetsuro Takeda, Peter Lin, Klaus M. Hahn, and Marilyn Gist Farquhar. 2001. "Galpha I3 Binding to Calnuc on Golgi Membranes in Living Cells Monitored by Fluorescence Resonance Energy Transfer of Green Fluorescent Protein Fusion Proteins." *Proceedings of the National Academy of Sciences of the United States of America* 98(26):14961–66.

Wettschureck, Nina, Alexandra Moers, Barbara Wallenwein, Albert F. Parlow, Christiane Maser-Gluth, and Steffan Offermanns. 2005. "Loss of Gq/11 Family G Proteins in the Nervous System Causes Pituitary Somatotroph Hypoplasia and Dwarfism in Mice." *Molecular and Cellular Biology* 25(5):1942–48.

Wickstead, Bill and Keith Gull. 2007. "Dyneins across Eukaryotes: A Comparative Genomic Analysis." *Traffic (Copenhagen, Denmark)* 8(12):1708–21.

Wilkie, Thomas M., Peggy A. Scherlet, Michael P. Strathmann, Vladlen Z. Slepak, and Melvin 1. Simon. 1991. *Characterization of G-Protein a Subunits in the Gq Class: Expression in Murine Tissues and in Stromal and Hematopoietic Cell Lines (Heterotrimeric GTP-Binding Protein/Signal Transduction/Multigene Family/Phospholipase C)*. Vol. 88.

Williams, Stacey L., Susanne Lutz, Nicole K. Charlie, Christiane Vettel, Michael Ailion, Cassandra Coco, John J. G. Tesmer, Erik M. Jorgensen, Thomas Wieland, and Kenneth G. Miller. 2007. "Trio's Rho-Specific GEF Domain Is the Missing Gα q Effector in C. Elegans." *Genes and Development* 21(21):2731–46.

Winter, Eitan E. and Chris P. Ponting. 2005. "Mammalian BEX , WEX and GASP Genes: Coding and Non-Coding Chimaerism Sustained by Gene Conversion Events." *BMC Evolutionary Biology* 5(1):54.

Wiśniewski, Jacek R., Nagarjuna Nagaraj, Alexandre Zougman, Florian Gnad, and Matthias Mann. 2010. "Brain Phosphoproteome Obtained by a Fasp-Based Method Reveals Plasma Membrane Protein Topology." *Journal of Proteome Research* 9(6):3280–89.

Wong, Edith D., Jennifer A. Wagner, Steven W. Gorsich, J. Michael McCaffery, Janet M. Shaw, and Jodi Nunnari. 2000. "The Dynamin-Related GTPase, Mgm1p, Is an Intermembrane Space Protein Required for Maintenance of Fusion Competent Mitochondria." *The Journal of Cell Biology* 151(2):341–52.

Wylie, Fiona, Kirsten Heimann, Tam Luan Le, Darren Brown, Glenn Rabnott, and Jennifer L. Stow. 1999. "GAIP, a $G\alpha_{i-3}$ - Binding Protein, Is Associated with Golgi-Derived Vesicles and Protein Trafficking." *American Journal of Physiology-Cell Physiology* 276(2):C497–506.

Xie, Long long, Feng Shi, Zheqiong Tan, Yueshuo Li, Ann M. Bode, and Ya Cao. 2018. "Mitochondrial Network Structure Homeostasis and Cell Death." *Cancer Science* 109(12):3686–94.

Yajima, Takaji, Ryotaro Inoue, Masako Yajima, Tadashi Tsuruta, Shinichiro Karaki, Tohru Hira, and Atsukazu Kuwahara. 2011. "The G-Protein on Cholesterol-Rich Membrane Microdomains Mediates Mucosal Sensing of Short- Chain Fatty Acid and Secretory Response in Rat Colon." *Acta Physiologica* 203(3):381–89.

Yakes, F. Michael and Bennett Van Houten. 1997. "Mitochondrial DNA Damage Is More Extensive and Persists Longer than Nuclear DNA Damage in Human Cells Following Oxidative Stress." *Proceedings of the National Academy of Sciences of the United States of America* 94(2):514–19.

Yamanaka, Koji, Seung Joo Chun, Severine Boillee, Noriko Fujimori-Tonou, Hirofumi Yamashita, David H. Gutmann, Ryosuke Takahashi, Hidemi Misawa, and Don W. Cleveland. 2008. "Astrocytes as Determinants of Disease Progression in Inherited Amyotrophic Lateral Sclerosis." *Nature Neuroscience* 11(3):251–53.

Yamano, Koji, Chunxin Wang, Shireen A. Sarraf, Christian Münch, Reika Kikuchi, Nobuo N. Noda, Yohei Hizukuri, Masato T. Kanemaki, Wade Harper, Keiji Tanaka, Noriyuki Matsuda, and Richard J. Youle. 2018. "Endosomal Rab Cycles Regulate Parkin-Mediated Mitophagy." *ELife* 7.

Yamaoka, Shohei, Masaki Nakajima, Masaru Fujimoto, and Nobuhiro Tsutsumi. 2011. "MIRO1 Influences the Morphology and Intracellular Distribution of Mitochondria during Embryonic Cell Division in Arabidopsis." *Plant Cell Reports* 30(2):239–44.

Yan, Jing, Dan L. Chao, Shiori Toba, Kotaro Koyasako, Takuo Yasunaga, Shinji Hirotsune, and Kang Shen. 2013. "Kinesin-1 Regulates Dendrite Microtubule Polarity in Caenorhabditis Elegans." *ELife* 2.

Yang, Fan, Bing Li, Yongyao Yang, Minhua Huang, Xinghui Liu, Yang Zhang, Hui Liu, Lan Zhang, Yujia Pan, Shui Tian, Yueting Wu, Lijuan Wang, and Long Yang. 2019. "Leptin Enhances Glycolysis via OPA1-Mediated Mitochondrial Fusion to Promote Mesenchymal Stem Cell Survival." *International Journal of Molecular Medicine* 44(1):301–12.

Yonekawa, Yoshiaki, Akihiro Harada, Yasushi Okada, Takeshi Funakoshi, Yoshimitsu Kanai, Yosuke Takei, Sumio Terada, Tetsuo Noda, and Nobutaka Hirokawa. 1998. "Defect in Synaptic Vesicle Precursor Transport and Neuronal Cell Death in KIF1A Motor Protein–Deficient Mice." *The Journal of Cell Biology* 141(2):431–41.

Yoshida, Kazuyuki, Yusuke Kusama, Moe Tategu, and Kenichi Yoshida. 2009. "FBXL16 Is a Novel E2F1-Regulated Gene Commonly Upregulated in P16INK4A- and P14ARF-Silenced HeLa Cells." *International Journal of Oncology* 36(2):479–90.

Yu, Fei, Tao Xu, Man Wang, Wenguang Chang, Peifeng Li, and Jianxun Wang. 2018. "Function and Regulation of Mitofusin 2 in Cardiovascular Physiology and Pathology." *European Journal of Cell Biology* 97(7):474–82.

Yu, Guoyong, Zhaotao Wang, Shulian Zeng, Sisi Liu, Chunping Zhu, Ruxiang Xu, and Ru-en Liu. 2019. "Paeoniflorin Inhibits Hepatocyte Growth Factor- (HGF-) Induced Migration and Invasion and Actin Rearrangement via Suppression of c-Met-Mediated RhoA/ROCK Signaling in Glioblastoma." *BioMed Research International* 2019:9053295.

Yu, Rong, Shao-Bo Jin, Urban Lendahl, Monica Nistér, and Jian Zhao. 2019. "Human Fis1 Regulates Mitochondrial Dynamics through Inhibition of the Fusion Machinery." *The EMBO Journal* 38(8):e99748.

Yu, Yiyi, Hao Chih Lee, Kuan Chieh Chen, Joseph Suhan, Minhua Qiu, Qinle Ba, and Ge Yang. 2016. "Inner Membrane Fusion Mediates Spatial Distribution of Axonal Mitochondria." *Scientific Reports* 6.

Yue, Chenglong, Mingshan Niu, Qian Qian Shan, Ting Zhou, Yiming Tu, Peng Xie, Lei Hua, Rutong Yu, and Xuejiao Liu. 2017. "High Expression of Bruton's Tyrosine Kinase (BTK) Is Required for EGFR-Induced NF-κB Activation and Predicts Poor Prognosis in Human Glioma." *Journal of Experimental & Clinical Cancer Research : CR* 36(1):132.

Zeng, Weizhong, Don-On Daniel Mak, Qin Li, Dong Min Shin, J. Kevin Foskett, and Shmuel Muallem. 2003. "A New Mode of Ca2+ Signaling by G Protein-Coupled Receptors: Gating of IP3 Receptor Ca2+ Release Channels by Gbetagamma." *Current Biology : CB* 13(10):872–76.

Zhang, Fan, Wenzhang Wang, Sandra L. Siedlak, Yingchao Liu, Jun Liu, Keji Jiang, George Perry, Xiongwei Zhu, and Xinglong Wang. 2015. "Miro1 Deficiency in Amyotrophic Lateral Sclerosis." *Frontiers in Aging Neuroscience* 7:100.

Zhang, Juan, Weihua Liu, Jianchao Liu, Weiming Xiao, Lei Liu, Chunsun Jiang, Xin Sun, Pingsheng Liu, Yushan Zhu, Chuanmao Zhang, and Quan Chen. 2010. "G-Protein Β2 Subunit Interacts with Mitofusin 1 to Regulate Mitochondrial Fusion." *Nature Communications* 1(7):101.

Zhang, Lili, Chen Chen, Marvin SH Mak, Junfeng Lu, Zeqing Wu, Qiuhe Chen, Yifan Han, Yuefeng Li, and Rongbiao Pi. 2019. "Advance of Sporadic Alzheimer's Disease Animal Models." *Medicinal Research Reviews* med.21624.

Zhang, Xuming. 2019. "Direct Gαq Gating Is the Sole Mechanism for TRPM8 Inhibition Caused by Bradykinin Receptor Activation." *Cell Reports* 27(12):3672-3683.e4.

Zhang, Xuming, Stephanie Mak, Lin Li, Andres Parra, Bristol Denlinger, Carlos Belmonte, and Peter A. McNaughton. 2012. "Direct Inhibition of the Cold-Activated TRPM8 Ion Channel by Gα Q." *Nature Cell Biology* 14(8):850–58.

Zhao, Chunjie, Junko Takita, Yosuke Tanaka, Mitsutoshi Setou, Terunaga Nakagawa, Sen Takeda, Hong Wei Yang, Sumio Terada, Takao Nakata, Yosuke Takei, Masaaki Saito, Shoji Tsuji, Yasuhide Hayashi, Nobutaka Hirokawa. 2001. "Charcot-Marie-Tooth Disease Type 2A Caused by Mutation in a Microtubule Motor KIF1Bbeta." *Cell* 105(5):587–97.

Zhao, Chunjie, Junko Takita, Yosuke Tanaka, Mitsutoshi Setou, Terunaga Nakagawa, Sen Takeda, Hong Wei Yang, Sumio Terada, Takao Nakata, Yosuke Takei, Masaaki Saito, Shoji Tsuji, Yasuhide Hayashi, and Nobutaka Hirokawa. 2001. "Charcot-Marie-Tooth Disease Type 2A Caused by Mutation in a Microtubule Motor KIF1Bβ." *Cell* 105(5):587–97.

Zheng, Bin, Christine Lavoie, Ting-Dong Tang, Phuong Ma, Timo Meerloo, Anthony Beas, and Marilyn G. Farquhar. 2004. "Regulation of Epidermal Growth Factor Receptor Degradation by Heterotrimeric Galphas Protein." *Molecular Biology of the Cell* 15(12):5538–50.

Zheng, Peng, Minmin Hu, Yuanyi Xie, Yinghua Yu, Hanna Jaaro-Peled, and Xu-Feng Huang. 2019. "Aripiprazole and Haloperidol Protect Neurite Lesions via Reducing Excessive D2R-DISC1 Complex Formation." *Progress in Neuro-Psychopharmacology and Biological Psychiatry* 92:59–69.

Zhu, Xiao-Hong, Hongyan Qiao, Fei Du, Qiang Xiong, Xiao Liu, Xiaoliang Zhang, Kamil Ugurbil, and Wei Chen. 2012. "Quantitative Imaging of Energy Expenditure in Human Brain." *NeuroImage* 60(4):2107–17.

Ziviani, Elena, Ran N. Tao, and Alexander J. Whitworth. 2010. "Drosophila Parkin Requires PINK1 for Mitochondrial Translocation and Ubiquitinates Mitofusin." *Proceedings of the National Academy of Sciences of the United States of America* 107(11):5018–23.

Züchner, Stephan, Irina V Mersiyanova, Maria Muglia, Nisrine Bissar-Tadmouri, Julie Rochelle, Elena L. Dadali, Mario Zappia, Eva Nelis, Alessandra Patitucci, Jan Senderek, Yesim Parman, Oleg Evgrafov, Peter De Jonghe, Yuji Takahashi, Shoij Tsuji, Margaret A. Pericak-Vance, Aldo Quattrone, Esra Battologlu, Alexander V Polyakov, Vincent Timmerman, J. Michael Schröder, and Jeffery M. Vance. 2004. "Mutations in the Mitochondrial GTPase Mitofusin 2 Cause Charcot-Marie-Tooth Neuropathy Type 2A." *Nature Genetics* 36(5):449–51.

RESUM EN CATALÀ

INTRODUCCIÓ

L'origen de les mitocòndries prové d'una simbiosi entre una bactèria ancestral i una cèl·lula eucariota. Amb el temps aquestes bactèries van anar evolucionant fins a convertir-se en orgànuls de la pròpia cèl·lula altament especialitzats en la producció d'energia a partir de nutrients i oxigen, tot i que actualment també realitzen altres funcions essencials com l'emmagatzematge d'ions (especialment calci) i la regulació de l'apoptosi. Les mitocòndries estan estructurades per una doble membrana amb una sèrie de plecs a la membrana interna, on s'acoblen la majoria dels complexes enzimàtics que participen a la fosforilació oxidativa. Aquest procés permet bombejar protons de la matriu mitocondrial a l'espai intermembrana a partir de l'energia que s'obté de l'oxidació de coenzims i el transport d'electrons entre les proteïnes dels complexes. El gradient de protons es restableix gràcies al complex de l'ATP sintasa, que permet generar ATP gracies a l'energia que obté del flux iònic.

Les mitocòndries son extremadament dinàmiques i pateixen constantment fenòmens de fissió i fusió per adaptar-se a les condicions de la cèl·lula. Aquests processos, juntament amb el transport de mitocòndries, es coneixen com a dinàmica mitocondrial i estan regulats per una gran quantitat de proteïnes. Els processos de fissió estan mediats principalment per la proteïna Drp1 i els contactes entre la mitocòndria i el reticle endoplasmàtic (ER), mentre que la fusió entre dues mitocòndries esta regulada per les mitofusines 1 i 2, que permeten la fusió de la membrana externa, i la proteïna Opa1, que ajuda a fusionar la membrana interna. Tant la Drp1 con les mitofusines i l'Opa1 son GTPases altament regulades per fosforilacions i modificacions post-transcripcionals.

A més de regular la seva morfologia, les mitocòndries han de ser transportades als llocs de la cèl·lula on les demandes energètiques o les necessitats de tamponar ions son elevades. Aquest transport es dona a totes les cèl·lules, però es especialment important en neurones degut a la seva morfologia excepcional. Les neurones son cèl·lules encarregades de transmetre impulsos del sistema nerviós, principalment a través de les sinapsis. Aquestes sinapsis consumeixen una

gran quantitat d'energia i requereixen molta capacitat per tamponar ions. Això fa que el transport de mitocòndries des del soma als extrems de les dendrites o els axons (on tenen lloc moltes sinapsis) sigui essencial. Aquest transport es dona majoritàriament a traves de microtúbuls gràcies a proteïnes motores com les kinesines o els complexes dineïna/dinactina. Aquestes proteïnes assoleixen moviment gracies a la seva capacitat d'obtenir energia amb la hidròlisi d' ATP. Mentre les kinesines permeten principalment el transport anteròg rad (cap als extrems del axons) les dïneina/dinactina regulen el retròg rad (cap al soma). Els dos complexes motors s'uneixen a les mitocòndries gràcies a uns adaptadors amb dominis coiled-coil coneguts com a milton. A mamífers s'hi troben dues isoformes anomenades TRAK1 i TRAK2, que tot i haver estat inicialment identificades com a reguladors del tràfic de vesícules, aviat es va trobar que permetien el transport de mitocòndries. Tot i que la TRAK2 permet el transport bidireccional de mitocòndries unint-se a kinesina o dineïna, TRAK1 regula majoritàriament el transport anteròg rad unint-se a kinesines.

Tant TRAK1 com TRAK2 permeten la unió de les proteïnes motores a les GTPases Miro, ancorades a la membrana mitocondrial externa. La proteïna dMiro es va identificar inicialment a *Drosophila*, i te 2 homòlegs a mamífers, Miro1 i Miro2. Les dues estan estructurades en 2 dominis GTPasa flanquejant un parell de dominis EF que alteren la conformació de la proteïna en presencia de calci. Quan les concentracions de calci al citosol son elevades (com ocorre a les sinapsis), els ions calci s'uniran als dominis EF i faran que Miro es desacobli de les proteïnes motores, fent aturar així les mitocòndries. Les proteïnes Miro, i especialment Miro1, estan molt regulades tant per processos de degradació (com ocorre al procés de mitofàgia) com per proteïnes que alteren la dinàmica mitocondrial, com poden ser DISC1, les pròpies mitofusines o les proteïnes amb dominis armadillo de la família armcx/armc10.

Les proteïnes armcx es van originar per processos de duplicació i recombinació al gen ancestral armc10. Totes tenen en comú la presencia de diversos dominis armadillo a la seva seqüencia, i moltes d'elles van estar originàriament considerades gens supressors de tumors degut a que la seva absència incrementava el risc de patir tumors epitelials, motiu pel cual es van anomenar Alex. Aviat es va trobar que localitzaven a la mitocòndria i tant l'armc10 com l'Alex3 podien unir-se a Miro1 i TRAK2 de forma dependent de calci i regular així el transport de mitocòndries. Tot i així, el mecanisme molecular pel qual les proteïnes Alex regulen Miro i TRAK es encara desconegut.

En aquest sentit, moltes de les senyals que regulen la fisiologia de les mitocòndries i altres orgànuls provenen de receptors amb set dominis transmembrana acoblats a proteïnes G, també coneguts com a GPCRs. Les proteïnes G estan formades per la subunitat Gα i l'heterodimer Gβγ. Clàssicament, la unió del lligands fa que el receptor actuï com a GEF per la Gα, estimulant el

canvi de GDP per GTP i la dissociació de la Gα del dímer Gβγ. D'aquesta manera, la Gα por interactuar amb els seus efectors i transmetre la senyal. A la vegada, molts d'aquests efectors actuaran com a GAP, induint la hidròlisis de GTP a la Gα i la seva reassociació amb la Gβγ. Aquest cicle està altament regulat per proteïnes com les GRKs, que fosforilen al receptor i permeten la unió de β-arrestines, promovent la internalització del receptor i l'aturada la senyal. D'altra banda, cada cop hi ha més evidències de l'activació de proteïnes Gα de forma independent als GPCRs. Un clar exemple son les proteïnes Ric8, que a mes d'actuar com a xaperones tenen activitat GEF i promouen l'activació de diverses Gα.

Tot i que les subunitats Gβγ també poden senyalitzar al dissociar-se, la major diversitat de senyals es transmesa a través de les Gα. Aquestes subunitats es poden classificar en 4 grans famílies segons la seva funció i similitud de seqüència: la $G\alpha_s$, la $G\alpha_i$, la $G\alpha_{12}$ i la $G\alpha_q$. Les dues primeres estimulen o inhibeixen l'activitat de l'adenilat ciclasa, respectivament. La família de la $G\alpha_{12}$ regula l'activació de proteïnes Rho a través de diverses GEF, mentre que la $G\alpha_q$ (que es composa majoritàriament per la $G\alpha_q$ i la $G\alpha_{11}$) estimula la senyalització per PLCβ.

No obstant, hi ha altres vies de senyalització que poden ser activades a partir de $G\alpha_q$ amb efectes diversos. Actualment s'han identificant altres efectors no canònics capaços d'interaccionar i transmetre senyals a partir de $G\alpha_q$, entre els quals es troben la quinasa de Bruton (BTK), rho GEFs, diverses caveolines i fins i tot components del citoesquelet. A més, estudis recents han demostrat que aquesta senyalització no només te lloc a la membrana plasmàtica, sinó també a diverses endomembranes, com el reticle endoplasmàtic o la mitocòndria. En aquest sentit, estudis previs del nostre grup van demostrar que la proteïna $G\alpha_q$ localitza a les membranes externa i interna de la mitocòndria i regula els processos de fissió i fusió. L'absència de $G\alpha_q$ i $G\alpha_{11}$ altera l'estructura de les crestes mitocondrials i dels complexes que formen la cadena de transport d'electrons i això es tradueix en alteracions en el potencial de membrana, un menor consum d'oxigen i una reducció en la producció d'ATP.

RESULTATS

Amb l'objectiu d'identificar possibles efectors de la $G\alpha_q$ a la mitocòndria capaços de produir els efectes observats, es va realitzar un anàlisi d'espectrometria de masses a partir d'immunoprecipitats (IP) de $G\alpha_q$ enriquits en la fracció mitocondrial. En concret, es va concentrar la fracció mitocondrial a llisats de MEF wt, MEF KO (utilitzades com a control), MEF KO+ $G\alpha_q$ i NIH3T3 i es va immunoprecipitar la $G\alpha_q$ endògena amb 2 anticossos diferents. L'anàlisi d'espectrometria de masses d'aquests immunoprecipitats va evidenciar la presència d'una gran quantitat de pèptids de proteïnes implicades en el transport i la dinàmica mitocondrial. Entre elles destaca la presencia de diversos pèptids de les proteïnes armadillo Alex3 i Armc10. Aquest

pèptids apareixen amb els 2 anticossos i varies línies cel·lulars, però no a les cèl·lules control que no expressen $G\alpha_{q/11}$.

La immunoprecipitació de l'Alex3 amb la $G\alpha_q$ es va validar a cèl·lules MEF, SHSY5Y i homogenats de cervell de ratolí . A més, es va demostrar que el mutant constitutivament actiu $G\alpha_q$R183C immunoprecipita més amb l'Alex3 i que aquesta associació es produeix a través de l'extrem C-terminal, on conté els dominis armadillo.

Com aquesta regió conté el lloc d'unió a la GTPasa Miro1, es va estudiar l'efecte de la $G\alpha_q$ en la interacció entre l'Alex3 i la Miro1. Fent servir proteïnes purificades es va demostrar que la interacció entre les dues proteïnes era directa. Experiments d'immunoprecipitació en llisats cel·lulars també van demostrar que aquesta interacció s'afavoreix en presencia de $G\alpha_q$. A més, es va veure que la $G\alpha_q$ també pot co-precipitar amb Miro1, i que aquesta possible interacció s'afavoreix en el mutant de Miro1 amb dominis EF no funcionals o en absència del domini GTPasa C-terminal. La interacció entre Miro1 i $G\alpha_q$ probablement estigui determinada per canvis conformacionals a la GTPasa, lo qual faria que en aquests mutants el lloc d'unió fos mes accessible. En aquest sentit, la presència d'alts nivells de calci aconsegueix reduir lleugerament la co-IP de $G\alpha_q$ amb Miro1, tot i que no en la mateixa mesura en que ho fa amb l'Alex3. La co-IP de la $G\alpha_q$ també es trova reduïda en el cas del mutant actiu insensible a regulacions per RGS $G\alpha_q$Q209L, però no pateix gaires variacions en el cas del mutant incapaç d'unir l'efector canònic PLCβ. Això suggereix que tant l'Alex3 com la Miro1 podrien ser efectors no canònics regulats de forma diferent i independent de PLCβ. Posteriorment es va demostrar la interacció directa entre la $G\alpha_q$ i l'Alex3 o la Miro1 fent servir proteïnes purificades, corroborant els resultats previs en que es veia més unió de $G\alpha_q$ a la regió C-terminal de l'Alex3. Utilitzant tècniques de microscòpia d'alta resolució, es va veure que la $G\alpha_q$ localitzava amb Miro1 en punts concrets de la membrana mitocondrial externa.

Per tal d'estudiar la importància d'aquesta possible regulació, es va analitzar en primer lloc el fenotip d'agregació mitocondrial produït per la sobreexpresió d'Alex3. Amb tècniques de microscopia confocal, es va observar que l'Alex3 produeix un fenotip d'hiperfusió mitocondrial que acava amb el col·lapse de les mitocòndries a la regió perinuclear. Degut a que aquesta fusió es produeix a la membrana mitocondrial externa però no a la interna, es va analitzar si el fenotip estava relacionat amb els efectes de les mitofusines 1 i 2. Es va comprovar que la sobreexpresió d'Alex3 era suficient per reduir la fragmentació mitocondrial produïda per l'absència de mitofusines. Experiments posteriors en cèl·lules MEF van demostrar que aquesta agregació estava incrementada en absència de $G\alpha_q$ i $G\alpha_{11}$, suggerint un efecte inhibitori de la $G\alpha_q$ sobre l'Alex3.

Per tal d'esbrinar si els efectes de $G\alpha_q$ en el fenotip d'Alex3 podien implicar una regulació en el transport de mitocòndries, es va avaluar l'impacte de $G\alpha_q$ a neurones d'hipocamp de ratolí. Fent servir shRNAs, es va veure que una reducció dels nivells de $G\alpha_q$ produeix un increment en la velocitat de les mitocòndries, així com una disminució en el nombre d'aturades i un augment en la tendència cap al moviment retrògrad. Aquest increment, però, es molt més reduït o absent en neurones provinents de ratolins KO per Alex3, indicant que aquesta proteïna es necessària per produir els efectes de $G\alpha_q$.

Posteriorment es va estudiar els efectes de la $G\alpha_q$ en experiments de co-expressió. En aquests estudis es va comprovar que l'increment en els nivells de $G\alpha_q$ augmenta el transport de mitocòndries en direcció anteròg rada. A més, es va demostrar que la $G\alpha_q$ pot co-immunoprecipitar amb la proteïna que s'encarrega del transport en aquesta direcció, la kinesina Kif5c, així com incrementar la seva unió a Miro1. Estudis posteriors fent servir mutants de $G\alpha_q$ units a GFP van demostrar que els efectes de $G\alpha_q$ a la dinàmica mitocondrial son dependents del seu domini GTPasa, i que l'expressió del mutant actiu $G\alpha_q$R183C atura el transport de mitocòndries en les dues direccions. Aquestes subunitats $G\alpha_q$ unides a GFP també van servir per evidenciar la localització dual de la proteïna, que es troba tant a la membrana plasmàtica com a la mitocòndria.

Tant l'increment del transport de mitocòndries cap a les terminals de l'axó degut a la sobreexpresió de $G\alpha_q$ com l'aturada del moviment induïda per l'expressió de $G\alpha_q$R183C es van tornar a posar de manifest en experiments expressant les proteïnes juntament amb el marcador de mitocòndries en vectors bicistrònics. Aquest efectes son específics per al transport de mitocòndries i no extrapolables al tràfic general, ja que no es van observar diferencies significatives en el transport de vesícules amb sinaptofisina. També es va veure que el bloqueig en la unió de GTP fent servir un inhibidor específic de $G\alpha_q$ impedeix l'aturada de mitocòndries. Experiments posteriors van demostrar l'aturada en el transport de mitocòndries a través de l'activació de receptors exclusivament acoblats a $G\alpha_q$, evidenciant que no només l'expressió del muntant actiu, sinó també la senyalització a través de la $G\alpha_q$ endògena son capaces d'aturar les mitocòndries.

Els efectes de la $G\alpha_q$ no es limiten però al transport de mitocòndries, sinó que afecten la dinàmica mitocondrial i repercuteixen en la fisiologia de les neurones. En aquest sentit, la reducció dels nivells de $G\alpha_q$ incrementa la longitud de les mitocòndries axonals, mentre que l'expressió del mutant actiu redueix la seva mida y complexitat i produeix canvis morfològics importants en la neurona, fent que es redueixi la longitud i l'arborització de les dendrites.

Per donar explicació al efectes observats tant en la dinàmica mitocondrial com el la fisiologia de les neurones, es van realitzar experiments amb les proteïnes adaptadores TRAK1 i 2. Estudis anteriors havien demostrat que la sobreexpresió de TRAK1 en cèl·lules HeLa promou el transport de mitocòndries cap a la perifèria, mentre que la TRAK2 feia l'efecte contrari, induint a l'agregació de les mitocòndries a la regió perinuclear. Aquests resultats es van reproduir als nostres experiments, i van permetre determinar que l'expressió de $G\alpha_q$R183C promovia la localització de la TRAK2 a la perifèria de les cèl·lules. La localització perifèrica de TRAK2 en presencia de $G\alpha_q$R183C es va evidenciar en cara més en cèl·lules MEF. Per esbrinar si aquest fenotip era degut a una interacció entre la $G\alpha_q$ i les TRAK, es van immunoprecipitar les dues proteïnes en presencia de $G\alpha_q$ o $G\alpha_q$R183C. Els resultats van evidenciar que la $G\alpha_q$ precipita més amb la TRAK2 que amb la TRAK1, especialment en la seva forma activa. A més, la presencia de $G\alpha_q$ incrementa la unió de TRAK2 a kinesina endògena i redueix la interacció amb Alex3 endògen, suggerint que la TRAK2 localitza menys a la mitocòndria.

Finalment, es va estudiar la localització de $G\alpha_q$ amb la miosina X, una altra proteïna identificada com a possible efector de la $G\alpha_q$ a l'anàlisi inicial d'espectrometria de masses. Diversos estudis suggereixen que la miosina X podria estar involucrada en el transport de mitocòndries a través de filaments d'actina. Aquest transport atípic es freqüent a les terminals sinàptiques i la seva regulació permet regular la velocitat a la que es mouen les mitocòndries quan es troben en moviment. Estudis d'immunofluorescència amb proteïnes endògenes van permetre detectar la localització de la miosina en punts molt concrets amb la $G\alpha_q$, així com la seva co-localització amb marcadors mitocondrials. Aquesta possible interacció explicaria l'increment de velocitat de les mitocòndries de neurones amb baixos nivells de $G\alpha_q$.

DISCUSSIÓ

Tenint en compte els resultats obtinguts, proposem que l'Alex3 podria actuar com a una proteïna acobladora, tant per a la $G\alpha_q$ com per la Miro1 i la TRAK2. Estudis previs van demostrar que l'Alex3 es necessari per el transport de mitocòndries, i que tant la seva absència com la seva sobreexpresió indueixen l'aturada de les mitocòndries. Una sobreexpresió d'Alex3 induiria un fenotip d'agregació mitocondrial, amb fusió de la membrana mitocondrial externa, que produiria una aturada. A més, podria formar dímers o agregats a la membrana mitocondrial externa, dificultant d'aquesta manera la unió de Miro1 amb els adaptadors TRAK1 i TRAK2. Per contra, l'absència d'Alex3 també reduiria la unió de Miro1 a les proteïnes TRAK i la unió de $G\alpha_q$ a aquestes dues proteïnes, reduint d'aquesta forma el moviment i induint a l'aturada. D'altra banda, l'Alex3 podria actuar com la proteïna Ric-8 i no només facilitar la interacció de $G\alpha_q$ amb les proteïnes Miro1 i TRAK2, sinó també estabilitzar-la a la mitocòndria i fins i tot promoure la seva activació.

La $G\alpha_q$, en la seva conformació amb GDP, interaccionaria amb Miro1 i promouria la seva interacció amb les TRAKs (sobretot amb TRAK1), afavorint d'aquesta manera el transport anteròg rad de mitocòndries a través de kinesines. Estímuls provinents tant de GPCRs de la membrana externa com de proteïnes mitocondrials (com podria ser l'Alex3) promouríen el canvi de GDP a GTP a la $G\alpha_q$, fent que aquesta interaccionés amb la TRAK2 i la desacoblés del complexe Miro1-Alex3, induint l'aturada del moviment. Aquesta aturada estaria complementada per l'increment en els nivells citosòlics de calci induïts per l'activació de la PLCβ. L'absència de $G\alpha_q$, per contra, podria afavorir la unió de TRAK2 a Miro1, i per tant, el transport retròg rad a través del complexe dineina/dinactina.